Exploring the Roles of Nuclear Deubiquitinating Enzymes BAP1 and MYSM1 in Hematopoiesis and Immune Cell Functions

Yue Liang

Department of Physiology
McGill University
Montreal, Quebec, Canada
April 2024

A thesis submitted to McGill University in partial fulfillment of the requirements of the degree of Doctor of Philosophy

TABLE OF CONTENTS

Abbreviations

Ab – antibody
ADCC – antibody-dependent cellular cytotoxicity
AGM – aorta-gonad-mesonephros
AID – activation-induced cytidine deaminase
APC – antigen presenting cell(s)
BAP1 – BRCA1-associated protein 1
BARD1 – BRCA1-associated RING domain protein 1
BCR – B-cell receptor
BER – base excision repair
BM – bone marrow
BRCA1 – breast cancer type 1 susceptibility protein
cDC – conventional dendritic cell
CDP – conventional dendritic cell progenitors
CLP – common lymphoid progenitor
CMP – common myeloid progenitor
CSR – class-switch recombination
DC – dendritic cell
D_H – diversity gene segment of the immunoglobulin heavy chain
DNMT – DNA methyltransferase
DSB – double-strand break
DZ – dark zone
E2A – E2A transcription factor
EBF1 – early B-cell factor 1
ECM – extracellular matrix
ETS – E26 transformation-specific
FDC – follicular dendritic cell
FO B – follicular B cell
FOXK1/2 – forkhead box kinase 1 and 2
GC – germinal center
GMP – granulocyte/macrophage progenitor
H2AK119ub – mono-ubiquitination at lysine 119 of histone H2A
H3K4me3 – tri-methylation at lysine 4 of histone H3
H3K27me3 –tri-methylation at lysine 27 of histone H3
H3S10p – phosphorylation at serine 10 of histone H3
H3K14ac – acetylation at lysine 14 of histone H3
HAT – histone acetyl transferases
HDR – homology-directed repair

HSC – hematopoietic stem cell
HSPC – hematopoietic stem and progenitor cell
ICOS – inducible T-cell co-stimulator
Ig – immunoglobulin
IgC – immunoglobulin constant domain
IgV – immunoglobulin variable domain
IFN – interferon
IL – interleukin
ILC – innate lymphoid cell
INO80 – INO80 chromatin remodeling complex
IP3R3 – inositol 1,4,5-trisphosphate receptor, type 3
IRF – interferon regulatory factor
J_L/J_H –joining gene segment of the immunoglobulin light/heavy chain
KDM1B – lysine-specific histone demethylase
KLF5 – Kruppel-like factor 5
LT-HSC – long-term hematopoietic stem cell
LMPP – lymphoid-primed multipotent progenitor
LZ – light zone
MEP – megakaryocyte erythroid progenitor
MHC – major histocompatibility complex
MMR – mismatch repair
MPP – multipotent progenitor cell
MSH2/6 – MSH2/6 mismatch repair complex
MYSM1 – Myb-like SWIRM and MPN domains 1
MZ B – marginal zone B cells
NHEJ – nonhomologous end joining
NK cell – natural killer cell
OGT – O-linked β-N-acetylglucosamine (O-GlcNAc) transferase
PAMP – pathogen-associated molecular pattern
PAX5 – paired box protein 5
PC – plasma cell
PCGF – Polycomb group ring finger subunit
PD1 – programmed cell death protein 1
pDC – plasmacytoid dendritic cell
PGC1α – peroxisome proliferator-activated receptor-γ coactivator 1-α
Pol – polymerase
PRC – polycomb repressive complex
RAD51 – RAD51 recombinase
Rag – recombination activation gene
RUNX1 – runt-related transcription factor 1

SHM – somatic hypermutation
ST-HSC – short-term hematopoietic stem cell
TCR – T cell receptor
Tfh – follicular helper T cell
TLR – Toll-like receptors
Treg – regulatory T cell
TrxG – trithorax groups
UBE2O – ubiquitin conjugating enzyme E2O
UNG – uracil DNA glycosylase
USP – ubiquitin-specific protease
V_L/V_H – variable gene segment of the immunoglobulin light/heavy chain
YY1 – Yin Yang 1

List of Figures

List of Tables

Additional tables including full genomic analysis results are available online at:

https://www.frontiersin.org/articles/10.3389/fimmu.2021.626418/full#supplementary-material

https://www.frontiersin.org/articles/10.3389/fimmu.2024.1353138/full#supplementary-material

Abstract

Hematopoiesis, the process by which the full repertoire of blood cells is established from the hematopoietic stem cells (HSCs), depends on a well-coordinated regulatory network of gene expression. BAP1 and MYSM1 are both deubiquitinases (DUBs) that can regulate gene expression and other cellular processes, through their direct catalytic activity on the repressive epigenetic mark histone H2AK119ub, as well as on several other substrates. In previous research, mutations of *Bap1* and *Mysm1* have been associated with defects in hematopoiesis in both mouse and human, yet our knowledge of the mechanistic role of these two DUBs in the development and the function of blood and immune cells remains limited. In the current study, we aim to explore the potential regulatory role of BAP1 and MYSM1 in hematopoietic cell development and immune response. We characterize a cell intrinsic role of BAP1 in B lymphocyte development and in antibody mediated immune response. We demonstrates its central role in the regulation of the genome-wide landscapes of histone H2AK119ub and downstream transcriptional programs of cell cycle progression, DNA damage response, and many other biological processes involved in B cell development, B cell activation, and humoral immunity. We also report a profound similarity in the developmental, hematopoietic, and immune phenotypes resulting from the loss of MYSM1 catalytic function and the full loss of MYSM1 protein, confirming that MYSM1 acts via its DUB catalytic activity specifically in early hematopoietic progenitors to allow normal development of hematopoietic cells, including lymphocytes and dendritic cells (DCs). Overall, our work expands the knowledge of the critical roles of BAP1 and MYSM1 in vivo in hematopoiesis, leukocyte development, immune responses, and other aspects of mammalian physiology.

Résumé

L'hématopoïèse, le processus par lequel le répertoire complet des cellules sanguines est établi à partir des cellules souches hématopoïétiques (CSH), dépend d'un réseau de régulation bien coordonné de l'expression génique. BAP1 et MYSM1 sont toutes deux des déubiquitinases (DUB) qui peuvent réguler l'expression des gènes et d'autres processus cellulaires, grâce à leur activité catalytique directe sur la marque épigénétique répressive histone H2AK119ub, ainsi que sur plusieurs autres substrats. Dans des recherches antérieures, des mutations de Bap1 et Mysm1 ont été associées à des défauts dans l'hématopoïèse tant chez la souris que chez l'homme, mais notre connaissance du rôle mécanique de ces deux DUB dans le développement et la fonction des cellules sanguines et immunitaires reste limitée. Dans la présente étude, nous cherchons à explorer le rôle régulateur potentiel de BAP1 et MYSM1 dans le développement des cellules hématopoïétiques et la réponse immunitaire. Nous caractérisons le rôle intrinsèque de BAP1 dans le développement des lymphocytes B et dans la réponse immunitaire médiée par les anticorps. Nous démontrons son rôle central dans la régulation des paysages génomiques de l'histone H2AK119ub et des programmes transcriptionnels en aval de la progression du cycle cellulaire, de la réponse aux dommages de l'ADN et de nombreux autres processus biologiques impliqués dans le développement des lymphocytes B, l'activation des lymphocytes B et l'immunité humorale. Nous rapportons également une profonde similarité dans les phénotypes développementaux, hématopoïétiques et immunitaires résultant de la perte de la fonction catalytique de MYSM1 et de la perte totale de la protéine MYSM1, confirmant que MYSM1 agit via son activité catalytique DUB spécifiquement dans les progéniteurs hématopoïétiques précoces pour permettre le développement normal des cellules hématopoïétiques, y compris les lymphocytes et les cellules dendritiques (DCs). Dans l'ensemble, notre travail élargit les connaissances sur les rôles critiques

de BAP1 et MYSM1 in vivo dans l'hématopoïèse, le développement des leucocytes, les réponses immunitaires et d'autres aspects de la physiologie des mammifères.

Preface

This thesis is written in the traditional format. The work presented in this thesis consists of experiments I have performed for the following publications:

Chapter 4.1:

Yun Hsiao Lin, **Yue Liang (co-author)**, HanChen Wang, Lin Tze Tung, Michael Förster, Poorani Ganesh Subramani, Javier M. Di Noia, Simon Clare, David Langlais, and Anastasia Nijnik. "Regulation of B lymphocyte development by histone H2A deubiquitinase BAP1." *Frontiers in immunology* 12 (2021): 626418.

Chapter 4.2:

Yue Liang (1st author), HanChen Wang, Noé Seija, Yun Hsiao Lin, Lin Tze Tung, Javier M. Di Noia, David Langlais, and Anastasia Nijnik. "B-cell intrinsic regulation of antibody mediated immunity by histone H2A deubiquitinase BAP1." *Frontiers in Immunology* 15 (2024): 1353138.

Chapter 4.3:

Yue Liang (1st author), Garvit Bhatt, Lin Tze Tung, HanChen Wang, Joo Eun Kim, Marwah Mousa, Viktoria Plackoska et al. "Deubiquitinase catalytic activity of MYSM1 is essential in vivo for hematopoiesis and immune cell development." *Scientific Reports* 13, no. 1 (2023): 338.

Marwah Mousa, **Yue Liang (co-1st-author)**, Lin Tze Tung, HanChen Wang, Connie Krawczyk, David Langlais, and Anastasia Nijnik. "Chromatin-binding deubiquitinase MYSM1 acts in hematopoietic progenitors to control dendritic cell development and to program dendritic cell responses to microbial stimulation." *Immunology* 172, no. 1 (2024): 109-126.

Contribution to Original Knowledge

This thesis furthers our understanding of the roles of two histone deubiquitinases, BAP1 and MYSM1, in hematopoiesis and immune cell functions. Our main findings and contribution to original knowledge are summarized below:

- We established BAP1 deficient Ba/F3 B cell precursor cell lines, and utilized them, together with control cell lines, to map the genome-wide DNA-binding sites of BAP1 and evaluate impact of BAP1 loss on histone H2AK119ub levels by ChIP-Seq. Overall, we propose that BAP1 plays a direct role in regulating the transcriptional programs essential for cell proliferation and cell cycle progression processes in pre-B cells, through its deubiquitinase (DUB) activity targeting histone H2AK119ub.

- We generated the *Bap1*$^{fl/fl}$ Cγ1-Cre mice, with Cre expression driven from the IgG1 heavy chain locus and Cre activity restricted to the activated, germinal center (GC), and downstream B cell populations. Through characterizing these mice, we demonstrate the direct and cell intrinsic role of BAP1 in the induction of B cell mediated immune response (including reduction of serum antibody titres, reduction in the ratio of dark zone (DZ) to light zone (LZ) GC B cells, and depletion of plasma cells), independent of its previously reported functions in B cell development. We, together with our collaborators, confirmed that BAP1 deficiency does not directly interfere with class switch recombination (CSR), and any reduction in class switched *Bap1*$^{fl/fl}$ Cγ1-Cre B cells can be attributed to impaired B cell proliferation.

- We established BAP1 deficient CH12F3 mature B cell lines. We utilized the described novel cell lines as well as control cell lines, with or without CSR induction, to map the genome-wide DNA-binding sites of BAP1 and evaluate impact of BAP1 loss on histone H2AK119ub levels

by ChIP-Seq. Also, we performed RNA-Seq gene expression analysis on GC B cells isolated from the spleen of *Bap1*$^{fl/fl}$ Cγ1-Cre and control *Bap1*$^{+/+}$ Cγ1-Cre mice in response to SRBC immunization, and identified novel transcriptional targets of BAP1 that are essential for the progression of GC-reaction and can contribute to the failure of humoral immunity with the loss of BAP1 function. Overall, we conclude that BAP1 acts as a DUB for H2AK119ub in B cells to regulate many transcriptional programs essential for normal cell physiology, as well as for B cell activation and the induction of humoral immune response.

- We, together with our collaborators, generated *Mysm1*^{D660N} mouse strains, in which the MYSM1 protein is expressed while its DUB catalytic activity is lost. Through characterizing these mice, we demonstrate that the loss of MYSM1 DUB catalytic activity results in a severe hematologic dysfunction (including depletion of lymphoid and myeloid immune cells, as well as their progenitors) with highly similarity to the previously characterized MYSM1 deficient mouse strains. Overall, we propose an essential and cell-intrinsic role of the MYSM1 DUB catalytic activity in the regulation of hematopoiesis.

- We confirmed that the loss of MYSM1 protein or of its DUB catalytic activity throughout the hematopoietic cell hierarchy severely impairs dendritic cell (DC) development using *Mysm1*^{D660N}, *Mysm1* deficient, and control mouse strains. We also analyzed the transcriptional profiles of DCs from the described mouse models with or without microbial stimulation, and conclude that the loss of MYSM1 function during DC-lineage development results not only in reduced DC numbers but also in altered DC immune activation and polarization states that could impact their immune functions.

Other Contributions not Included in this Thesis

In addition, I have had the opportunity to contribute to the following publications that are not included in this thesis:

Yun Hsiao Lin, Michael Forster, **Yue Liang**, Mansen Yu, HanChen Wang, Francis Robert, David Langlais, Jerry Pelletier, Simon Clare, and Anastasia Nijnik. "USP44 is dispensable for normal hematopoietic stem cell function, lymphocyte development, and B-cell-mediated immune response in a mouse model." *Experimental Hematology* 72 (2019): 1-8.

Joo Eun Kim, Lin Tze Tung, Roselyn R. Jiang, Mitra Yousefi, **Yue Liang**, Danielle Malo, Silvia M. Vidal, and Anastasia Nijnik. "Dysregulation of B lymphocyte development in the SKG mouse model of rheumatoid arthritis." *Immunology* 170, no. 4 (2023): 553-566.

Amanda Fiore, **Yue Liang**, Yun Hsiao Lin, Jacky Tung, HanChen Wang, David Langlais, and Anastasia Nijnik. "Deubiquitinase MYSM1 in the hematopoietic system and beyond: a current review." *International Journal of Molecular Sciences* 21, no. 8 (2020): 3007.

Contribution of Authors

This thesis was written by **Yue Liang** and kindly reviewed by Dr. Anastasia Nijnik.

Chapter 3.1

Experiments were designed by Dr. Anastasia Nijnik, **Yue Liang**, and Dr. David Langlais, and the experimental work was carried out and data acquired by **Yue Liang**, with assistance from Hanchen Wang, Lin Tze Tung, and Dr. Anastasia Nijnik. Bioinformatics data analyses were performed by Hanchen Wang and **Yue Liang**, with the supervision of Dr. David Langlais. Dr. Simon Clare provided the mouse line, genotyping protocols, and scientific advice for the studies. Dr. Javier M. Di Noia and Poorani Ganesh Subramani provided valuable scientific advice and reagents for the project, including the protocols for the derivation of CRISPR/Cas9 cell lines, and valuable input on data analyses and interpretation.

Chapter 3.2

Experiments were designed by Dr. Anastasia Nijnik, **Yue Liang**, and Dr. David Langlais. The majority of the experimental work was carried out and data acquired by **Yue Liang**, with assistance from Hanchen Wang, Lin Tze Tung, and Dr. Anastasia Nijnik. Dr. Javier M. Di Noia and Noé Seija designed and performed the analysis for Figure 4.2.7 and Figure 4.2.8 A-B, as well as provided valuable scientific advice and reagents for the project, including the protocols for the derivation of CRISPR/Cas9 cell lines and valuable input on data interpretation. Bioinformatics data analyses were performed by **Yue Liang** and Hanchen Wang, with the supervision of Dr. David Langlais.

Chapter 3.3

Experiments were designed by Dr. Anastasia Nijnik, and **Yue Liang** for the mouse hematologic immunophenotyping analysis, by Dr. Bhushan Nagar and Anna A. Georges for the enzymatic studies, and by Linda Henneman and Dr. Ivo J. Huijbers for mouse gene targeting. Dr. Connie Krawczyk and Dr. David Langlais provided advice for the experimental design. Experimental studies in mouse models were performed by **Yue Liang**. with the support and assistance from Lin Tze Tung, HanChen Wang, Joo Eun Kim, Marwah Mousa, and Viktoria Plackoska, and with the supervision of Dr. Anastasia Nijnik. Studies of MYSM1 enzymatic functions were performed by Garvit Bhatt, with the support of Katalin Illes and the supervision of Dr. Bhushan Nagar, Anna A. Georges, and Dr. Philippe Gros. Linda Henneman and Dr. Ivo J. Huijbers established the *Mysm1*^{D660N} mouse strain, with subsequent breeding and crosses to other mouse lines conducted by **Yue Liang** with the supervision of Dr. Anastasia Nijnik.

Acknowledgements

I would like to express my deepest gratitude to my supervisor, Dr. Anastasia Nijnik, for her continuous guidance, support, and encouragement over the course of my degree. Her immense knowledge, patience, and detail-oriented attitude have motivated me in all the time of my academic research and daily life.

I would like to also express my sincere thanks to my supervisory committee members: Dr. Daniela Quail, Dr. Danielle Malo, Dr. Jorg H. Fritz, Dr. Silvia Vidal, and Dr. Volker Blank, as well as David Langlais and Dr. Javier M. Di Noia, for their invaluable advice and encouragement. Special thanks to Dr. Ursula Stochaj, for starting my research journey before I joined the Nijnik lab.

I would like to thank all of my lab mates who have been amazing colleagues and friends: Amanda Fiore, Dania Shaban, HanChen Wang, Joo Eun (June) Kim, Lin Tze (Jacky) Tung, Marwah Mousa, Nay Najm, Roselyn Jiang, Viktoria Plackoska, and Yun Hsiao (Minnie) Lin. I could not have undertaken this journey without their friendship and support.

I would like to thank Julien Leconte and Camille Stegen from the Cell Vision Flow cytometry core for assistance with cell sorting; thank Sarah Boissel and other members of the Molecular Biology and Functional Genomics Facility of the Institut de Recherches Cliniques de Montréal (IRCM) for next generation sequencing and the Digital Research Alliance of Canada and Calcul Québec for the resources for bioinformatics data analyses; thank Catherine Gagné, Tanya Koch and other staff of the McGill Comparative Medicine and Animal Resources Centre (CMARC) for mouse colony management; thank Akansha Gupta, Andrew Yim, Connor Prosty, Dania Shaban, Gabriela Blaszczyk, Hieu Nguyen, Nayoung Cha, Orthy Aiyana, Sarah Elliott, Selin Birgen, Temi Oladeji, Xuanning Chen, and Yurim Park for mouse genotyping; thank Adithi Sundarakrishnan and Andrew

Yim for technical assistance related to protein purification and enzymatic assays; and thank the CMARC Diagnostics Laboratory for the hematology analyses of mouse blood.

I would like to acknowledge generous financial support from the Fonds de la recherche en santé du Québec, and from the Department of Physiology and the Faculty of Medicine and Health Sciences of McGill University.

Finally, I would like to express my gratefulness to my family members, especially my parents, Xianmin Liang and Qun Fu, for their unwavering support and encouragement throughout my academic journey. Their belief in me and their constant encouragement, no matter the time or circumstance, have been invaluable.

Chapter 1: Introduction and Literature Review

1.1 Hematopoiesis

Blood, being one of the most highly regenerative tissues in mammals, is comprised of cells with various populations and limited lifespans. The replenishment of blood cells is sustained across the entire life. Hematopoiesis is the process by which all lineages of blood cells, including erythrocytes, platelets, myelocytes, and lymphocytes, are generated[1, 2].

Except during early embryonic development, hematopoiesis originates from a rare population of self-renewing and multipotent cells, known as hematopoietic stem cells (HSCs). These cells first emerge in the aorta-gonad-mesonephros (AGM) region of the embryo; as embryonic development goes on, they migrate to other tissues such as the fetal liver; at birth, the HSCs majorly colonize the bone marrow (BM), where they reside and sustain the life-long production of blood cells[3, 4, 5].

1.1.1 The hierarchical tree model of hematopoiesis

Although details are still in debate, hematopoiesis is commonly depicted by the model of a hierarchical tree, which roots from HSCs, branches to a series of progenitor cells with gradual loss of lineage differentiation potential, and eventually gives rise to mature blood cells[2, 6, 7, 8, 9]. The immediate progeny of HSCs are multipotent progenitor cells (MPPs). These cells have reduced self-renewal ability but maintains full potential to differentiate into the common myeloid progenitors (CMPs) or the common lymphoid progenitors (CLPs). CMPs are conventionally considered to give rise to oligopotent progenitors such as megakaryocyte erythroid progenitors (MEPs) and granulocyte/macrophage progenitors (GMPs), which further differentiate into cells of the myeloid lineage, including erythrocytes, megakaryocytes, granulocytes, and monocytes.

Likewise, CLPs are thought to be responsible for the generation of a series of unilineage progenitors and mature precursors which eventually differentiate into cells of the lymphoid lineage, including B and T lymphocytes, natural killer (NK) cells, and innate lymphoid cells (ILCs)[6, 7, 10, 11]. However, later discovery reveals that there are cells like dendritic cells (DCs) that can derive from either the myeloid or the lymphoid pathway[12], suggesting further complexity and flexibility of the hematopoietic cell development program.

Figure 1.1.1 Hierarchical tree model of hematopoiesis.

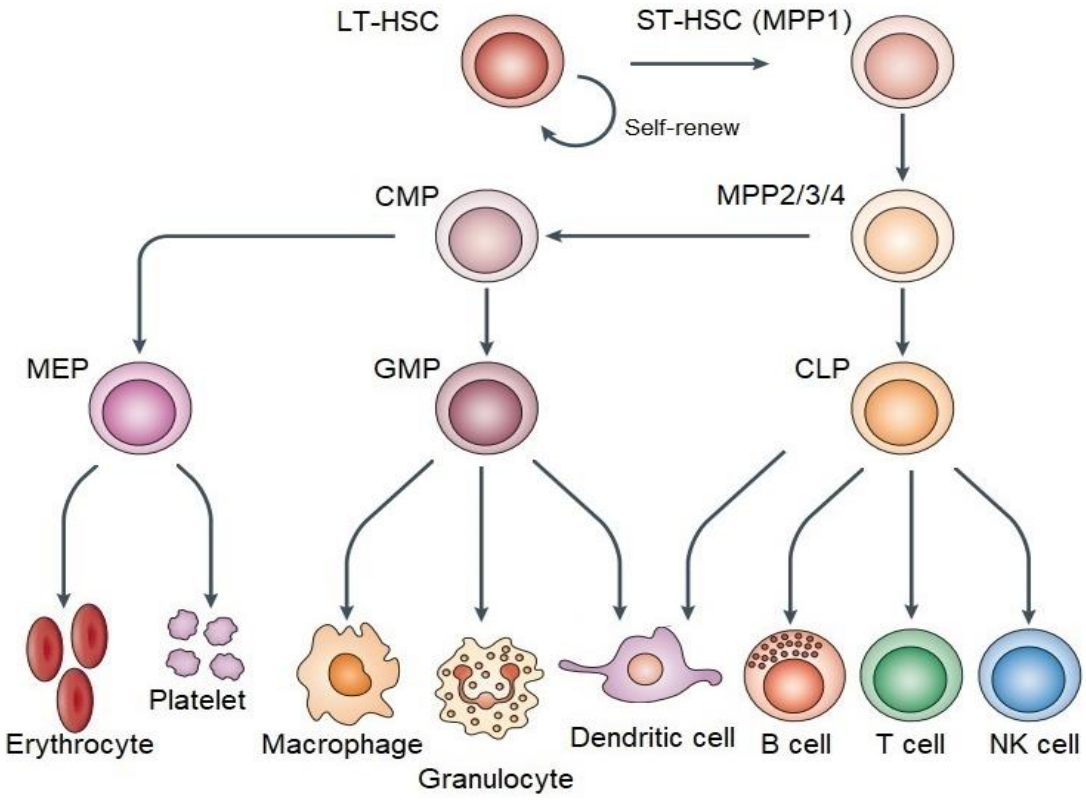

Hematopoiesis is usually depicted as a hierarchical cell fate tree. One of the most widely accepted models is displayed here. LT-HSC: long-term hematopoietic stem cell; ST-HSC: short-term hematopoietic stem cell; MPP: multipotent progenitor cell; CMP: common myeloid progenitor; CLP: common lymphoid progenitor; MEP: megakaryocyte erythroid progenitor; GMP: granulocyte/macrophage progenitor; NK cells: natural killer cells.
This figure is adapted from King, K.Y. and Goodell, M.A. (2011)[8].

1.1.2 Hematopoietic stem and progenitor cells (HSPCs)

In adult mammals, HSCs are a rare population of cells found in the bone marrow, comprising less than 0.01% of the total leukocyte population. HSCs are characterized by their capability to reconstitute cells of all blood lineages in a recipient of bone marrow transplantation[2, 8]. In mice, HSCs are found in the $Lin^{-}/Sca\text{-}1^{+}/cKit^{+}$ (LSK) fraction of bone marrow cells and are commonly gated as $CD150^{+}/CD48^{-}$ LSK cells[13]. These cells can be further classified into two subsets: $CD34^{-}$ long-term hematopoietic stem cells (LT-HSCs) and $CD34^{+}$ short-term hematopoietic stem cells (ST-HSCs)[9]. LT-HSCs are cells maintaining maximum self-renewal potential over the lifespan of the host, designated according to their capacity for sustained hematopoietic reconstitution in a recipient for a prolonged period (more than 4 months). They are usually found in the quiescent state and divide infrequently, entering cell cycles in response to hematopoietic stress signals and switching back to dormancy afterwards[2, 14, 15, 16]. On the other hand, ST-HSCs, also known as multipotent progenitors 1 (MPP1), are progenies of LT-HSCs. These cells, compared to LT-HSCs, have limited self-renewal capacity and short-term hematopoietic reconstitution ability (typically less than 4 months), but are more proliferative and more committed to differentiation into all blood cell lineages[2, 9, 17]. Although the precise mechanisms are still being elucidated, various factors in the bone marrow niche have been reported to contribute to the regulation of the transition from LT-HSCs to ST-HSCs (MPP1s), including cytokine signaling, cell-cell interactions, extracellular matrix (ECM) components, and metabolic factors[18, 19, 20]. Recently, inflammatory signals, such as pathogen-associated molecular patterns (PAMPs) and pro-inflammatory cytokines, have been reported to directly trigger HSC response, leading to the exit from their quiescent state[8, 21].

It is worth noticing that the stage-wise classification of HSPC differentiation has its limitations – single-cell transplantation experiments have revealed the heterogeneous engraftment behaviors of HSCs carrying identical surface markers, indicating that these cells may span a continuum of activation states instead of belonging to clearly defined populations[13]. However, for the ease of explanation, we continue to use HSC and MPP subpopulations to describe them in this review. Although not obvious as distinct cell populations in recent single-cell RNA-seq analysis[22], the MPPs are classically further divided into multiple sub-populations in flow cytometry experiments[6, 9]. Here we adopt a model where MPP subtypes are separated into MPP1–4 contained within the LSK compartment. Except for the described MPP1 (ST-HSCs), MPP2/3/4 are believed to sit on the same level of the hematopoietic hierarchical tree – each MPP population is independently produced by HSCs. Moreover, MPP2/3/4 have lower self-renewal capacity and demonstrate fully multipotent but lineage-biased hematopoietic reconstitution potential. To be more specific, MPP2/3/4 are primed towards different blood cell lineages: MPP2 and MPP3 are myeloid-biased subsets (where the former is primed more towards the megakaryocyte/erythroid lineage and the later is primed more towards the granulocyte/ macrophage lineage), whereas MPP4 (also known as lymphoid-primed multipotent progenitors or LMPPs) is a lymphoid-biased subset[9, 13]. Overall, the heterogeneity within the HSPC populations highlights the complexity of hematopoietic differentiation.

1.2 Blood Cells in the Immune System

The immune system is a complex network of organs, cells and chemicals that forms two lines of protection in the mammalian body: I) the innate immune response, which induces rapid but non-specific defense against pathogens and II) the adaptive immune response, which provides specific

protection to pathogens and develops immunological memory[10, 23]. Blood cells are essential players in both the innate and the adaptive immune responses. These cells circulate through blood and lymphatic vessels and reside in most tissues, coordinating a wide range of activities within the body, encompassing tissue remodeling, wound healing, tumor surveillance, and notably, defending against intruding pathogens[10].

1.2.1 The innate immune system and important cells involved

The innate immune system consists of three major components: physical barriers (e.g. skin and mucous membranes), chemical mediators (e.g. chemokines that direct immune cell migration and antimicrobial peptides that kill bacteria), and cellular components. To be more specific, cells involved in the innate immune system include granulocytes (such as neutrophils, eosinophils, and basophils), monocytes, macrophages, and DCs, as well as NK cells and other innate lymphoid cells (ILCs)[10, 23]. Upon encountering a pathogen or danger signal, each cell type fulfills a functionally or temporally distinct role to address and eliminate the threat. Tissue-resident macrophages, which locate throughout the body and are often found in proximity to sites of injury or infection, ingest pathogens and release chemokines to rapidly recruit neutrophils (in case of bacterial or fungal infections) or eosinophils and basophils (in case of parasitic infections)[10]. In humans, neutrophils are the most abundant type of white blood cells and are among the first responders of the innate immune system. Like macrophages, they can engulf invading microorganisms through phagocytosis, as well as release antimicrobial peptides and reactive oxygen species to break down and destroy pathogens. Distinctively, neutrophils are able to commit to cell death and release their intracellular content; the released DNA, histones, and antimicrobial proteins form web-like neutrophil extracellular traps to capture and neutralize pathogens[10]. However, if these attempts

prove ineffective, antigen presenting cells (APCs) such as DCs phagocytose pathogens, carry processed pathogen fragments (antigens) from the site of infection to nearby secondary lymphoid organs, and present the antigens with their cell surface major histocompatibility complex (MHC) molecules to adaptive immune cells such as $CD4^+$ helper T cells and $CD8^+$ cytotoxic T cells[10]. Thereby, DCs act as a bridge between innate and adaptive immune system to induce pathogen clearing in a targeted manner.

1.2.2 The adaptive immune system and important cells involved

The adaptive immune system takes longer to respond to invading pathogens compared to the innate immune system but provides specific and long-lasting protection. Key cells involved in the adaptive immune response include B lymphocytes (B cells) and T lymphocytes (T cells)[10]. Although both originate from HSCs in the bone marrow, B cells and T cells are named based on the different site of their development – the bone marrow (BM) and the thymus, respectively[24]. Precisely, in adult mammalian body, these lymphocytes originate from HSCs, develop in the described two primary (central) lymphoid organs (i.e. BM and thymus), and then undergo maturation in secondary (peripheral) lymphoid organs (i.e. spleen, lymph nodes, and others), serving distinct and diverse roles in the adaptive immune responses[10, 24].

B cells primarily mediate humoral immune response by differentiating into plasma cells that produce antibodies (Abs), of which the functions include antigen neutralization, Fc receptor-binding mediated antibody-dependent cellular cytotoxicity (ADCC, leading to cell lysis or apoptosis), and activation of the complement cascade (leading to recruitment of inflammatory cells and phagocytosis)[25]. Thereby, B cells are important in controlling bacterial, viral, and parasitic

infections[10, 26, 27, 28]. Some B cells develop into memory B cells, which persist within the host and can launch a more rapid and potent response upon re-encountering the pathogen. B cells can also act as APCs and initiate T cell-mediated immune response[10, 24, 26].

The T cell-mediated immune responses (also known as cellular immune responses) are primarily driven by $CD8^+$ cytotoxic T cells, which is a subset of mature T cells that recognize and eliminate infected or abnormal cells, and thus play essential roles in fighting against viral infections and tumors. Apart from the $CD8^+$ cytotoxic T cells, $CD4^+$ helper T cells are another important subset of mature T cells. These cells coordinate the activation of other immune cells (e.g. B cells, $CD8^+$ cytotoxic T cells, and macrophages)[10, 24]. Since the identification of the Th1/Th2 $CD4^+$ T cell dichotomy, numerous additional T-helper (Th) subsets have been discovered, including Th17, Th22, Th9, and Treg cells, each characterized by a distinct cytokine profile and believed to play a unique role in immune response[29, 30]. For instance, regulatory T cells (Treg) act to suppress excessive immune responses to protect the body from autoimmunity and chronic inflammatory diseases[10, 24, 30, 31]. In addition, like B cells, a small fraction of $CD4^+$ or $CD8^+$ effector T cells can develop into long-lived memory T cells, enabling the host to mount a quicker and more robust immune response upon re-exposure to the same antigen[32].

1.3 B Cell Development and Functions

B cells are one of the central mediators of the immune response, particularly in the adaptive immune system. These cells are characterized by their expression of clonally diverse cell surface immunoglobulins (Ig) that can recognize specific antigenic epitopes[26]. Since their discovery in the middle of the 20th century, B cells have been extensively studied in mice and humans in terms of

their highly ordered program of early development in the bone marrow and later maturation in the secondary lymphoid organs, as well as their functions including antibody production, memory cell formation, and others[10, 24, 26].

Figure 1.3.1 B cell development.

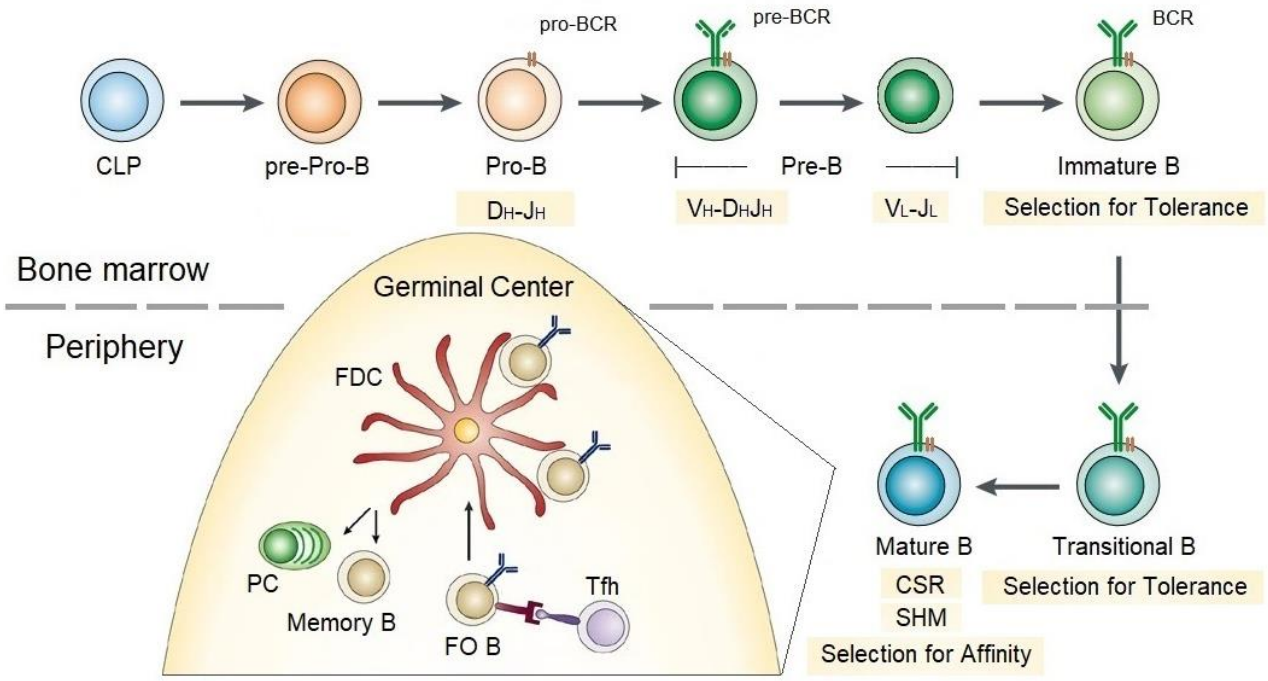

Early B cell development occurs in the bone marrow, whereas later B cell maturation occurs in the periphery. CLP: common lymphoid progenitor; FDC: follicular dendritic cell; PC: plasma cell; FO B: follicular B cell; Tfh: follicular helper T cell; CSR: class-switch recombination; SHM: somatic hypermutation.
This figure is adapted from I) Kurosaki, T., Shinohara, H., and Baba, Y. (2009)[33], II) Ceredig, R., and Rolink, T. (2002)[34], and III) De Villartay, J. P., Fischer, A., and Durandy, A. (2003)[35].

1.3.1 Early stages of B cell development and the V(D)J recombination

In adult mice and humans, the early stages of B cell development occur in the BM, during which allelic exclusion of Ig genes, established via the V(D)J recombination, is crucial for the mono-specificity of B cells[36]. Ig molecules are typically Y-shaped heterodimeric proteins consisting of

two heavy (H) chains and two light (L) chains, with each chain composed of a variable domain (IgV) and one or more constant domains (IgC)[37]. Specifically, each variable domain is encoded by independent gene segments: variable (V_L) and joining (J_L) gene segments in the L chain, as well as variable (V_H), diversity (D_H), and joining (J_H) gene segments in the H chain[10, 37]. During early B cell development, these segments undergo stochastic, error-prone rearrangements. Productive V(D)J rearrangements lead to the cell surface expression of a unique B cell receptor (BCR) on each clone of B cells, therefore allowing B cells to obtain functional specificity and generating the diversity of B cell repertoire[10, 26].

Like other blood cells, the production of new B lymphocytes originates from HSCs. HSCs that exit their quiescent state can generate lymphoid-biased MPP4s that are primed to give rise to CLPs, which then differentiate into the earliest committed B-lineage cells, known as pre-pro-B cells[10, 33] (Figure 1.3.1). Upon entering the pro-B stage (also referred to as pre-B1 stage in some studies)[38], the cells gain surface expression of Igα, Igβ, and calnexin, which are occasionally referred to as the pro-B-cell receptor (pro-BCR)[33]. Notably, in the pro-B stage, expression of recombination activating genes (*Rag1* and *Rag2*), together with other regulatory molecules (such as Artemis that is ubiquitously expressed as part of the NHEJ pathway)[39], allows the initiation of the diversity to joining segments (D_H-J_H) rearrangement of the Ig heavy chain transcription units[10, 33, 34]. The following pre-B cell stage can be further divided into the large pre-B stage (also known as large pre-B2 stage) and the subsequent small pre-B stage (also known as small pre-B2 stage)[38, 40]. As B cells develop from the pro-B stage to the large pre-B stage, the variable segment to the adjoined diversity and joining segments (V_H-DJ_H) rearrangement is completed, which enables the production of an intact Ig heavy chain (μ H chain)[10, 33]. The Ig heavy chain assembles with an

invariant surrogate light chain (encoded by λ5 and VpreB)[41], as well as the previously described Igα and Igβ subunits. The consequent complex, known as the pre-B-cell receptor (pre-BCR), is presented at the cell surface, acting as the key feature of large pre-B cells[33, 38]. Signaling via pre-BCR triggers clonal expansion of the large pre-B cell population, followed by the cessation of Ig heavy chain rearrangement and the termination of pre-BCR expression[33, 38]. Upon the loss of cell-surface pre-BCR, the B cells enter the small pre-B cell stage, where they decrease in size and initiate rearrangements of their light chain[33, 38]. Productive light chain V-J_L rearrangement eventually results in the cell-surface expression of a unique and functional BCR that belongs to the IgM class (named according to the μ H chain), which marks the immature B stage[10, 33, 42]. Because of the imprecise and random nature of V(D)J recombination, immature B cells express an exceedingly varied IgM repertoire, comprising over 10^9 specificities, among which a lot can exhibit reactivity to host tissues[42]. To minimize the risk of autoimmune reactions, a negative selection for tolerance occurs at the immature B cell stage: at this checkpoint, cells possessing a surface expression of autoreactive IgM molecules are directed to receptor editing, deletion, or anergy[33, 42, 43, 44].

1.3.2 B cell maturation

Transitional B cells represent an essential link between the early development of B cells in the bone marrow and the later maturation of B cells in the spleen. IgM^+ immature B cells that pass the mentioned central tolerance checkpoint exit the bone marrow, enter the blood as transitional B cells that can co-express IgM and IgD molecules due to alternative splicing of the Ig constant domain[45, 46]. These transitional B cells migrate to the spleen, where they undergo maturation and eventually join the pool of long-lived naive mature B cells[47]. To be more specific, in mice,

transitional B cells can be further classified into T1 cells (IgM^+ $CD23^-$) that are found in blood, bone marrow and spleen, T2 cells (IgM^+ $CD23^+$) that are only found in the spleen and are thought to be derived from the T1 cells, and T3 cells (IgM^{low} $CD23^+$) cells seem to be an anergic splenic population that does not progress into the mature stage[48]. Notably, it is reported that transitional B cells are still susceptible to the negative selection for auto-reactive BCR in the periphery (known as the peripheral tolerance checkpoint), which serves to further reduce potential autoimmune responses[44, 47, 49]. Moreover, transitional B cells that circulate to non-splenic secondary lymphoid organs (e.g. lymph nodes) may encounter antigens before they acquire maturation. In such circumstances, reactive transitional B cell clones are eliminated via the process of negative selection as well[47, 50].

Once entering the spleen, transitional B cells of the conventional B-2 lineage can give rise to mature B cells that are fully capable of participating in immune responses, among which the majority are follicular (FO) B cells and the minority are marginal zone (MZ) B cells [10, 33, 51, 52]. MZ B cells, named due to their location in proximity to the marginal region of the spleen that filters the blood, are characterized by high level of IgM expression and act as part of the frontline of antigen detection[10, 51, 52, 53]. In contrast, FO B cells, exhibiting lower level of surface IgM, reside in follicles and make up the bulk of the peripheral B cell pool, contributing to highly specific antibody (Ab) responses in cooperation with T follicular helper (Tfh) cells[10, 51, 52].

Other than the conventional B-2 cells, there is also the B-1 cell lineage, which include the B-1a and B-1b subsets. Although the details of the developmental pathway are not fully understood, it is believed that B-1 cells are from a distinct progenitor population generated from fetal tissues

(including fetal liver and fetal omentum)[54]. In terms of their functions, B-1 cells are considered as significant contributors to the B-cell mediated immune responses: B-1a cells are able to rapidly produce "innate-type" natural antibodies along with MZ B cells in a T-cell independent manner during the early humoral response, whereas B-1b cells act as essential antibody producers against specific pathogens in the later phase of humoral response[55, 56, 57, 58].

Figure 1.3.2 Ig gene diversification and affinity maturation.

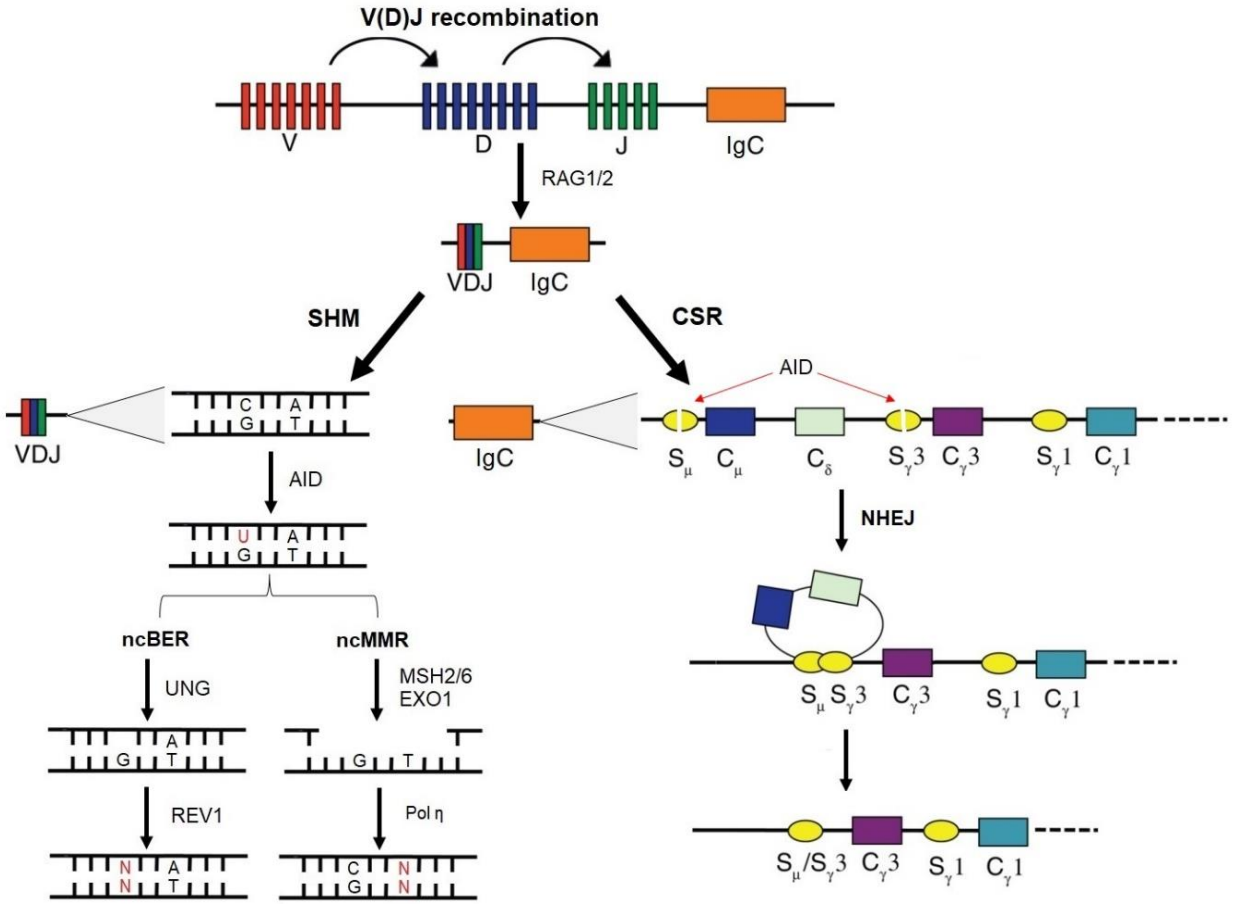

Schematic representation of the Ig gene diversification and affinity maturation, using the heavy chain locus as an example. VDJ: variable, diversity, joining gene segments; IgC: immunoglobulin constant domains; RAG1/2: RAG1/2 recombination activation complex; SHM: somatic hypermutation; CSR: class-switch recombination; C: deoxycytidine; G: deoxyguanosine; A: deoxyadenosine; T: deoxythymidine; AID: activation-induced cytidine deaminase; ncBER: non-canonical base excision repair; ncMMR: non-canonical mismatch repair; UNG: uracil DNA glycosylase; REV1: REV1 DNA directed polymerase; MSH2/6: MSH2/6 mismatch repair

complex; EXO1: exonuclease 1; Pol η: DNA polymerase η; S: switching regions; NHEJ: nonhomologous end joining.
This figure is adapted from I) Delker, R.K., Fugmann, S.D. and Papavasiliou, F.N. (2009)[59] and II) Feng, Y., Seija, N., Di Noia, J.M. and Martin, A. (2020)[60].

1.3.3 B cell activation and germinal center reaction

After encountering antigens, naive FO B cells can undergo activation and further affinity maturation. To be more specific, in the spleen, naive B-2 FO cells that bind antigens via their surface Ig receptor upregulate the expression of chemokine receptor (e.g. CCR7) and migrate towards the boundary of B cell follicles and T cell zones, seeking Tfh cells[33, 61, 62, 63]. Tfh cells, through their expression of a range of molecules including CD40 ligand (CD40L), inducible T-cell co-stimulator (ICOS), and CD28, form dynamic conjugates with FO B cells, triggering their activation and rapid proliferation[64, 65]. Activated FO B cells can undergo differentiation via one of two routes: the follicular pathway, leading to the formation of germinal centers (GCs), and the extrafollicular pathway, resulting in the development of short-lived plasma cells (PCs) [33, 63]. Compared to the short-lived PCs which provide rapid but transient production of antibodies, B cells committed to the follicular pathway are able to elicit long-lasting antibody reactions with high specificity and affinity[10, 63].

A germinal center is structurally characterized by a dark zone (DZ) and a light zone (LZ), named according to their histological appearance in mice and humans[10, 63]. The dark zone, located in proximity to the T cell zone, contains a high density of rapidly proliferating B cells known as centroblasts[63]. The light zone, in contrast, is comprised of nonmitotic B cells known as centrocytes, as well as a network formed by follicular dendritic cells (FDCs)[63]. Such compartmentalization results from the differential gradient of chemokines in germinal center (DZ with higher

concentration of CXCL12 generated by Tfh cells versus LZ with higher concentration of CXCL13 generated by FDCs), as well as the regulated expression of chemokine receptors in GC B cells (CXCR4^{hi} DZ cells vs. CXCR5^{hi} LZ cells)[63, 66].

In terms of its function, the germinal center is essential for providing the microenvironment to support antibody affinity maturation, of which the basis is a process known as somatic hypermutation (SHM)[10, 63, 67]. Highly proliferative GC B cells that undergo SHM in the dark zone exit the cell cycle and re-express surface Ig as they migrate to the light zone, where they interact with antigen-carrying FDCs[63]. High affinity for antigen provides a competitive advantage for B cell survival, known as the affinity selection[10, 63]. B cells that pass the affinity selection re-enter the dark zone to undergo additional rounds of proliferation and SHM, whereas apoptotic B cells are engulfed by specialized macrophages residing within germinal centers[63]. Thereby, cyclic re-entry of GC B cells between the dark and light zones allows a survey of efficacy, prompting the survival of cells that gain high affinity to Ag through SHM. Consequently, survived B cells that differentiate into Ab-secreting plasma cells or long-lived memory B cells are able to better deal with pathogens in a highly specific manner[10, 51, 63]. On the other hand, class switch recombination (CSR), a process critical for the diversification of antibody effector functions, was widely depicted as another hallmark of the GC reaction – it was believed that CSR, like SHM, also predominantly occurs in germinal centers[10, 63]. However, recent discoveries revealed that CSR is induced by T cell priming prior to the GC B cell differentiation, and is largely ceased in germinal centers[67]. Nevertheless, both SHM and CSR are critical for the maturation of antibody responses, and their mechanisms will be discussed in the following sections.

1.3.4 Somatic hypermutation

SHM typically occurs in the dark zone, triggering high rates (~0.1% per base per generation) of point mutations in the variable domain of Ig (IgV)[61, 63]. Precisely, deoxycytidine bases in IgV genes are targeted by activation-induced cytidine deaminase (AID) for deamination, introducing deoxycytidine (C) to deoxyuridine (U) conversion, thereby leading to a base pair mismatch between U and deoxyguanosine (G)[61, 63]. Such U:G mismatch can be repaired through different pathways. In the base excision repair (BER) pathway, the uracil is recognized and excised from the deoxyribose-phosphate backbone by uracil DNA glycosylases (predominantly UNG and subordinately SMUG1), generating an abasic gap[60, 61, 63]. Except for the canonical error-free repair (mediated by enzymes such as APE1 and DNA polymerase β) that restores the C:G base pair, error-prone translesion DNA synthesis (mediated by DNA polymerases such as REV1) may also occur, resulting in the introduction of random nucleotide substitution (either transition or transversion) at the original C:G base pair[60, 61, 63]. Alternatively, in the mismatch repair (MMR) pathway, U:G mismatch can be detected by the MSH2/MSH6 heterodimer complex, followed by further excision surrounding the U:G mismatch by enzymes such as the PMS2/MLH heterodimer (also known as the MutLα complex) and the exonuclease EXO1. The excised DNA fragment, likewise, can be repaired with relatively low fidelity by error-prone DNA polymerases such as DNA polymerase η, generating mutations at A:T base pairs[60, 61]. Both non-canonical mutagenic translesional repair pathways are crucial in SHM, leading to stochastic changes in BCR affinity and specificity[60, 61, 63].

1.3.5 Class-switch recombination

CSR, on the other hand, induces combinatorial deletion of exon segments between switch (S) regions in the heavy chain constant domains of Ig (IgC), bringing selected heavy chain IgC exons

in proximity to IgV. This enables the diversification of Ig expression from IgM and IgD to IgG, IgE or IgA without changing the antigen-binding specificity[60, 63, 68]. Similar to SHM, the CSR process is also initiated by AID recruitment. Typically, AID preferably deaminates deoxycytidine bases in S regions (1–10 kb in length), which are G rich regions located upstream of all heavy chain IgC exons except for Cδ[60, 63, 68]. Via ncBER or nc MMR pathways, AID-introduced U:G mismatch can be converted to DNA double-strand breaks (DSBs), which are repaired by nonhomologous end joining (NHEJ) rather than homology-directed repair (HDR) in CSR[60, 63, 68]. Briefly, NHEJ involves the recognition of broken DNA ends by Ku70/80 heterodimer, the recruitment of DNA protein kinases (DNA-PKcs), the removal of damaged or mismatched nucleotides from the broken ends by nucleases such as Artemis and PALF, and the ligation of processed DNA ends by DNA ligation complex (XLF, XRCC4, and DNA Ligase IV)[69, 70]. During CSR, the recruitment of NHEJ proteins to S regions requires the function of AID C terminus; in contrast, during SHM, the N terminus function of AID is more important[61, 68]. NHEJ is essential in CSR as it can occur as an intrachromosomal deletional recombination and bridge two S regions with DSBs. Notably, the two S regions need to be in contact via the formation of a chromosomal loop, which is induced by the interactions of Eμ and 3′Eα enhancers[68, 71, 72]. Proteins such as YY1[73] have been proposed as potential regulators of the chromosomal loop formation during CSR, although the mechanism is not fully understood.

1.4 Dendritic Cell Development and Functions

Dendritic cells (DCs) are professional APCs found in all mammalian tissues, playing a crucial role in the initiation and regulation of both innate and adaptive immune responses[74, 75]. Since their discovery in the 1970s[76], many subtypes of DCs are classified based on their tissue of origin,

pathway of differentiation, surface marker expression, transcriptional profiles, phenotype similarities, and others[74, 75, 77, 78]. Here, we briefly review the development and functions of two major subtypes: conventional DCs (cDCs) and plasmacytoid DCs (pDCs)[74, 75, 77]. Other subsets, such as monocyte-derived DCs (moDCs) that are found on sites of inflammation but are absent from homeostasis, will not be discussed here.

1.4.1 Conventional dendritic cells

cDCs, featured by their potent antigen presenting abilities, develop from conventional dendritic cell progenitors (CDPs) in the bone marrow[74, 75]. Characterized by their functions, cDCs were historically categorised into lymphoid tissue resident cDC (exist within the lymphoid tissues in the steady state, surveying the blood and lymph for signs of infection) and migratory cDC (exist in peripheral tissues, capturing antigen and migrating to the draining lymph node)[79]. The latter include multiple subsets which are found in tissues such as lungs, intestines and kidneys[79]. In terms of their development, cDCs were thought to originate from monocytes, but this was subsequently disproved. Later research showed that CDPs derive from both the myeloid and the lymphoid pathway[12, 75]. In mice, it was originally thought that $CD8\alpha^+$ cDCs are lymphoid-derived whereas $CD8\alpha^-$ cDCs are myeloid-derived[80, 81]. However, later DC reconstitution experiments challenged this model – CLPs and CMPs purified from mouse bone marrow showed a similar potential to generate both subsets of cDCs in the irradiated recipient mice[80, 81]. On the other hand, CMPs are 10-fold more abundant than CLPs, and consequently the majority of DCs being studied originate from CMPs, making the myeloid versus lymphoid distinction challenging but less useful in DC research[81]. Nowadays, cDCs in mice are commonly further classified into cDC1 and cDC2 by their differential surface expression (e.g. Clec9a and XCR1 for cDC1 vs. SIRPα for cDC2)[75, 77, 78].

cDC1s make up around 30-40% of total cDCs in most tissues, but are enriched in the thymus and Peyer's patches[75]. In mouse, lymphoid-organ-resident cDC1s are typically $CD8^+$ [74, 75]. These cDC1s can be activated by PAMPs via their Toll-like receptors (TLRs) and produce cytokines such as IL-12, IL-6, TNF-α, and type III IFNs[74]. Moreover, cDC1s are proficient in cross-presenting antigens (especially the antigens associated with dead cells) on MHC class I molecules and cross-priming $CD8^+$ T cells. cDC1s are, therefore, considered as important inducers of anti-viral and anti-tumor immune responses[74].

cDC2s, in contrast, are more abundant and heterogeneous than cDC1s. In mice, lymphoid-organ-resident cDC2s are typically $CD8^-$, among which a fraction express $CD4^+$ [74, 75]. In terms of their functions, cDC2s have exceptionally high levels of cytosolic nucleic acid sensors, NOD-like receptors, and other inflammation associated signaling molecules at the steady state, enabling them to detect a wide spectrum of danger signals[74, 78]. Furthermore, these cells can act as the sources of many cytokines, including IL-12, IL-10, IL-1β, IL-6, IL-8, and IL-23[74]. Distinct from cDC1s, cDC2s are able to provide T cell survival signals and are more efficient activators of $CD4^+$ T cells[74]. For instance, Th1 and Th17 cells have been reported to be induced by cDC2s[74, 78].

1.4.2 Plasmacytoid dendritic cells

pDCs, compared to cDCs, are not proficient in classical antigen presentation and T cell priming[74]. Whether the origin of pDCs is of the myeloid or the lymphoid lineage has been a topic of debate for a long time, partially due to their similarities to both cDCs and B-cells[79]. Currently, pDCs are believed to differentiate from CDPs by some researchers, but are considered as descendants of precursors that are distinct those giving rise to cDCs by others[75, 79]. In mice, pDCs migrate from

the bone marrow to the peripheral lymphoid organs and acquire their maturation[74]. Due to their unique constitutive expression of IRF7 (independent of the IFN-α/β receptor positive feedback loop required in other cells), pDCs are major producers of type I interferons (IFNs)[74]. Through the IFN production, pDCs regulate the function of other immune effector cells, including cDCs, NK cells, $CD4^+$ and $CD8^+$ T cells, and thereby act as an important mediator of anti-viral immune responses[74].

1.4.3 Re-classification of DCs based on single cell RNA sequencing (scRNA-seq)

More recently, single-cell RNA-seq analyses improved the understanding of DC subsets. Through unbiased transcriptomic classification, six sub-populations were identified in human DCs[82]. Among these six groups, the classic cDC1s, pDCs, and monocyte-derived DCs (moDCs) are present, whereas the cDC2s are found as heterogeneous and sub-divided into cDC2A and cDC2B (or, in some studies, cDC2 and cDC3, characterized by different surface markers)[82, 83]. Such subdivision is confirmed in mice as well[83]. In addition, a novel subset of DCs named AS DCs ($AXL^+SIGLEC6^+$ DCs) was identified, yet the precursor of this subset still needs to be identified[82].

1.5 Regulations of Hematopoietic Cell Development and Functions

The production, differentiation, and maturation of hematopoietic cells are under delicate control of complex networks of regulatory pathways. Various factors exert cell-specific and temporarily defined regulations on hematopoietic cells to determine their developmental stage and lineage potential, as well as their survival and functions. These regulatory factors include cell-extrinsic ones, such as cytokine signaling, cell-cell interactions, and ECM components[18, 19, 20], and cell-intrinsic ones, such as transcriptional and epigenetic regulators[2, 84]. Here, we focus more on the

transcriptional and epigenetic modulations of gene expression, as external signals must interact with these intrinsic parameters to instruct the fate of hematopoietic cells.

1.5.1 Transcription factors in early B cell development

Taking B lymphocytes as an example, many transcription factors have been identified as crucial regulators of B cell development. E2A transcription factor (E2A), early B-cell factor 1 (EBF1) and paired box protein 5 (PAX5) are three interdependent and indispensable factors controlling the commitment from CLPs to the B cell lineage[10, 85, 86]. Absence of any of these transcription factors leads to an early block in B-cell development[87, 88, 89]. Specifically, PAX5, known as the master regulator of B lymphopoiesis, constrains the potential developmental pathways of lymphoid progenitors to the B cell lineage by suppressing the transcription of lineage-inappropriate genes (such as *Flt3* and *Ly6a*/*Sca1* controlling the proliferation and differentiation of hematopoietic progenitors, *Csf1r* necessary for myeloid cell development, and *Notch1* required for T cell lineage specification) while also promoting the expression of genes essential for B cells (including *Aicda* encoding AID enzyme, *Mb-1*/*Cd79a* encoding the Igα subunit of BCR, and genes encoding cell surface receptors CD19, CD40, CD21, CD23, and others)[90]. E2A and EBF1 are necessary for PAX5 expression, whereas the expression of EBF1 depends on autoregulation and low dosage of purine-rich sequence binding factor 1 (PU.l), and the level of EBF1, in turn, affects E2A expression[91]. Interestingly, an induction of transcription factors that are not B-cell-specific, including EGR1, NR4A2, and KLF4, was observed before the onset of the E2A-EBF1-PAX5 regulatory circuit, implicating a transcriptional priming mechanism of early B cell development[92]. Moreover, the E2A-EBF1-PAX5 circuit is believed to be responsible for regulating the expression of *Rag1* and *Rag2* essential for the VDJ rearrangements of Ig genes[85, 90, 91]. Precisely, E2A binding

sites have been identified in the *Rag1* promoter region, while PAX5 has been reported to bind to the *Rag2* promoter region in murine B cells[93, 94]. Moreover, E2A and EBF1 bind coordinately with FOXO1, while FOXO1 is a key transcription factor that activates the transcription of *Rag1* and *Rag2* genes in primary murine B cells[95, 96]. B cell precursors undergoing VDJ recombination are also regulated by other transcription factors, such as LEF1 and SOX4 supporting cell survival and proliferation of pro-B cells, as well as IRF4 and IRF8 controlling the cessation of pre-BCR signalling and facilitating the differentiation into small pre-B cells engaged in light-chain gene rearrangements[97]. Overall, the coordinated activities of transcription factors play a critical role in regulating B cell lineage commitment and early stages of B cell development.

1.5.2 Transcription factors in B cell maturation and GC reaction

Beyond the commitment and differentiation of early B cells progenitors, the fate of mature B cells is also subject to the regulation of gene expression. For instance, PAX5, mentioned as a critical regulator of early B cell development in the previous section, exhibits persistent level of expression from the pro-B cell stage to the mature B cell stage, but needs to be repressed during terminal plasma cell differentiation in order to enable the expression of plasma cell regulators BLIMP1 and XBP1, as well as surface receptors CD28 and CCR4 necessary for normal plasma cell function[90]. Other examples include the E26 transformation-specific (ETS) and interferon regulatory factor (IRF) family transcription factors, such as PU.1, SPIB, IRF8, and IRF4, which are all crucial for MZ B / FO B lineage selection, BCR signaling, and cell survival[98].

Likewise, the GC reaction also depends on the regulation of various transcription factors. For instance, octamer transcription factors OCT1 and OCT2, as well as their transcription coactivator

OBF1, are identified as essential contributors to the initiation of GC reaction downstream of BCR signalling[99]. These regulators directly activate the transcription of *Bcl6*, which encodes a zinc finger transcription factor[99]. Known as the master regulator of GC reaction, BCL6 regulates expression of a wide range of genes (such as those encoding CD80, PD-L1, CXCR4, p53, CDKN1A, etc.)[100], and contributes to the stabilization of FO B / Tfh cell-cell interactions in DZ, the DZ GC B cell chemotaxis, the tolerance of GC B cells to DNA damage, and many other processes[99, 100]. The expression of *Bcl6* is regulated by many other transcription factors, including IRF8, IRF4, MEF2B, BLIMP1, and TP53[99]. Specifically, IRF4 controls the transcription of BCL6 and OBF1 at the very early phase of GC B cell differentiation in response to T-cell-dependent antigen stimulation, whereas IRF8 induces the upregulation of BCL6 and MDM2 and consequently promotes GC B cell survival[99, 101, 102]. Other transcription factors crucial for the initial stages of GC establishment include cMYC, which is essential for GC maintenance[99, 103]. Notably, the expression of *Myc* gene is repressed by BCL6 in DZ B cells and is only transcribed in a small fraction of LZ B cells that are primed for re-entry into the DZ[104].

On the other hand, the later stage of GC reaction, involving SHM, is also modulated by various transcription factors. PAX5, E2A, and IRF8 have been reported to regulate the expression of AID , thereby contributing to BCR affinity maturation[99]. The expression level of Id3 affects germinal center B cell maturation[105]. YY1 is necessary for the rapid proliferation of DZ cells via, at least partly, inhibition of cell apoptosis[99, 106]. FOXO1 is a key transcription factor maintaining the DZ program, as it can inhibit the expression of BLIMP1 and consequently supress the differentiation of GC B cells into plasma cells[99, 107]. As B cells exit from the GC reaction, however, BLIMP1, together with IRF4, play a critical role in terminating the expression of AID, BCL6, PAX5 and

cMYC while promoting the expression of XBP1, thereby driving the transition from GC B cells to plasma cells and enabling antibody production[99, 108]. In contrast, ABF-1 favors the differentiation of GC B cells into memory B cells[99, 109]. In summary, transcription factors are important regulators of the GC reaction and fate decision of mature B cells.

1.5.3 Epigenetic regulation in B cell development

The regulation of B cell development also involves epigenetic mechanisms. In brief, epigenetic modifications, including DNA methylation, histone modification and non-coding RNA associated gene silencing, regulate gene expression by altering chromatin structure and DNA accessibility without directly affecting the genomic sequence[110, 111]. DNA methylation, mediated by DNA methyltransferases (DNMTs) and predominantly occuring at CpG dinucleotides, is associated with repression of gene transcription[111, 112]. The DNA methylation pattern across the genome undergoes dynamic changes during hematopoiesis and exhibits locus-specific variations – the level of methylation can increase in certain genomic regions while decrease in others[113]. DNA methylation is an important regulatory mechanism during B cell development. For instance, the promoter of the *Mb-1* gene, which encodes the Igα subunit of BCR, is fully methylated in HSCs, partially demethylated in CLPs, and completely demethylated in pre-B cells. The changing methylation status of *Mb-1* promoter is regulated by EBF1 in cooperation with runt-related transcription factor 1 (RUNX1), and is required for the activation of *Mb-1* gene transcription by PAX5 at the pre-B cell stage[85]. Likewise, histone modifications and microRNAs (miRNAs) also play important roles in B cells, about the former we will discuss more in the following sections. An example of the involvement of these two mechanisms in B cells is the regulation of CSR: the S-regions are enriched for histone modifications (H3K4me3, H3K36me3 and H3K27ac) that are believed to

have a role in AID binding, whereas miRNAs (miR-155, miR-181b, and miR-361) can reduce the expression of AID and supress the production of hypermutated auto-antibodies[112, 114, 115]. Many other epigenetic regulators, such as SMARCA4 and EZH2, are also implicated in establishment of the B-cell fate[86]. Overall, the epigenetic regulatory networks are essential for supporting their normal development and functions of B cells.

1.5.4 Transcription factors in DC development

Many transcription factors have been implicated in the development of different DC subsets. For instance, STAT3 is shown to function early in the commitment process to the DC lineage, as STAT3-deficient murine HSCs are unable to produce CDPs in response to Flt3 ligand treatment[116]. Likewise, PU.1, involved in the induction and maintenance of Flt3 expression in DC precursors, is also essential for development of cDCs and pDCs[117]. Another important example is IRF8. IRF8 deficiency leads to reduction or elimination of both cDC and pDC subsets in human patients[118, 119]. Consistently, it is reported that early expression of IRF8 in HSC-MPP creates a predisposition towards the cDC1 lineage[120]. Moreover, the ratio of IRF8/IRF4 expression levels in pre-DCs is indicative of their commitment, with higher IRF8 expression associated with the cDC1 lineage and higher IRF4 expression associated with the cDC2 lineage[121].

Other important transcription factors involved in cDC development include BATF3, RelB, and Id2[79, 119]. BATF3 is a basic leucine zipper transcription factor, and its deficiency in mice results in a reduction of $CD8^+$ and $CD103^+$ cDC1s without affecting the $CD8^-$ and $CD11b^+$ cDC2s[122]. Consistentky, silencing of BATF3 in HSCs leads to impaired cDC1 differentiation *in vitro*, but not in humanized mice[123]. On the other hand, mice lacking RelB, a member of the NF-κB/Rel family

proteins, exhibit a drastic reduction of $CD8^-$ resident cDCs[124]. In addition, Id2, a DNA binding inhibitor belonging to the family of basic helix-loop-helix (HLH) transcription factors, is needed for cDC development while exerting an inhibitory effect on pDC development – mice with Id2 deficiency have reduced number of $CD8^+$ and $CD103^+$ cDCs and increased number of pDCs[122, 125].

Likewise, there are many other transcription factors involved in pDC development, such as Ikaros, SpiB, and E2-2[79, 119]. Ikaros is a zinc finger DNA binding protein, of which the deficiency leads to reduced pDC numbers in mice and humans[126, 127]. It was later found that Ikaros regulates the development from CDPs to pDCs by antagonizing the TGFβ pathway, since inhibition of TGFβ signaling rescues Ikaros-deficient pDC development *in vitro*[128]. Furthermore, DC progenitors from Ikaros-deficient mice exhibited reduced expression levels of Flt3, IRF4, IRF8, and SpiB, indicating that Ikaros functions upstream of these factors[79]. SpiB, interestingly, is necessary for pDC development in humans[129], yet whether its function is indispensable for pDC development in mice remains in debate[130, 131]. In contrast, E2-2, which is a member of the HLH protein family and is antagonized by the Id proteins, plays a crucial role not only in the development but also in the maintenance of pDCs[79, 132, 133]. In summary, the development of DCs, including cDC and pDC subsets, is governed by various transcription factors.

1.6 Histone Modifications and Gene Regulation

Eukaryotic DNA is structured into chromatin, which exists in two primary forms: euchromatin (less condensed and genetically active) and heterochromatin (highly condensed and genetically inactive)[113, 134, 135]. Nucleosome, a section of DNA winding around the octamer of core histones (composed of H2A-H2B and H3-H4 dimers), form the basic units of chromatin that is responsible

in part for the compactness of a chromosome[113, 134, 135]. Histone modifications constitute an extra regulatory layer on top of the DNA sequence. Common histone modifications, including acetylation, methylation, phosphorylation, and ubiquitination, can affect nucleosome assembly or disassembly, influencing the accessibility and expression potential of the adjacent genes[136, 137, 138].

The complexity of histone modifications can be reflected by the diversity of chromatin modifying enzymes and protein complexes as well as the functional variety of histone marks. For example, among the mediators of histone modifications, the trithorax groups (TrxG) and the polycomb repressive complexes (PRCs) are the most studied protein complexes[110]. TrxG mediated tri-methylation at lysine 4 of histone H3 (H3K4me3) results in an open chromatin configuration, and, therefore, marks active transcription[137, 139, 140, 141]. Conversely, PRC1 mediated H2A mono-ubiquitination at lysine 119 (H2AK119ub) and PRC2 mediated H3 tri-methylation at lysine 27 (H3K27me3) lead to chromatin condensation and consequent repression of gene expression[137, 139, 140, 141].

Moreover, different histone modifications may function in an interactive manner. For instance, increased level of H3K27me3 is associated with enhanced PRC1 recruitment and H2A mono-ubiquitination[142, 143, 144], whereas the H2AK119Ub, in turn, promotes PRC2 binding and H3K27 tri-methylation[145, 146]. H2AK119ub also exerts an inhibitory effect on di- and tri-methylation of H3K4, leading to repression of transcription initiation in vitro[144]. Also, phosphorylation of histone H3 at serine 10 (H3S10p) promotes the histone acetyl transferases (HATs) mediated acetylation at H3 lysine 14 (H3K14ac)[147]. Many aspects of the dynamic, covalently linked histone modification mechanisms remain to be explored.

Figure 1.6.1 Different modes of ubiquitination lead to different substrate fates.

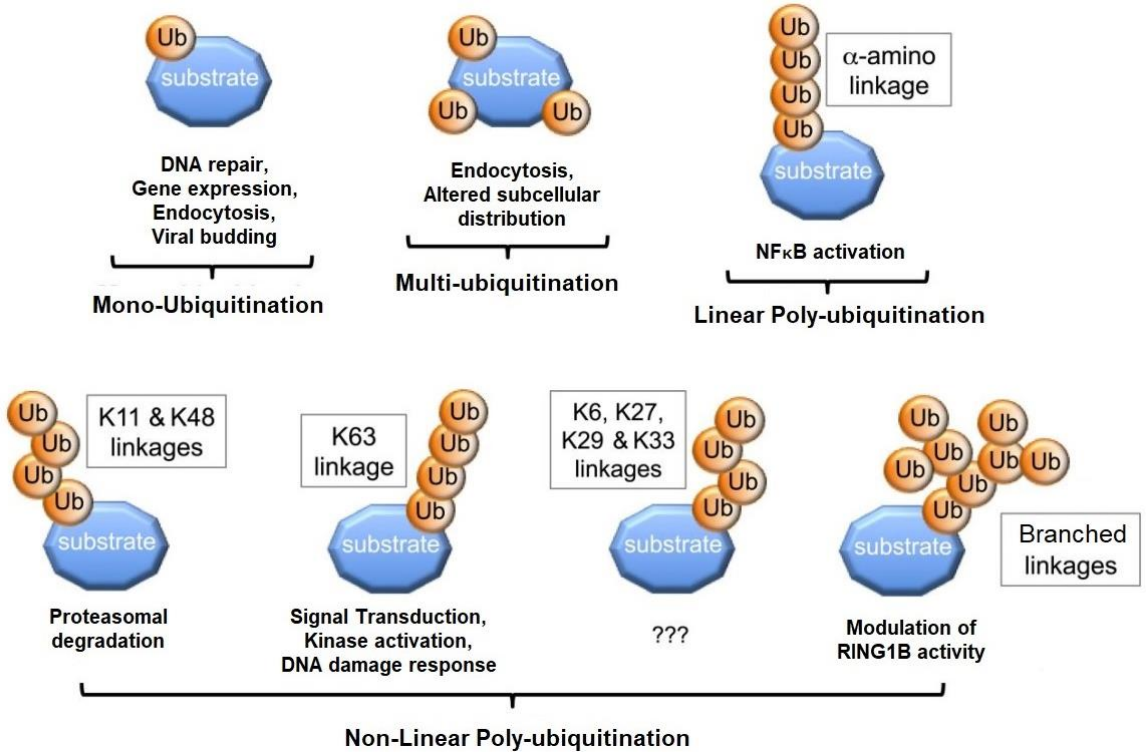

Attachment of single or multiple ubiquitin molecule(s) onto histone or non-histone substrates leads to diverse cellular responses. Ub: ubiquitin; K: lysine.
This figure is adapted from I) Suryadinata, R., Roesley, S. N. A., Yang, G., & Šarčević, B. (2014)[148], and II) Sadowski, M., & Sarcevic, B. (2010)[149].

1.6.1 Ubiquitination of histone and non-histone substrates

Ubiquitination, the process of conjugating the 76-amino-acid ubiquitin (Ub) to the side chain of a lysine residue of the substrate protein, is a complex process involving several enzyme-catalyzed steps. Sequentially, the C-terminal glycine residue of Ub is first attached to the catalytic cysteine residue of ubiquitin activating enzyme (E1) via a thioester bond in an ATP dependent manner, then transferred to ubiquitin conjugating enzyme (E2), and eventually appended to the lysine residue of target molecule by ubiquitin-protein isopeptide ligase (E3)[149, 150, 151]. Moreover, multiple lysine residues on the substrates, as well as residues on the substrate conjugated Ub, can be utilized by

ubiquitinases to catalyze further cycles of ubiquitination, resulting in multi-ubiquitination or poly-ubiquitination, respectively[149, 150, 151]. Specifically, polyubiquitination can be categorised into two types: I) linear ubiquitination (also known as α-amino linkage), during which a peptide bond forms between the C-terminal glycine residue of one Ub molecule and the N-terminal methionine residue of another Ub molecule, and II) non-linear ubiquitination, during which a peptide bond forms between the C-terminal glycine residue of one Ub molecule and one of the seven lysine residues (K6, K11, K27, K29, K33, K48 and K63) within another Ub molecule[148, 152].

Depending on the locus and the type of ubiquitination, substrates have distinct fates. For example, mono-ubiquitination often contributes to the regulation of gene expression and DNA repair, whereas poly-ubiquitination is usually associated with proteasomal degradation (K11- and K48-poly-Ub) or non-degradative cellular processes such as signal transduction (K63-poly-Ub)[148, 149, 153, 154]. Notably, there may be certain crosstalk between different types of ubiquitination: the self-ubiquitination of the E3 ligase RING1B (the catalytic subunit of PRC1, also known as RNF2 or RING2) results in branched K6, K27, and K48 ubiquitin chains, which is essential for its catalytic activity to induce histone H2A monoubiquitination[155].

Although histone ubiquitination is proposed to serve as an indispensable regulator of nuclear and cellular processes, it is not as intensively studied as histone methylation and acetylation[137]. Historically, histone H2A was the first identified ubiquitinated protein, and shortly after the discovery, researchers found that rather than poly-ubiquitination, a single Ub molecule was conjugated to H2A at the highly conserved lysine 119 (H2AK119) residue in vertebrates (isoforms include H2AK118 in *Drosophila* and H2AK121 in *Arabidopsis*)[135, 150, 156, 157]. H2A ubiquitination

was linked to gene silencing as it was found enriched in inactive X chromosome in early studies, and was later reported to be widely distributed across the genome, including transcription start sites (TSS), gene bodies, and intergenic regions[135]. Thus far, H2AK119ub is the most abundant form of histone ubiquitination (up to 10% in vertebrate genome) and is confirmed to be associated with repressed genes by ChIP-seq analyses[135, 151]. H2B mono-ubiquitination at lysine 120 (H2BK120ub), as well as the less prevalent H3 and H1 ubiquitination (site remain unclear), have also been discovered[151].

1.6.2 Functions of H2A (de)ubiquitination

In spite of several reports associating both H2A ubiquitination and deubiquitination with transcriptional activation, H2AK119ub is generally considered as a mark of gene silencing, whereas the removal of the mono-ubiquitin opposes this repressive effect[150, 151, 158]. The PRC1 complex that mediates H2A monoubiquitination is considered to be recruited to the same genomic regions after PRC2 is recruited and deposits H3K27me3, which seems to indicate that H2AK119ub deposition is dependent on H3K27me3[135]. However, such proposal was challenged by the observation in *Drosophila* that PRC1 can be directly recruited to chromatin (by PhoRC, of which the vertebrate ortholog is YY1) independent of H3K27me3[135]. Follow up studies in mammals confirmed that H3K27me3 is dispensable for H2AK119ub[135]. On the other hand, as mentioned before, the transcriptional repressive function of H2AK119ub can be associated with its role in inhibiting H3K4 methylation[144]. Furthermore, H2AK119ub has been shown to enhance the recruitment of remodeling and spacing factor 1 (RSF1) and the binding of the linker histone H1, indicating the possibility that H2AK119ub contributes to transcriptional repression by remodeling higher-order chromatin structure[150, 159, 160].

Other than its role in regulating gene expression, H2A (de)ubiquitination may also contributes to the DNA damage repair process. Phosphorylation of the histone H2A variant H2AX (γ-H2AX), the most robust histone modification in response to DNA damage (especially DSBs), has been proposed as prerequisite for H2A ubiquitination, suggesting the possible involvement of H2A ubiquitination in DNA damage response[161]. To be more precise, H2AX phosphorylation is primarily mediated by ataxia telangiectasia mutated (ATM) kinase[161, 162]. Subsequently, mediator of DNA damage checkpoint protein 1 (MDC1) is recruited to the γ-H2AX locus, becomes phosphorylated by ATM, and promotes the binding of E3 ligases RNF8 and RNF168, which can target H2A and H2AX for mono- or poly-ubiquitination at K13 and K15[162, 163]. Although the mechanistic role or these poly- and mono-Ub marks is not fully understood, it has been reported that H2AK15 mono-ubiquitination together with H4K20 dimethylation, or K63-linked polyubiquitination of H2AK15, is able to enhance the recruitment of 53BP1, which is essential for DSB repair by NHEJ pathway[162, 163, 164]. Furthermore, the K125, K127 and K129 residues on H2A can be targeted for mono-ubiquitination by breast cancer type 1 susceptibility protein (BRCA1) and its binding partner BRCA1-associated RING domain protein 1 (BARD1)[165]. Specifically, H2AK127ub and H2AK129ub facilitate the recruitment of chromatin remodeling protein SMARCAD1, which promotes DNA end resection and DSB repair by HR pathway[165]. Consistently, UV irradiation has been shown to result in elevated level of H2A mono-ubiquitination in mammalian cells, although the residue to which mono-ubiquitin is added remains unclear[166, 167]. Overall, H2A ubiquitination, either at steady state or in response to damage, is required for many biological processes, including regulation of gene expression and DNA repair.

1.6.3 H2A (de)ubiquitinating enzymes

As mentioned earlier, the process of ubiquitination depends on E1/E2/E3 enzymes, among which the E2 and E3 enzymes are responsible for the attachment of Ub molecules to histone or non-histone substrates. Mammals possess more than 30 E2 enzymes and over 500 E3 enzymes, the diverse combinations of which contribute to the generation of various structures of ubiquitinated proteins[148]. In humans, RING1B is the most well-characterized H2AK119-specific E3 ligase[150, 168]. It is the primary catalytic component of the PRC1 complex and is believed to be an essential regulator of transcriptional repression[148, 150, 168]. The RING1A subunit, in contrast, is less studied but also exhibits independent E3 ligase activity and can potentially compensate for RING1B[169]. To be more precise, the catalytic core of either the canonical PRC1 (cPRC1) or the non-canonical (ncPRC1) complex consists of the Ring finger protein subunit (RING1B or RING1A) and the Polycomb group ring finger (PCGF) subunit (PCGF1/RNF68, PCGF2/RNF110, PCGF3/RNF3, PCGF4/BMI1/RNF51, PCGF5/RNF159, or PCGF6/RNF134)[170]. RING proteins are sufficient for H2A ubiquitination, while PCGF proteins are reported to enhance the activity of RING proteins *in vitro*[170, 171]. Interestingly, a study using mouse embryonic stem (ES) cells revealed that although RING1B mediates chromatin compaction and is necessary for gene repression, their gene expression regulatory role can be independent of their ubiquitin ligase activity[172]. Moreover, despite the many reports that RING1B regulates the repression of many important developmental genes in mouse ES cells, it is dispensable for the initiation and maintenance of X chromosome inactivation (characterized by chromosome-wide histone modifications, including H3K27me3, H4K20me, and, importantly, H2AK119ub)[173]. Other E3 ligases, including RNF8/168 that target H2AK13/K15 and BRCA1/BARD1 that target H2AK127/K129, also play critical roles in biological processes such as DNA damage repair[148].

On the other hand, the removal of Ub tags is mediated by deubiquitinating enzymes (DUBs), including six families of cysteine proteases and one family of JAMM/MPN domain-associated metalloproteases[174, 175]. Mechanistically, DUBs belonging to the cysteine protease families catalyze the removal of ubiquitin molecules via peptide bond cleavage using a nucleophilic thiol from a cysteine (which is typically found in a catalytic triad that also involves histidine). In contrast, DUBs belonging to the metalloprotease family mediate deubiquitination by peptide bond cleavage using a nucleophilic hydroxyl group generated in a zinc-dependent manner[175]. Till now, many H2A DUBs have been identified, including BRCC36 hydrolyzing the K63-linked poly-ubiquitin chains on H2AK15[176], ubiquitin-specific proteases (USPs) USP3 and USP51 hydrolyzing the mono-ubiquitin on H2AK13/K15[177, 178], and USP48 hydrolyzing the mono-ubiquitin on H2AK127/K129[179]. Likewise, the removal of mono-ubiquitin mark on H2AK119 can be mediated by DUBs such as USP3, USP21, USP22, and USP44, as well as BRCA1-associated protein-1 (BAP1) and Myb-like SWIRM and MPN domains 1 (MYSM1)[148, 167, 180]. Notably, MYSM1 (also known as KIAA1915) was discovered to be necessary in the maintenance and differentiation of HSCs, as well as in the normal development of lymphoid and erythroid lineage cells[167, 180]. Since then, Dr. Nijnik's research team has been investigating the functions of H2A deubiquitinating enzymes (H2A-DUBs) in hematopoiesis and humoral immune responses. Previous works of our lab have demonstrated that USP44, which has specificity for both H2AK119ub and H2BK120ub, is dispensable for normal HSC function, lymphocyte development, and B-cell-mediated immune response[181]. In the current study, we focus on exploring the uncharacterized functions of two H2A-DUBs, BAP1 and MYSM1, with an emphasis on their gene expression regulatory roles during B cell development and B cell mediated immune responses, as well as during DC development.

Figure 1.6.2 DUB classifications.

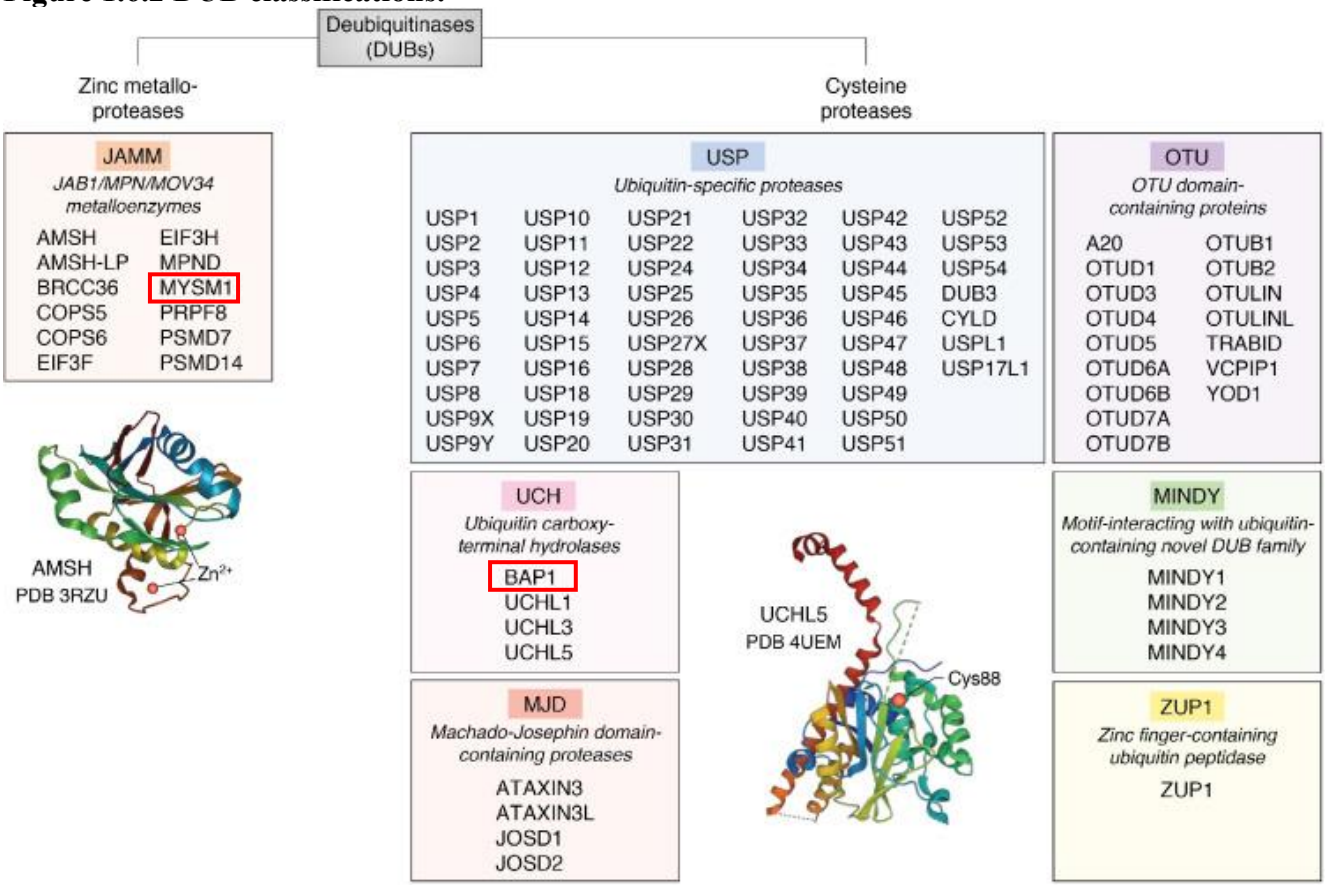

Seven classes of DUBs have been identified so far and are represented in different colors, out of which six are cysteine proteases (USP: ubiquitin-specific proteases; OTU: ovarian-tumor proteases; UCH: ubiquitin carboxyl-terminal hydrolases; MINDY: motif-interacting with ubiquitin-containing novel DUB family; MJD: Machado-Joseph disease protein domain proteases; ZUP1: zinc finger-containing ubiquitin peptidase 1) and one is metalloprotease (JAMM, JAMM/MPN domain-associated metallopeptidases).
This figure is adopted from Estavoyer, B., Messmer, C., Echbicheb, M., Rudd, C. E., Milot, E., & Affar, E. B. (2022)[175].

1.7 BRCA1-Associated Protein-1 (BAP1)

BAP1 was discovered in 1998, isolated as a binding partner of BRCA1[182]. Initially, BAP1 was thought to function by releasing ubiquitin from BRCA1, and was later found to enhance BRCA1's suppressive effect on tumor growth without deubiquitinating it[182, 183]. Indeed, deletions of the BAP1 encoding gene were commonly seen in breast cancers and lung cancers[184]. Later studies

further revealed the BRCA1-independent tumor suppressive role of BAP1. The human *Bap1* gene is located on chromosome 3p21.3, a genomic region frequently deleted or rearranged in various cancers[185]. BAP1 mutations are linked to many types of human malignancies, including sporadic uveal melanomas, mesotheliomas, renal cell carcinomas, hepatocellular carcinomas[186, 187, 188, 189]. The association between BAP1 mutations and hematopoietic malignancies was less reported, although BAP1-interacting ASXL proteins are commonly mutated in myeloproliferative disorders[190, 191]. Nowadays, it is widely accepted that BAP1, through its gene expression regulatory role, is involved in many key biological processes, including cell cycle, cell proliferation, metabolism, cell death, DNA damage response and others[148, 151, 182, 185, 192, 193, 194, 195, 196].

Figure 1.7.1 Overview of BAP1 functions.

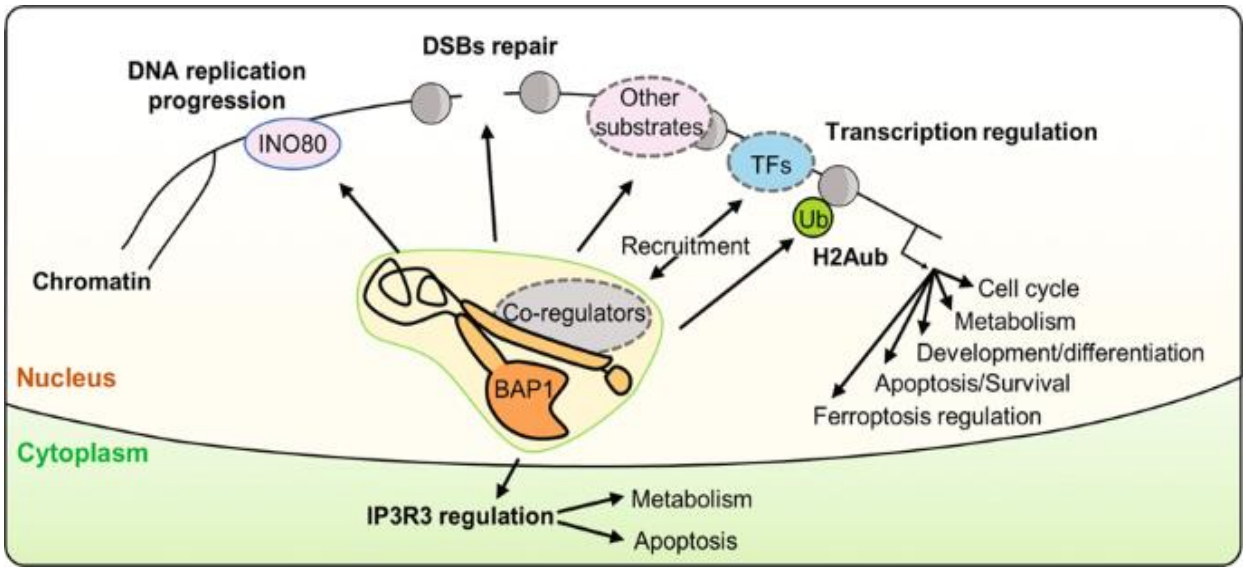

BAP1 plays essential roles in various biological processes. TF: transcription factors; H2Aub: histone H2AK119 mono-ubiquitin; INO80: INO80 chromatin remodeling complex; IP3R3: inositol 1,4,5-trisphosphate receptor, type 3.
This figure is adopted from Masclef, L., Ahmed, O., Estavoyer, B., Larrivée, B., Labrecque, N., Nijnik, A., & Affar, E. B. (2021)[186].

1.7.1 BAP1 structure and cellular functions

BAP1 is a 90 kDa protein (729 amino acids) with an N-terminal ubiquitin carboxyl hydrolase (UCH) domain, two C-terminal nuclear localization signal (NLS) motifs, and multiple protein-interacting domains[184]. As a member of the UCH subfamily of DUBs, BAP1 possesses a conserved catalytic domain containing an invariant cysteine, histidine, and conserved UCH aspartic acid catalytic residues (C91, H169, and D184)[172, 182, 197, 198]. This key catalytic domain mediates the auto-deubiquitination of BAP1 at its C-terminal nuclear localization signals (NLS), facilitating the nuclear import of BAP1[199]. BAP1 is known to have substrates both in the nucleus and the cytosol[186]. When binding to chromatin, BAP1 specifically removes the H2AK119ub via its catalytic domain, thereby mediating chromatin modulation and transcriptional regulation[200]. Moreover, BAP1 can coordinate the transcription machinery by interacting with different transcription factors, including forkhead box kinase 1 and 2 (FOXK1/2)[201, 202], Yin Yang 1 (YY1)[197], Kruppel-like factor 5 (KLF5)[203], and peroxisome proliferator-activated receptor-γ coactivator 1-α (PGC1α)[204], additional sex combs like transcription regulators (ASXLs)[183, 198], host cell factor 1 (HCF1)[197, 205], and O-linked β-N-acetylglucosamine (O-GlcNAc) transferase (OGT)[183, 206]. Consistent with the variety of its substrates and binding partners, BAP1 can contribute to the regulation of a wide range of cellular processes, including proteasomal degradation, signal transduction, protein trafficking, cell-cycle regulation, DNA damage response, cell survival and proliferation, metabolism, cell death, and others[148, 151, 182, 185, 192, 193, 194, 195, 196]. Beyond its gene expression modulatory role, studies have revealed BAP1's involvement in promoting apoptosis by deubiquitinating and stabilizing IP3R3 and consequently regulating the endoplasmic reticulum (ER) Ca^{2+} flux[207], and in facilitating DNA damage repair of the HR pathway by deubiquitinating and stabilizing INO80 and recruiting RAD51[186, 208].

1.7.2 BAP1 protein-protein interactions and gene regulatory roles

Researchers have been investigating the interactions between BAP1 and other proteins, as well as their involvement in chromatin modification and transcriptional regulation. The most studied BAP1-associated proteins include additional sex combs like 1 and 2 (ASXL1/2), host cell factor 1 (HCF1), Yin Yang 1 (YY1), and O-linked β-N-acetylglucosamine (O-GlcNAc) transferase (OGT) [148, 193, 194, 197]. These proteins are considered to associate with BAP1 and form a chromatin-associated core complex [205, 209, 210, 211]. Many other proteins, including previously mentioned transcription factors FOXK1/2, KLF5, and PGC1α, as well as histone acetyltransferase HAT1[212], the lysine-specific histone demethylase KDM1B (also known as LSD2)[197], and the ubiquitin ligase UBE2O[199], have been reported as binding partners of BAP1.

ASXL proteins are considered to be indispensable for the enzymatic activity of BAP1, since they can bind to the DEUBAD domains of BAP1 and activate BAP1 by increasing its affinity for ubiquitin[186, 194, 210]. The BAP1-ASXL complex is referred to as the polycomb repressive deubiquitinase (PR-DUB) complex in some literature[213, 214], with respect to its *Drosophila* homolog (Calypso-AXL)[215]. The PR-DUB complex, together with the PRC1 complex, regulates the transcriptional activation of various genes by exerting opposing effects and orchestrating a dynamic balance of H2A mono-ubiquitin modification[200, 215]. Moreover, resent studies suggest that BAP1 may repress PRC2 activity and thereby the H3K27me3 mediated transcriptional silencing, adding extra complexity to the regulatory network of gene expression[216].

HCF1, on the other hand, is a transcription regulator that can modulate G1–S transition and cell proliferation[197]. Through an HCF1-binding motif located in its middle region, BAP1 bind to HCF1 and preferentially hydrolyzes the K48-linked over the K63-linked polyubiquitin chains[183, 197, 217]. As a consequence, BAP1 prevents the proteasomal degradation of HCF1 and promotes its scaffolding effect to recruit histone-modifying enzymes to, for instance, promoters which are targets of the E2F family of transcription factors[183, 217]. Consistently, evidence supporting the cell proliferation regulatory role of BAP1 can be found in many reports, although many aspects of the underlying mechanism remain unknown[211, 217]. Similarly, BAP1 is shown to deubiquitinate and stabilize the HCF1-associated protein OGT, which modulates chromatin remodeling, metabolic stress, cell cycle progression, and many other processes[183, 193, 218, 219].

BAP1 and HCF1 can also form a complex with the transcription factor YY1, which enhances the recruitment of the resulting BAP1-HCF1-YY1 complex to gene promoters[197]. Researchers have proposed that the BAP1-HCF1-YY1 complex contributes to the transcriptional regulation of several mitochondrial and general metabolism genes[197].

To sum up, through selective interactions with different proteins, BAP1 exerts a wide range of regulatory effects on gene expression, and, therefore, is crucial in various biological processes. The context-dependent roles of different BAP1-involving protein complexes indicate the possibility that BAP1 may have cell type-specific and temporarily defined functions. Hence, we are interested in the potential role of BAP1 in hematopoiesis, especially in the development and function of B lymphocytes.

Figure 1.7.2 Functional domains of BAP1.

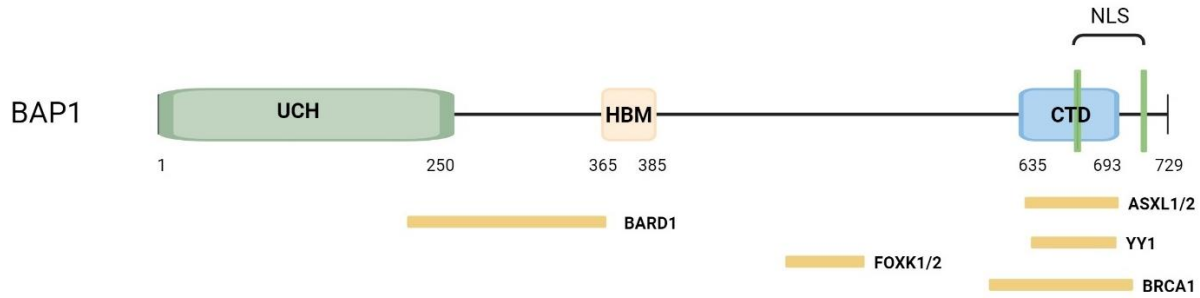

Domain organization of BAP1 and the protein–protein interaction interface between BAP1 and other factors in humans. Ubiquitin carboxy hydrolase (UCH) domain (1–250); BARD1-binding region (182–365); HCF1 binding (HBM) domain (365–385); FOXK1/K2 binding region (477–526); BRCA1 binding region (596–721); C-terminal binding domain (CTD) and ASXL1/2 binding domain (635–693); Nuclear localization signals (NLS) (656–661 and 717–722); Yin Yang 1 (YY1) binding domain (642–686).
This figure is adapted from Louie BH and Kurzrock R. (2020)[220].

1.7.3 BAP1 in hematopoiesis

Although BAP1 mutations have been linked to disorders such as lung cancers, mesothelioma, and uveal melanoma for a long time, their effects in hematologic pathology were not thoroughly studied. Recently, researchers identified a somatic heterozygous BAP1 mutation in a patient with de novo myelodysplastic syndrome (MDS)[183]. Remarkably, ASXL1, the binding partner of BAP1, is commonly mutated in acute myeloid leukemia (AML), chronic myelomonocytic leukemia (CMML) and other cancers[183, 210]. These findings encourage us to further explore the functions of BAP1 in the blood and immune system.

Although a systemic constitutive loss of BAP1 leads to embryonic lethality in mouse models[221], inducible BAP1 deletion in adult mice resulted in an expansion of HSCs, CMPs, and GMPs, indicating the importance of BAP1 in early stages of hematopoiesis[222]. Moreover, BAP1 is required for the normal development of myeloid lineage blood cells, as these mice developed

splenomegaly, monocytosis, neutrophilia and anemia, which are features comparable to the human MDS[221]. In terms of the lymphoid lineage, BAP1 deletion in these mice leads to severe thymic atrophy and reduction of T cells[222]. B cell depletion was also observed in these mice, yet whether it is due to intrinsic BAP1 function in B cells or its role in the earlier progenitor cells remains unknown. To address this question, our lab generated a *Bap1*$^{fl/fl}$mb1-Cre mouse line and demonstrated that B-cell specific BAP1 deletion resulted in impaired B cell development in the bone marrow (Figure 1.7.3)[223]. Precisely, these mice exhibit impaired B cell differentiation from the pro-B to pre-B and immature B cell stages, as well as reduced systemic B cells and compromised Ab response to immunization[223]. In this project, we decide to further investigate the mechanistic role of BAP1 in B cell development and humoral immunity.

Figure 1.7.3 Reduced antibody levels and impaired antibody mediated immune response in *Bap1*$^{fl/fl}$ mb1-Cre mice.

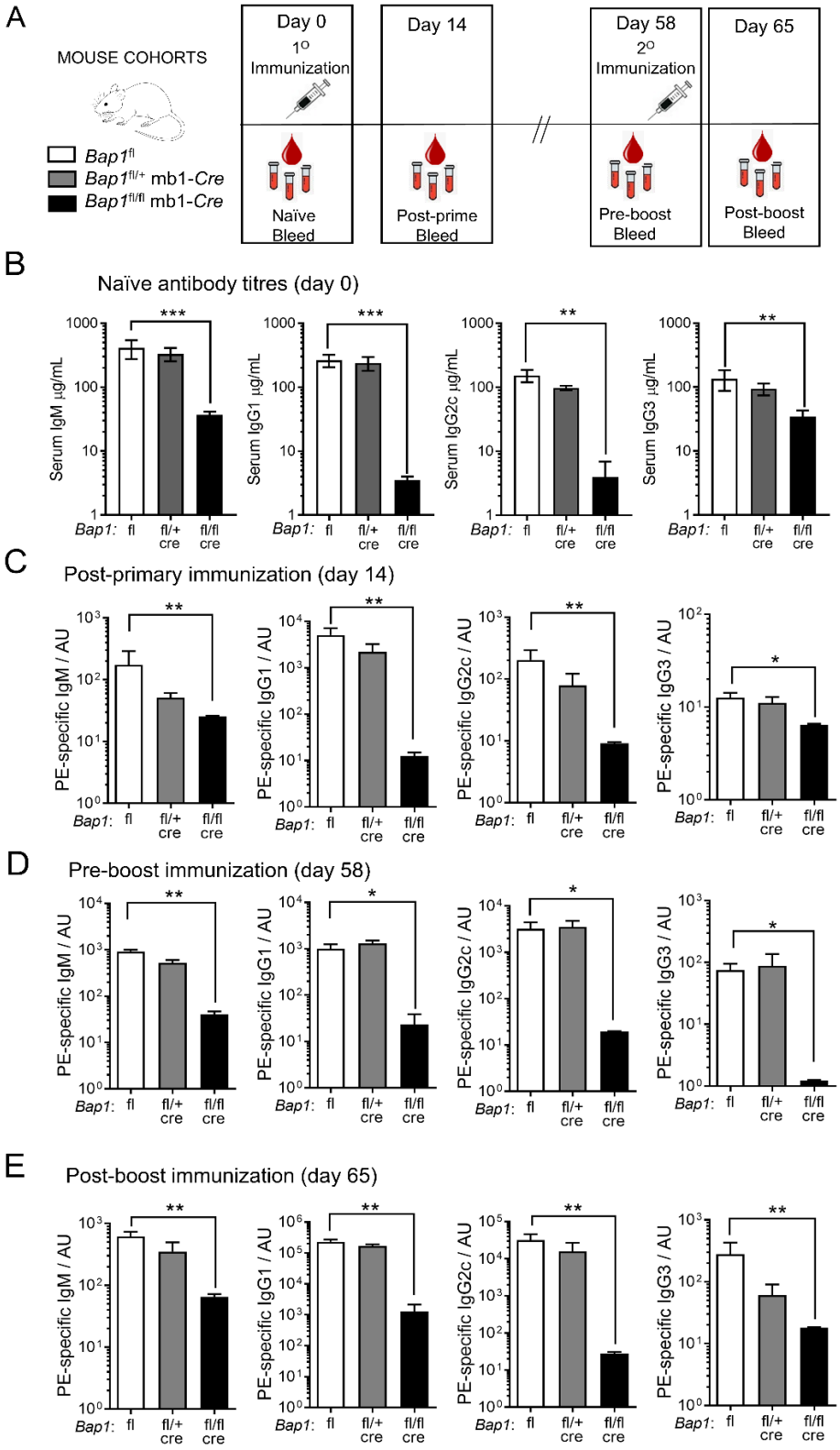

(A) Schematic of the experimental plan and timeline for the analyses of antibody production in *Bap1*$^{fl/fl}$ mb1-Cre and control *Bap1*^{fl} and *Bap1*$^{fl/+}$ mb1-Cre mice. The mice received primary (day 0) and boost (day 58) immunizations of PE in CFA; post-primary immunization serum samples were acquired on day 14, pre-boost serum samples on day 58, and post-boost serum samples on day 65. **(B)** Levels of total IgM, IgG1, IgG2c, and IgG3 antibody isotypes in the serum of naïve mice of *Bap1*$^{fl/fl}$ mb1-Cre and control *Bap1*^{fl} and *Bap1*$^{fl/+}$ mb1-Cre genotypes. The data for IgM, IgG1, and IgG3 is from 6-11 mice per genotype, and for IgG2c from 3-6 mice per genotype, consolidated from two independent experiments. **(C-E)** Antigen specific antibody titres in the mice of *Bap1*$^{fl/fl}$ mb1-Cre and control *Bap1*^{fl} and *Bap1*$^{fl/+}$ mb1-Cre genotypes, immunized and bled as outlined in (A). Data is from 3-6 mice per genotype. Bars represent means ± SEM; statistical analyses used non-parametric Kruskal-Wallis multiple comparison test with Dunn's post-hoc test in GraphPad Prism 9.5.1; * p<0.05, ** p<0.01, *** p<0.001; AU - arbitrary units.

1.8 Myb-like SWIRM and MPN domains 1 (MYSM1)

MYSM1 was discovered as an epigenetic modulator that activates the transcription of androgen receptor target genes in prostate cancer cell lines[224]. Later research revealed its essential regulatory roles in hematopoiesis, immune response, and various other aspects of mammalian physiology. MYSM1 predominantly acts as a nuclear chromatin-interacting protein and has orthologues exclusively in vertebrate species[225]. This indicates its more recent evolutionary development and suggests that it has specialized biological functions. Notably, recent discoveries have linked mutations in MYSM1 in humans to a rare hereditary disorder known as bone marrow failure syndrome (IBMFS), characterized by leukopenia, anemia, and other hematopoietic and developmental abnormalities, which highlights the biomedical significance of investigating MYSM1 functions[225, 226, 227].

1.8.1 MYSM1 structure and cellular functions

As a DUB of the metalloprotease family, MYSM1 is comprised of the Myb-like SANT domain which can bind to DNA *in vitro*, the SWIRM domain which is essential for the protein to be recruited to DNA and interact with histones *in vivo*, and the MPN domain which carries catalytic

activity[225]. In particular, the MPN metalloprotease domain of MYSM1 is characterized by a JAB1-MPN-MOV34 (JAMM) motif which consists of a consensus sequence (E-x[2]-H-S/T-Hx[7]-S-x[2]-D). It allows MYSM1 to coordinate with Zn^{2+} and selectively hydrolyze ubiquitin-linked isopeptide bonds[225, 227, 228].

In the nucleus, MYSM1 can act as a DUB by targeting H2AK119ub and consequently de-repress gene expression[225]. Moreover, MYSM1 can interact with other transcriptional regulators such as the histone acetyltransferase pCAF[224], the BRG1 and BRM catalytic components of the chromatin remodeling complex SWI/SNF[225], and many essential hematopoietic transcription factors including E2A, PU.1, GATA2, RUNX1, and cMYC[229, 230, 231, 232]. MYSM1 activity has also been associated with DNA damage response, as MYSM1-deficient murine or human cells exhibit elevated genotoxic stress (increased baseline level of γ-H2AX, increased UV-induced ROS production, increased post-irradiation p53 level and cell death, and others)[180, 226]. A recent study shows that the mechanistic role of MYSM1 during DNA damage response is not to promote DSB repair, but to enable the normal cessation of DNA damage response signaling[233]. Furthermore, MYSM1 is also shown to exert a constitutive inhibitory effect on the p53 stress response pathway, as inducible deletion of MYSM1 in mice leads to enhanced p53 protein levels and activation of p53-regulated stress response genes, such as PUMA and p21 encoding genes[234].

On the other hand, cytoplasmic functions of MYSM1 are also reported. In macrophages, MYSM1 is reported as a potential regulator of signal transduction pathways of innate immunity by targeting cytosolic substrates. Precisely, MYSM1 can cleave the K63-polyubiquitin chains on Toll-like receptor (TLR) signaling pathway components TRAF3 and TRAF6, as well as the K63/K27/M1-

polyubiquitin chains on RIP2 downstream of NOD2, thereby repressing the innate immune and inflammatory responses of macrophages[225, 235, 236]. Interestingly, the SWIRM and MPN domains, but not the SANT domain, are essential for the described cytosolic activity of MYSM1[225, 235, 236].

Figure 1.8.1 Functional domains of MYSM1.

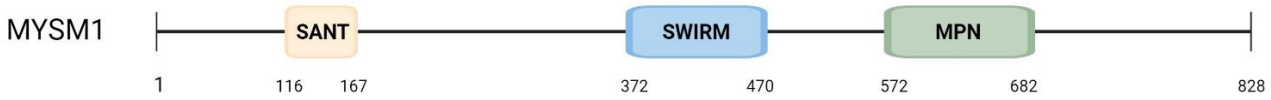

Domain organization of MYSM1 in humans. SANT domain (116-167); SWIRM domain (372-470), and MPN metalloprotease domain (572-682) containing a JAMM-motif.
This figure is adapted from Fiore, A., Liang, Y., Lin, Y. H., Tung, J., Wang, H., Langlais, D., & Nijnik, A. (2020)[225].

1.8.2 MYSM1 regulates the expression of key transcription factors in hematopoiesis

Since being discovered, MYSM1 was most extensively studied in hematopoietic cells with a focus on its transcription regulatory role. Previous reports showed that MYSM1 can mediate the removal of H2AK119ub at a range of gene loci that are essential for the maintenance, differentiation, and lineage specification of hematopoietic cells, including *Gfi1* in HSCs, *Flt3* in dendritic cell precursors, *Id2* in NK cell progenitors, *Ebf1* in B cell progenitors, *Pax5* in naïve B cells, and *miR150* in B1a cells[225, 230, 231, 232]. Also, MYSM1 can promote the recruitment of important transcription factors, such as PU.1 to the *Flt3* locus, NFIL3 to the *Id2* locus, E2A to the *Ebf1* locus, and GATA2 together with RUNX1 to the *Gfi1* locus[229, 230, 231, 232]. Consistently, depletion of MYSM1 leads to increased recruitment of PRC1 at these loci and consequent disruptions of HSC quiescence and function, dendritic cell development, NK cell maturation, B cell lineage specification and differentiation, and other defects[225]. Hence, by orchestrating the histone H2A deubiquitination status, MYSM1 is able to de-repress gene transcription and act as an intrinsic

regulator of hematopoietic cells. In addition, MYSM1 has also been proposed to mediate transcription activation by forming a complex with the HAT pCAF in a prostate cancer cell line, although there are no similar reports suggesting a link between MYSM1-mediated histone deubiquitination and acetylation in hematopoietic cells yet[224].

Consistent with the described role of MYSM1 as a transcriptional and epigenetic regulator, *Mysm1*$^{-/-}$ mouse with MYSM1 deficiency exhibits a severe depletion of HSPCs, including the DC precursors[237]. Specifically, MYSM1 deficiency results in increased H2A monoubiquitin level, and consequently leads to decreased *Flt3* expression and disrupted PU.1 recruitment to the *Flt3* promoter, suggesting that MYSM1 acts as a DUB in regulating the early checkpoints during DC development[237]. However, the roles of MYSM1 at later stages in DC differentiation, maturation, activation, and effector functions remain unknown, which encourages us to further examine the role of MYSM1 in the transcriptional regulation of DC biology, including in DC maturation and effector functions.

Figure 1.8.2 Overview of the reported roles of MYSM1 in the transcriptional regulation of hematopoiesis.

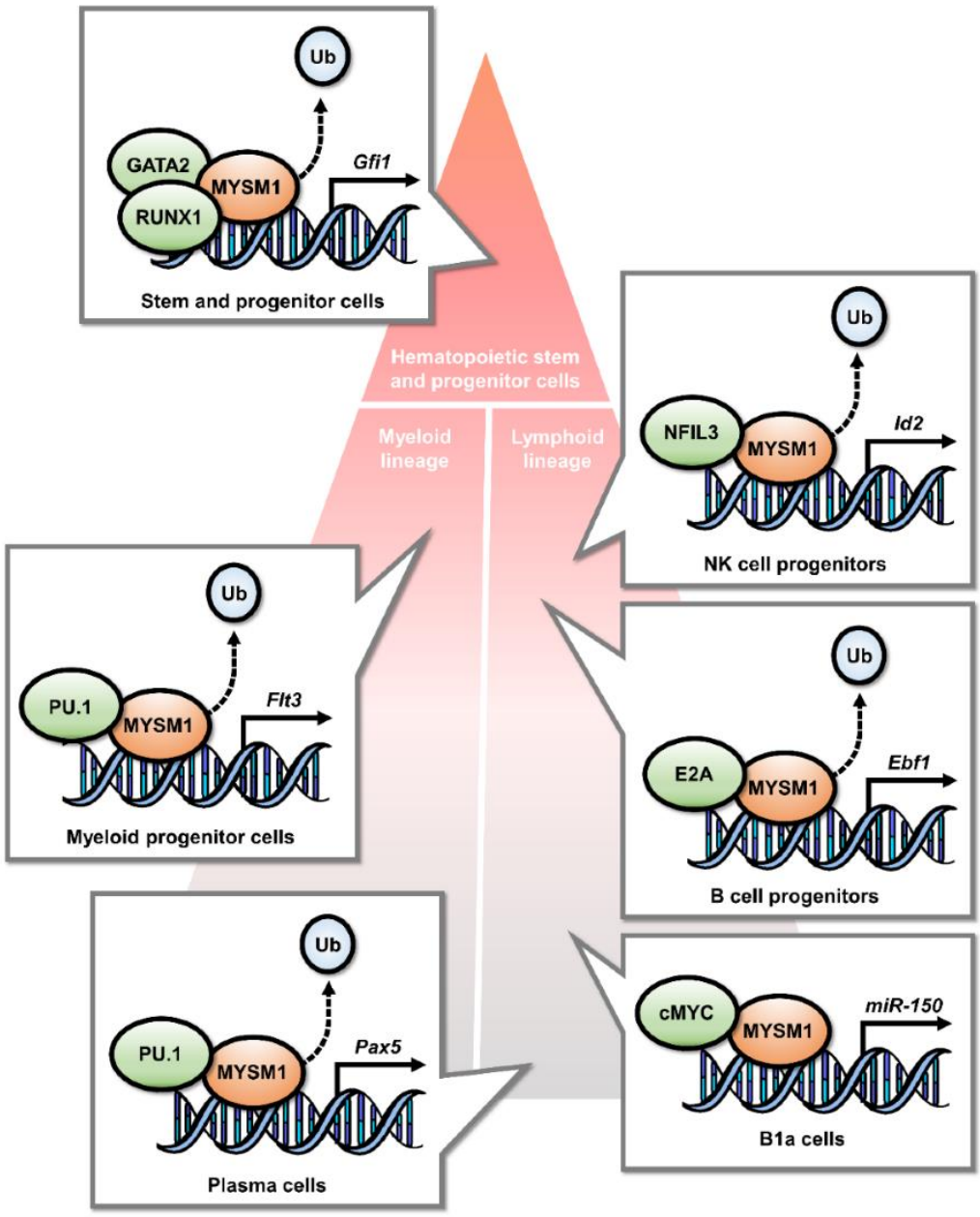

MYSM1 was shown to de-repress the expression of *Ebf1* in B cell progenitors, *Pax5* in naïve B cells, miR150 in B1a cells, *Id2* in NK cell progenitors, *Flt3* in dendritic cell precursors, and *Gfi1* in hematopoietic stem and progenitor cells, through deubiquitination of histone H2AK119ub, and interactions with hematopoietic transcription factors E2A, PU.1, GATA2, RUNX1, cMYC, and NFIL3.
This figure is adopted from Fiore, A., Liang, Y., Lin, Y. H., Tung, J., Wang, H., Langlais, D., & Nijnik, A. (2020)[225].

1.8.3 MYSM1 maintains ribosomal protein gene expression in HSCs

Previous works of our lab demonstrated the critical role of MYSM1 in the early stages of hematopoiesis and, possibly to a lesser extent, in humoral immune response[238, 239]. We and others characterized p53 activation as the common feature of MYSM1 deficiency and the driving mechanism for hematopoietic failure and other associated pathologies, as demonstrated by the rescue of *Mysm1*$^{-/-}$ phenotypes in the *Mysm1*$^{-/-}$*p53*$^{-/-}$ double knockout mice[238, 239, 240, 241]. We proposed that MYSM1 deficiency is a new form of ribosomopathy, as MYSM1 exerts a key regulatory role in the expression of genes encoding ribosomal-protein (*RP*-genes) and in the repression of the p53 pathway[242, 243]. We conducted the first genome-wide analysis for MYSM1-regulated genes in mouse HSCs and confirmed that MYSM1 maintains the expression of *RP*-genes [244]. However, MYSM1 deficiency did not lead to detectable elevation of H2AK119ub levels at the MYSM1-binding sites within these *RP*-gene promoters[244], suggesting other modes for their transcriptional regulation by MYSM1. Hence, we decide to further explore the regulatory role of MYSM1 in the hematopoietic system by investigating whether all biologically significant MYSM1 functions are universally dependent on its DUB catalytic activity and whether MYSM1 catalytic activity is essential for the maintenance of hematopoiesis in vivo.

Chapter 2: Rationale and Objectives

2.3 Rationale

BAP1 and MYSM1 are important regulators of gene expression. Previous studies revealed the essential roles of these two DUBs in hematopoiesis. Precisely, BAP1 deficiency in mice resulted in MDS-like hematopoietic abnormalities (including splenomegaly, monocytosis, neutrophilia, and anemia)[221] as well as thymic atrophy and reduction of T cells[222], suggesting that BAP1 is crucial to myeloid cell development and T lymphocyte development, respectively. B cell depletion was also reported, but not analyzed in detail[222]. Our research team examined the influence of BAP1 deficiency on B lymphocytes by characterizing a novel *Bap1*$^{fl/fl}$mb1-Cre mouse line. This demonstrated that B-cell specific BAP1 deletion resulted in impaired B cell differentiation from the pro-B to pre-B and immature B cell stages, as well as reduced systemic B cells and compromised Ab responses to immunization[223]. These results suggest a B-cell intrinsic role of BAP1 to regulate B cell development. However, whether BAP1 modulates B cell development by regulating gene expression via its H2A-DUB activity, and whether BAP1 also plays a role in B cell maturation and activation, remain largely unknown. Hence, we hypothesize that BAP1 functions as an important regulator of the transcriptional programs of I) B cell development and II) B cell mediated immune response. One focus of the current work is to further investigate the mechanistic role of BAP1 in B cell development, B cell activation, and antibody mediated immune response.

MYSM1, on the other hand, has been reported as a key regulator in the early stages of hematopoiesis and, possibly to a lesser extent, in humoral immune response[238, 239]. Previous studies showed that MYSM1, as a H2A-DUB, is able to remove H2AK119ub and regulate the expression

of key genes (including *Gfi1*, *Flt3*, *Id2*, *Ebf1*, *Pax5*, and *miR150*) involved in the maintenance, differentiation, and lineage specification of hematopoietic cells, including lymphocytes and DCs[225, 230, 231, 232]. Nevertheless, the DUB catalytic activity of MYSM1 is associated with many but not all of its functions. Previously, we and others demonstrated the importance of MYSM1-p53 axis in HSPC development and function[238, 239, 240, 241, 242, 243]. More recently, we conducted the first genome-wide analysis for MYSM1-regulated genes in mouse HSCs and confirmed that MYSM1 maintains the expression of genes encoding ribosomal proteins (*RP*-genes)[244]. However, during transcriptomic analyses of our MYSM1-deficient mouse lines, the lack of detectable elevation of H2AK119ub at the MYSM1-binding sites within these *RP*-gene promoters made us wonder whether MYSM1 mediates such transcriptional regulation by acting as a DUB or though protein-protein interactions[244]. Therefore, we decides to further explore the regulatory role of MYSM1 in the hematopoietic system. We hypothesize that the DUB catalytic activity of MYSM1 is essential for the maintenance of hematopoiesis. In the current study, we focus on investigating whether the loss of MYSM1 catalytic function and the loss of MYSM1 protein exert comparable effects to various hematopoietic cell lineages. In addition, we also further examine the role of MYSM1 in the transcriptional regulation of DC biology, including in DC maturation and effector functions.

2.4 Objectives

Aim 1: To explore the role of BAP1 in B cell development.

Aim 2: To explore the role of BAP1 in B cell mediated immune response.

Aim 3: To explore the role of MYSM1 and its DUB activity in hematopoiesis.

Chapter 3: Methodology

3.4 Materials and Methods for Exploring the Role of BAP1 in B Cell Development

3.1.1 Cell culture

Murine pro-B lymphocyte cell line Ba/F3 was maintained at 0.5-2 x10^6 cells/mL in RPMI-1640 (Wisent) with 10% Fetal Calf Serum (FCS, Wisent), 2mM L-Glutamine, 100µg/mL streptomycin, 100U/mL penicillin (Wisent), and 5% WEHI conditioned media as the source of IL-3. Ba/F3 cell lines stably expressing triple-FLAG-tagged murine BAP1 were derived as previously described[239], and maintained under 2µg/mL puromycin selection (Wisent).

3.1.2 CRISPR-Cas9 gene targeting

pSpCas9(BB)-2A-GFP (PX458) was obtained through Addgene (#48138). gRNA fragments targeting *Bap1* were designed using the Zhang lab software (*http://crispr.mit.edu*) and ligated into BbsI (NEB) digested PX458. Plasmids were transformed into DH5α competent cells, purified using PureLink HiPure Plasmid Filter Midiprep Kit (Invitrogen), and verified by Sanger sequencing. To introduce the constructed plasmid into Ba/F3 cells, nucleofection was performed using Amaxa Cell Line Nucleofector Kit V (Lonza) according to the manufacturer's protocols. Single GFP^+ cells were sorted 48 hours after the nucleofection and then expanded over two weeks to generate single cell clones. The loss of BAP1 protein expression in the cell line clones was validated via Western blotting, with the following antibodies: anti-BAP1 (D7W7O, Cell Signaling Technology), anti-β-Actin (D6A8, Cell Signaling Technology), HRP-conjugated anti-mouse-Ig (eB144, Rockland), and HRP-conjugated anti-rabbit-Ig (eB182, Rockland).

3.1.3 Chromatin immunoprecipitation (ChIP)

ChIP was performed as described previously [245], with minor modifications. Briefly, cells were fixed with 1% formaldehyde in the culture media for 10 minutes at room temperature, followed by addition of 0.125M of glycine to stop fixation. Nuclei were extracted with 5 minutes lysis in 0.25% Triton buffer, followed by 30 minutes in 200mM NaCl buffer. Nuclei were resuspended in sonication buffer and sonicated for twelve cycles of 30 seconds with a digital sonifier (Branson Ultrasonics) at 80%, with 30 seconds rest in cooled circulating water.

Beads immunocomplexes were prepared overnight by conjugating 40µL of Dynabeads Protein G (Invitrogen, Life Technologies) with antibodies: anti-BAP1 (Cell Signaling Technology, D1W9B, 52.8 µg), anti-FLAG M2 (Sigma, F1804, 5 µg) or anti-H2AK119Ub (Cell Signaling Technology, D27C4, 5 µg). Immunoprecipitation was performed by overnight incubation of antibody-bead matrices with sheared chromatin from the equivalent of $5x10^6$ cells. For BAP1-FLAG ChIP, 4 washes were performed with medium-stringency buffers, while 6 low-stringency washes were used for histone ChIP. Samples were de-crosslinked by overnight incubation at 65°C in 1% SDS buffer, and following RNaseA and Proteinase K enzymatic treatments, ChIP DNA was purified using Qiaquick PCR Cleanup kit (Qiagen).

ChIP-seq libraries were prepared using the Illumina TruSeq kit and sequenced on an Illumina HiSeq 4000 sequencer in paired-end 50bp configuration, with input DNA from the same cells sequenced as negative control. The reads were mapped to the UCSC mouse mm9 reference genome with Bowtie 1.0.0 [246], and BAP1 binding sites identified using peak detection algorithm MACS1.4 [247], with comparisons for read enrichment against control input DNA from the same cells. Normalized sequence read density profiles (bigwig) were generated with Homer tool [248] and visualized with IGV [249]. Gene ontology (GO) and disease ontology enrichment analyses on genes

associated with BAP1 ChIP-Seq binding clusters were performed on GREAT 4.0.4 [250] with Basal plus extension option, searching for genes within 2kb upstream, 2kb downstream, and 200kb in distal.

3.1.4 ChIP-Seq and RNA-Seq data consolidation

Full gene annotations with transcription start site (TSS) were obtained from the UCSC mouse mm9 reference genome. An in-house Python script was developed to load the genomic locations of ChIP-Seq binding sites and the TSS locations of RNA-Seq dysregulated genes, and search for gene TSS located within a specific distance to each ChIP-Seq binding site.

3.1.5 Statistical analyses

Statistical analyses used Prism 7.01 (GraphPad Inc.), with Student's *t*-test for two datasets and ANOVA for multiple comparisons. Further information for each dataset is provided in the Figure Legends.

3.5 Materials and Methods to Explore the Role of BAP1 in B cell Mediated Immune Response

3.2.1 Mice

The *Bap1*$^{tm1c(EUCOMM)Hmgu}$ mouse strain carries a conditional (floxed) allele of the *Bap1* gene; it was generated by the Wellcome Trust Sanger Institute Mouse Genetics Project and Infrafrontier/ EMMA (*www.infrafrontier.eu*) [251, 252, 253], and described in our recent work [223]. The strain was bred to the transgenic line expressing Cre recombinase under the control of the B cell lineage specific promoter mb1-Cre (from Prof. Michael Reth, MPI für Immunbiologie und Epigenetik, Germany) [254], and to the B6.129P2(Cg)-*Ighg1*$^{tm1(cre)Cgn}$/J mouse strain (Jackson Labs: 010611, Cγ1-cre)

expressing Cre recombinase from the endogenous immunoglobulin heavy constant gamma 1 locus (*Ighg1*) [255]. As we previously described [223], the loxP sites flank exons 6-12 (ENSMUSE00000121807-00000121801) of the main ENSMUST00000022458.10 *Bap1* transcript, and the $Bap1^{\Delta}$ allele is predicted to disrupt BAP1 protein coding sequence from amino acid 126 (out of 728), precluding full expression of the N-terminal UCH catalytic domain and all the downstream domains of the protein. All lines were on the C57BL/6 genetic background. Both male and female animals were used in experiments, sex-matched between test and control groups. Experiments were in accordance with the guidelines of the Canadian Council on Animal Care and protocol MCGL-2011-6029 approved by the McGill Animal Care Committee. Genotyping was performed in house using the DreamTaq DNA Polymerase (Thermo Fisher Scientific) and primers from IDT Technologies.

3.2.2 Cell culture

Mouse B cell line CH12F3, which is a widely used model for the study of B cell activation and class switching [256], was maintained at 0.5-2 $x10^6$ cells/mL in RPMI-1640 (Thermo Fisher Scientific) with 10% Fetal Calf Serum (FCS, Thermo Fisher Scientific), 2mM L-Glutamine, 100µg/mL streptomycin, 100U/mL penicillin (Thermo Fisher Scientific), and 5% NCTC (Sigma-Aldrich).

3.2.3 CRISPR-Cas9 gene targeting

$Bap1^{\Delta/\Delta}$ CH12F3 cells were generated through CRISPR-Cas9 gene editing according to our previously described protocols [223]. gRNAs were designed with *http://crispr.mit.edu* online tools [257]: gRNA_Bap1_Exon4_Chr14:32,066,155: *gcaaatggatcgaagagcgc*,

gRNA_Bap1_Exon5_Chr14:32,066,654: *ggcgtgagtggcacaagagt*, and cloned into the pSpCas9(BB)-2A-GFP (PX458) plasmid (Addgene, #48138). Sequence-verified plasmids were introduced into CH12F3 cells through nucleofection using the Amaxa Cell Line Nucleofector Kit V (Lonza) according to the manufacturer's protocol. Single GFP^+ IgA^- cells were sorted on day-2, and expanded for further 14 days to generate single cell clones. Loss of BAP1 protein was validated with Western blotting and the following antibodies: anti-BAP1 (D7W7O, Cell Signaling Technology) and anti-β-Actin (D6A8, Cell Signaling Technology).

3.2.4 CH12F3 cell assays

AlamarBlue fluorogenic assay (ThermoFisher Scientific) was performed according to the manufacturer's protocols, as we previously described [223]. Cells were seeded into 96-well plates at 10^5 /mL, rested overnight, and the AlamarBlue reagent added at 10% (v/v). Fluorescence intensity was recorded at the 4-hour timepoint on the EnSpire Plate reader (Perkin Elmer), at the 560nm excitation and 590nm emission wavelengths. For the CFSE-dilution assay, 5×10^6 cells were incubated in 2 μM CellTrace™ CFSE (ThermoFisher Scientific) in 1mL of PBS for 10 min at 37°C. The cells were washed in PBS with 5% FBS, followed by a second wash in PBS. The cells were re-suspended in complete media at 2×10^5 /mL and maintained in culture overnight at 37°C 5% CO_2. The cells were counterstained with Fixable Viability Dye eFluo780 (ThermoFisher Scientific), and the data were acquired on the BD Fortessa and analyzed with FlowJo (Tree Star, BD Biosciences) software. In some assays the CH12F3 cells were stimulated with TGF-β (1ng/ml, R&D Systems), IL-4 (10 ng/ml, Peprotech), and anti–CD40 (1μg/ml, BD Biosciences).

3.2.5 Primary B cell cultures

The protocols were as described in our recent work [258]. Briefly, naïve primary mouse B cells were purified from splenocytes using EasySep™ Mouse B Cell Isolation Kit (19854, Stem Cell Technologies) and were cultured at 37°C with 5% CO_2 in iGB media: RPMI-1640 (Wisent), supplemented with 10% FBS (Wisent), 1% penicillin/streptomycin (Wisent), 0.1 mM 2-mercaptoethanol (BioShop), 10 mM HEPES, and 1 mM sodium pyruvate. Mouse primary B cells were labeled with 2.5μM CellTrace™ Violet (C34557, Invitrogen) in PBS for 20 minutes at 37°C before quenching as recommended by the supplier. For switching to IgA, B cells were stimulated with mouse recombinant IL-21 (20ng/mL, Peprotech), TGF-β1 (5ng/mL), retinoic acid (1μM, Sigma), F(ab')2 goat anti-mouse IgM (5μg/mL, Jackson ImmunoResearch) and anti-CD40 mAb FGK45 (5μg/mL, prepared in-house from hybridoma), as previously described [259]. To measure class switching to IgA, cells were treated with mouse FcR blocking reagent (130-092-575, Miltenyi Biotec) then stained with anti IgA-PE (1040-09, Southern Biotech). Dead cells were excluded using eBioscience™ Fixable Viability Dye eFluor™ 780 (65-0865-14, Invitrogen). Induced GC B cells (iGBs) were generated on 40LB feeder cells (a gift from Dr. Daisuke Kitamura, Tokyo University of Science, Tokyo, Japan) [260]. One day prior to B cell plating, 40LB cells were treated with 10μg/mL mitomycin C (SKU M-1108, AG Scientific) at 0.5×10^6 cells per mL in 10cm dishes with DMEM media supplemented with 10% FBS (Wisent) and 1% penicillin/streptomycin (Wisent). After treatment, the cells were washed 6 times with 10 mL of PBS and plated at 1.3×10^5 cells per well in 0.5 mL (24-well plate). Subsequently, purified naive B cells were plated onto the 40LB feeders at $2x10^5$ cells in 1mL of iGB media, supplemented with 1 ng/mL IL-4 (214-14, Peprotech). On days 3, 4 and 5, the cells were either harvested for downstream analyses in PBS with 0.5% BSA and 2 mM EDTA or fed with 1 mL of fresh iGB

media with 1 ng/mL IL-4. Class switching to IgG1 was analyzed by flow cytometry, treating with mouse FcR blocking reagent and staining the cells with anti-IgG1 PE (550083, A85-1, BD Pharmingen) and anti-IgM BV421 (562595, R6-60.2, BD Pharmingen). For the analyses of cell division, iGBs were stained with 2.5μM CellTrace™ Violet on the day of plating, according to the manufacturer's protocol. Cell numbers for the iGBs growth curves were calculated using Countess 3 Automated Cell Counter.

3.2.6 Mouse immunization

For the phycoerythrin (PE) immunization the mice were injected subcutaneously with immunogen emulsion comprising 100 μl CFA (Thermo Fisher Scientific), 15 μg of R-PE (ProZyme, Cedarlane), and 100 μl PBS, vortexed for 45 min prior to the injection. For the immunization with sheep red blood cells (SRBCs), the mice were injected intravenously with 10^9 SRBCs (Innovative Research IC10-0210, Cedarlane) in 300uls of PBS. Immunization protocols were previously described [261, 262].

3.2.7 Analyses of antibody titres

ELISA analyses of total immunoglobulin levels in the serum of naive mice (or in the supernatants from B cell cultures) used rat anti-mouse capture antibodies IgM II/41, IgG1 A85-3, and IgG3 R2-38 (BD Biosciences, 1 μg/ml) followed by detection with goat anti-mouse IgG(H+L)-HRP (Southern Biotechnologies). For the analysis of total IgG2c levels capture antibody goat anti-mouse Ig (H+L) and detection antibody goat anti-mouse IgG2c-biotin (Southern Biotechnologies), followed by streptavidin-HRP (Thermo Fisher Scientific) were used. Purified mouse IgM, IgG1, IgG2c, and IgG3 isotype control antibodies (BioLegend) were used as standards for the calculation

of immunoglobulin concentrations. In the ELISA assays for the detection of PE-specific antibodies, the plates were coated with R-PE (10 μg/ml, ProZyme, Cedarlane), and developed with biotin goat anti-mouse IgM, IgG1, IgG2c, or IgG3 (Southern Biotechnologies), followed by streptavidin-HRP (Thermo Fisher Scientific). All the ELISAs were developed with SuperAquaBlue substrate (Thermo Fisher Scientific), and data acquired at 405 nm on EnSpire 2300 plate reader (PerkinElmer). Throughout the ELISA procedure, PBS with 0.05% Tween-20 was used as the Wash Buffer, PBS with 1% bovine serum albumin (Wisent) as the Blocking Buffer, and PBS with 0.1% bovine serum albumin (Wisent) as the Assay Diluent.

The detection of SRBC-specific antibodies was performed by flow cytometry, as described previously [263]. Briefly, mouse serum samples were pre-diluted 1:60 in PBS and incubated with 3x 10^5 SRBC for 30 min on ice. The SRBCs were washed and stained with goat anti-mouse IgG AlexaFluor488 (Poly4053, BioLegend, 1:200), or with goat anti-mouse IgM-biotin (1020-08, Southern Biotechnologies, 1:750), or IgG1-biotin (1070-08, Southern Biotechnologies, 1:750), followed by streptavidin – PerCP-Cy5.5 (BioLegend). Following thorough washing, the samples were analyzed on BD Fortessa and data processed with FlowJo software (Tree Star, BD Biosciences). SRBCs pre-incubated with serum of naive mice and stained as described above were analyzed as negative controls.

3.2.8 Flow cytometry

Cell suspensions of mouse tissues were prepared in RPMI-1640 (Thermo Fisher Scientific) with 2% (v/v) FCS, 100μg/ml streptomycin and 100U/ml penicillin (Thermo Fisher Scientific). The cells were stained for surface-markers in PBS with 2% FCS for 20 min on ice, with the following antibodies: Alexa Fluor 488 anti-GL7 (GL7, Biolegend); APC anti-CD21/CD35 (7E9, Biolegend),

anti-CD86 (GL-1, Biolegend), anti-CD267/TACI (ebio8F10-3, eBioscience), and anti-IgD (11-26c.2a, BioLegend); APC-eFluor780 anti-CD45R/B220 (RA3-6B2, ThermoFisher); APC-Cy7 anti-CD5 (53-7.3, Biolegend); Brilliant UltraViolet 395 anti-CD43 (S7, BD Biosciences); Brilliant Violet 421 anti-CD95/Fas (Jo2, BD Biosciences) and anti-CD138 (281-2, BioLegend); Brilliant Violet 650 anti-CD45R/B220 (RA3-6B2, BioLegend); Biotin anti-IgG1 (polyclonal, 1070-08, Southern Biotech); eFluor450 anti-CD45R/B220 (RA3-6B2, Thermo Fisher); FITC anti-CD23 (B3B4, Invitrogen) and anti-Ki67 (SolA15, eBioscience); Pacific Blue anti-IgD (11-26c.2a, BioLegend); PE anti-Blimp-1 (5E7, Biolegend), anti-CD184/CXCR4 (L276F12, Biolegend) and anti-IgM (II/41, Thermo Fisher); PE-Cy7 anti-CD19 (6D5, BioLegend), anti-CD21/CD35 (eBio8D9, Invitrogen), and anti-CD38 (90, Invitrogen); PerCP-Cy5.5 anti-CD4 (RM4-4, Biolegend), anti-CD8a (53-6.7, Biolegend), anti-CD11b (M1/70, eBioscience), anti-CD19 (1D3, Tonbo Biosciences), anti-CD45R/B220 (RA3-6B2, BioLegend), anti-IgD (11-26c.2a Biolegend), anti-CD93 (AA4.1, Biolegend), anti-NK1.1 (PK136, Biolegend), and anti-TER119 (Ly-76, Biolegend). Brilliant Violet 785 Streptavidin (Biolegend) was used to detect biotin-conjugated antibodies. Viability Dye eFluor® 506 (eBioscience) was used to discriminate dead cells. Compensation was performed with BD CompBeads (BD Biosciences). The data were acquired on BD Fortessa and analyzed with FlowJo software (Tree Star, BD Biosciences).

3.2.9 Cell isolation and sorting

Total B cells were isolated from mouse spleens via magnetic enrichment using the EasySep Mouse CD19 Positive Selection Kit II (Stem Cell Technologies). For the FACS-sorting of B cell subsets, mouse spleens were mechanically dissociated in PBS with 0.1% BSA and 2mM EDTA, passed through 40 μm cell-strainers, and subjected to red blood cell lysis in ACK buffer (0.15M NH_4Cl,

10mM KHCO3, 0.1mM EDTA). Cells were stained with the following antibodies: Alexa Fluor 488 anti-GL7 (GL7, BioLegend), Brilliant Violet 421 anti-CD95/Fas (Jo2, BD Biosciences), and Brilliant Violet 650 anti-CD45R/B220 (RA3-6B2, BioLegend). Viability Dye 7-AAD (Biolegend) was used to discriminate dead cells. Sorting was performed on the FACSAria (BD Biosciences).

3.2.10 Chromatin immunoprecipitation (ChIP)

ChIP was performed as described previously [223, 245]. Cells were fixed with 1% formaldehyde in cell culture media for 10 min at room temperature, followed by addition of 0.125 M glycine to stop the fixation. Nuclei were extracted with 5 min lysis in 0.25% Triton buffer, followed by 30 minutes in 200mM NaCl buffer. Nuclei were resuspended in sonication buffer and sonicated for 12 cycles of 30 sec with a digital sonifier (Branson Ultrasonics) at 80%, with 30 sec rest in cooled circulating water. Beads immunocomplexes were prepared overnight by conjugating 40µL of Dynabeads Protein G (Thermo Fisher Scientific) with antibodies anti-BAP1 (Cell Signaling Technology, D1W9B, 52.8 µg) or anti-H2AK119ub (Cell Signaling Technology, D27C4, 5 µg). Immunoprecipitation was performed with an overnight incubation of the antibody-bead matrices with sheared chromatin from the equivalent of $5x10^6$ cells. Six washes were performed with low-stringency buffers, and samples de-crosslinked by overnight incubation in 1% SDS buffer at 65℃. Following treatments with RNaseA and Proteinase K, ChIP DNA was purified using Qiaquick PCR Cleanup kit (Qiagen).

ChIP-seq libraries were prepared using the Illumina TruSeq kit and sequenced on the Illumina NovaSeq 6000 in a paired-end 100bp configuration, with input DNA from the same cells sequenced as the negative controls. The reads were mapped to the UCSC mouse mm9 reference genome with Bowtie 1.0.0 [246], and BAP1 binding sites identified using the MACS1.4 peak

detection algorithm [247], comparing for read enrichment against input DNA from the same cells. Normalized sequence read density profiles (bigwig) were generated with Homer [248] and visualized with IGV [249]. Gene ontology (GO) enrichment analysis on the genes associated with the BAP1 ChIP-Seq binding clusters was performed on GREAT 4.0.4 [250] with Basal plus extension, searching for genes within 2kb upstream, 2kb downstream, or 200kb in distal.

3.2.11 RNA sequencing

RNA-seq protocols were as previously described [223, 264]. Briefly, RNA was isolated using the Mag-MAX total RNA kit (Ambion) and quality assessed using Bioanalyzer RNA Pico chips (Agilent). rRNA depletion and library preparation were performed using the SMARTer Stranded RNA-Seq kit (Takara Clontech). The libraries were sequenced on an Illumina Novaseq 6000 in a paired-end 100 bp configuration aiming for $50x10^6$ reads per sample. The quality of the sequencing reads was confirmed using the FastQC tool (Babraham Bioinformatics), and low-quality bases were trimmed from the read extremities using Trimmomatic v.0.33 [265]. The reads were then mapped to the mouse UCSC mm9 reference genome assembly using Hisat2 v2.2.1 [266, 267, 268]. Gene expression was quantified by counting the number of uniquely mapped reads with featureCounts using default parameters [269]. We retained genes that had an expression level of at least 5 counts per 10^6 reads (CPM) in at least 4 of the samples [270]. TMM normalization and differential gene expression analyses were conducted using the edgeR Bioconductor package [271]. Dimension reduction analysis was performed using the Principal Component and Partial Least Squares regression method [272]. Pairwise comparisons were performed between genotypes or between treatments, and genes with changes in expression $\geq |2.0|$ fold and Benjamini-Hochberg adjusted p values ≤ 0.05 were considered significant. Gene ontology (GO) enrichment analyses on differentially expressed gene

clusters were performed with DAVID Bioinformatics Resources 6.8 [273], and Gene Set Enrichment Analysis (GSEA) was performed with GSEA tool v4.3.2 using MSigDB v2022.1 with default configuration and permutation within gene sets [274]. For the RNA-Seq data consolidation with the ChIP-Seq data, full gene annotations were obtained from UCSC mouse mm9 reference genome. An in-house Python script was developed to load the genomic locations of ChIP-Seq binding sites and RNA-Seq dysregulated genes, and search for gene TSS within a specific distance to each ChIP-Seq binding site, as previously described [244].

3.2.12 Statistical analyses

Statistical analyses used Prism 9.5.1 (GraphPad Inc.), with Student's *t*-test for two datasets and ANOVA for multiple comparisons, with further information provided in Figure Legends.

3.6 Materials and Methods to Explore the Role of MYSM1 DUB Activity in Hematopoiesis

3.3.1 Generation of Mysm1^{D660N} mice

Mysm1^{D660N} mice were generated on a C57BL/6JRj background using pronuclear microinjection in mouse zygotes. Zygotes isolated from C57BL/6JRj mice were co-injected with Cas9 protein (200ng/µl) and *Mysm1* exon 16-targeting guide RNA (5'-GTGTCAATATCTCGTAAAGA-3'; 25ng/µl) from px330 plasmid, along with oligonucleotide repair templates (20ng/µl) for the introduction of the D660N mutation (see below). Founder mice were screened for the desired point mutation by PCR amplification and Sanger sequencing using the following primers: 5'-GGCATTATAGTGCACTCTGGAA-3' and 5'-TATACTCAACTGCTGACCTTCCA-3'. *Mysm1*^{D660N} founders were backcrossed once onto C57BL/6JRj and maintained for the desired experimental genotype.

ssDNA D660N HDR repair template:

GGCTACAGTGTCATTGGGTGGTACCATTCTCATCCTGCATTTGATCCTAATCCATCTT

TAAGGAATATTGACACACAAGCCAAATACCAGGTGTGTTGTTACATACCTACATTTT

GTAAATTATTA

ssDNA silent mutation HDR repair template:

GGCTACAGTGTCATTGGGTGGTACCATTCTCATCCTGCATTTGATCCTAATCCATCTTTA

AGGGACATTGACACACAAGCCAAATACCAGGTGTGTTGTTACATACCTACATTTTGTA

AATTATTA

3.3.2 Other mouse lines and genotyping

Mouse lines *Mysm1*$^{-/-}$ and *Mysm1*$^{fl/fl}$ carry the loss-of-function and the conditional alleles of *Mysm1* gene, respectively, and were previously described [180, 234, 275]. *Mysm1*$^{fl/fl}$ *Cre*^{ERT2} mice were derived for tamoxifen-inducible *Mysm1* deletion by crossing *Mysm1*$^{fl/fl}$ and Gt(ROSA)26Sor$^{tm1(cre/ERT2)}$ strains, as previously described [234]. All lines were on the C57BL/6 genetic background. The mice were maintained under specific pathogen-free conditions and sex-matched across experimental groups. All experiments were in accordance with the guidelines of the Canadian Council on Animal Care and protocol AUP-2011-6029 approved by the McGill Animal Care Committee.

Mouse genotyping for the *Mysm1*^{D660N} allele was performed with a custom designed TaqMan SNP Genotyping assay and TaqMan Genotyping Master Mix on a StepOnePlus instrument (all reagents from ThermoFisher Scientific). Other genotyping was performed by conventional genomic PCR with DreamTaq DNA Polymerase (ThermoFisher Scientific) and primers from Integrated DNA Technologies.

3.3.3 Tamoxifen mouse treatment

For tamoxifen-induced *Mysm1*-gene deletion, mice of *Mysm1*$^{fl/fl}$ Cre^{ERT2}, *Mysm1*$^{fl/DN}$ Cre^{ERT2}, and control genotypes were injected intraperitoneally with tamoxifen (Sigma-Aldrich, T5648) in sterilized corn oil at 0.12 mg/gram per injection, with 8 doses administered in total over 16 days, as in our previous work [234, 244, 276]. Successful deletion of *Mysm1* exon 3 was validated by PCR analyses of the genomic DNA from lymphoid organs and BMDCs of the mice, as described previously [234], and the loss of MYSM1 protein expression in lymphoid tissues was validated by Western blotting [277].

3.3.4 Mouse bone marrow transplantation

For competitive bone marrow transplantations, recipient wild type B6.SJL-PtprcaPepcb/Boy (JAX002014, congenic for CD45.1) mice were irradiated with 2 doses of 4.5Gy, delivered 3 hours apart, in an RS2000 irradiator (Rad Source). Wild-type CD45.1-marked bone marrow cells were mixed in a 1:1 ratio with bone marrow cells from mice of *Mysm1*$^{fl/+}$*Cre*^{ERT2}, *Mysm1*$^{fl/fl}$*Cre*^{ERT2}, or *Mysm1*$^{fl/DN}$*Cre*^{ERT2} genotypes, and the mixes transplanted into three independent cohorts of recipient mice via intravenous injection. The mice were kept on neomycin in drinking water (2g/l, BioShop) for 3 weeks. Successful reconstitution of the hematopoietic system by donor cells was confirmed with a bleed and flow cytometry analysis at 12 weeks, and was followed with tamoxifen treatment to induce *Mysm1*^{fl} to *Mysm1*$^{\Delta}$ allele conversion and further studies to compare hematopoietic function across the *Mysm1* genotypes.

*3.3.5 **BMDC cultures and stimulation***

For BMDC derivation, mouse bone marrow was resuspended at 10^7 cells/mL and seeded dropwise at 75 µLs per well into 6-well non-tissue culture treated plates (Fisher Scientific) containing 3 mL/well of RPMI-1640 media, with 10% fetal calf serum (FCS) (both from ThermoFisher Scientific), 2 mM L-glutamine (Wisent), 100 U/mL penicillin/streptomycin (Wisent), 50 µM β-mercaptoethanol (Millipore-Sigma), and 20 ng/mL granulocyte-macrophage colony-stimulating factor (GM-CSF, 315-03, Peprotech) The cultures were fed with fresh media at days 3 and 6. After 8-9 days, BMDCs were harvested and seeded at 10^6 cells/mL for stimulation with lipopolysaccharide (LPS, *E. coli* O111:B4, Millipore-Sigma), polyinosinic–polycytidylic acid (poly(I:C), Millipore-Sigma), or (1→3)-β-D-glucan from *Alcaligenes faecalis* (Millipore-Sigma).

*3.3.6 **BMDC antigen presentation assays***

BMDCs derived from tamoxifen treated mice of *Mysm1*$^{fl/DN}$ Cre^{ERT2} and control *Mysm1*$^{fl/+}$ Cre^{ERT2} genotypes were either untreated or stimulated with LPS (10 ng/mL, *E. coli* O111:B4, Millipore-Sigma) and whole OVA (1 mg/mL, Worthington, LS003061) for 18 h. OT-II CD4 T cells were isolated from B6.Cg-Tg(TcraTcrb)425Cbn/J mice (Jackson Laboratories, JAX 004194) using the EasySep™ Mouse CD4$^+$ T Cell Isolation Kit (Stem Cell Technologies, 19852). In some assays, the T cells were pre-loaded with 10 µM Cell Proliferation Dye eFluor™ 450 (ThermoFisher Scientific), according to the manufacturer's protocol. BMDCs were co-cultured with OT-II CD4 T cells in round-bottom 96-well plates for 3–4 days, at 10^4 BMDCs and 10^5 T cells per well (1:10 ratio), in IMDM media with 10% fetal calf serum (FCS) (ThermoFisher Scientific), 2 mM L-glutamine (Wisent), 100 U/mL penicillin/streptomycin (Wisent), and 50 µM β-mercaptoethanol (Millipore-Sigma). The cultures were analysed by flow cytometry at day 3, for

T cell activation markers (CD44, CD69) and for the Cell Proliferation Dye eFluor™ 450, pre-gating on live $CD3^+CD4^+$ T cells. Alternatively, for the analyses of cytokine production, the cultures were stimulated on day 4 with Cell Activation Cocktail (BioLegend, 423302, 1:500), containing ionomycin and phorbol 12-myristate-13-acetate (PMA) for 4 h, with the addition of Brefeldin A and Monensin to block cytokine secretion (BioLegend 420701, 420601, 1:1000) over the last 2 h. The cells were stained for intracellular cytokines IFNγ, IL-2, IL-4, and IL-10 using the BD Fixation/Permeabilization Solution Kit (BD Biosciences, 554714) and the antibodies listed below:

Table 3.3.6.1 Antibodies and other reagents used in the flow cytometry analyses.

Fluorophore	Target	Company	Clone	Catalogue
Alexa Fluor 647	IL-4	BioLegend	11B11	504112
APC	CD44	ThermoFisher	IM7	17-0441-83
APC	CD86	BioLegend	GL-1	105012
APC	CD371 (CLEC12A)	BioLegend	5D3/CLEC12A	143405
APC/Cy7	XCR1	BioLegend	ZET	148223
Biotin	CD3	BioLegend	17A2	100243
BUV395	CD3	BD Biosciences	145-2C11	563565
BUV395	CD45	BD Biosciences	30-F11	564279
BUV737	CD11c	BD Biosciences	HL3	612796
BUV737	CD16/CD32	BD Biosciences	2.4G2	612783
BUV737	CD45.1	BD Biosciences	A20	612811
BV421	CD34	BD Biosciences	RAM34	562608
BV421	IL-2	BioLegend	JES6-5H4	503825
BV650	CD117 (c-kit)	BioLegend	ACK2	135125
BV785	CD45.2	BioLegend	104	109839
BV785	F4/80	BioLegend	BM8	123141
eFluor 450	CD11b	ThermoFisher	M1/70	48-0112-82
eFluor 450	CD45R (B220)	ThermoFisher	RA3-6B2	48-0452-82
FITC	CD40	BioLegend	HM40-3	102906
FITC	CD69	BioLegend	H1.2F3	104506
FITC	CD317 (BST2, PDCA-1)	BioLegend	927	127007, 127008
PE	CD3	BioLegend	17A2	100206
PE	CD45.1	BioLegend	A20	110708
PE	CD80	ThermoFisher	16-10A1	12-0801-82
PE	CD135 (Flt3)	ThermoFisher	A2F10	12-1351-83

PE	CD172a (SIRPα)	BioLegend	P84	144011
PE	IFNγ	BioLegend	W18272D	163503
PE/Cy7	CD45.2	BioLegend	104	109830
PE/Cy7	CD64 (FcγRI)	BioLegend	X54-5/7.1	139313, 139314
PE/Cy7	CD115 (CSF-1R)	BioLegend	AFS98	135523
PE/Cy7	CD274 (B7-H1, PD-L1)	BioLegend	10F.9G2	124314
PerCP/Cy5.5	CD3	BioLegend	17A2	100217
PerCP/Cy5.5	CD4	BioLegend	RM4-4	116012
PerCP/Cy5.5	CD19	Tonbo Bio	1D3	65-0193-U100
PerCP/Cy5.5	CD172a (SIRPα)	BioLegend	P84	144009
PerCP/Cy5.5	CD273 (B7-DC, PD-L2)	BioLegend	TY25	107218
PE/Cy7	IL-10	BioLegend	JES5-16E3	505025
APC	Ly-6A/E (Sca-1)	ThermoFisher	D7	17-5981-83
BV650	MHCII	BioLegend	M5/114.15.2	107641
PerCP/Cy5.5	NK-1.1	BioLegend	PK136	108727
BV785	Streptavidin	BioLegend	-	405249
-	TrueStain fcX(anti-mouse)	BioLegend	93	101320

3.3.7 Flow cytometry

Cell suspensions of mouse tissues were prepared in RPMI-1640 (Wisent) with 2% (v/v) fetal calf serum (FCS), 100μg/ml streptomycin and 100U/ml penicillin (Wisent). The cells were stained for surface-markers in PBS with 2% FCS for 20 minutes on ice, using antibodies and gating strategies listed below:

Table 3.3.7.1 Antibodies and other reagents used in the flow cytometry analyses.

Fluorophore	Target	Manufacturer	Catalog Number	Clone
AF488	GL7	BioLegend	144612	GL7
APC	CD21/CD35	Biolegend	123412	7E9
APC	CD86	BioLegend	105012	GL-1
APC	CD267/TACI	Invitogen	17-5942-82	ebio8F10-3
Biotin	IgG1	Southern Biotech	1070-08	polyclonal
BV421	CD138	BioLegend	142508	281-2
BV421	CD95/Fas	BD Bioscience	562633	Jo2
BV650	CD45R/B220	BioLegend	103241	RA3-6B2
BV785	Streptavidin	BioLegend	405249	n/a
FITC	KI67	eBioscience	11-5698-80	SolA15
FITC	CD23	Invitrogen	A15820	B3B4

Pacific Blue	IgD	BioLegend	405712	11-26c.2a
PE	Blimp-1	BioLegend	150005	5E7
PE	CD184/CXCR4	BioLegend	146505	L276F12
PE	IgM	Invitogen	12-5790-83	II/41
PE-Cy7	CD19	BioLegend	115520	6D5
PE-Cy7	CD21/CD35	Invitogen	13-0211-82	eBio8D9
PE-Cy7	CD38	Invitogen	25-0381-82	90
PerCPCy5.5	CD11b	eBioscience	45-0112-82	M1/70
PerCPCy5.5	CD4	BioLegend	116012	RM4-4
PerCPCy5.5	CD8a	BioLegend	100734	53-6.7
PerCPCy5.5	IgD	BioLegend	405709	11-26c
PerCPCy5.5	NK1.1	BioLegend	108727	PK136
PerCPCy5.5	Ter119	BioLegend	116228	Ly-76
PerCPCy5.5	CD19	Tonbo Biosciences	50-105-4943	1D3
PerCPCy5.5	CD45R/B220	BioLegend	103236	RA3-6B2
PerCPCy5.5	CD93	BioLegend	136512	AA4.1
eFluor506	Viability Dye	eBioscience	65-0866-18	n/a

Table 3.3.7.2 Flow cytometry gating strategies to identify B cell subpopulations in mouse tissues.

Cell Subsets	**Markers used for gating**
B cells	$B220^{+}$
Memory B cells	$B220^{+}$, $CD38^{+}$, $GL7^{-}$
Germinal centre (GC) B cells	$B220^{+}$, $CD95/Fas^{+}$, $GL7^{+}$
DZ GC B cells	$B220^{+}$, $CD95/Fas^{+}$, $GL7^{+}$, $CD86^{-}$, $CXCR4^{+}$
LZ GC B cells	$B220^{+}$, $CD95/Fas^{+}$, $GL7^{+}$, $CD86^{+}$, $CXCR4^{-}$
Plasmablasts/Plasma cells	Lin^{-} ($CD11b^{-}$, $TER119^{-}$, $CD4^{-}$, $CD8^{-}$, $NK1.1^{-}$), $CD138^{+}$, $TACI^{+}$
Plasmablast	Lin^{-} ($CD11b^{-}$, $TER119^{-}$, $CD4^{-}$, $CD8^{-}$, $NK1.1^{-}$), $CD138^{+}$, $TACI^{+}$, $CD19^{+}$, $B220^{+}$
Early Plasma cells	Lin^{-} ($CD11b^{-}$, $TER119^{-}$, $CD4^{-}$, $CD8^{-}$, $NK1.1^{-}$), $CD138^{+}$, $TACI^{+}$, $CD19^{+}$, $B220^{-}$
Mature Plasma cells	Lin^{-} ($CD11b^{-}$, $TER119^{-}$, $CD4^{-}$, $CD8^{-}$, $NK1.1^{-}$), $CD138^{+}$, $TACI^{+}$, $CD19^{-}$, $B220^{-}$
Plasmablast	Lin^{-} ($CD11b^{-}$, $TER119^{-}$, $CD4^{-}$, $CD8^{-}$, $NK1.1^{-}$), $CD138^{+}$, $TACI^{+}$, $CD19^{+}$, $B220^{hi}$, $Ki67^{+}$
Early Plasma cells	Lin^{-} ($CD11b^{-}$, $TER119^{-}$, $CD4^{-}$, $CD8^{-}$, $NK1.1^{-}$), $CD138^{+}$, $TACI^{+}$, $Blimp1^{+}$, $B220^{lo}$, $Ki67^{-}$

Late Plasma cells	Lin^{-} ($CD11b^{-}$, $TER119^{-}$, $CD4^{-}$, $CD8^{-}$, $NK1.1^{-}$), $CD138^{+}$, $TACI^{+}$, $Blimp1^{+}$, $B220^{-}$, $Ki67^{-}$
T1 Transitional B cells	$CD19^{+}$, $B220^{+}$, $CD93^{+}$, IgM^{+}, CD23-
T2 Transitional B cells	$CD19^{+}$, $B220^{+}$, $CD93^{+}$, IgM^{+}, $CD23^{+}$
T3 Transitional B cells	$CD19^{+}$, $B220^{+}$, $CD93^{+}$, IgM^{lo}, $CD23^{+}$
Follicular (FO) B cells	$CD19^{+}$, $B220^{+}$, $CD93^{-}$, IgM^{+}, $CD21^{+}$, IgD^{+}
FO I B cells	$CD19^{+}$, $B220^{+}$, $CD93^{-}$, IgM^{lo}, $CD21^{+}$, IgD^{+}
FO II B cells	$CD19^{+}$, $B220^{+}$, $CD93^{-}$, IgM^{hi}, $CD21^{+}$, IgD^{+}
Marginal Zone (MZ) B cells	$CD19^{+}$, $B220^{+}$, $CD93^{-}$, IgM^{hi}, $CD21^{hi}$, $CD23^{lo}$
MZ Precursor (MZP) B cells	$CD19^{+}$, $B220^{+}$, $CD93^{-}$, IgM^{hi}, $CD21^{hi}$, $CD23^{hi}$
B1a B cells	$CD19^{+}$, $B220^{lo}$, $CD43^{+}$, $CD5^{+}$
B1b B cells	$CD19^{+}$, $B220^{lo}$, $CD43^{+}$, $CD5^{-}$

Viability Dye eFluor® 506 (ThermoFisher Scientific) was used to discriminate dead cells. Compensation was performed with BD™ CompBeads (BD Biosciences). The data were acquired on BD Fortessa and analyzed with FACS Diva (BD Biosciences) or FlowJo (Tree Star) software.

3.3.8 Western blotting

Western blotting was performed as previously described [239], with cells lysed in RIPA buffer supplemented with protease and phosphatase inhibitors (ThermoFisher Scientific). Protein concentration was measured using the BCA assay (ThermoFisher Scientific) on an EnSpire 2300 multilabel reader (PerkinElmer). Protein lysate samples were boiled in Laemmli buffer and 1.25% β-mercaptoethanol (Sigma-Aldrich) before loading onto gels, alongside Precision Plus Kaleidoscope standards (Bio-Rad). Upon gel-to-membrane transfer, nitrocellulose membranes (GE Healthcare) were blocked with 5% milk in TBS-T and probed with antibodies against MYSM1 (EPR18657, Abcam) and β-Actin (D6A8, Cell Signaling Technology) at 4°C overnight, followed by secondary antibodies Abcam - goat anti-rabbit IgG H&L (HRP) - ab6721 horseradish

peroxidase (HRP)-conjugated or Rockland - Rabbit TrueBlot: anti-rabbit IgG HRP - 18-8816-31 at room temperature for 1 hour, with TBS-T washes after each incubation. Protein bands were detected using Western Lightning Plus-ECL (PerkinElmer) and HyBlot CL autoradiography films (Harvard Apparatus Canada).

3.3.9 RNA isolation and RT-qPCR

RNA was extracted using the MagMAX™ Total RNA Isolation Kit (Invitrogen, Thermo Fisher Scientific) or the EZ-10 DNAaway RNA kit (Bio Basic), according to manufacturer's protocol, and quantified with NanoDrop (ThermoFisher Scientific). cDNA was prepared using the Moloney murine leukemia virus (MMLV) reverse-transcription kit and quantitative PCRs run on a StepOnePlus instrument with PowerSYBR master mix (all from Thermo Fisher Scientific). Primers were purchased from Integrated DNA Technologies, as shown below:

Table 3.3.9.1 Primers for RT-qPCR analyses.

Target	Forward primer	Reverse primer
Cd274	TGCGGACTACAAGCGAATCACG	CTCAGCTTCTGGATAACCCTCG
Il10	TGGAGCAGGTGAAGAGTGATTTTA	CACTGCAGGTGTTTTAGCTTTTCA
Il12b	GGCTGGTGCAAAGAAACATGGACT	AGAGACGCCATTCCACATGTCACT
Il1b	CAGGATGAGGACATGAGCACC	CTCTGCAGACTCAAACTCCAC
Il6	CATGTTCTCTGGGAAATCGTG	TTCTGCAAGTGCATCATCG
Mysm1	TGTGGATGTGGAAGGAGATG	TGGTGCTATCCAGAGTCCAA
Tnfa	CGGACTCCGCAAAGTCTAAG	CAGTTCTATGGCCCAGACCCT
Gapdh	TGCAGTGGCAAAGTGGAGAT	ACTGTGCCGTTGAATTTGCC

3.3.10 In vitro fluorescence catalytic activity assay

Genes for wild-type and mutated mouse MYSM1 were sub-cloned into pFastBac vectors, which contain an N-terminal hexahistidine tag. The D660N mutation was introduced using standard site-directed mutagenesis protocols. MYSM1 proteins were expressed in Sf9 cells, infected with

recombinant baculovirus and grown at 27℃ for ~66 hours. Proteins were purified by sonicating the cells, followed by Ni-NTA affinity, Mono-Q and size exclusion chromatography (Superdex 200i). The final yield was ~0.8 mg/ L of cells.

Enzymatic assays were conducted in assay buffer comprised of 20 mM Tris pH 8.1, 100 mM NaCl, 0.01% BSA, 1 mM DTT at room temperature in 96-well low binding black plates. 12.5µL of either MYSM1 or MYSM1^{D660N} at 300 nM was added to the 96-well plate followed by the addition of 12.5µL of serially diluted substrate (0.02 - 40 µM) and immediately placed into a fluorescence spectrophotometer with excitation/emission wavelengths set to 485/535 nm, respectively.

3.3.11 RNA sequencing

RNA-seq protocols were as previously described [223, 264]. Briefly, RNA yields and quality were assessed using Bioanalyzer (Agilent). rRNA depletion and library preparation were performed using the KAPA RNA HyperPrep Kit with RiboErase (Roche). The libraries were sequenced on an Illumina Novaseq 6000 in a paired-end 100 bp configuration aiming for 50x10^6 reads per sample. The quality of the sequencing reads was confirmed using the FastQC tool (Babraham Bioinformatics), and low-quality bases were trimmed from the read extremities using Trimmomatic v.0.33 [265]. The reads were then mapped to the mouse UCSC GRCm39/mm39 reference genome assembly using Hisat2 v2.2.1 [266, 267, 268]. Gene expression was quantified by counting the number of uniquely mapped reads with featureCounts using default parameters [269]. We retained genes that had an expression level of at least 5 counts per 10^6 reads (CPM) in at least 3 of the samples [270]. TMM normalization and differential gene expression analyses were conducted using the edgeR Bioconductor package [271]. Dimension reduction analysis was performed using the Principal Component and Partial Least Squares regression method [272]. Pairwise comparisons were

performed between genotypes or between treatments, and genes with changes in expression ≥ |1.5| fold and Benjamini-Hochberg adjusted *p* values ≤ 0.01 were considered significant. Gene ontology (GO) enrichment analyses on differentially expressed gene clusters were performed with DAVID Bioinformatics Resources 6.8 [273], and Gene Set Enrichment Analysis (GSEA) was performed with GSEA tool v4.3.2 using MSigDB v2022.1 with default configuration and permutation within gene sets [274].

3.3.12 Statistical analyses

Statistical analyses used Prism 7.01 (GraphPad Inc.), with Student's two-tailed *t*-test for two datasets and ANOVA for multiple comparisons; $p<0.05$ was considered significant.

Chapter 4: Results

4.1 Role of BAP1 in the Development of B Lymphocytes

4.1.1 Loss of BAP1 impairs B cell development, viability, and cell cycle progression

In previous studies, we investigated the role of BAP1 in B lymphocyte development by generating and characterizing the *Bap1*$^{fl/fl}$ *mb1*-Cre mouse strain[223], where BAP1 depletion occurs specifically in B cells upon *mb1* expression starting from the pre-pro-B cell stage[254]. Through flow cytometry analysis, we found that the loss of BAP1 resulted in a systemic reduction in B cell numbers[223]. Precisely, multiple splenic B cell subpopulations, including transitional B cell subsets (T2-3), follicular B cell subsets (FOL I-II), and marginal zone progenitor (MZP) B cells, were depleted in *Bap1*$^{fl/fl}$ *mb1*-Cre mice[223]. Moreover, chimeric analysis confirmed the cell intrinsic role of BAP1 in B cells[223]. Consistently, we observed a significant reduction in both the frequencies and the absolute numbers of large pre-B cells and mature B cells, as well as an expansion of pro-B cells in the bone marrow of *Bap1*$^{fl/fl}$ *mb1*-Cre mice compared to the controls[223]. This indicates a cell intrinsic requirement for BAP1 for normal progression of B cell development. Further analysis using Annexin V staining revealed an increase in the proportion of late apoptotic/necrotic cells within the large pre-B cells, indicating impaired cell viability[223]. Likewise, Ki67 and histone H3S10p staining of bone marrow cells from the *Bap1*$^{fl/fl}$ *mb1*-Cre mice demonstrated a significant increase in the proportion of G0 cells and a corresponding decrease in G1-S-G2 cells within the large pre-B, small pre-B, immature, and mature B cell subpopulations, indicating that the loss of BAP1 impairs cell cycle progression[223]. Furthermore, RNA-Seq transcriptomic analysis of pre-B and immature B cells from the *Bap1*$^{fl/fl}$ *mb1*-Cre mice revealed that the dysregulated genes resulted from BAP1 deficiency are enriched in biological pathways including “cell proliferation”, “DNA replication”, and “cell division” (Figure 4.1.1) [223]. Thus, we proposed that BAP1 regulates B cell

development, possibly by modulating B cell proliferation and cell cycle progression. In the current study, we sought to further explore the mechanistic role of BAP1 in B cells.

Figure 4.1.1 RNA-Seq analysis of *Bap1*-deficient pre-B and immature B cells.

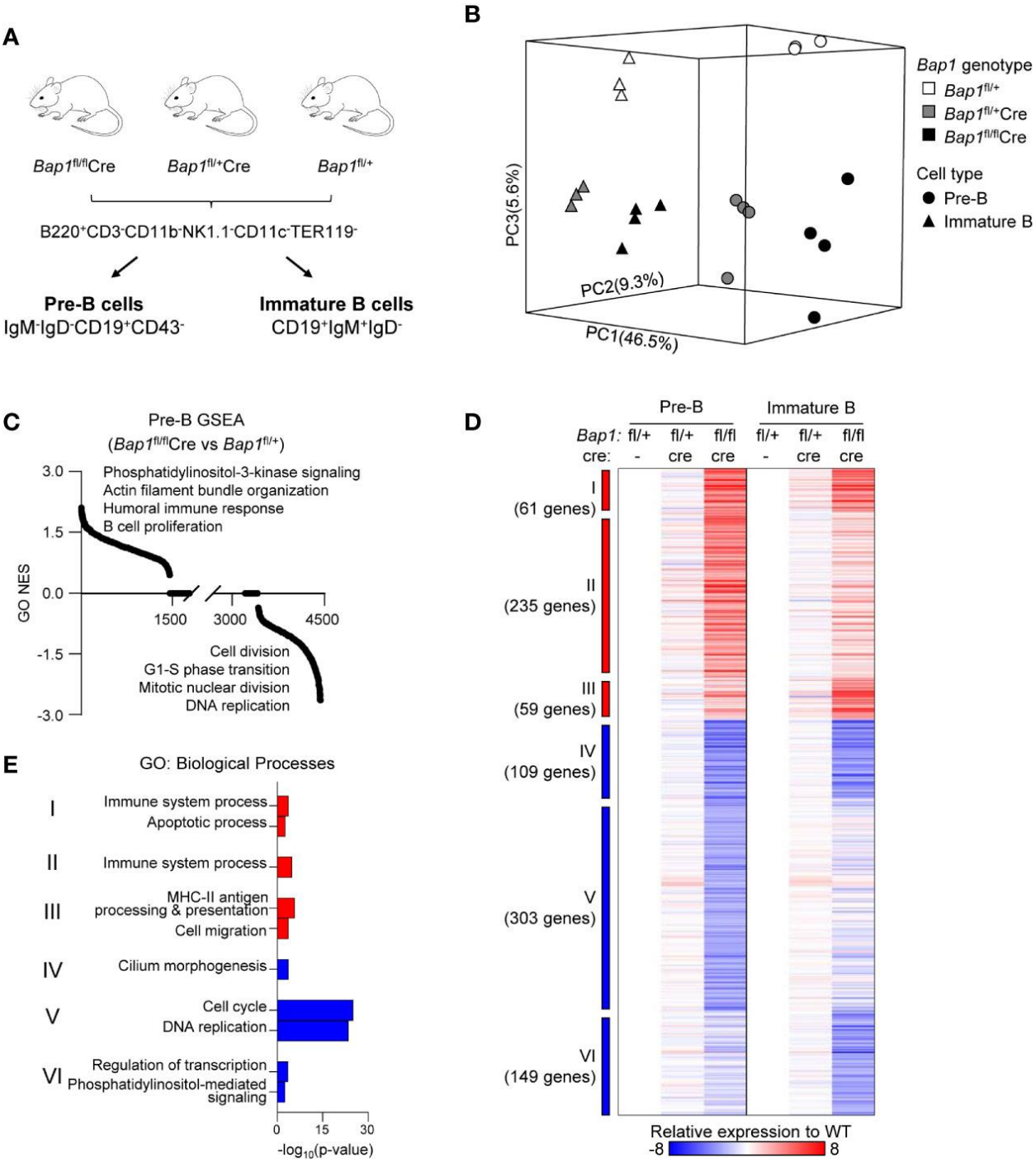

Data presented are from 3-4 mice per genotype. **(A)** Schematic representation of the mouse genotypes and cell sorting protocols for the RNA-Seq experiment. **(B)** 3D principal component analysis model demonstrating the gene expression profiles of each RNA-Seq sample: differences between cell types are described by principal component 1 (PC1, 46.5% variability) and differences between genotypes are described by PC2 and PC3 (9.3% and 5.6% variability, respectively). **(C)** Normalized enrichment scores (NES) of 4,436 pre-established biological processes expression signatures used in the gene set enrichment analysis (GSEA). **(D)** Heat map displaying 916 significantly dysregulated genes when comparing *Bap1*$^{fl/fl}$*Cre* and control *Bap1*$^{fl/+}$ cells. The significance threshold is fold change ≥ 1.5 and False Discovery Rate (FDR) ≤0.01. Relative gene expression to the average of pre-B and immature B control *Bap1*$^{fl/+}$ groups are used to generate the heat map. Genes are grouped into Clusters I-VI based on their expression pattern across the two cell types and three genotypes. **(E)** Gene ontology (GO) enrichment analysis on the genes from the Clusters I-VI described in **(D)**. The top two enriched biological processes terms per cluster are displayed.

4.1.2 Impaired cell proliferation in BAP1-deficient B cell precursor cell lines

To further analyze the impact of BAP1 loss on B cell survival and proliferation and the molecular mechanisms involved, *Bap1* gene was targeted with CRISPR/Cas9 in the B cell precursor cell line Ba/F3. Two gRNAs were designed to target *Bap1* exons 4 and 5 that encode the key N-terminal catalytic domain of the protein (Figure 4.1.2A). Cell clones were screened by PCR for deletions within the *Bap1* locus, and six clones were selected and further analyzed by Western blotting to confirm the loss of BAP1 protein (Figure 4.1.2B). There was no defect in the viability of *Bap1*$^{\Delta/\Delta}$ cell lines, as demonstrated by equivalent frequencies of live, early apoptotic, and late apoptotic/necrotic cells between the *Bap1*$^{\Delta/\Delta}$ and control cell cultures (Figure 4.1.2C). The effect of BAP1 loss on the proliferation of the B cell lines was further analyzed with two approaches: a colorimetric alamarBlue assay conducted in bulk cell population, and a flow cytometric CFSE-dilution assay providing proliferation data at single cell resolution. Both approaches demonstrated a reduction in cell proliferation for all the *Bap1*$^{\Delta/\Delta}$ clones tested, reaching statistical significance for the majority of the clones (Figure 4.1.2D-F). This further confirmed the role of BAP1 in the

regulation of B cell proliferation and indicated the *Bap1*$^{\Delta/\Delta}$ Ba/F3 cell lines as a model for further analyses of the molecular mechanisms involved.

Figure 4.1.2 Impaired proliferation in CRISPR/Cas9 BAP1-deficient B cell precursor cell line Ba/F3.

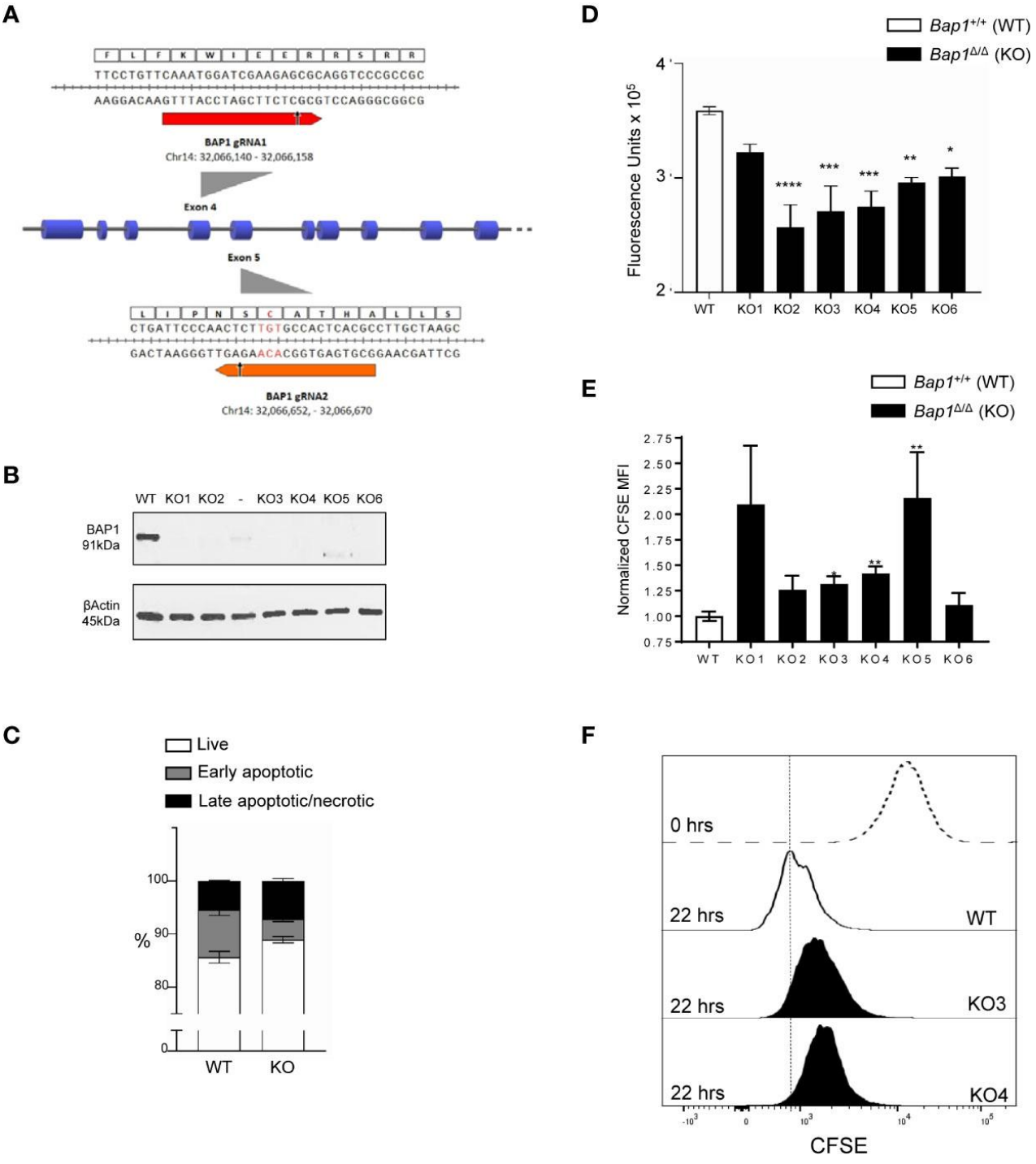

(A) gRNA targeted cleavage on *Bap1* gene sequence. gRNA1 and gRNA2 were designed to target exons 4 and 5 of mm9 *Bap1* gene, respectively. The gRNA-targeted DNA fragments of exons 4 and 5, as well as the corresponding amino acids of BAP1 protein are displayed in detail. Arrows indicate predicted sites of Cas9 mediated double strand break (DSB). Both the cleavage sites are upstream of the key catalytic residue of BAP1 protein Cys-91 (red). **(B)** Loss of BAP1 protein expression in $Bap1^{\Delta/\Delta}$ cell line clones 1-6, demonstrated with Western blotting, using β-Actin as the loading control. Additional clone with residual BAP1 expression, analyzed on the gel between clones 2 and 3, was excluded from subsequent analysis. **(C)** Cell viability analysis with flow cytometry, staining the cells with Annexin V and Viability Dye, to identify live ($AnxV^-V506^-$), early apoptotic ($AnxV^+V506^-$), and late apoptotic/necrotic ($AnxV^+V506^+$) cells; consolidated data from 6 $Bap1^{\Delta/\Delta}$ cell clones is presented. **(D)** Cell proliferation analysis with colorimetric alamarBlue assay, demonstrating reduced proliferation of $Bap1^{\Delta/\Delta}$ cell clones. Data presented is from one experiment and was reproduced in a second independent experiment. **(E)** Cell proliferation analyses with a flow cytometry based CFSE-dilution assay, gating on live cells. Consolidated data from two independent experiments is presented, normalizing the CFSE mean fluorescence intensity (MFI) of $Bap1^{\Delta/\Delta}$ cell clones in each experiment to their corresponding WT control. In **(C–E)**, bars represent mean ± SEM; statistical analyses were performed using ANOVA; *p < 0.05, **p < 0.01, ***p < 0.001, ****p < 0.0001, or not significant if significance is not indicated. **(F)** Representative histograms showing CFSE fluorescence of WT and $Bap1^{\Delta/\Delta}$ clones KO3 and KO4, at 22 hours of culture, gating on live cells. A histogram showing CFSE fluorescence of WT cells prior to culture (0 hours, dotted line) is included as a control.

4.1.3 Mapping BAP1 binding across the B cell genome

To identify the genes directly regulated by BAP1, we mapped the genome-wide DNA-binding sites of BAP1 by ChIP-Seq. The experiment was carried out in the B cell precursor cell line Ba/F3: a) using wild type cells with an anti-BAP1 antibody, and b) using cells stably expressing 3xFLAG-tagged BAP1 protein with an antibody against the FLAG epitope[221]. We identified a total of 13,163 BAP1 binding sites (or peaks) across the genome, with a very high concordance between the two datasets (Figure 4.1.3A). Ordering the BAP1-binding sites based on their distance to the nearest gene transcription start site (TSS), 74% were located within 1kb of the nearest TSS and were therefore classified as gene-proximal (≤1kb to TSS, 9,680 sites), and the remaining 26% were classified as gene-distal (>1kb to TSS, 3,483 sites). To gain functional insight into the transcriptional targets of BAP1 in B cells, gene ontology analysis was performed on the genes in the vicinity of each BAP1 binding site using the Genomic Regions Enrichment of Annotations

Tool (GREAT)[250]. This demonstrated that the genes near the gene-proximal BAP1 binding sites were highly enriched for biological process ontology terms “cell cycle” and “DNA metabolic process” (Figure 4.1.3B), suggesting the direct involvement of BAP1 in the regulation of the transcriptional programs required for B cell proliferation.

Figure 4.1.3 ChIP-Seq analysis of BAP1 binding sites and the impact of BAP1 loss on histone H2AK119ub levels, in the B cell precursor cell line Ba/F3.

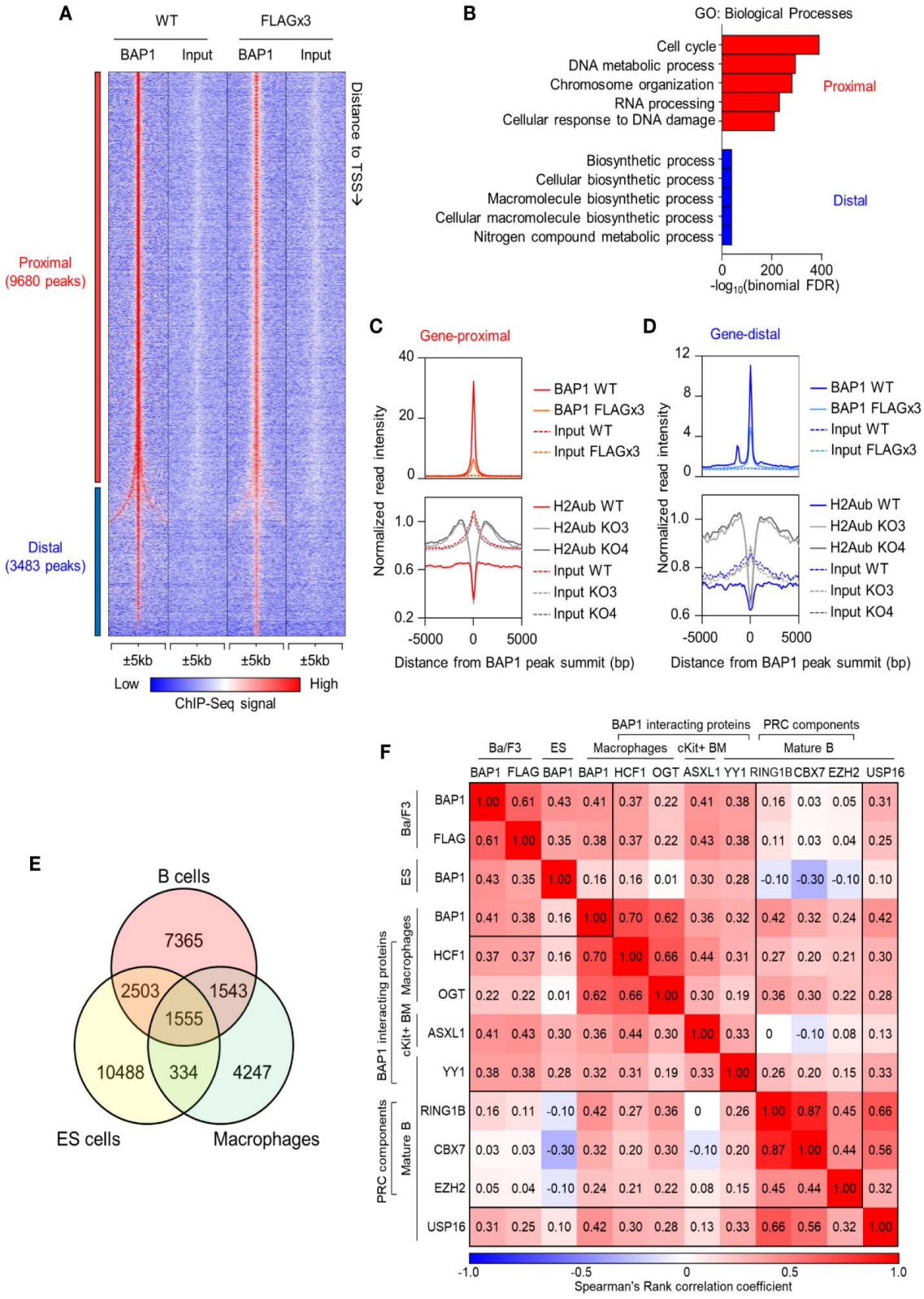

(A) Heat map showing the tag density of 13,163 BAP1 binding sites identified in ChIP-Seq experiments from wild type Ba/F3 B cell lineage precursor cells (WT) and Ba/F3 cells stably expressing triple-FLAG-tagged BAP1 (FLAG x3). The sites are ranked based on their distance to the nearest gene transcriptional start site (TSS). Gene-proximal sites are defined as having the nearest gene TSS within 1kb, and gene-distal sites are defined as having the nearest gene TSS further than 1kb. **(B)** Gene Ontology analysis of the nearest genes to each BAP1 binding site, performed on the GREAT website[250]. The -$\log_{10}$(binomial FDR) value for each term is plotted. **(C, D)** Histograms showing the average normalized tag densities of BAP1 and histone H2AK119ub around the gene-proximal **(C)** and gene-distal **(D)** BAP1 binding sites. The tag densities of BAP1 are determined from the ChIP-Seq data of WT and FLAG x3 Ba/F3 cells, and the tag densities of histone H2AK119ub are from the ChIP-Seq data of WT and two *Bap1*$^{\Delta/\Delta}$ (KO) Ba/F3 cells lines. **(E)** Venn diagram comparing the BAP1 binding sites identified in our ChIP-Seq datasets from B cells with BAP1 binding sites identified in previous studies in ES-cells and macrophages[221, 278]. **(F)** Analyses of the co-localization of BAP1 binding sites identified in our ChIP-Seq data with the binding sites for other functionally related transcriptional regulators in previously published studies. Heatmap displaying the Spearman rank correlations between all pairwise comparisons for the BAP1 ChIP-Seq data and the ChIP-Seq datasets of other functionally related transcriptional regulators. Spearman correlations were calculated using the normalized tag densities (± 100bp around peak summit) across the entire set of binding sites identified from the ChIP-Seq experiments. The BAP1 ChIP-Seq from Ba/F3 cells represents our datasets and is described in **(A, B)**. The others are public datasets, downloaded and re-analyzed using our pipeline: BAP1 ChIP-Seq from ES cells[278], the BAP1, HCF1, and OGT ChIP-Seq from bone marrow derived macrophages[221], the ASXL1 ChIP-Seq from c-Kit^{+} bone marrow cells[279], the RING1B, CBX7, EZH2, and USP16 ChIP-Seq from quiescent CD43^{-} resting splenic B cells[280], and the YY1 ChIP-Seq from follicular B cells (CD19^{+}AA4^{-}CD21^{lo}CD23^{hi})[281]; all datasets are from mouse.

4.1.4 <u>BAP1 functions as a deubiquitinase for histone H2AK119ub in B cells</u>

To gain insights into the mechanisms of BAP1 transcriptional and epigenetic regulation in the B cell lineage, we performed ChIP-Seq analysis for the repressive histone mark H2AK119ub, comparing the *Bap1*$^{\Delta/\Delta}$ and control Ba/F3 B cell precursor cell lines. Two clones of *Bap1*$^{\Delta/\Delta}$ cells were selected, KO3 and KO4, based on full loss of BAP1 protein and a proliferation defect representing an average of that seen across all the available clones (Figures 4.1.2D, E). The ChIP-Seq data demonstrated that on average the genomic regions surrounding the BAP1 binding sites had low levels of histone H2AK119ub in wild type Ba/F3 cells, consistent with their predominant localization at promoters of expressed genes (Figures 4.1.3C, D). Importantly, the levels of histone H2AK119ub at these BAP1-bound genomic sites were significantly elevated in *Bap1*$^{\Delta/\Delta}$ relative

to wild-type cells (Figures 4.1.3C, D). This indicated the non-redundant role of BAP1 as a DUB for histone H2AK119ub in the B cell lineage, as previously also reported for other cell types[194, 200, 209, 215].

To compare the roles of BAP1 in transcriptional regulation in B cells and other cell types, we consolidated our BAP1 ChIP-Seq and previously published BAP1 ChIP-Seq datasets, with macrophages and ES cells being the source of the available data[221, 278]. Spearman rank correlation analysis was performed for all pairwise comparisons. The results demonstrate a considerable overlap in the genomic location of BAP1 binding across the cell types, and also highlight a subset of BAP1 binding sites potentially specific to B cells (Figures 4.1.3E, F). Genes nearest to each of the "shared" and the "cell-type specific" subsets of BAP1 binding sites were further analyzed for enrichment of biological process GO-terms, demonstrating shared BAP1 binding at the genes involved in many housekeeping biological processes, including "cell-cycle", across the different cell lineages.

To gain mechanistic insights into BAP1 cross-talk with other transcriptional regulators, we further consolidated our BAP1 ChIP-Seq with ChIP-Seq datasets for BAP1-associated transcriptional regulators ASXL1[194, 200, 209, 215], HCF1[197, 205, 211], OGT[204, 221], and YY1[197], for components of PRC complexes RING1B, CBX7, and EZH2[141, 143, 282] and with a dataset for DUB USP16[280], using data from murine B cells (where available) and also datasets from macrophages and hematopoietic progenitors[221, 248, 280, 283]. A significant correlation in genomic localization was observed between BAP1 and BAP1-interacting proteins ASXL1, HCF1, YY1 and to a lesser extent OGT (Figure 4.1.3F), suggesting that BAP1 acts in cooperation with these proteins in the B cell lineage, as in

other cell types. Weak correlation was observed between the genomic localization of BAP1 and the RING1B catalytic subunit of the histone H2A ubiquitin ligase PRC1, and no correlation was seen with the PRC2 catalytic subunit EZH2 (Figure 4.1.3F), supporting the antagonistic roles of BAP1 and PRCs in transcriptional regulation. Interestingly, a positive correlation was observed between BAP1 and USP16, indicating that these DUBs may target some common genomic locations, and suggesting cooperative or complementary functions (Figure 4.1.3F).

4.1.5 Exploring BAP1 Regulated Transcriptional Programs in B Cell Development

We consolidated our ChIP-Seq and RNA-Seq datasets and identified in total 591 genes that had BAP1 binding sites in their proximity and were dysregulated in expression in BAP1 deficiency. Repeating the analysis for each cluster of genes dysregulated in BAP1-deficient B cells, we observed a strong and significant overrepresentation of BAP1 binding sites at the genes in the downregulated Clusters IV-VI (Figure 4.1.4A, Figure 4.1.1D, E). In particular, the strongest overrepresentation of genes with BAP1 binding sites was seen for Cluster V, enriched for the genes involved in cell cycle progression and downregulated in expression in BAP1-deficient pre-B cells (Figure 4.1.4A, Figure 4.1.1D, E). Overall, this demonstrates a strong concordance between our RNA-Seq and ChIP-Seq datasets, consistent with the primary function of BAP1 as a transcriptional activator. The strong correlation between BAP1 occupancy, histone H2AK119ub levels, and gene expression suggests a direct role of BAP1 in the regulation of genes essential for normal cell cycle progression in pre-B cells.

Gene ontology (GO) analysis further confirmed that the set of genes in proximity of BAP1 binding sites and downregulated in expression in BAP1-deficient pre-B cells was strongly enriched for

GO-terms “cell cycle” and “DNA replication” (Cluster V, Figure 4.1.4B). Notably, this gene set included the key genes encoding: regulators of G1/S cell cycle transition (*Ccne2*, *Cdc25a*) and the initiation of DNA replication (*Cdc6*, *Cdc45*, *Cdt1*); components of the core DNA replication machinery (*Pola1*, *Pold1*, *Pole*, *Pole2*, *Pcna*, *Rfc1*, *Dna2*, *Lig1*, *Mcm2-7*) and enzymes involved in deoxyribonucleotide synthesis (*Rrm1*, *Rrm2*); regulators of G2/M cell cycle transition (*Bub1*, *Cdc25a*, *Espl1*, *Plk1*), mitotic spindle dynamics (*Haus4, Haus5*, *Ndc80*, *Kif2c*, *Kif23*, *Kif11*, *Kntc1*), and cytokinesis (*Anln*, *Ect2*, *Prc1*); key regulators of chromatin structure through the S and M phases of the cell cycle (*Esco2*, *Ncapd2*, *Ncapg2*, *Uhrf1*); and several general biomarkers of cell proliferation (*Foxm1*, *Mki67*) (Figure 4.1.4C). Overall, our data suggests a direct role of BAP1 in the regulation of the transcriptional programs of cell proliferation, linked to its requirement for cell cycle progression in pre-B cells and for normal B cell development.

To gain insights into the putative mechanisms through which BAP1 may regulate the transcriptional programs of cell cycle progression in B cell development, we assessed the levels of the repressive histone mark H2AK119ub in *Bap1*$^{\Delta/\Delta}$ relative to control Ba/F3 B cell precursor cell lines from our ChIP-Seq data, specifically focusing on the BAP1 binding sites within the promoters Cluster V genes downregulated in expression in BAP1 deficient pre-B cells and assigned GO-terms “cell cycle”, “DNA replication”, and “cell division” (69 genes). Importantly, a significant increase in histone H2AK119ub levels was observed in *Bap1*$^{\Delta/\Delta}$ relative to control cells at these promoters (Figure 4.1.4D, E). This strongly suggests that BAP1 regulates the expression of the genes essential for cell proliferation and cell cycle progression in B cell development at least in part *via* the deubiquitination of histone H2AK119ub.

In summary, we previously analyzed the role of BAP1 in B cells using the *Bap1*$^{fl/fl}$ mb1-Cre mouse model, which has a selective loss of BAP1 throughout the B cell lineage, and demonstrated the cell-intrinsic requirement for BAP1 in the normal progression of B cell development [223]. In the current study, we established BAP1's role as a DUB for histone H2AK119ub in the regulation of the transcriptional programs of cell proliferation in pre-B cells [223].While BAP1 remains highly expressed throughout the B cell lineage [284], its role in the regulation of B cell activation and humoral immune response remains unknown and would be the focus of our next step.

Figure 4.1.4 BAP1 in the regulation of genes involved in cell proliferation and cell cycle progression in pre-B cells.

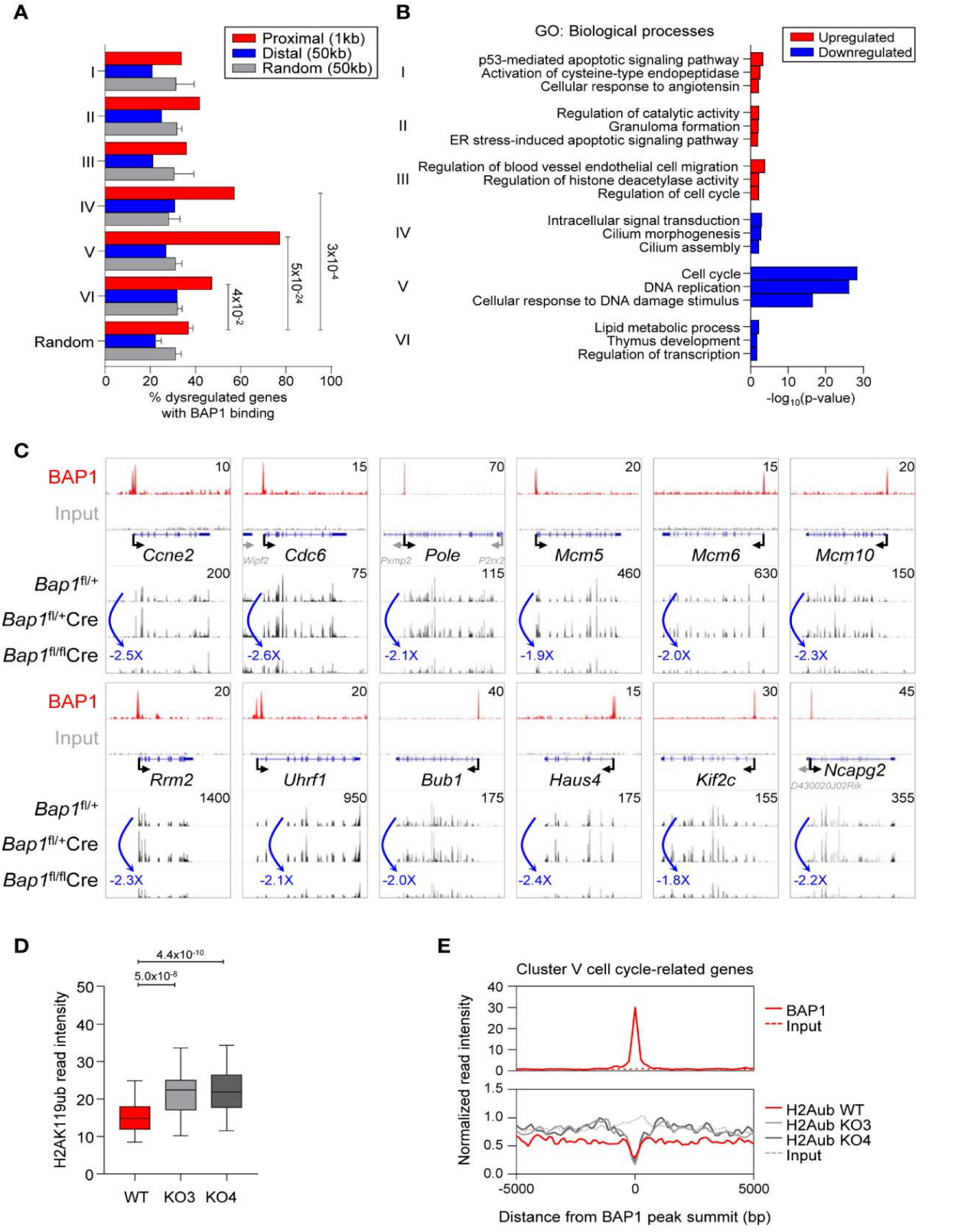

(A) Consolidation of the RNA-Seq and ChIP-Seq datasets, described in Figure 4.1.1 and 4.1.3, showing the percentages of genes dysregulated in expression in *Bap1*$^{fl/fl}$*Cre* cells with at least one BAP1 binding site within the indicated range of their TSS. Analysis is performed for each of the Cluster I-VI of the genes dysregulated in *Bap1*$^{fl/fl}$*Cre* cells, as defined in Figure 4.1.1D. The random genes cluster consists of ten groups of 300 genes randomly selected from 24,421 genes in the mm9 genome. The random binding sites consist of ten groups of 10,000 genomic locations randomly selected from the mm9 genome. Fisher Exact Test is used to calculate the *p*-values. **(B)** Gene ontology (GO) enrichment analysis for the Clusters I-VI genes, dysregulated in expression in *Bap1*$^{fl/fl}$*Cre* cells, and containing a proximal or distal BAP1 binding site. Top three enriched biological process terms per Cluster are displayed. **(C)** Genomic snapshots of selected genes that represent the putative direct transcriptional targets of BAP1 in pre-B cells. The genes are selected from Cluster V genes that are downregulated in expression in *Bap1*$^{fl/fl}$*Cre* pre-B cells, carry a proximal or distal BAP1 binding site, and are functionally linked to cell proliferation and cell cycle progression. ChIP-Seq tracks for BAP1 and input DNA are shown on the top two lanes. The gene feature track is shown in the middle. Averaged RNA-Seq tracks for pre-B cells are in the bottom three lanes, with fold changes comparing expression levels in *Bap1*$^{fl/fl}$*Cre* and control *Bap1*$^{fl/+}$ samples indicated. The maximum data range of each track is indicated at the top-right corner of the track. **(D)** Box plot showing histone H2AK119ub read intensities ±2.5kb to BAP1 binding sites near putative BAP1-regulated Cluster V genes, functionally linked to cell proliferation and cell cycle progression; (GO terms: GO:0007049 ~cell cycle; GO:0006260 ~DNA replication; GO:0051301 ~cell division; mmu04110: Cell cycle; and/or mmu03030: DNA replication, 69 genes in total). The Mann-Whitney U test was used to calculate the *p*-values. **(E)** Histograms showing the average normalized read intensities of BAP1 and histone H2AK119ub at the BAP1 binding sites proximal to the select subset of Cluster V genes, functionally linked to cell proliferation and cell cycle progression, as specified above. The read intensities of BAP1 are determined from the ChIP-Seq data of WT and FLAG x3 Ba/F3 cells, and the read intensities of histone H2AK119ub are from the ChIP-Seq data of WT and two *Bap1*$^{\Delta/\Delta}$ (KO) Ba/F3 cell lines.

4.2 Role of BAP1 in B cell mediated immune response

4.2.1 B-cell specific loss of BAP1 results in impaired antibody production

In previous studies, we hypothesized that BAP1 may function as an essential transcriptional regulator of B cell mediated immune response, and characterized the *Bap1*$^{fl/fl}$ mb1-Cre mouse model, in which BAP1 is specifically depleted throughout the B cell lineage[223]. We observed significant reductions in antibody titres (including IgM isotype and class-switched IgG1, IgG2c, and IgG3 isotypes) in the serum of naïve *Bap1*$^{fl/fl}$ mb1-Cre mice compared to *Bap1*$^{fl/+}$ and *Bap1*$^{fl/+}$ mb1-Cre control mice, either at the naïve state or following primary and boost immunizations (Figure 1.7.3). This indicates that BAP1 expression in the B cell lineage is crucial for the induction of B cell mediated immune response. Moreover, as mentioned in the previous sections, *Bap1*$^{fl/fl}$ mb1-Cre mice lack BAP1 expression throughout the B cell lineage, resulting in impaired B cell development and reduced B cell numbers in lymphoid organs [223], which could in part account for the impaired antibody production in these mice. Hence, in this study, our objective is to test the direct role of BAP1 in the regulation of B cell mediated immune response, independently of its functions in B cell development.

4.2.2 Cell-intrinsic role of BAP1 in mature activated B cells in humoral immune response

To test the direct regulatory role of BAP1 in B cell mediated immune response while minimizing the influence of its functions in B cell development, we generated the *Bap1*$^{fl/fl}$ Cγ1-Cre mice, with Cre expression driven from the IgG1 heavy chain locus and Cre activity restricted to the activated, germinal centre (GC), and downstream B cell populations [255]. In contrast to the *Bap1*$^{fl/fl}$ mb1-Cre mice [223], naïve *Bap1*$^{fl/fl}$ Cγ1-Cre mice had normal numbers of splenic pre-GC B cells, including the transitional, follicular, and marginal zone subsets (Figure 4.2.1). At the same time, the effective

Cre-mediated *Bap1*^{fl} to *Bap1*$^{\Delta}$ allele conversion was demonstrated by PCR-genotyping of the genomic DNA from *ex vivo* stimulated *Bap1*$^{fl/fl}$ Cγ1-Cre and control *Bap1*$^{+/+}$ Cγ1-Cre B cells (Figure 4.2.2A-B). Furthermore, RNA-seq analyses of splenic *Bap1*$^{fl/fl}$ Cγ1-Cre GC B cells demonstrated a strong reduction in the transcript reads mapping to the *Bap1* floxed exons 6-12, as compared to the GC B cells from mice of control *Bap1*$^{+/+}$ Cγ1-Cre genotype (Figure 4.2.2C-D).

Cohorts of naïve *Bap1*$^{fl/fl}$ Cγ1-Cre mice were analyzed for total serum antibody levels and demonstrated a significant reduction in IgG1 but not IgM titres relative to the *Bap1*$^{+/+}$ Cγ1-Cre control group (Figure 4.2.3A). Further cohorts of *Bap1*$^{fl/fl}$ Cγ1-Cre and control *Bap1*$^{+/+}$ Cγ1-Cre mice were immunized, either subcutaneously with PE/CFA or intravenously with sheep red blood cells (SRBCs) and analyzed for antigen specific antibody titres over a time-course post-prime and post-boost immunization. A strong reduction in the antigen-specific antibody levels in *Bap1*$^{fl/fl}$ Cγ1-Cre mice relative to the control *Bap1*$^{+/+}$ Cγ1-Cre group was observed across both immunization models and most time-points (Figure 4.2.3B-E). Overall, these findings demonstrate the direct and cell intrinsic role of BAP1 in the induction of B cell mediated immune response, independent of its previously reported functions in B cell development [223].

Figure 4.2.1 Analysis of splenic B cell populations in naïve *Bap1*$^{fl/fl}$ Cγ1-Cre mice.

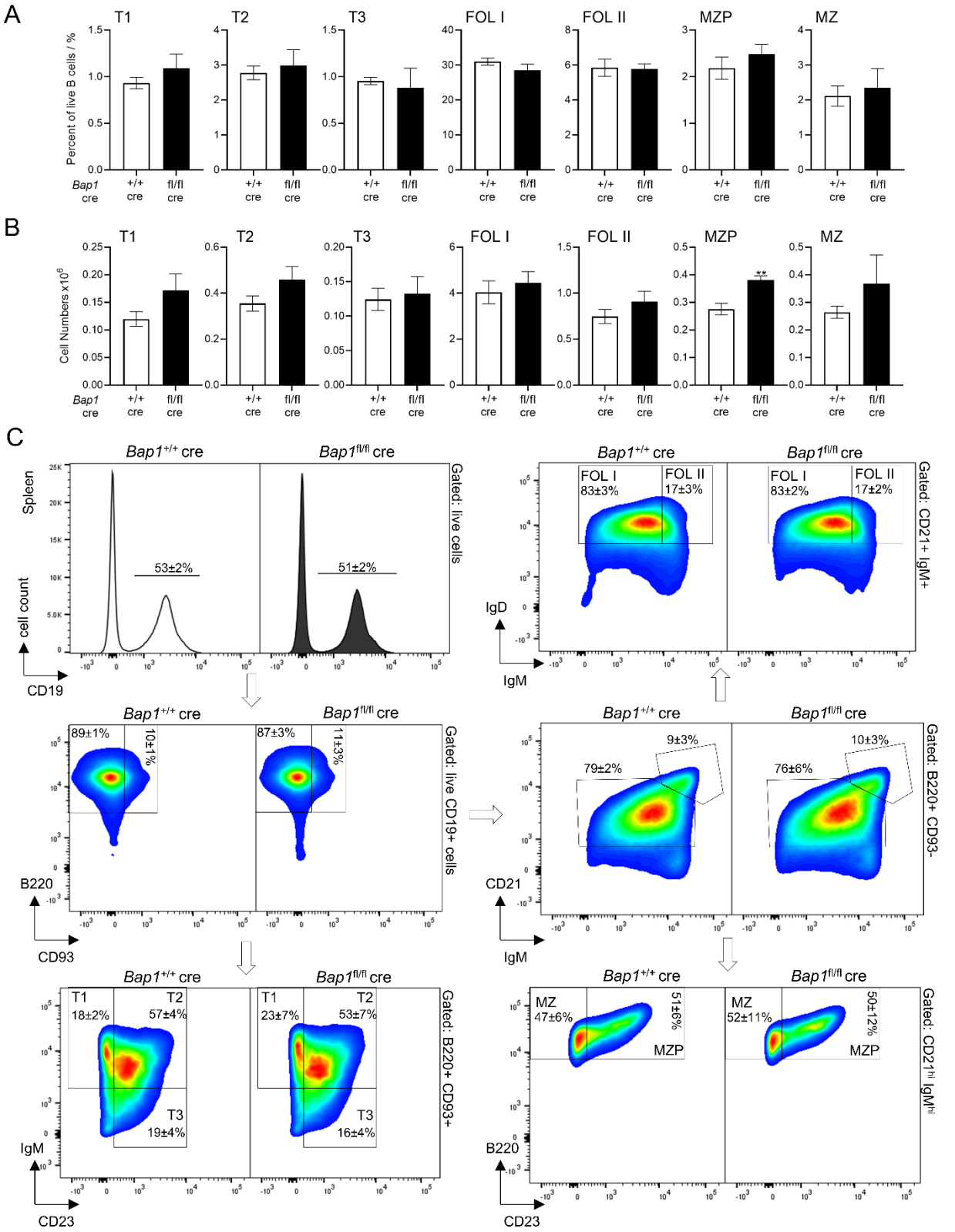

(A-B) Quantification of transitional T1, T2, and T3, follicular FOL I and FOL II, marginal zone progenitor (MZP) and marginal zone (MZ) B cell population in the spleen of *Bap1*$^{fl/fl}$ Cγ1-Cre and control *Bap1*$^{+/+}$ Cγ1-Cre mice, presented **(A)** as a percentage of live CD19^{+} B cell lineage splenocytes, and **(B)** as an absolute cell number per mouse spleen. Cells are gates as live CD19^{+} B cells, followed by B220^{+}CD93^{+}IgM^{+}CD23^{-} for T1, B220^{+}CD93^{+}IgM^{+}CD23^{+} for T2, and B220^{+}CD93^{+}IgM^{lo}CD23^{+} for T3 transitional B cells, B220^{+}CD93^{-}CD21^{+}IgM^{+}IgD^{+} for FOL I and B220^{+}CD93^{-}CD21^{+}IgM^{hi}IgD^{+} for FOL II follicular B cells, B220^{+}CD93^{-}CD21^{hi}IgM^{hi}CD23^{+} for MZP and B220^{+}CD93^{-}CD21^{hi}IgM^{hi}CD23^{-} for MZ B cells, as previously described [285]. Data are from 4 mice per genotype. Bars represent mean ± SEM; statistical analysis by *t*-test; ** $p<0.01$; not significant if not indicated. **(C)** Representative flow cytometry plots of the spleen of naïve *Bap1*$^{fl/fl}$ Cγ1-Cre and control *Bap1*$^{+/+}$ Cγ1-Cre mice, showing the gating for T1, T2, T3, FOL I, FOL II, MZP, and MZ B cell populations, according to the markers listed above. Percentages of cells within each gate relative to the parent gate for each mouse genotype are presented as mean ± S.D.

Figure 4.2.2 Confirmation of Cre-mediated *Bap1*-gene inactivation in stimulated *Bap1*$^{fl/fl}$ Cγ1-Cre B cells.

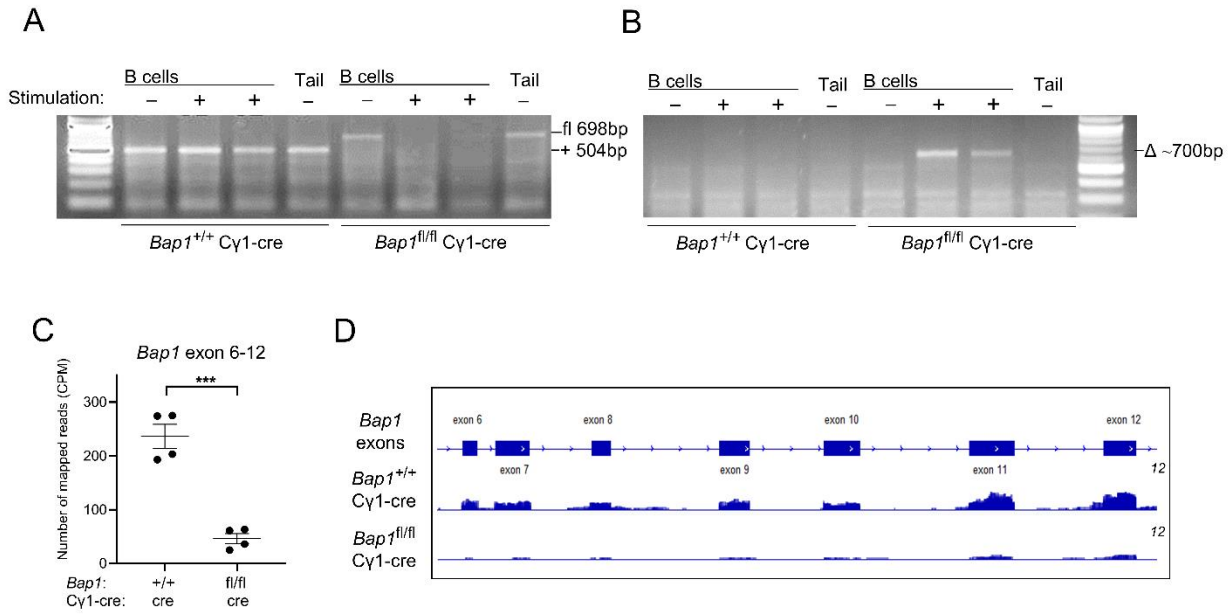

(A-B) Genomic PCR analyses of splenic B cells of *Bap1*$^{fl/fl}$ Cγ1-Cre and control *Bap1*$^{+/+}$ Cγ1-Cre genotypes, with and without *in vitro* stimulation with LPS + IL-4 or anti-CD40 + IL-4. Tail-clip samples from the same mice are included as additional negative controls. **(A)** Loss of *Bap1*-floxed allele and **(B)** gain of *Bap1*-null allele in the stimulated *Bap1*$^{fl/fl}$ Cγ1-Cre B cells but not in control samples. PCR primers were *Bap1*_Fw TGGGGATGTCTGGGGTAAAG with **(A)** *Bap1*_Rv TGGTGGCAAATGAGACCTTG and **(B)** *Bap1*_ex13_Rv2 AGTGCCATCCTACTCAGCAAA. **(C-D)** Loss of expression of the *Bap1*-floxed exons 6-12 in the RNA-seq data from primary GC B cells of *Bap1*$^{fl/fl}$ Cγ1-Cre genotype relative to control *Bap1*$^{+/+}$ Cγ1-Cre genotype. **(C)** Dot plot showing the number of sequencing reads mapped to *Bap1* exons 6-12 in the RNA-seq data from GC B cells of *Bap1*$^{fl/fl}$ Cγ1-Cre and control *Bap1*$^{+/+}$ Cγ1-Cre genotypes. Statistical analysis used

Student's *t*-test; *** $p < 0.001$. **(D)** Genomic snapshots of the RNA-seq tracks of *Bap1* floxed exons 6-12 from GC B cells of *Bap1*$^{fl/fl}$ Cγ1-Cre and control *Bap1*$^{+/+}$ Cγ1-Cre genotypes. The maximum data range (y-axis scale) of the tracks is 12.

Figure 4.2.3 Reduced antibody levels and impaired antibody mediated immune response to immunization in *Bap1*$^{fl/fl}$ Cγ1-Cre mice

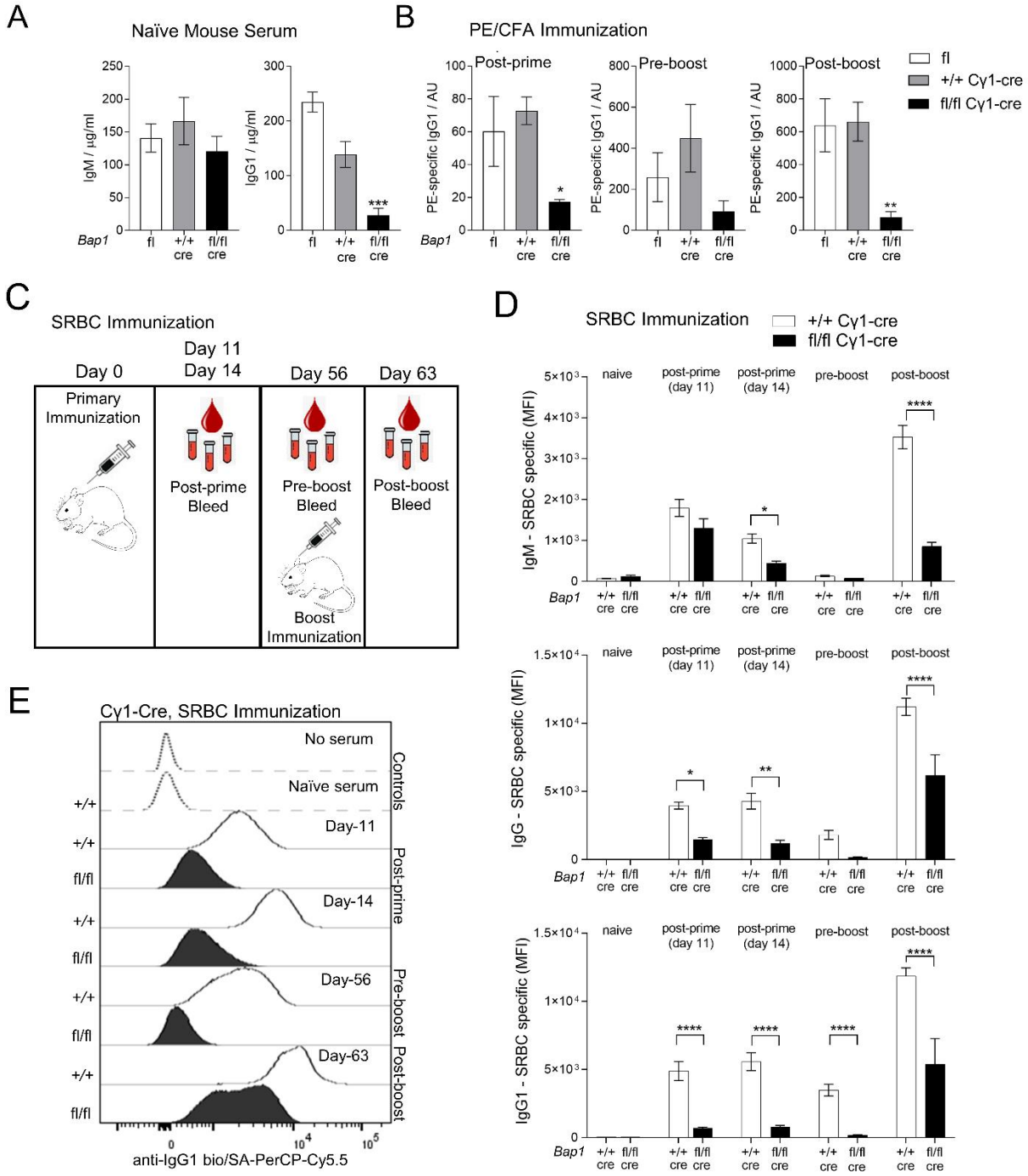

(A) Levels of total IgM and IgG1 antibody isotypes in the serum of naïve mice of *Bap1*$^{fl/fl}$ Cγ1-Cre and control *Bap1*^{fl} and *Bap1*$^{+/+}$ Cγ1-Cre genotypes, assessed by ELISA. Data are from 9-11 mice per genotype, consolidated from two independent experiments. **(B)** Antigen specific antibody titres in the mice of *Bap1*$^{fl/fl}$ Cγ1-Cre and control *Bap1*^{fl} and *Bap1*$^{+/+}$ Cγ1-Cre genotypes, immunized with PE in CFA adjuvant, as outlined above; data acquired with ELISA from 3-5 mice per genotype. **(C)** Experimental plan and timeline for the analyses of *Bap1*$^{fl/fl}$ Cγ1-Cre and control *Bap1*$^{+/+}$ Cγ1-Cre mouse responses to sheep red blood cell (SRBC) immunization. **(D)** Antigen specific antibody titres in the serum of mice of *Bap1*$^{fl/fl}$ Cγ1-Cre and control *Bap1*$^{+/+}$ Cγ1-Cre genotypes following SRBC immunization. Data are from 6-8 mice per genotype and reproduced in two independent experiments. Bars represent means ± SEM; statistical analyses used ANOVA with Sidak's post-hoc test comparing *Bap1*$^{fl/fl}$ Cγ1-Cre and *Bap1*$^{+/+}$ Cγ1-Cre groups; * $p<0.05$, ** $p<0.01$, *** $p<0.001$, **** $p<0.0001$, or not significant if not indicated; AU – arbitrary units; MFI – mean fluorescence intensity. **(E)** Representative flow cytometry analyses of mouse serum for SRBC-binding antibody levels, involving the incubation of SRBCs with the serum followed by the staining of SRBCs for antibody binding, as previously described [263].

4.2.3 Germinal center dysfunction and plasma cell depletion with the loss of BAP1

To understand the impact of BAP1-loss on the cellular dynamics of humoral immune response, mice of *Bap1*$^{fl/fl}$ Cγ1-Cre and control *Bap1*$^{+/+}$ Cγ1-Cre genotypes, both naïve and challenged with SRBC-immunization (as shown in 4.2.4C), were analyzed for the numbers of germinal centre (GC) B cells, memory B cells, and plasma cells using flow cytometry (Figure 4.2.4). While there was no significant change in the absolute numbers of GC B cells in *Bap1*$^{fl/fl}$ Cγ1-Cre relative to control mice at day 11 following the SRBC-immunization (Figure 4.2.4A), we observed a significant reduction in the ratio of dark zone (DZ) to light zone (LZ) GC B cells (Figure 4.2.4B), primarily due to an expansion in the number of LZ B cells (data not shown). Importantly, *Bap1*$^{fl/fl}$ Cγ1-Cre mice showed a reduction in the numbers of class switched IgG1^{+} GC B cells (Figure 4.2.4C), with a significant depletion of IgG1^{+} cells within both the DZ and LZ subpopulations (data not shown), as well as a reduction in IgG1^{+} memory B cells (Figure 4.2.4D). Absolute numbers of plasma cells were also significantly reduced in both the spleen and bone marrow of *Bap1*$^{fl/fl}$ Cγ1-Cre mice (Figure 4.2.4F), with a particularly strong depletion of the IgG1^{+} class-switched plasma cells (Figure 4.2.4G). Further analysis of the plasma cell population demonstrated a more significant

depletion of plasmablasts and early plasma cells as compared to late plasma cells in the *Bap1*$^{fl/fl}$ Cγ1-Cre mice (Figure 4.2.5A-B), and a reduction in the proportion of plasma cells positive for the Ki-67 marker of cell proliferation at least in the bone marrow (Figure 4.2.5C). Overall, the significant depletion of plasma cells likely contributes to the failure to produce and sustain normal antibody titres in the *Bap1*$^{fl/fl}$ Cγ1-Cre mice.

The mice were further analyzed for GC B cells, memory B cells, and plasma cells at day 7 after the boost SRBC immunization, and the data are presented in Figure 4.2.6. Surprisingly, an increase in GC B cells was observed in *Bap1*$^{fl/fl}$ Cγ1-Cre mice relative to the control cohort after the booster immunization (Figure 4.2.6A), and this may reflect the modulatory effects of pre-existing high antibody titres on B cell recruitment into the GC in the control group [286]. Furthermore, the numbers of IgG1^{+} class-switched GC and memory B cells in the *Bap1*$^{fl/fl}$ Cγ1-Cre mice were restored to normal after the booster immunization (Figure 4.2.6C-D), consistent with the considerable rise in their antibody titres at this time point (Figure 4.2.2D-E). However, the reduced ratio of DZ to LZ GC B cells and the significant depletion of class switched IgG1+ plasma cells persisted even after the booster immunization in *Bap1*$^{fl/fl}$ Cγ1-Cre mice (Figure 4.2.6B, G). The persisting plasma cell phenotype likely contributes to the ongoing reduction in the antibody titres in *Bap1*$^{fl/fl}$ Cγ1-Cre mice.

Figure 4.2.4. Analyses of germinal centre (GC) B cells, memory B cells, and plasma cells in *Bap1*$^{fl/fl}$ Cγ1-Cre mice.

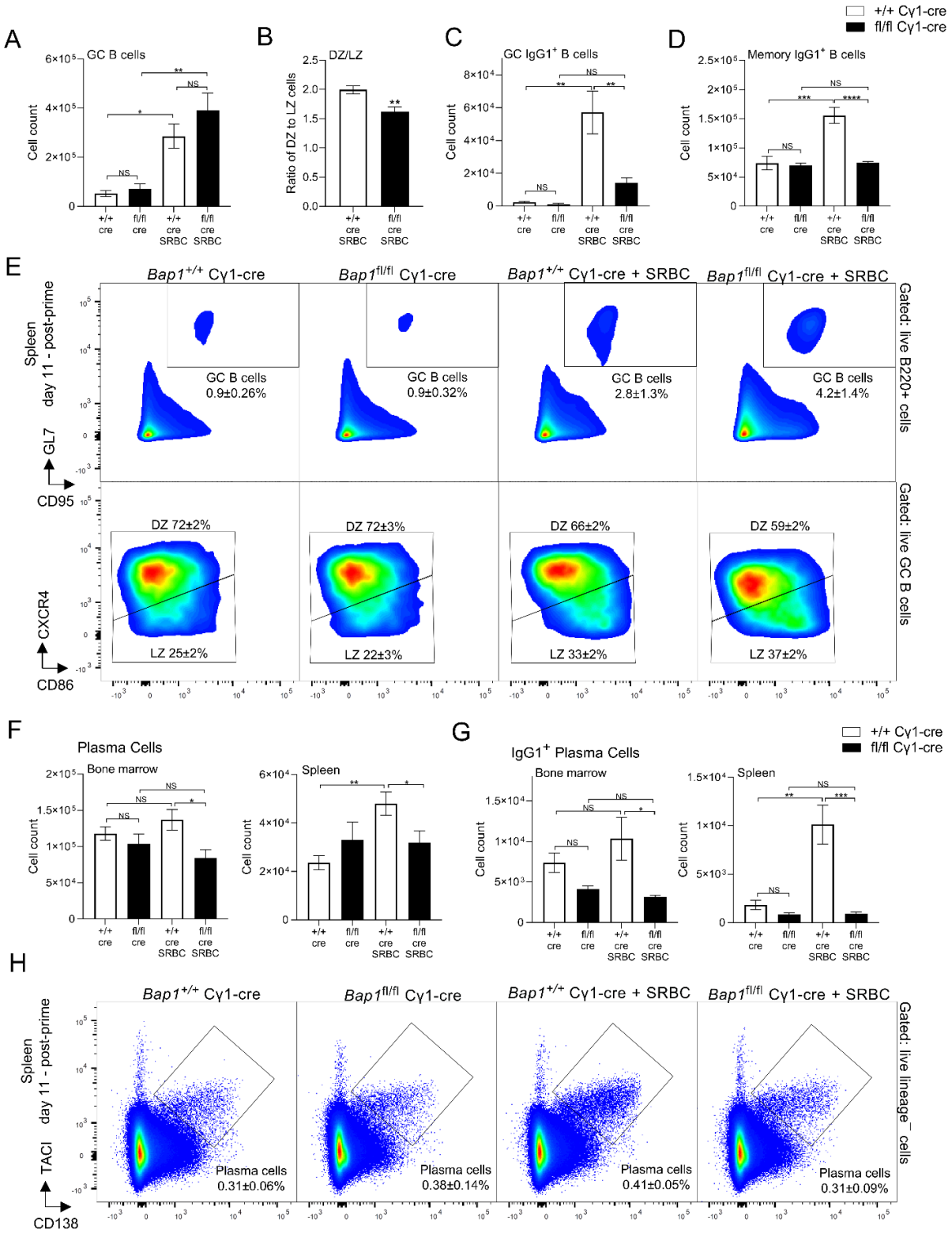

Mice of *Bap1*$^{fl/fl}$ Cγ1-Cre and control *Bap1*$^{+/+}$ Cγ1-Cre genotypes, both naïve and at day 11 post-primary SRBC-immunization, were analyzed by flow cytometry. **(A)** Absolute numbers of GC B cells per mouse spleen, **(B)** ratio of dark zone (DZ) to light zone (LZ) GC B cells, **(C)** absolute numbers of IgG1^{+} GC B cells per mouse spleen, and **(D)** absolute numbers of IgG1^{+} memory B cells per mouse spleen, comparing between the *Bap1* genotypes and immunization conditions. **(E)** Representative flow cytometry plots analyzing splenic GC B cells; average percentage of cells in each gate relative to the parent gate for all the mice in each group is indicated as mean ± SD. **(F-G)** Absolute numbers of total plasma cells and IgG1^{+} plasma cells in the bone marrow and spleen, comparing between the *Bap1* genotypes and immunization conditions. **(H)** Representative flow cytometry analyses of plasma cells in the spleen of *Bap1*$^{fl/fl}$ Cγ1-Cre and control *Bap1*$^{+/+}$ Cγ1-Cre mice, both naïve and at day 11 post-primary SRBC-immunization; average percentage of cells in each gate relative to the parent gate for all the mice in each group is indicated as mean ± SD. Bars represent means ± SEM; statistical analyses used ANOVA with Sidak's post-hoc test to compare between the *Bap1*$^{fl/fl}$ Cγ1-Cre and *Bap1*$^{+/+}$ Cγ1-Cre genotypes and immunization conditions; * $p<0.05$, ** $p<0.01$, *** $p<0.001$, **** $p<0.0001$. GC B cells were gated as live B220^{+}GL7^{+}CD95^{+} cells and divided into CXCR4^{+}CD86^{-} dark zone (DZ) and CXCR4^{-}CD86^{+} light zone (LZ) cell. Plasma cells were gated as live CD138 $^{+}$TACI $^{+}$ cells, negative for the lineage markers CD11b, TER119, CD4, CD8, and NK1.1.

Figure 4.2.5 Further analyses of plasma cells in *Bap1*$^{fl/fl}$ Cγ1-Cre mice.

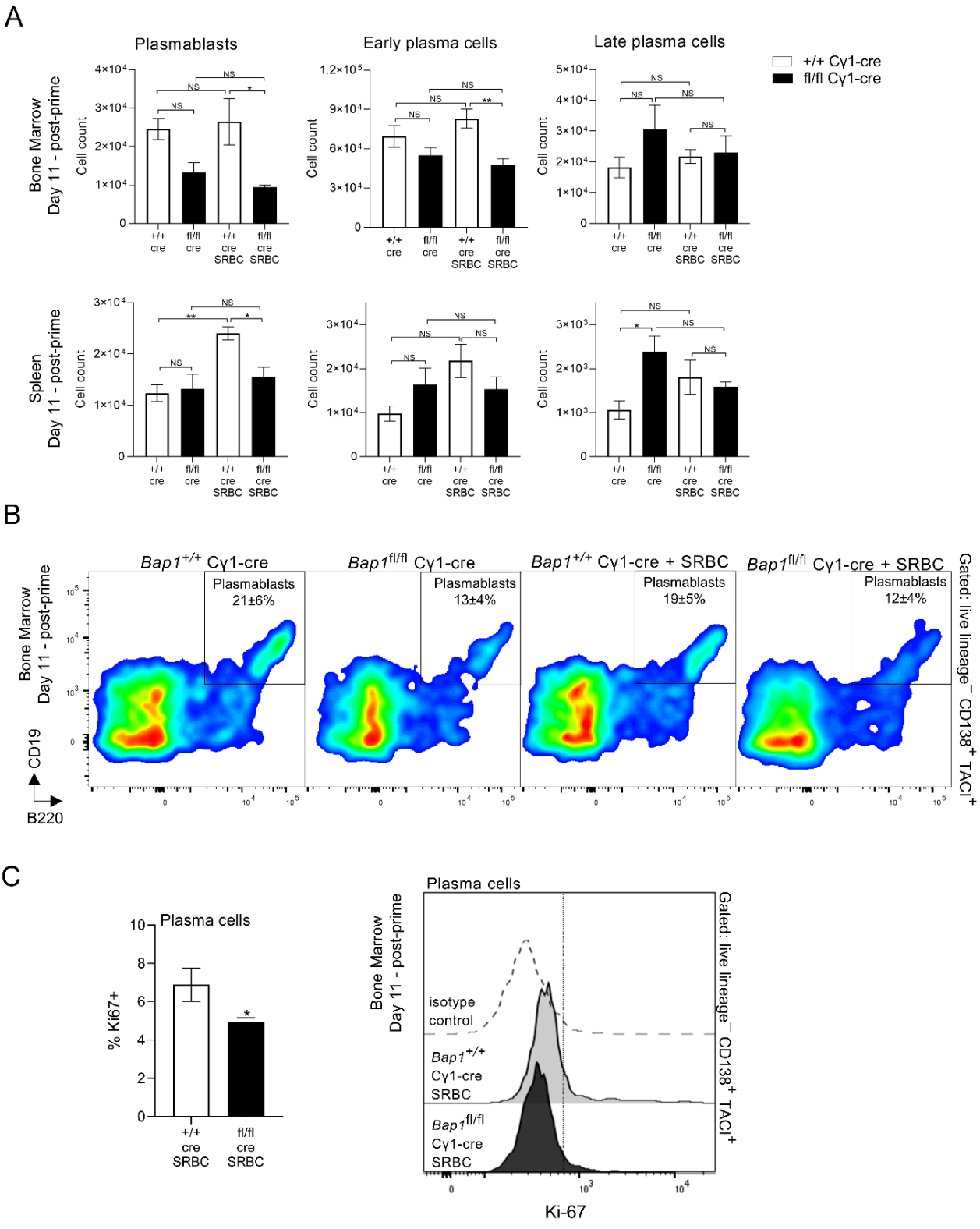

Mice of *Bap1*$^{fl/fl}$ Cγ1-Cre and control *Bap1*$^{+/+}$ Cγ1-Cre genotypes, both naïve and at day 11 post-primary SRBC-immunization, were analyzed by flow cytometry. **(A)** Absolute numbers of plasmablasts, early plasma cells, and late plasma cells in mouse bone marrow (top panel) and spleen (bottom panel), comparing between the *Bap1* genotypes and immunization conditions. **(B)** Representative flow cytometry plots analyzing bone marrow plasma cells, gated as live Lin^{-} CD138^{+} TACI^{+}, and showing the staining for the CD19^{+}B220^{+} plasmablast subpopulation; average percentage of cells in each gate relative to the parent gate for all the mice in each group is indicated as mean ± SD. **(C)** Analyses of bone marrow plasma cells for Ki-67 marker of cell proliferation, including quantification of the percentage of Ki-67+ plasma cells (left panel), and representative flow cytometry histogram gated on plasma cells and showing Ki-67 staining (right panel). All bars represent means ± SEM; statistical analyses used ANOVA with Sidak's post-hoc test to compare between the *Bap1*$^{fl/fl}$ Cγ1-Cre and *Bap1*$^{+/+}$ Cγ1-Cre genotypes and immunization conditions; * $p<0.05$, ** $p<0.01$, *** $p<0.001$. Plasma cells were gated as live CD138^{+} TACI^{+} cells, negative for the lineage markers CD11b, TER119, CD4, CD8, and NK1.1, and classified into CD19^{+}B220^{+} plasmablasts, CD19^{+}B220^{-} early plasma cells, and CD19^{-}B220^{-} late plasma cells. Intracellular staining for BLIMP1 transcription factor was used to validate plasma cell gating (data not shown). Furthermore, alternative staining for plasmablasts as B220^{hi} Ki67^{+}, early plasma cells as BLIMP1^{+} B220^{lo} Ki67^{-}, and late plasma cells as BLIMP1^{+} B220^{-} Ki67^{-} gave similar results and conclusions (data not shown).

Figure 4.2.6 Analyses of germinal centre (GC) B cells, memory B cells, and plasma cells in *Bap1*$^{fl/fl}$ Cγ1-Cre mice post-boost immunization.

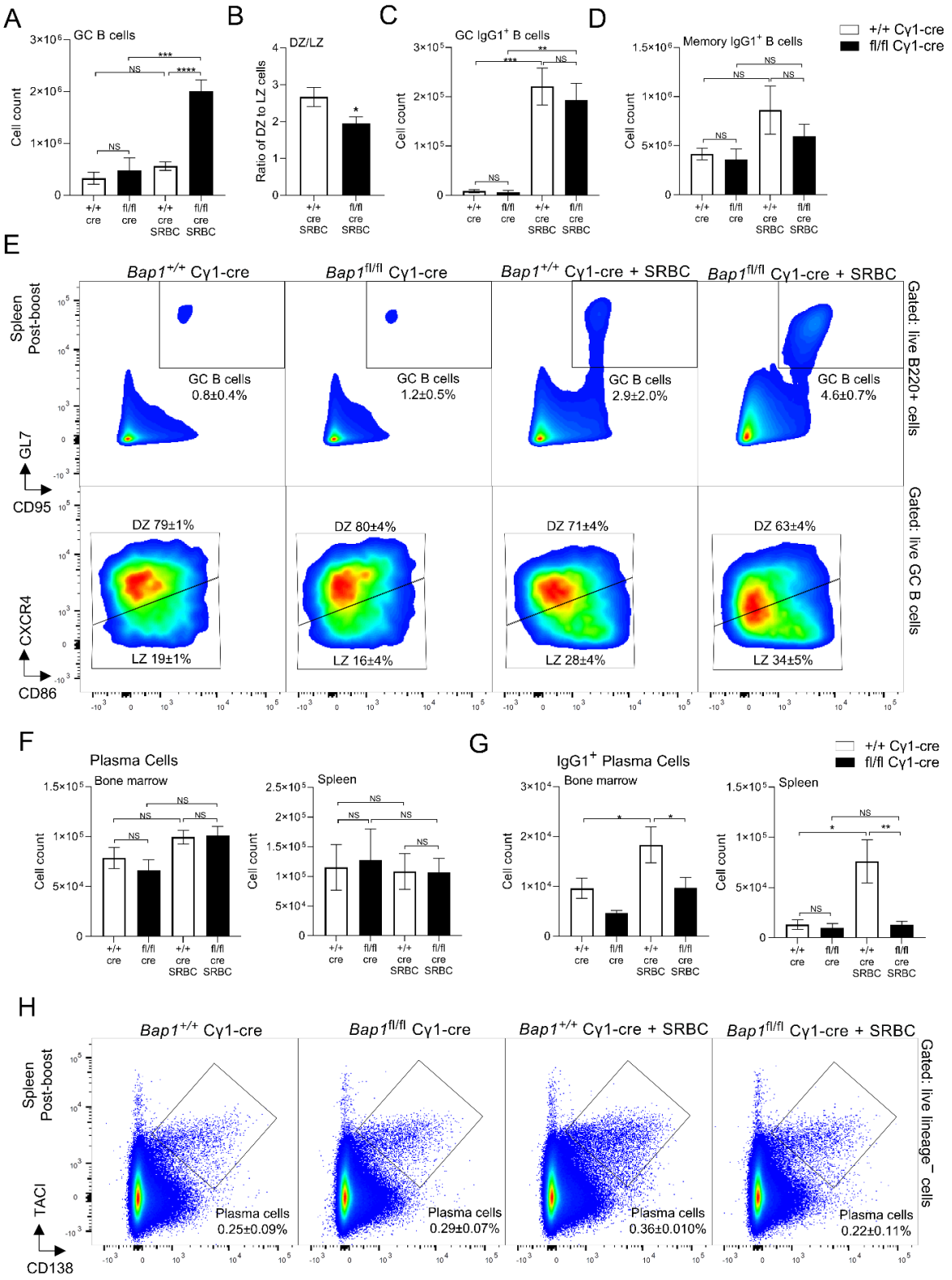

Mice of *Bap1*$^{fl/fl}$ Cγ1-Cre and control *Bap1*$^{+/+}$ Cγ1-Cre genotypes, both naïve and at day 7 post-boost SRBC-immunization, were analyzed by flow cytometry. **(A)** Absolute numbers of GC B cells per mouse spleen, **(B)** ratio of dark zone (DZ) to light zone (LZ) GC B cells, **(C)** absolute numbers of IgG1$^+$ GC B cells per mouse spleen, and **(D)** absolute numbers of IgG1$^+$ memory B cells per mouse spleen, comparing between the *Bap1* genotypes and immunization conditions. **(E)** Representative flow cytometry plots analyzing splenic GC B cells; average percentage of cells in each gate relative to the parent gate for all the mice in each group is indicated as mean ± SD. **(F-G)** Absolute numbers of total plasma cells and IgG1$^+$ plasma cells in the bone marrow and spleen, comparing between the *Bap1* genotypes and immunization conditions. **(H)** Representative flow cytometry analyses of plasma cells in the spleen of *Bap1*$^{fl/fl}$ Cγ1-Cre and control *Bap1*$^{+/+}$ Cγ1-Cre mice, both naïve and at day 7 post-boost SRBC-immunization; average percentage of cells in each gate relative to the parent gate for all the mice in each group is indicated as mean ± SD. Bars represent means ± SEM; statistical analyses used ANOVA with Sidak's post-hoc test to compare between the *Bap1*$^{fl/fl}$ Cγ1-Cre and *Bap1*$^{+/+}$ Cγ1-Cre genotypes and immunization conditions; * $p<0.05$, ** $p<0.01$, *** $p<0.001$. GC B cells were gated as live B220$^+$GL7$^+$CD95$^+$ cells and divided into CXCR4$^+$CD86$^-$ dark zone (DZ) and CXCR4$^-$CD86$^+$ light zone (LZ) cell. Plasma cells were gated as live CD138 $^+$TACI $^+$ cells, negative for the lineage markers CD11b, TER119, CD4, CD8, and NK1.1.

4.2.4 Loss of BAP1 in primary B cells does not impair antibody class switching

While the more significant impact of BAP1-loss on the numbers of IgG1$^+$ rather than total GC B cells and plasma cells in the *Bap1*$^{fl/fl}$ Cγ1-Cre model may reflect the higher expression of Cre in the IgG1$^+$ cells [255], it may also suggest a role for BAP1 in B cell immunoglobulin class switching. We therefore proceeded to directly test the effects of *Bap1*-loss on B cell class switching *in vitro*. Induced GC B cells (iGBs) of *Bap1*$^{fl/fl}$ Cγ1-Cre and control *Bap1*$^{+/+}$ Cγ1-Cre genotypes were generated on the 40LB feeder cells that provide CD40L and BAFF, as described previously [258, 260]. iGBs were analyzed at day 4 for class switching to IgG1 and demonstrated no significant differences between the *Bap1*$^{fl/fl}$ Cγ1-Cre and control *Bap1*$^{+/+}$ Cγ1-Cre cultures (Figure 4.2.7A-B). We further analyzed B cell proliferation in the iGBs cultures, using either the CellTrace Violet (CTV) dilution method with flow cytometry (Figure 4.2.7C-D, day 4) or manual cell counting (Figure 4.2.7E, days 0-6). This demonstrated a significant impairment in the proliferation for *Bap1*$^{fl/fl}$ Cγ1-Cre relative to control *Bap1*$^{+/+}$ Cγ1-Cre B cells under these culture conditions (Figure

4.2.7C-E). Further analyses of the B cell class switching rates per cell division in this model confirmed that the loss of *Bap1* does not directly interfere with B cell class switching, and any reduction in class switched *Bap1*$^{fl/fl}$ Cγ1-Cre B cells can be attributed to impaired B cell proliferation (Figure 4.2.7C,F).

Primary B cells from *Bap1*$^{fl/fl}$ Cγ1-Cre and control *Bap1*$^{+/+}$ Cγ1-Cre mice were also stimulated in culture to class-switch to IgA with IL-21, anti-CD40, anti-IgM, TGF-β, and retinoic acid, as reported previously [259]. Again, *Bap1*$^{fl/fl}$ Cγ1-Cre B cells demonstrated normal levels of class switching over 4 days in culture (Figure 4.2.8A-B), though *Cre*-mediated *Bap1*^{fl} to *Bap1*$^{\Delta}$ allele conversion was observed as early as days 3, albeit without full loss of the *Bap1*^{fl} allele (Figure 4.2.8C-D). It is notable that no loss of cell proliferation was observed in these cultures, and this may reflect biological differences in the responses of *Bap1*-deficient B cells to different stimulation conditions or the lower efficiency of Cγ1-Cre in the cells undergoing class switching to IgA relative to IgG1, as shown by the persistent detection of the *Bap1*^{fl} allele in these cells (Figure 4.2.8D).

We further evaluated class switching using splenic B cells from *Bap1*$^{fl/fl}$ mb1-Cre and control *Bap1*$^{+/+}$ mb1-Cre mice, as in this model the Cre-mediated *Bap1*-allele deletion takes place from the early stages in B cell lineage development, and the full loss of BAP1 protein in *Bap1*$^{fl/fl}$ mb1-Cre splenic B cells has been validated through Western blotting in our previously published studies [223]. Thus, to further assess the role of BAP1 in antibody class switching, *Bap1*$^{fl/fl}$ mb1-Cre and control *Bap1*$^{+/+}$ mb1-Cre B cells were stimulated in culture with IL-21, anti-CD40, anti-IgM, TGF-β, and retinoic acid to class-switch to IgA and analyzed at day 3 (Figure 4.2.7G-K). While *Bap1*$^{fl/fl}$ mb1-Cre B cells showed a trend toward impaired cell proliferation relative to the control B cells

(Figure 4.2.7G,I,J), there were no differences in class switching per cell division between the *Bap1*-genotypes (Figure 4.2.7K), consistent with our findings with the *Bap1*$^{fl/fl}$ Cγ1-Cre B cells (Figure 4.2.7F, 4.2.8B). Overall, we conclude that BAP1 is not directly required for the normal progression of antibody class switching.

Given the impaired proliferation of *Bap1*-deficient B cells under some of the stimulation conditions presented above, we further analyzed the effects of BAP1 on B cell viability. No significant differences in cell viability were observed between *Bap1*$^{fl/fl}$ Cγ1-Cre and control *Bap1*$^{+/+}$ Cγ1-Cre germinal centre B cells, memory B cells, or plasma cells, freshly isolated from naive mice or from mice at day 11 post-SRBC immunization (Figure 4.2.9A-D). Further analysis of the plasma cell populations as plasmablasts, early plasma cells, and mature plasma cells also demonstrated no differences in viability based on the *Bap1*-genotype of the cells (data not shown). However, such analyses may not detect subtle changes in cell viability due to the rapid clearance of dead cells in healthy tissues, and we therefore further analyzed the viability of primary B cells of *Bap1*$^{fl/fl}$ Cγ1-Cre and control *Bap1*$^{+/+}$ Cγ1-Cre genotypes in culture, stimulated over 5 days with either anti-CD40 and IL-4, or with LPS and IL-4. This demonstrated a mild but statistically significant reduction in the viability of *Bap1*$^{fl/fl}$ Cγ1-Cre relative to control *Bap1*$^{+/+}$ Cγ1-Cre B cells under both stimulation conditions (Figure 4.2.9E). Overall, we conclude that the loss of BAP1 can impair the viability of activated B cells.

Figure 4.2.7 Loss of BAP1 does not impair immunoglobulin class switching in primary B cells.

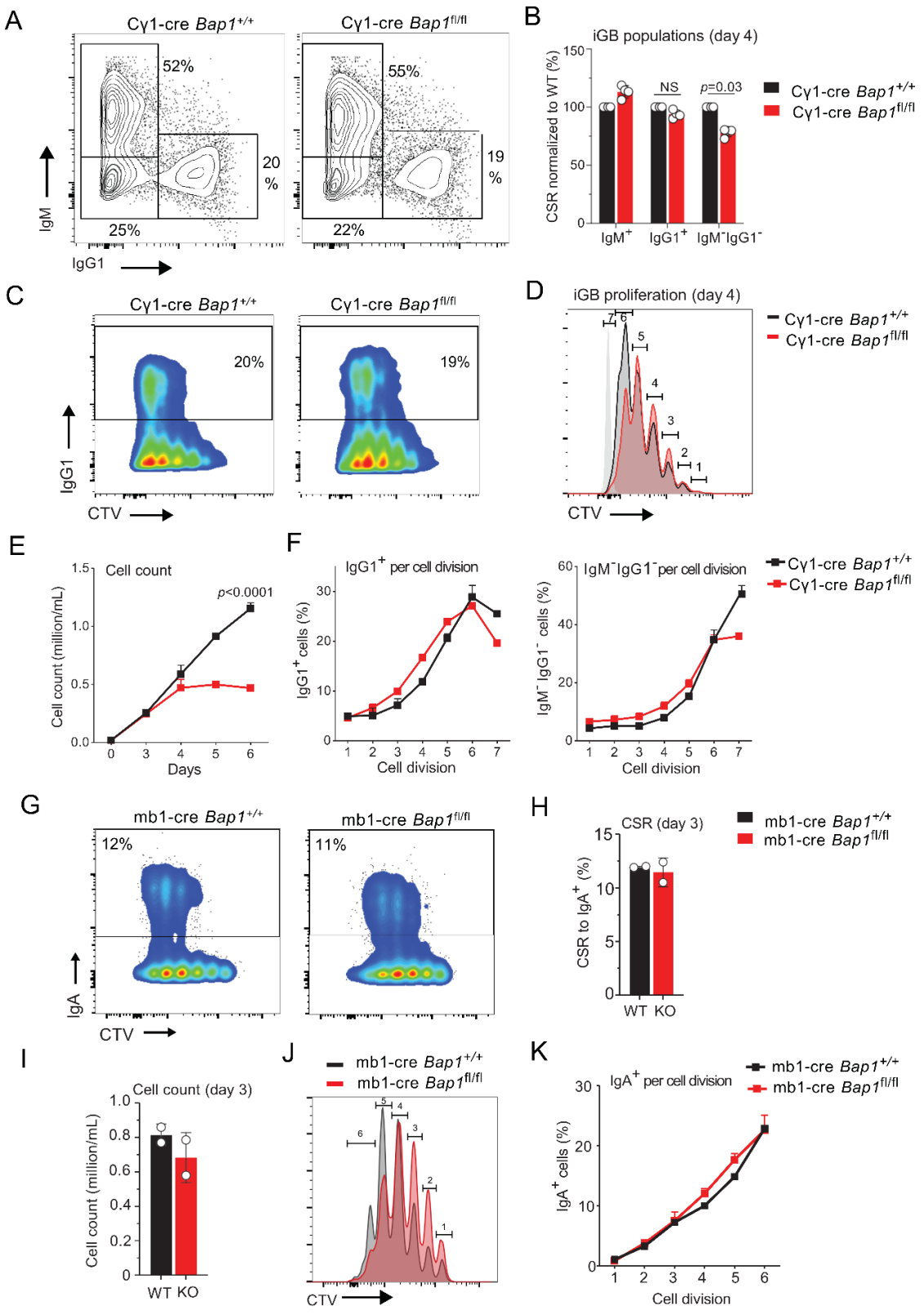

Induced GC B cells (iGB) of *Bap1*$^{fl/fl}$ Cγ1-Cre and control *Bap1*$^{+/+}$ Cγ1-Cre genotypes were generated on 40LB feeders, as described previously [258, 260], and analyzed at day 4 of culture for **(A-C)** immunoglobulin class switching to IgG1, and **(C-D)** cell proliferation using the CellTrace Violet (CTV) dilution method. **(E)** Growth curves of iGBs of *Bap1*$^{fl/fl}$ Cγ1-Cre and control *Bap1*$^{+/+}$ Cγ1-Cre genotypes over a 6-day time course, evaluated with cell counting and demonstrating the impaired proliferation of *Bap1*-deficient B cells. **(F)** Antibody class switching per cell division, comparing *Bap1*$^{fl/fl}$ Cγ1-Cre and control *Bap1*$^{+/+}$ Cγ1-Cre iGBs at day 4 and showing no differences between the genotypes. Bars represent means ± SEM, with two mice per genotype. **(G-K)** Primary splenic B cells of *Bap1*$^{fl/fl}$ mb1-Cre and control *Bap1*$^{+/+}$ mb1-Cre genotypes were stimulated in culture to induce class switching to IgA. **(G)** Analyses of the cultures at day 3 of stimulation for class-switching to IgA and for cell proliferation using the CTV-dilution method demonstrated no differences in class switching between the *Bap1*-genotypes. **(H)** Quantification of the B cell cultures for class-switching to IgA demonstrated no differences between the *Bap1*-genotypes. **(I-J)** Analyses of B cell proliferation using **(I)** cell counting or **(J)** CTV-dilution method demonstrated a trend toward decreased proliferation of *Bap1*$^{fl/fl}$ mb1-Cre relative to the control *Bap1*$^{+/+}$ mb1-Cre B cells. **(K)** Antibody class switching per cell division comparing *Bap1*$^{fl/fl}$ mb1-Cre and control *Bap1*$^{+/+}$ mb1-Cre B cells showed no differences between the genotypes. Bars represent means ± SEM with two mice per genotype. Statistical analyses used **(B, H, I)** unpaired two-tailed Student's *t*-test or **(E, K)** two-way ANOVA with Sidak's multiple comparison test; *p*-values are indicated in the figure or not-significant (NS) if not indicated.

Figure 4.2.8 Partial *Bap1*-deletion does not impair immunoglobulin class switching to IgA isotype in primary B cells.

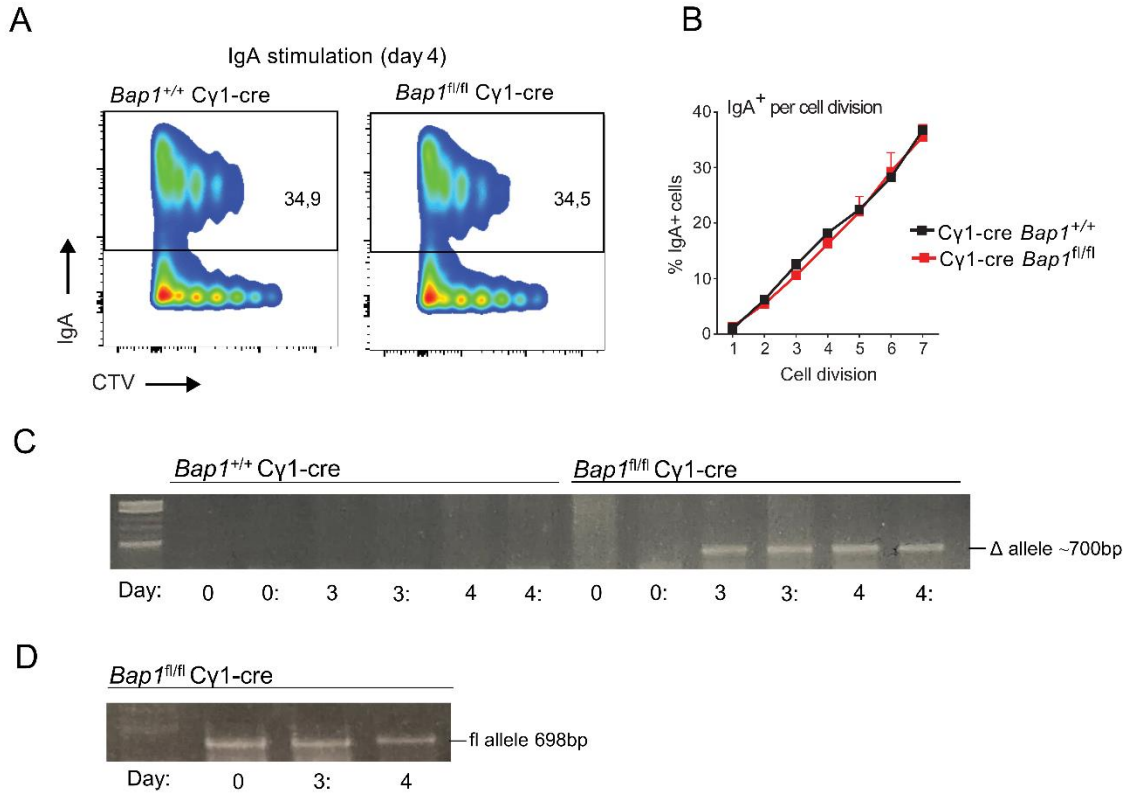

Primary splenic B cells from *Bap1*$^{fl/fl}$ Cγ1-Cre and control *Bap1*$^{+/+}$ Cγ1-Cre mice were stimulated in culture to induce class switching to IgA. **(A)** Analyses of the B cell cultures on day 4 of stimulation for class-switching to IgA and for cell proliferation using the CFSE-dilution method demonstrated no differences between the *Bap1*-genotypes. **(B)** Analyses of the B cell cultures for class-switching to IgA quantified per cell division demonstrated no differences between the *Bap1*-genotypes. **(C-D)** Genomic PCR analyses of the *Bap1*$^{fl/fl}$ Cγ1-Cre and control *Bap1*$^{+/+}$ Cγ1-Cre B cell cultures, either unstimulated on day 0 or on days 3-4 of stimulation. Gain of the *Bap1*-null allele **(C)**, but without the loss of the *Bap1*^{fl} allele **(D)** in stimulated *Bap1*$^{fl/fl}$ Cγ1-Cre B cells is demonstrated, indicating that Cγ1-Cre is only partially effective. Primers were *Bap1*_Fw TGGGGATGTCTGGGGTAAAG with **(C)** *Bap1*_ex13_Rv2 AGTGCCATCCTACTCAGCAAA or **(D)** *Bap1*_Rv TGGTGGCAAATGAGACCTTG.

Figure 4.2.9 Analyses of the viability of *Bap1*-deficient B cells.

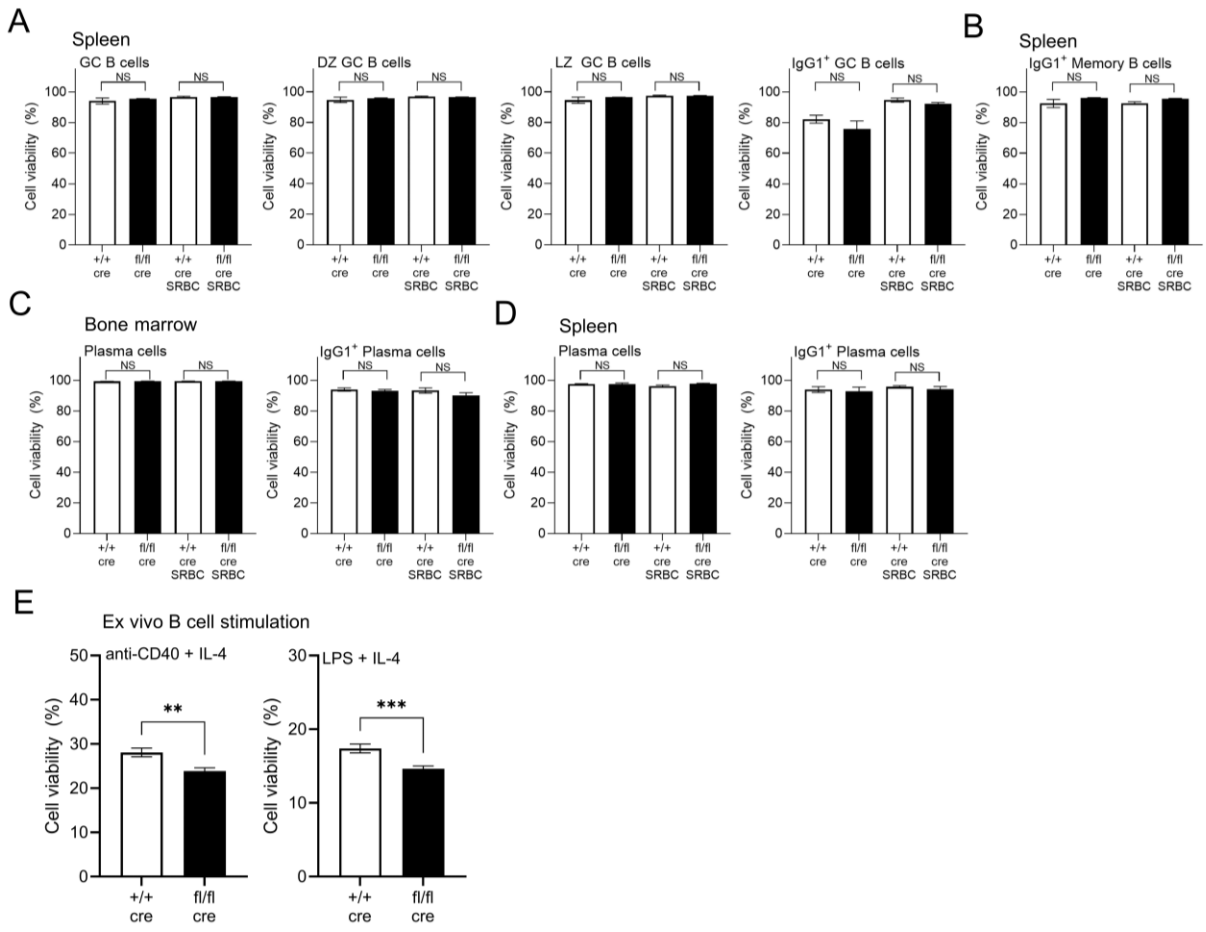

(A-D) Viability of primary B cells from the spleen and bone marrow of the mice of *Bap1*$^{fl/fl}$ Cγ1-Cre and control *Bap1*$^{+/+}$ Cγ1-Cre genotypes, either naïve or at day 11 post-primary SRBC-immunization, analyzed by flow cytometry based on fixable viability dye exclusion. **(A)** Splenic germinal centre (GC) B cells, dark zone GC B cells, light zone GC B cells, and IgG1^{+} GC B cells, **(B)** splenic IgG1^{+} memory B cells, and **(C-D)** total plasma cells and IgG1^{+} plasma cells in the bone

marrow and spleen show no differences in cell viability between the *Bap1*-genotypes. GC B cells were gated as live $B220^{+}GL7^{+}CD95^{+}$ cells and divided into $CXCR4^{+}CD86^{-}$ dark zone (DZ) and $CXCR4^{-}CD86^{+}$ light zone (LZ) cell. Plasma cells were gated as live $CD138^{+}TACI^{+}$ cells, negative for the lineage markers CD11b, TER119, CD4, CD8, and NK1.1. Bars represent means ± SEM; statistical analyses used ANOVA with Sidak's post-hoc test to compare $Bap1^{fl/fl}$ Cγ1-Cre and $Bap1^{+/+}$ Cγ1-Cre groups; no significant differences in B cell viability based on the *Bap1*-genotype were detected. **(E)** Viability of primary splenic B cells of $Bap1^{fl/fl}$ Cγ1-Cre and control $Bap1^{+/+}$ Cγ1-Cre genotypes at day 5 of *in vitro* stimulation with anti-CD40 (2 μg/ml) and IL-4 (5 ng/ml), or with LPS (1 μg/mL) and IL-4 (5 ng/ml), analyzed by flow cytometry based on fixable viability dye exclusion. Bars represent means ± SEM; statistical analyses used used Student's *t*-test; ** $p<0.01$, *** $p<0.001$.

4.2.5 Impaired proliferation in Bap1 CRISPR/Cas9 gene targeted CH12F3 B cells

To further explore the roles and mechanisms of BAP1 activity in B cells, we targeted *Bap1* gene using CRISPR/Cas9 in the CH12F3 B cell lymphoma line [256], which is a commonly used model for the analyses of B cell activation, class switching, and associated cellular processes. gRNAs were designed to target *Bap1* exons 4 and 5 that encode the N-terminal catalytic domain of the protein (Figure 4.2.10A), and single-cell clones screened by PCR for deletions within the targeted regions of the *Bap1* locus. Further analyses of five $Bap1^{\Delta/\Delta}$ single-cell clones by Western blotting confirmed the full loss of BAP1 protein expression (Figure 4.2.10B).

Based on the impaired proliferation of $Bap1^{fl/fl}$ Cγ1-Cre primary B cells in the iGB cultures (Figure 4.2.7) and on our previous report of impaired proliferation in $Bap1^{fl/fl}$ mb1-Cre pre-B cells [223], we analyzed the $Bap1^{\Delta/\Delta}$ CH12F3 cell clones for defects in proliferation, using the AlamarBlue resazurin/resorufin-based assay in bulk cell cultures, and the flow cytometry based CFSE dilution method. The assays demonstrated a significant reduction in cell proliferation for the $Bap1^{\Delta/\Delta}$ CH12F3 cell clones relative to control wild type CH12F3 cells (Figure 4.2.10C-E), as well as the reduced viability of $Bap1^{\Delta/\Delta}$ CH12F3 cell at least under unstimulated culture conditions (Figure 4.2.10F). This demonstrates the conservation of *Bap1*-deficiency phenotypes between CH12F3

cells and primary B cells and establishes the *Bap1*$^{\Delta/\Delta}$ CH12F3 cells as a model for further analyses of BAP1 functions in B cell biology.

Figure 4.2.10 CRISPR/Cas9-mediated *Bap1*-deletion in CH12F3 B cells, and the impaired proliferation of *Bap1*-deficient CH12F3 cell clones.

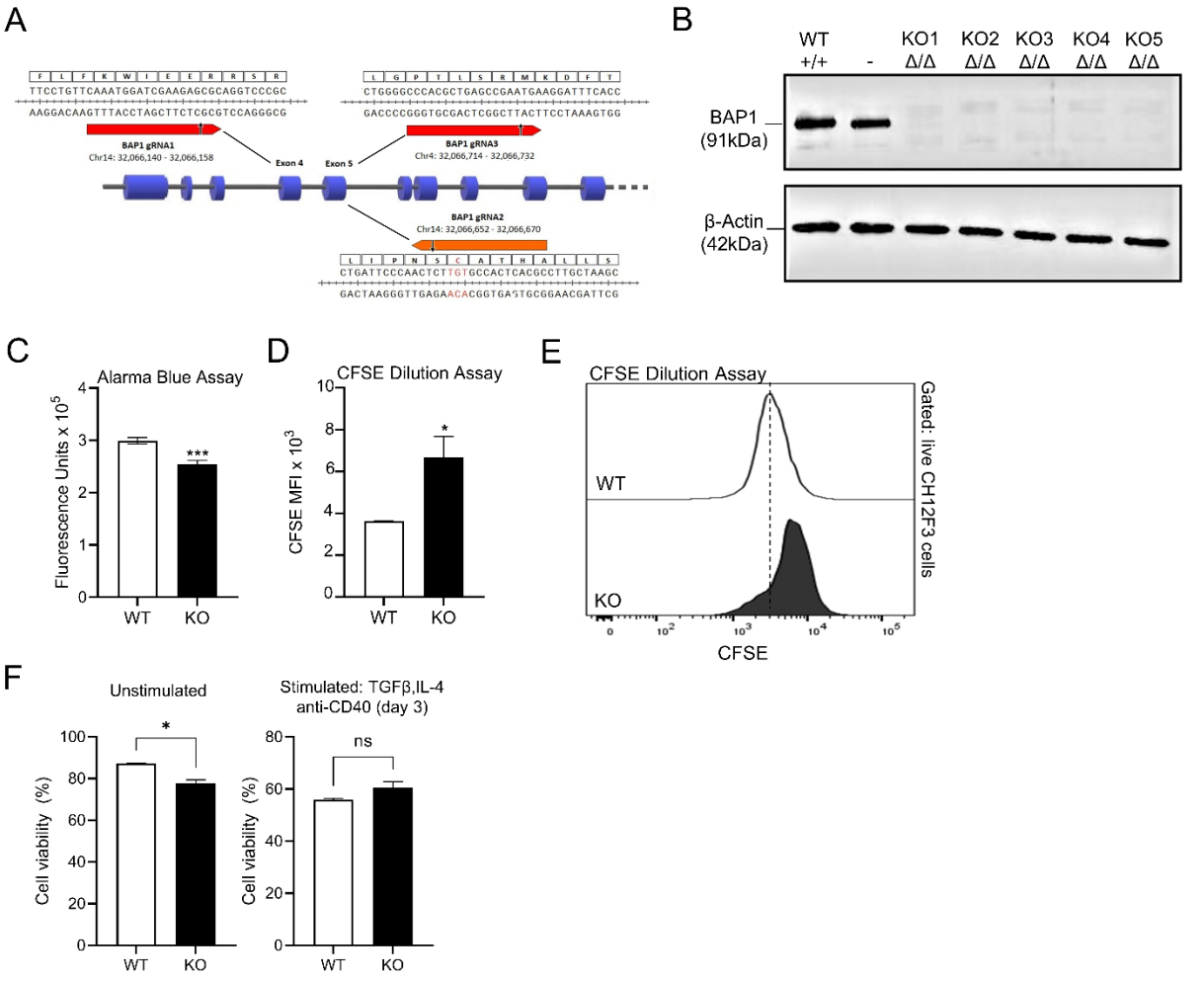

(A) *Bap1* gene targeting strategy: *gRNA1* was designed to target exon 4, and *gRNA2* and *gRNA3* were designed to target exon 5 of *Bap1* gene, encoding the BAP1 catalytic domain (mm9 genome assembly). gRNAs were used in pairs to improve the efficiency of PCR screening for the deletions. The diagram shows the gRNA-targeted fragments of exons 4 and 5, as well as the corresponding amino acids of BAP1 protein. Arrows indicate the predicted sites of Cas9-mediated double strand breaks (DSB), and the key catalytic residue of BAP1 protein Cys91 is indicated in red. **(B)** Western blot validating the loss of BAP1 protein expression in *Bap1*$^{\Delta/\Delta}$ CH12F3 clones 1-5, using β-Actin as the loading control. The CH12F3 clones with successful *Bap1*-deletions were targeted with *gRNA2* and *gRNA3*. **(C-E)** Analyses of the effects of BAP1 loss of CH12F3 cell proliferation. **(C)**

AlamarBlue assay demonstrates reduced proliferation of *Bap1*$^{\Delta/\Delta}$ CH12F3 cells; data is averaged from clones 1-5. **(D-E)** Cell proliferation analyses using a flow cytometry based CFSE-dilution assay, with the CH12F3 cells pre-loaded with CFSE and maintained in culture overnight. **(D)** Quantification of the CFSE mean fluorescence intensity (MFI) of *Bap1*$^{\Delta/\Delta}$ CH12F3 clones 1-5 relative to control wild type CH12F3 cells, demonstrating the reduced proliferation of *Bap1*$^{\Delta/\Delta}$ CH12F3 cells. **(E)** Representative CFSE dilution histograms, gated on live cells and demonstrating reduced proliferation of *Bap1*$^{\Delta/\Delta}$ relative to control wild type CH12F3 cells. **(F)** Viability of CH12F3 cells, analyzed by flow cytometry based on fixable viability dye exclusion, comparing *Bap1*$^{\Delta/\Delta}$ clones 1-5 to control wild type cells, using either unstimulated cells or cells at day 3 of stimulation with TGF-β (1 ng/ml), IL-4 (10 ng/ml), and anti–mouse CD40 (1μg/ml). **(C-D, F)** Bars represent mean ± SEM; statistical analyses used Student's *t*-test; * $p<0.05$, *** $p<0.001$, ns – not significant.

*4.2.6 **BAP1 genome-wide binding in B lymphocytes***

To identify the genomic regions directly regulated by BAP1 in mature B cells, we conducted ChIP-seq to map BAP1 genome-wide DNA-binding sites using an anti-BAP1 antibody and wild type CH12F3 cells, with and without stimulation with TGF-β, IL-4, and anti-CD40 over 72 hours. While there are limitations to using CH12F3 cells as a model of primary GC B cells, BAP1 is a challenging target, with most previously published ChIP-seq datasets using cells that express an epitope-tagged BAP1 protein [214, 221, 287]. We have therefore also repeated the ChIP-seq analysis using CH12F3 cells stably expressing 3xFLAG-tagged BAP1 with an antibody against the FLAG epitope, as previously described [221, 223]. We identified a total of 1,499 BAP1 binding sites (or peaks) across the genome (Figure 4.2.11A, Figure 4.2.12A), with the high concordance between the dataset from unstimulated and stimulated CH12F3 cells, indicating that BAP1 recruitment to chromatin is constitutive rather than induced with B cell stimulation. Among the BAP1 binding sites 88% were classified as gene-proximal based on their distance to the nearest gene transcription start site (≤1kb to TSS). To gain insights into the biological functions of the BAP1 transcriptional target genes, ontology analyses were performed on the genes in the vicinity of the BAP1 binding sites using the Genomic Regions Enrichment of Annotations Tool (GREAT) [250]. This

demonstrated a highly significant association of the gene-proximal BAP1 binding sites with the genes involved in proteosome-dependent protein degradation, DNA damage response, and protein trafficking, and the association of the gene-distal BAP1 binding sites with the genes involved in the regulation of transcription and RNA processing (Figure 4.2.11B). This suggests the role of BAP1 in the regulation of many transcriptional programs essential for normal cell physiology, as well as for the induction of B cell activation and humoral immune response.

To compare the role of BAP1 as a transcriptional regulator in mature B cells to its role in other cell types, we consolidated our newly acquired BAP1 ChIP-Seq with the previously published BAP1 ChIP-Seq datasets from Ba/F3 pro-B cells [223], ES cells [278], and macrophages [221]. This indicated a considerable overlap in BAP1 genomic binding and suggested shared BAP1 functions in the regulation of housekeeping transcriptional programs across many cell types (Figures 4.2.13A). To gain further insights into the cross-talk between BAP1 and other transcriptional regulators, we also consolidated our BAP1 ChIP-Seq data with the public ChIP-Seq datasets for BAP1-associated transcriptional regulators, including HCF1 and OGT in macrophages [221], and ASXL1 in hematopoietic stem and progenitor cells (HSPC) [279]. A significant overlap in the genomic localization was observed between BAP1 and BAP1-interacting proteins ASXL1, HCF1, and to a lesser extent OGT (Figure 4.2.12B), indicating that BAP1 may act in cooperation with these transcriptional regulators in B cells, as in other cell types. Furthermore, we consolidated our BAP1 ChIP-seq data with the public ChIP-seq datasets from primary murine B cells for the other major regulators of the histone H2AK119ub epigenetic mark, including polycomb proteins RING1B, CBX7, YY1, EZH2 and deubiquitinase USP16 [280, 281]. We observed an overlap in the genomic binding of BAP1 with components of the polycomb repressive complex 1 (PRC1), including its

E3 ubiquitin ligase catalytic subunit RING1B (Figure 4.2.12B). This suggests that BAP1 and PRC1 may co-regulate histone H2AK119ub levels and turnover at shared genomic locations. Interestingly, we also observed an overlap in the genomic binding of BAP1 and another well-known H2AK119ub-deubiquitinase USP16 (Figure 4.2.12B), suggesting their cooperative or complementary functions.

Figure 4.2.11 ChIP-seq analyses of BAP1 genome-wide binding and the effects of BAP1-loss on the histone H2AK119ub levels in CH12F3 B cells.

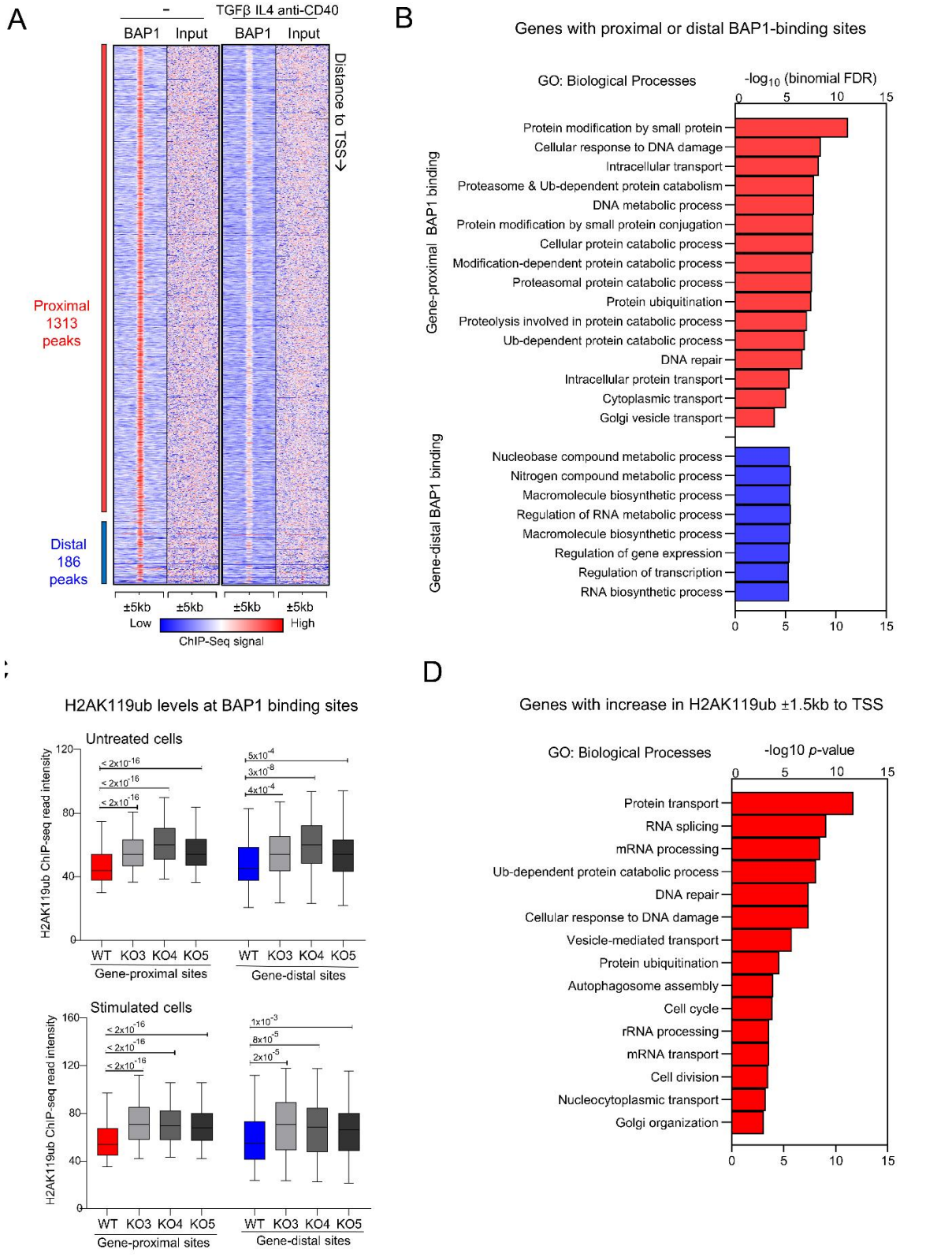

(A) Heat-map showing the tag densities of 1,499 BAP1 binding sites identified in the ChIP-Seq experiments from wild type CH12F3 cells, untreated and at 72-hours of stimulation with TGFβ, IL-4, and anti-CD40. The sites are ranked based on their distance to the nearest gene transcription start site (TSS), and the gene-proximal sites are defined based on their location within 1kb to the nearest gene TSS. **(B)** Gene ontology (GO) analysis performed on the GREAT website, showing the biological process GO-terms enriched for the genes nearest to each BAP1 binding site, plotting the $-\log_{10}$(binomial FDR) for each GO-term. **(C)** ChIP-Seq analyses of histone H2AK119ub levels at the BAP1 binding sites in CH12F3 cells, including wild type (WT) control cells and three independent clones of CRISPR/Cas9 edited *BAP1*-knockout cells (KO3-4-5). Box plots show the H2AK119ub read intensities ±5kb to the gene-proximal and gene-distal BAP1 binding sites, comparing WT and KO cells; the *p*-values are calculated using Mann-Whitney U-test. **(D)** Gene ontology enrichment analyses on the genes that undergo an increase in the levels of histone H2AK119ub (fold change ≥ 2.0) around their transcription start sites (±1.5kb to TSS) in $Bap1^{\Delta/\Delta}$ versus control CH12F3 B cells; the -log10(*p*-values) are listed for selected top GO-terms.

Figure 4.2.12 ChIP-seq analyses of the BAP1 genomic binding sites in CH12F3 cells in consolidation with other relevant public ChIP-seq datasets. (A-B)

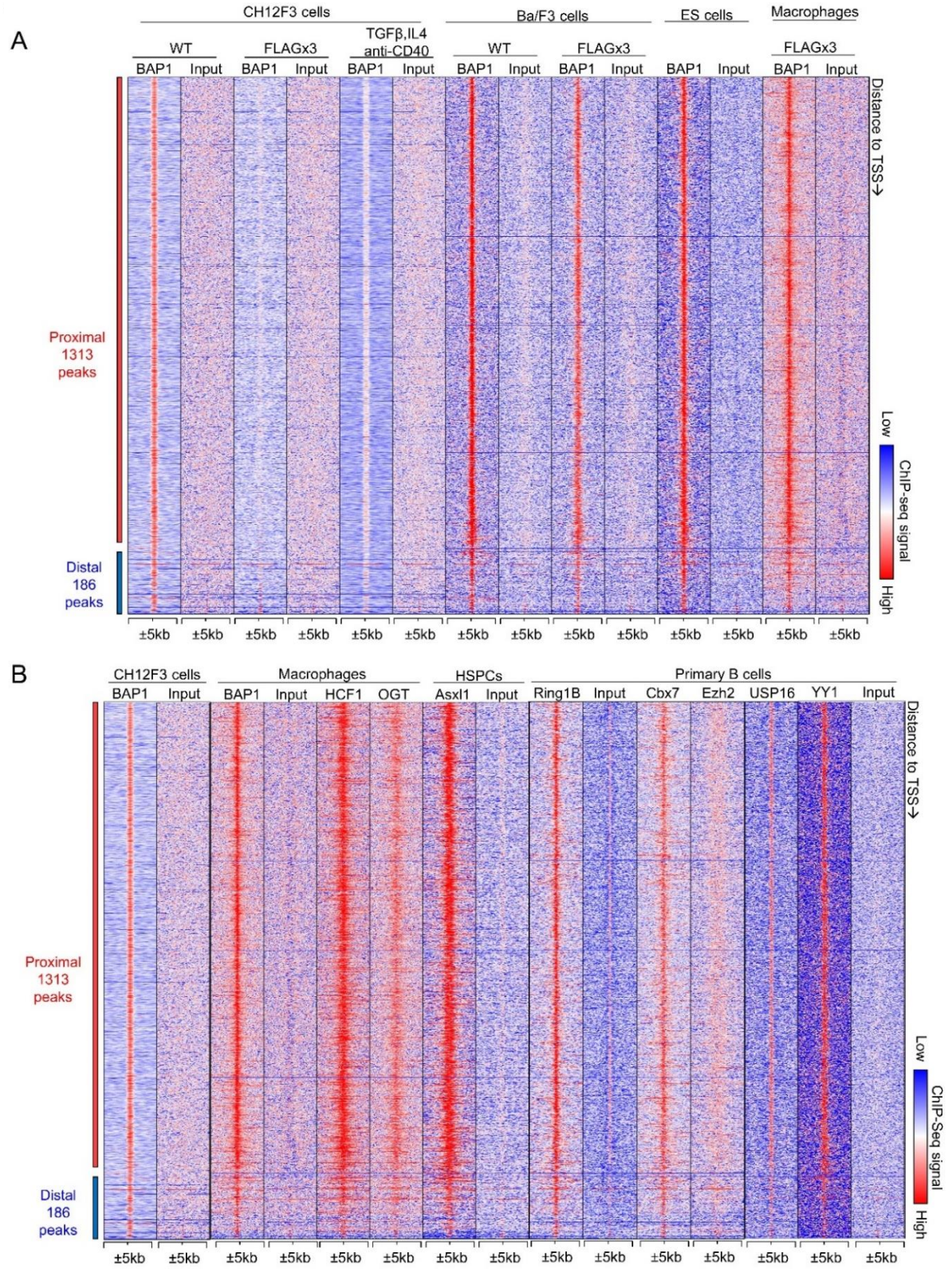

Heatmaps showing the tag densities of 1,499 BAP1 binding sites identified in our ChIP-seq analyses of CH12F3 cells, including from left to right wild type (WT) cells analyzed with anti-BAP1 antibody, cells stably expressing FLAGx3-tagged BAP1 analyzed with anti-FLAG antibody, and WT cells stimulated with TGFβ, IL-4, and anti-CD40 for 72 hours and analyzed with anti-BAP1 antibody. **(A)** The BAP1 ChIP-seq datasets from CH12F3 cells are consolidated with the available public BAP1 ChIP-seq datasets, including from Ba/F3 pro-B cells [223], ES cells [278], and bone marrow derived macrophages [221], to analyze for BAP1 binding site colocalization across different cell types. **(B)** The BAP1 ChIP-seq datasets from CH12F3 cells are consolidated with the public ChIP-seq datasets for BAP1 associated transcriptional regulators, including HCF1 and OGT in bone marrow derived macrophages [221] and ASXL1 in bone marrow hematopoietic stem and progenitor cells (HSPCs, $cKit^{+}$) [279], as well as ChIP-seq datasets for other regulators of histone H2AK119ub, including polycomb proteins RING1B, CBX7, EZH2 and deubiquitinase USP16 from quiescent $CD43^{-}$ resting splenic B cells [280] and polycomb protein YY1 from follicular splenic B cells ($CD19^{+}AA4^{-}CD21^{lo}CD23^{hi}$) [281]. All public ChIP-seq datasets are from mouse, downloaded and re-analyzed using our pipelines.

4.2.7 Non-redundant role of BAP1 as a deubiquitinase for histone H2AK119ub in B cells

To assess the role of BAP1 as a DUB for histone H2AK119ub in activated B cells, consistent with its reported function in other cell types [186], further ChIP-Seq analyses were performed to quantify the histone mark H2AK119ub. The study compared control wild type (WT) and BAP1-deficient $Bap1^{\Delta/\Delta}$ CH12F3 B cell lines, analyzing three independent clones of CH12F3 cells (KO3-4-5) and repeating the analyses at steady-state and following cell activation (TGFβ, IL-4, anti-CD40, 72 hours). ChIP-Seq data demonstrated that the loss of BAP1 resulted in a highly significant increase in histone H2AK119ub levels at the BAP1 binding sites and surrounding genomic regions (±5kb) in all the three $Bap1^{\Delta/\Delta}$ clones and under both untreated and stimulated conditions (Figures 4.2.12C). This establishes the non-redundant role of BAP1 as a DUB for histone H2AK119ub in B lymphocytes.

Next, we set out to interrogate the biological functions of the genes regulated via the BAP1 DUB-activity for H2AK119ub. We therefore re-analyzed our ChIP-seq datasets to identify the genes with a >2-fold increase in H2AK119ub within ±1.5kb to their TSS in the $Bap1^{\Delta/\Delta}$ relative to control

CH12F3 B cells. GO-term analysis on this gene-set indicated that the genes undergoing an increase in H2AK119ub with the loss of BAP1 encode regulators of protein transport, Ub-dependent protein degradation, DNA damage response and repair, RNA processing, as well as autophagosome assembly and cell cycle progression (Figure 4.2.11D). This demonstrates a strong concordance in the biological functions of this gene-set with the genes marked by BAP1-binding (Figure 4.2.11B, D). Overall, we conclude that BAP1 acts as a DUB for H2AK119ub in B cells to regulate many transcriptional programs essential for normal cell physiology, and for B cell activation and the induction of humoral immune response.

For further insights into BAP1 functions as a DUB for H2AK119ub in the transcriptional networks of B cell mediated immune response, we performed supplementary analyses to consolidate our ChIP-seq datasets with the published RNA-seq data characterizing the transcriptional response of wild type CH12F3 cells to stimulation [288], and the transcriptional change with the transition from follicular to GC in primary B cells [289]. In both cases, we identified a subset of differentially expressed genes that in our datasets have proximal BAP1 binding and sustain an increase in H2AK119ub with the loss of BAP1. Such datasets may represent a starting point for future studies to validate and characterize genes under the direct transcriptional control of BAP1 in activated B cells.

4.2.8 BAP1-regulated transcriptional programs of germinal center B cells

To further analyze the role of BAP1 in the transcriptional regulation of B cell activation, RNA-Seq gene expression analysis was conducted on GC B cells isolated from the spleen of *Bap1*$^{fl/fl}$ Cγ1-Cre and control *Bap1*$^{+/+}$ Cγ1-Cre mice at day 11 post-SRBC immunization, with the cells

gated for FACS-sorting as shown in Figure 4.2.13. As already discussed, a strong reduction in the expression of the *Bap1*^{fl} exons was demonstrated in the RNA-seq datasets from *Bap1*$^{fl/fl}$ Cγ1-Cre relative to control GC B cells (Figure 4.2.2C-D), confirming an effective Cre-mediated *Bap1* gene inactivation in the cells captured for the RNA-seq. Importantly, dimension reduction analysis of the gene expression profiles revealed a clear segregation of the *Bap1*$^{fl/fl}$ Cγ1-Cre and control *Bap1*$^{+/+}$ Cγ1-Cre GC datasets (Figure 4.2.14A, PC1 – 31% and PC2 –14% variance), which indicates a significant transcriptional change in GC B cells with the loss of BAP1.

To explore the biological functions of the genes dysregulated in *Bap1*-deficient GC B cells, gene set enrichment analysis (GSEA) was performed [274]. This demonstrated a significant downregulation of the transcriptional signatures involved in B cell engagement with T-helper cells, such as 'positive regulation of T cell proliferation' and 'positive regulation of IL2 production' in the *Bap1*$^{fl/fl}$ Cγ1-Cre GC B cells, as well as an upregulation of the transcriptional signatures linked to mitochondrial function such as 'inner mitochondrial membrane organization', 'ATP biosynthetic process', and 'oxidative phosphorylation' (Figure 4.2.14B). We also conducted a differential gene expression analysis between the *Bap1*$^{fl/fl}$ Cγ1-Cre and control *Bap1*$^{+/+}$ Cγ1-Cre GC B cells, at the fold change (FC) ≥ |2.0| and false discovery rate (FDR) ≤ 0.05, which identified 94 upregulated and 76 downregulated genes in the *Bap1*$^{fl/fl}$ Cγ1-Cre GC B cells. Applying gene ontology (GO) analysis, we note the downregulation of the transcriptional signature of 'intracellular signal transduction' in the *Bap1*$^{fl/fl}$ Cγ1-Cre GC B cells (Figure 4.2.14C), with the downregulated genes including important positive and negative regulators of B cell receptor signaling, such as *Nfam1* [290], *Camk2d* [291], *Lrrk2* [292], *Dgka* [293], and *Cblb* [294, 295] (Figure 4.2.14D). As an example, *Cblb* encodes an E3 ubiquitin ligase that targets CD79a, CD79b, and IRF4 to regulate the initiation and

progression of the GC-reaction [294, 295]. Overall, the cell intrinsic loss of BAP1 in GC B cells resulted in a dysregulation of the transcriptional programs essential for normal induction of humoral immune response.

We consolidated the RNA-seq and ChIP-seq datasets to identify putative genes under the direct transcriptional control of BAP1 in B cells, as the genes dysregulated in *Bap1*$^{fl/fl}$ Cγ1-Cre GC B cells and with BAP1-binding at their promoters in CH12F3 and/or BaF3 B cell lines. While our datasets showed no evidence for BAP1 regulation of the genes encoding the major mediators of B cell lineage choice, GC reaction, or plasma cell differentiation (*Bach2*, *Batf*, *Bcl6*, *Blimp1*/*Prdm1*, *Irf4*, *Irf8*, *Myc*, *Pax5*, *Xbp1*), we identified 73 putative BAP1-regulated genes. Such genes included the regulators of B cell receptor signaling *Dgka* and *Cblb*, already discussed above (Figure 4.2.14D-E) [293, 294, 295]. The genes also included *Litaf* that encodes a repressor of *Bcl6*-expression and a regulator of autophagy and apoptosis in B cell lymphoma [296, 297], as well as *Igf2bp3* that encodes a reader of the N6-methyladenosine (m6A) RNA-modification, specifically induced in GC B cells and essential for normal induction of humoral immune response (Figure 4.2.14D-E) [298]. In summary, our study identifies novel transcriptional targets of BAP1 that are essential for the progression of GC-reaction and can contribute to the failure of humoral immunity with the loss of BAP1 function.

Figure 4.2.13 Gating strategy used for the FACS-sort of GC B cells for RNA-seq analyses.

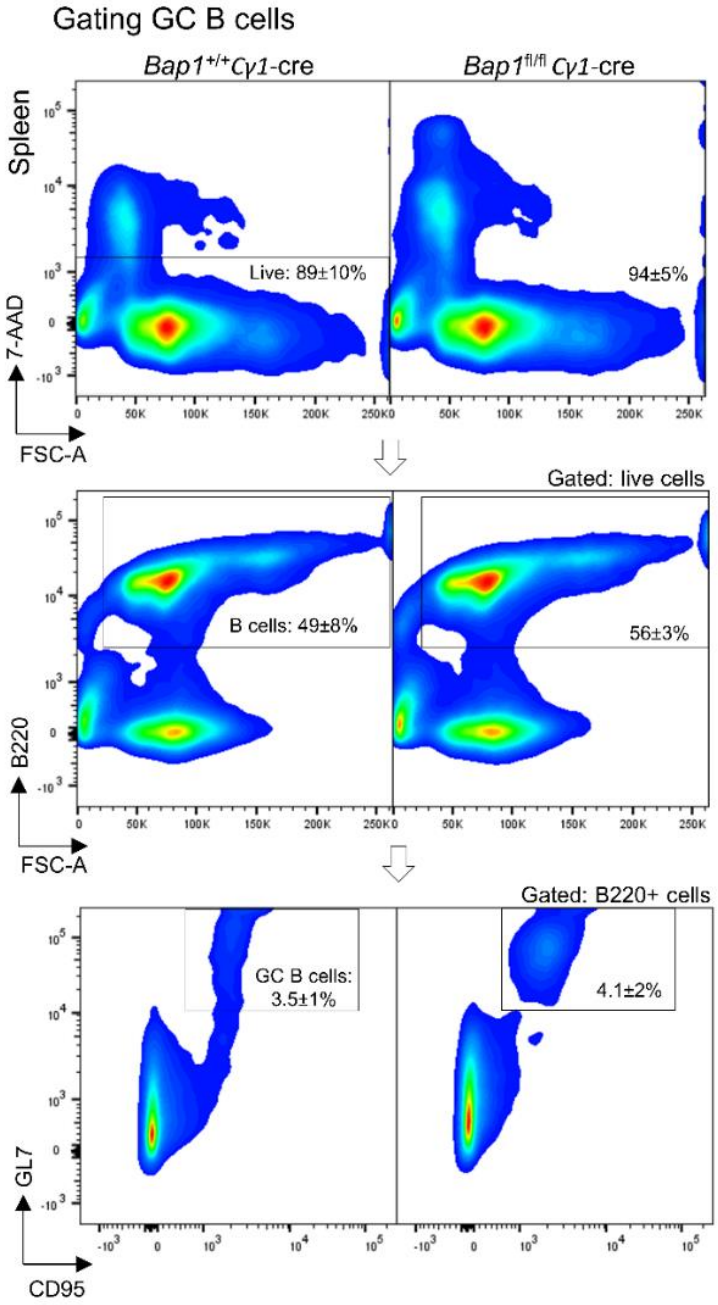

GC B cells were FACS-sorted from total splenocytes of *Bap1*$^{fl/fl}$ *Cγ1-Cre* and control *Bap1*$^{+/+}$ *Cγ1-Cre* mice at day 11 after the primary intravenous immunization with SRBC. Representative flow cytometry plots show the gating for GC B cell population as live B220^{+}GL7^{+}CD95^{+} cells. Percentages of cells within each gate relative to the parent gate for each mouse genotype are presented as mean ± S.D.

Figure 4.2.14 RNA-Seq analysis of the transcriptome of *Bap1*$^{fl/fl}$ Cγ1-Cre and control *Bap1*$^{+/+}$ Cγ1-Cre GC B cells.

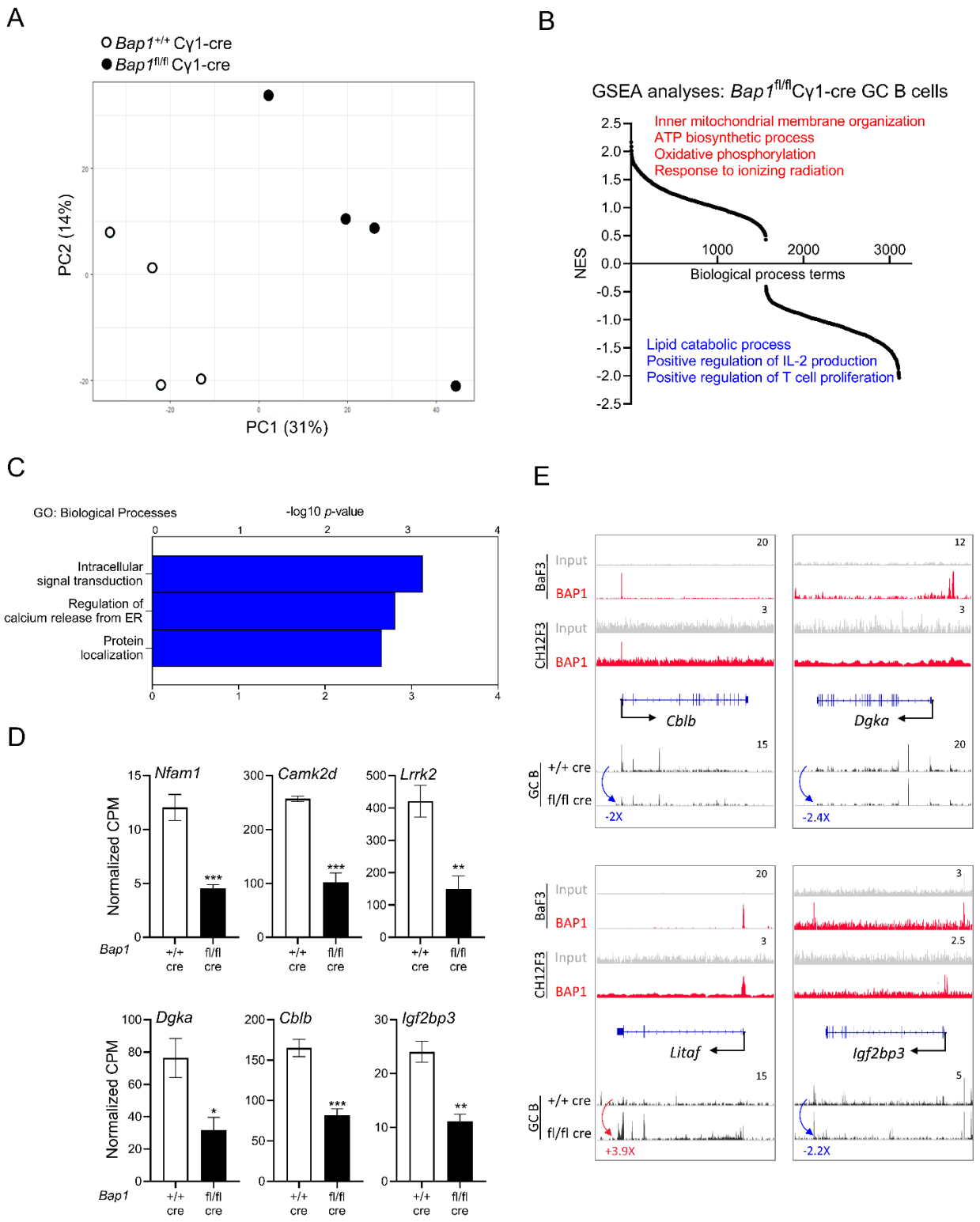

(A) Principal component analysis plot demonstrating the gene expression profiles of the RNA-Seq samples: differences between the *Bap1* genotypes are described by principal component 1 (PC1, 31% variability) and PC2 (14%). **(B)** Gene set enrichment analysis (GSEA) showing the normalized enrichment scores (NES) of 3,107 pre-established biological processes transcriptional signatures in $Bap1^{fl/fl}$ Cγ1-Cre relative to control $Bap1^{+/+}$ Cγ1-Cre GC B cells. **(C)** Gene ontology enrichment analysis of the genes downregulated in $Bap1^{fl/fl}$ Cγ1-Cre relative to control $Bap1^{+/+}$ Cγ1-Cre GC B cells, at fold change (FC) ≥ |2.0| and false discovery rate (FDR) ≤0.05; -log10(*p*-values) for the top GO-terms are presented. **(D)** Examples of the genes downregulated in $Bap1^{+/+}$ Cγ1-Cre GC B cells and encoding important regulators on B cell receptor signaling, GC reaction, and humoral immunity; data presented as normalized read counts per million (CPM); bars represent mean ± SEM; * $p< 0.05$, ** $p<0.01$, *** $p<0.001$. **(E)** Genomic snapshots of selected genes representing the putative direct transcriptional targets of BAP1 in B cells, based on their altered expression in the $Bap1^{fl/fl}$ Cγ1-Cre GC B cells RNA-seq data and on BAP1 binding at their promoters in the ChIP-seq data. ChIP-Seq tracks for BAP1 and input DNA are shown on the top two lanes, including new data from CH12F3 B cells and previously published data from Ba/F3 pre-B cells [223]. The gene feature track is shown in the middle, and averaged RNA-Seq tracks are in the bottom, with fold changes comparing expression in $Bap1^{fl/fl}$ Cγ1-Cre and control $Bap1^{+/+}$ Cγ1-Cre GC B cells indicated. The maximum data range of each track is indicated at the top-right corner.

4.3 Role of MYSM1 and its DUB Activity in Hematopoiesis

4.3.1 Loss of MYSM1 impairs HSC function and hematopoietic cell differentiation

MYSM1 is another focus of our study. Like BAP1, MYSM1 is also a deubiquitinase (DUB) that is able to target histone H2AK119ub and is a potential regulator of gene expression in hematopoietic and immune systems. Previous studies revealed the importance of MYSM1 in hematopoiesis. Mice with systemic loss of MYSM1 show partial embryonic lethality, growth retardation, and severe hematopoietic defects[180, 232], which resemble the inherited bone marrow failure syndrome (IBMFS) of human patients with *Mysm1* mutations[225, 226, 227, 299]. Through characterizing *Mysm1*$^{-/-}$ inducible knockout mouse models, we and others found that the loss of MYSM1 resulted in impaired HSC quiescence, apoptosis of hematopoietic progenitors, and a severe depletion of erythroid cells, lymphocytes, DCs, and other hematopoietic lineages [180, 232, 237]. Moreover, we and others characterized p53 activation as the common feature of MYSM1 deficiency and the driving mechanism for the described hematopoietic pathologies, which is demonstrated by the rescue of *Mysm1*$^{-/-}$ phenotypes in the *Mysm1*$^{-/-}$*p53*$^{-/-}$ double knockout mice [238, 239, 240, 241, 300]. However, although several mechanisms for p53 activation in MYSM1 deficiency were proposed, no clear link to MYSM1 DUB catalytic activity has emerged so far [239, 240, 244, 301]. In fact, it is important to stress that not all MYSM1 functions are directly linked to its DUB catalytic activity, and it also engages in many functionally significant protein-protein interactions [224, 225]. Recently, we conducted the first genome-wide analysis for MYSM1-regulated genes in mouse HSCs and reported that MYSM1 maintains the expression of genes encoding ribosomal proteins [244], however with MYSM1-loss the levels of H2AK119ub at the MYSM1-binding sites within these gene promoters remained below the level of detection, suggesting other modes for their transcriptional regulation by MYSM1 [244]. Overall, it remains unknown whether all

biologically significant MYSM1 functions are universally dependent on its DUB catalytic activity and whether MYSM1 catalytic activity is essential for the maintenance of hematopoiesis *in vivo*. In the current study, we generated and characterized mouse strains carrying a *Mysm1*^{D660N} point mutation predicted to render MYSM1 protein catalytically inactive without affecting its stability and expression (referred to as *Mysm1*$^{DN/DN}$ and *Mysm1*$^{fl/DN}$Cre^{ERT2} mouse strains with a constitutive and an inducible loss of MYSM1 DUB catalytic activity, respectively). We sought to compare the developmental, hematopoietic, and immune phenotypes resulting from the loss of MYSM1 catalytic function versus the full loss of MYSM1 protein in mouse models, and further explore the role of MYSM1 and its DUB catalytic activity in development and functions of hematopoietic cells.

4.3.2 Loss of catalytic activity in the MYSM1 ^{D660N} mutant protein

To generate an allele encoding a catalytically inactive MYSM1 in mouse we chose to introduce the *Mysm1*^{D660N} point mutation at the highly conserved aspartic acid 660 residue within the JAMM motif of the MPN catalytic domain (Figure 4.3.1A). This residue is considered essential to the catalytic mechanism and is predicted to interact with both Zn^{2+} and the substrate [228, 302]. To confirm that the catalytic activity of MYSM1^{D660N} is indeed impaired, we expressed and purified both wild-type MYSM1 and MYSM^{D660N} proteins from Sf9 insect cells, and performed an *in vitro* catalytic activity assay using Ubiquitin-Rhodamine 110 as substrate. The proteins were purified from Sf9 insect cells at a similar yield (0.78 mg/L of cells for wild type MYSM1, 0.83 mg/L of cells for MYSM1^{D660N}) and eluted in a retention volume slightly lower than 13 mL in size exclusion chromatography, demonstrating that they were not aggregated and likely not misfolded (Figure 4.3.2A). We found that wild-type MYSM1 cleaved the substrate in a dose-dependent manner with

a K_m of 8.5 μM for the substrate, whereas the activity of $MYSM^{D660N}$ was completely abrogated (Figure 4.3.1B). This confirms that the D660N mutation inactivates the catalytic activity of mouse MYSM1 protein.

Figure 4.3.1 Development and validation of the mouse model expressing a catalytically inactive MYSM1.

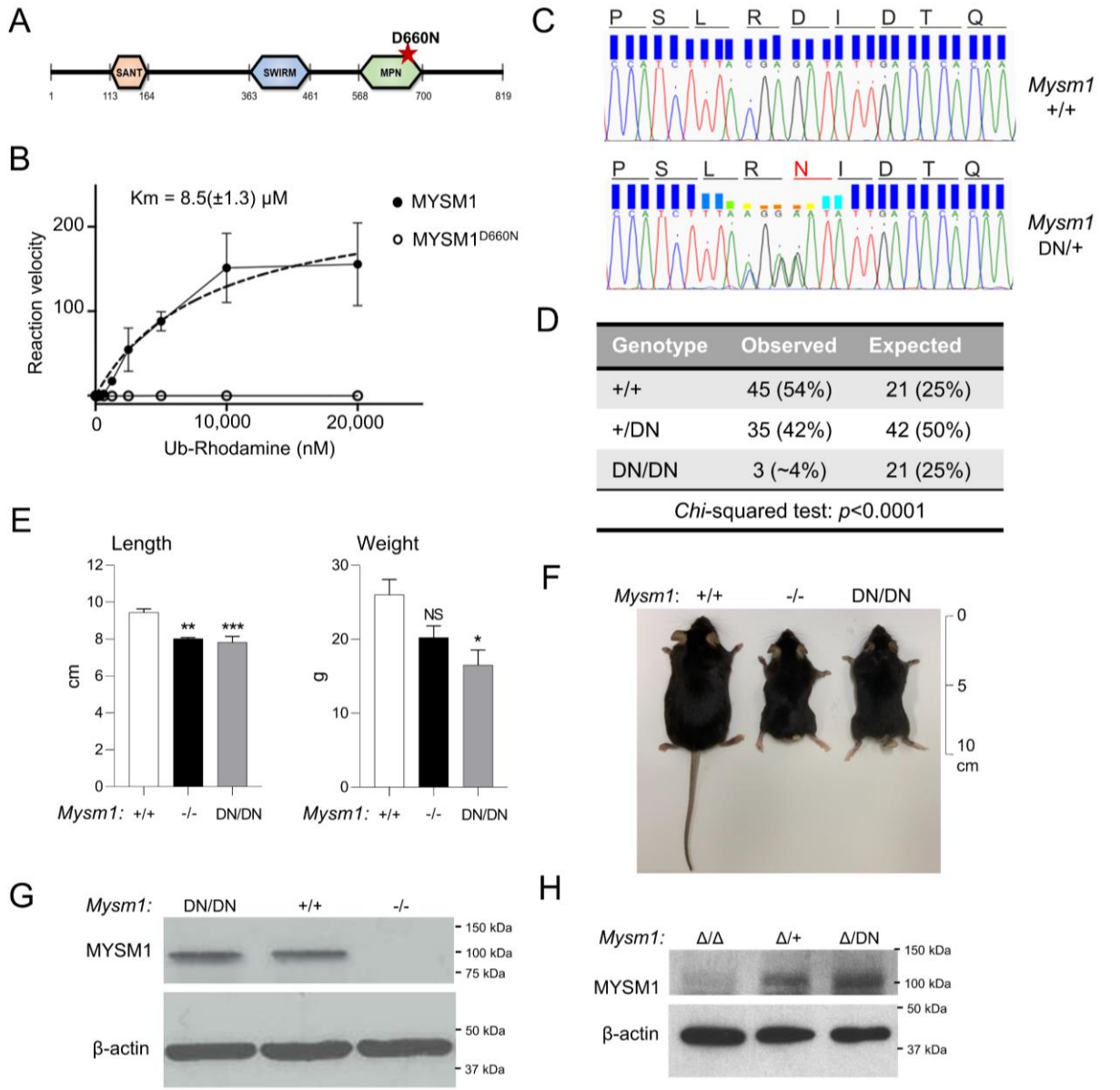

(A) Domain structure of the mouse MYSM1 protein indicating the mutation in the MPN catalytic domain predicted to render the protein catalytically inactive. **(B)** Catalytic activity assay of recombinant mouse MYSM1 against ubiquitin-Rhodamine substrate demonstrates that the D660N mutation results in a full loss of the DUB catalytic activity. **(C)** Sanger sequencing of the *Mysm1* locus in the genomic DNA of wild type control and *Mysm1*$^{DN/+}$ heterozygous mice, indicating the DNA sequences and the corresponding amino acid sequences of the wild type and mutant proteins. **(D)** High embryonic lethality of *Mysm1*$^{DN/DN}$ mice: offspring genotypes obtained from the mating of two *Mysm1*$^{+/DN}$ heterozygous parents show strong deviation from expected Mendelian ratios. **(E)** Length and weight of the age- and sex- matched mice of *Mysm1*$^{+/+}$, *Mysm1*$^{-/-}$ and *Mysm1*$^{DN/DN}$ genotypes; bars represent means ± SEM, statistical analysis with ANOVA comparing each group to the control, * p<0.05, ** p<0.01, *** p<0.001, NS - not significant. **(F)** Representative image of the age- and sex- matched mice of *Mysm1*$^{+/+}$, *Mysm1*$^{-/-}$ and *Mysm1*$^{DN/DN}$ genotypes, showing reduced body size and tail dysmorphology. **(G)** Western blot of mouse bone marrow cell lysates showing comparable MYSM1 protein levels in *Mysm1*$^{+/+}$ and *Mysm1*$^{DN/DN}$ samples. **(H)** Western blot of splenocyte lysates from tamoxifen-treated Cre^{ERT2} transgenic mice of *Mysm1*$^{fl/+}$, *Mysm1*$^{fl/fl}$, and *Mysm1*$^{fl/DN}$ genotypes, showing strong depletion of MYSM1 protein in the *Mysm1*$^{\Delta/\Delta}$ cells, and comparable MYSM1 protein levels between *Mysm1*$^{\Delta/+}$ and *Mysm1*$^{\Delta/DN}$ samples. β-actin is used as a loading control in (G-H).

Figure 4.3.2 Supplemental analyses of MYSM1D660N protein and transcript.

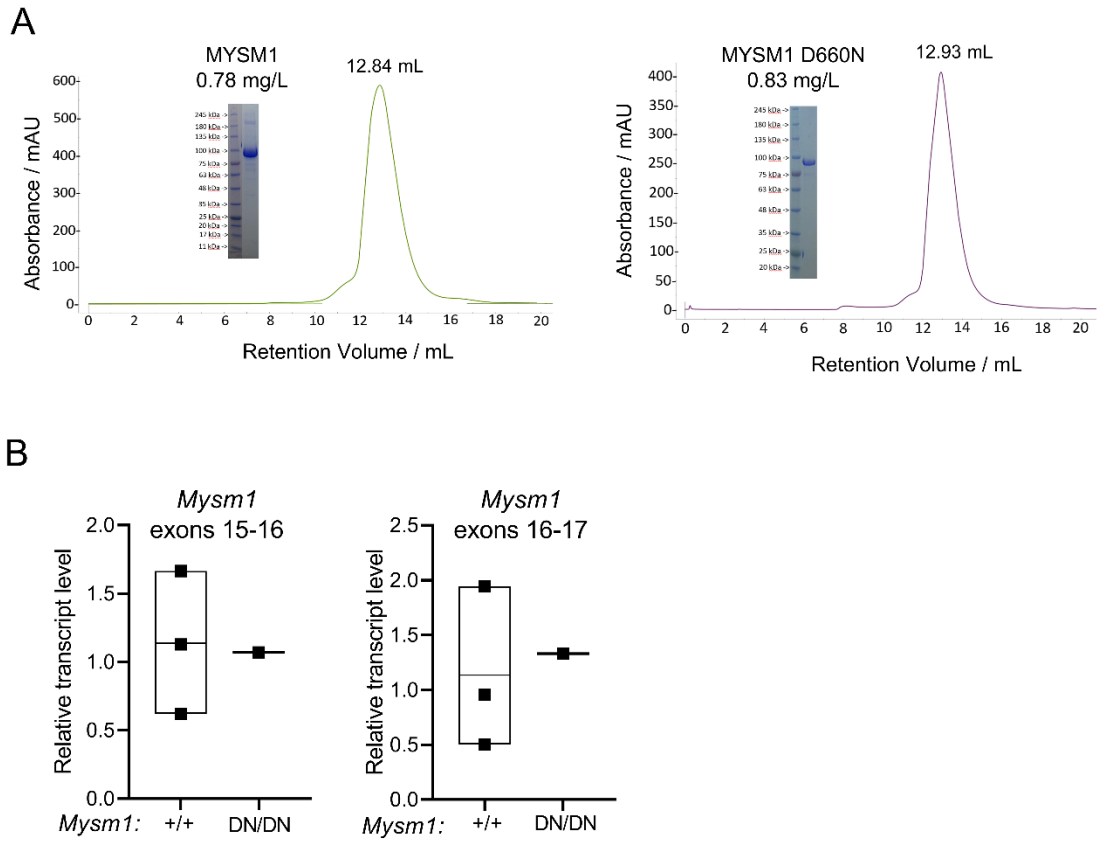

(A) Size exclusion chromatography of murine wild type MYSM1 (green) and MYSM1^{D660N} (purple) proteins, recombinantly expressed in Sf9 insect cells, with associated SDS-PAGE. The Superdex 200 increase analytical column (GE Healthcare) was eluted at a flow rate of 0.75 mL/min with 20 mM Tris (pH 8.1), 150 mM NaCl, 1 mM DTT. Fractions containing the cleanest samples were pooled and concentrated to ~10 mg/mL. The yields of the wild type and mutant proteins were 0.78 mg/L and 0.83 mg/L of insect cell culture, respectively. **(B)** RT-qPCR analysis of the *Mysm1* transcript in mouse bone marrow cells using new primer pairs spanning the *Mysm1* exon junctions 15-16 and 16-17, demonstrating no change in the levels of *Mysm1* transcript spliced across these exon junctions in *Mysm1*$^{DN/DN}$ relative to *Mysm1*$^{+/+}$ control cells. Each dot represents a different mouse; transcript levels are normalized to *Hprt* housekeeping control transcript and then to the mean *Mysm1* transcript levels in the *Mysm1*$^{+/+}$ control mice.

4.3.3 Generation of the Mysm1 ^{D660N} mouse strain

We used CRISPR/Cas9-mediated genome editing in zygotes to introduce the point mutation into exon 16 of *Mysm1*. C57BL/6 zygotes were co-injected with Cas9 protein and a gRNA, along with two homology-dependent recombination (HDR) templates. Since conventional knockout of MYSM1 causes partial embryonic lethality, we used two HDR templates to increase the efficiency of the procedure: one HDR template for the introduction of the D660N mutation and a second template introducing silent mutations to disrupt the gRNA recognition site [303]. The founder harboring both the D660N and silent mutations was backcrossed onto C57BL/6 mice to generate heterozygous *Mysm1*^{D660N} mice lacking the silent mutations on the other *Mysm1* allele. Sanger sequencing of the genomic DNA demonstrated successful introduction of the point mutation that translates into the MYSM1^{D660N} amino acid substitution in the protein (Figure 4.3.1C). The sequencing window covered 371 nucleotides (NCBI GRCm39 *Mysm1*, Gene ID: 320713, range from 94840309 to 94840679), and included the entire *Mysm1* exon-16 and ≥80 nucleotides of the flanking introns at both ends, and demonstrated no other mutations apart from those shown in Figure 4.3.1C and resulting in the D660N substitution in the protein. As the mutations are located >20 nucleotides away from the 3' splice site of *Mysm1* exon-16 they are not expected to disrupt splicing [304]; and further analysis of the *Mysm1*^{D660N} allele with the Spliceator online tool

(*www.lbgi.fr/spliceator/*) predicted no changes in splicing. Furthermore, RT-qPCR analysis of mouse bone marrow cells with the primer pairs spanning *Mysm1* exon junctions 15-16 and 16-17 demonstrated no changes in the levels of *Mysm1* transcript successfully spliced across these exon junctions in *Mysm1*$^{DN/DN}$ compared to *Mysm1*$^{+/+}$ control cells (Figure 4.3.2B).

4.3.4 Mysm1 $^{DN/DN}$ mouse model: partial embryonic lethality and developmental phenotypes

Mysm1$^{DN/DN}$ mice were born in sub-Mendelian numbers, with only ~4% of offspring from an intercross of two heterozygous parents having the *Mysm1*$^{DN/DN}$ genotype, indicating that the loss of MYSM1 catalytic activity causes increased embryonic lethality (Figure 4.3.1D). At adulthood, *Mysm1*$^{DN/DN}$ mice were significantly smaller in length and weight than their littermates (Figure 4.3.1E-F), and had abnormally short tails (Figure 4.3.1F), as previously seen in the *Mysm1*$^{-/-}$ mice [180, 232]. Importantly, we demonstrated similar levels of MYSM1 protein in *Mysm1*$^{DN/DN}$ and control *Mysm1*$^{+/+}$ bone marrow cells, and the expected loss of MYSM1 protein expression in *Mysm1*$^{-/-}$ cells (Figure 4.3.1G). Overall, we highlight the similarity in the gross developmental phenotypes of the *Mysm1*$^{DN/DN}$ and *Mysm1*$^{-/-}$ mouse strains, and establish the essential role of the MYSM1 DUB catalytic activity *in vivo*.

4.3.5 Mysm1 $^{fl/DNCreERT2}$ mouse model for an inducible loss of the MYSM1 catalytic activity

Given the partial embryonic lethality and low availability of the *Mysm1*$^{DN/DN}$ mice, we crossed the mice to the *Mysm1*$^{fl/fl}$Cre^{ERT2} mouse strain that allows highly efficient *Mysm1*^{fl} to *Mysm1*$^{\Delta}$ allele conversion with tamoxifen treatment, as demonstrated in our previous studies [234, 244]. Here we derived cohorts of Cre^{ERT2}-transgenic mice of *Mysm1*$^{fl/+}$, *Mysm1*$^{fl/fl}$, and *Mysm1*$^{fl/DN}$ genotypes, which were born in normal Mendelian numbers, lacked any obvious developmental phenotypes,

and bred normally (data not shown). Following tamoxifen treatment, we demonstrated a strong depletion of MYSM1 protein in *Mysm1*$^{\Delta/\Delta}$ mouse splenocytes, but comparable retention of MYSM1 protein levels in *Mysm1*$^{\Delta/+}$ and *Mysm1*$^{\Delta/DN}$ samples (Figure 4.3.1H). The *Mysm1*$^{fl/DN}$ Cre^{ERT2} model will test the effects of the loss of MYSM1 DUB catalytic activity on the maintenance of hematopoiesis, leukocyte development, and other aspects of mammalian physiology, independently of its roles in mouse development and the significant developmental phenotypes seen in the *Mysm1*$^{DN/DN}$ mouse strain.

4.3.6 Severe hematologic dysfunction in Mysm1 $^{DN/DN}$ and Mysm1 $^{fl/DN}$ Cre^{ERT2} mice

Hematology analyses of the blood of *Mysm1*$^{DN/DN}$ and *Mysm1*$^{-/-}$ mice relative to the *Mysm1*$^{+/+}$ controls, demonstrated severe hematopoietic dysfunction, characterized by macrocytic anemia, with reduction in blood erythrocyte counts, hematocrit, and hemoglobin concentration, as well as an increased in mean corpuscular volume (MCV, Figure 4.3.3A). Severe depletion of leukocytes and lymphocytes in *Mysm1*$^{DN/DN}$ relative to control *Mysm1*$^{+/+}$ mice was also observed (Figure 4.3.3A). Overall, the reported anemia and leukopenia phenotypes of *Mysm1*$^{DN/DN}$ mice are highly consistent with those observed in the *Mysm1*$^{-/-}$ mouse model (Figure 4.3.3A), and also clinically in the patients with *MYSM1* loss-of-function mutations [225, 226, 227, 299].

We conducted further hematology analyses on tamoxifen-treated Cre^{ERT2} transgenic mice of *Mysm1*$^{+/fl}$, *Mysm1*$^{fl/fl}$, and *Mysm1*$^{DN/fl}$ genotypes, and observed highly similar hematopoietic phenotypes in the *Mysm1*$^{\Delta/DN}$ mice, including macrocytic anemia, leukopenia, and lymphocyte depletion (Figure 4.3.3B). We further observed an increase in platelets in *Mysm1*$^{DN/\Delta}$ mice (Figure 4.3.3B), while platelets were not quantified in the *Mysm1*$^{DN/DN}$ model due to increased clotting of

the blood samples. Elevated platelet counts were previously reported for the *Mysm1*$^{-/-}$ mouse strain [180, 225], and although the mechanisms remain poorly understood they may be linked to elevated inflammatory response in *Mysm1*$^{-/-}$ mice [235, 236, 305], as thrombocytosis is a common feature of systemic inflammation [306]. Overall, we demonstrate that the loss of MYSM1 DUB catalytic activity in either constitutive or inducible mouse models results in a severe hematologic dysfunction with highly similar phenotypes to the previously characterized *Mysm1*$^{-/-}$ and *Mysm1*$^{\Delta/\Delta}$ mouse strains.

Figure 4.3.3 Hematologic dysfunction in the mouse models with the loss of MYSM1 DUB catalytic activity.

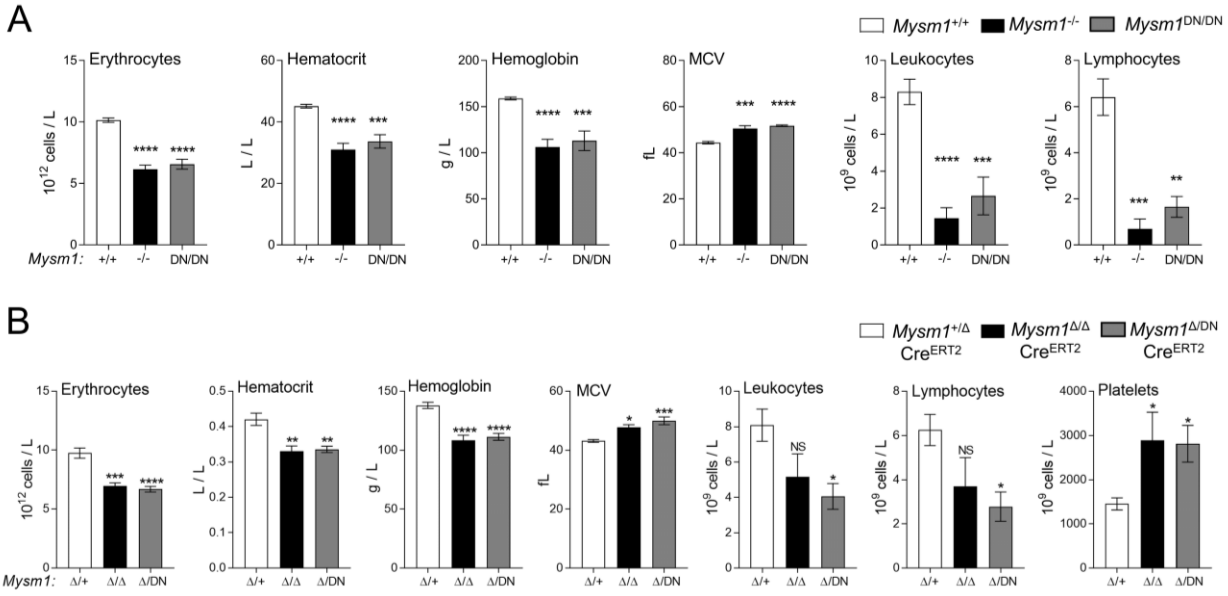

Hematology analyses were conducted on the blood of **(A)** *Mysm1*$^{+/+}$, *Mysm1*$^{-/-}$, and *Mysm1*$^{DN/DN}$ mice, and **(B)** Cre^{ERT2}-transgenic tamoxifen-treated mice of *Mysm1*$^{fl/+}$, *Mysm1*$^{fl/fl}$, and *Mysm1*$^{fl/DN}$ genotypes. Data is from (A) 3-8 mice per genotype consolidated from two independent experiments, or (B) 5-6 mice per genotype consolidated from two independent experiments. Bars represent means ± SEM; statistical analysis with ANOVA comparing each group to the control, * p<0.05, ** p<0.01, *** p<0.001, NS - not significant; MCV - mean corpuscular volume.

4.3.7 Depletion of lymphoid and myeloid immune cells in the Mysm1 $^{DN/DN}$ mice

Severe reduction in lymphocyte numbers, including B cells, CD4 T cells, CD8 T cells, and NK cells, was also observed in the spleen of the *Mysm1*$^{DN/DN}$ and *Mysm1*$^{\Delta/DN}$ mice, with the overall phenotype being highly similar to that of the *Mysm1*$^{-/-}$ and *Mysm1*$^{\Delta/\Delta}$ mouse models (Figure 4.3.4A-D). An increase in the proportion of dead cells was also observed, particularly for splenic B cells and NK cells in *Mysm1*$^{DN/DN}$ relative to control *Mysm1*$^{+/+}$ mice (Figure 4.3.5A). Further analyses confirmed the depletion of splenic transitional (T1-3) and follicular B cells in the *Mysm1*$^{DN/DN}$ and *Mysm1*$^{\Delta/DN}$ mice, with a somewhat milder depletion of the marginal zone B cell population (Figure 4.3.6A-B). The numbers of myeloid cells, including monocytes, macrophages, and neutrophils, were somewhat more variable across the experimental groups, but also showed a depletion in the *Mysm1*$^{DN/DN}$ and *Mysm1*$^{\Delta/DN}$ mice (Figure 4.3.4E-F, Figure 4.3.5B).

Figure 4.3.4 Depletion of splenic lymphoid and myeloid immune cells with the loss of MYSM1 DUB catalytic activity.

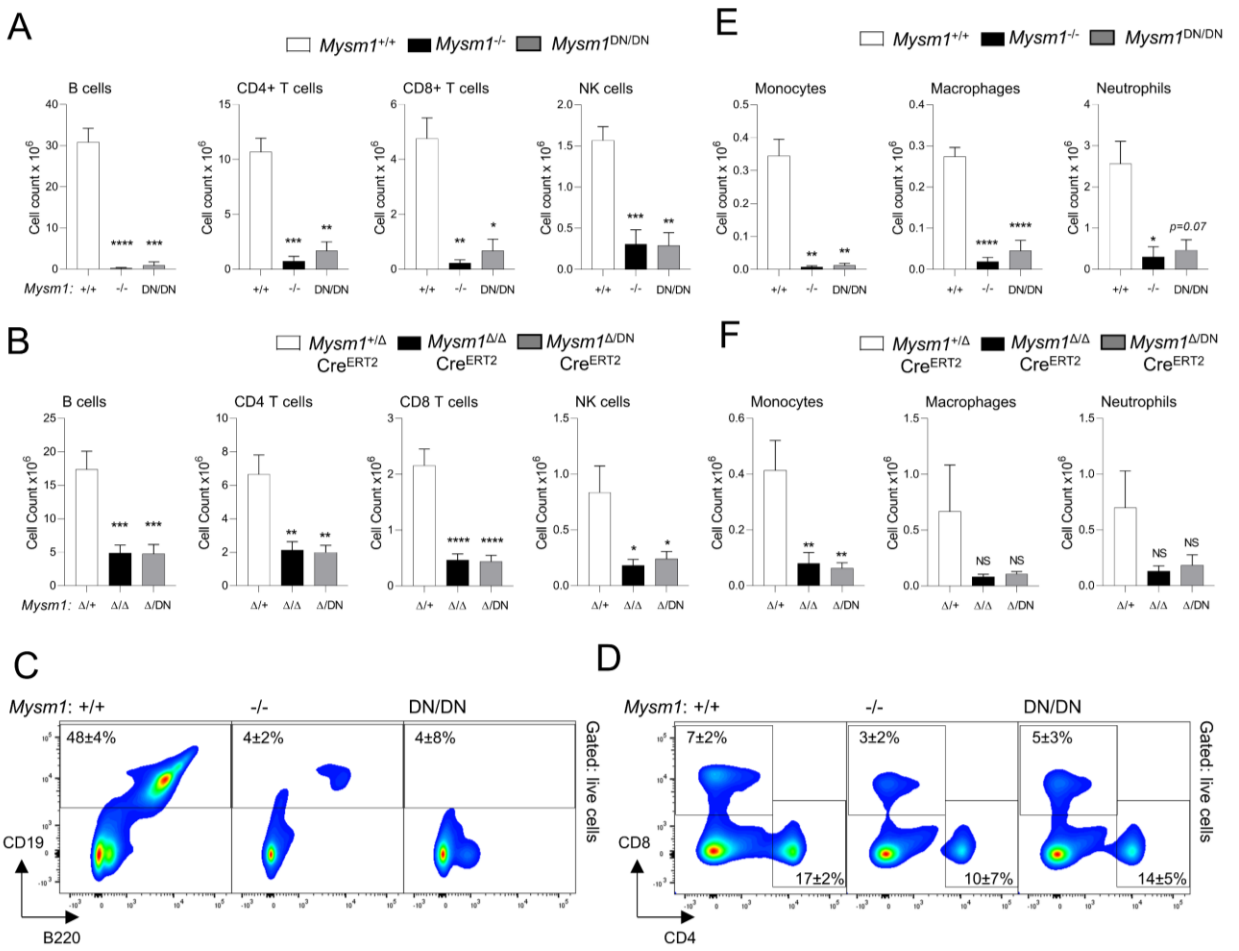

Flow cytometry analyses were performed on **(A,C-E)** *Mysm1*$^{+/+}$, *Mysm1*$^{-/-}$, and *Mysm1*$^{DN/DN}$ mice, and **(B,F)** Cre^{ERT2} transgenic mice of *Mysm1*$^{fl/+}$, *Mysm1*$^{fl/fl}$, and *Mysm1*$^{fl/DN}$ genotypes at >20 weeks after tamoxifen treatment, to quantify **(A-B)** B cells (CD19^{+}CD3^{-}), CD4 T cells (CD3^{+}CD4^{+}CD8^{-}), CD8 T cells (CD3^{+}CD4^{-}CD8^{+}), NK cells (CD3^{-}NK1.1^{+}), and **(E-F)** monocytes (CD45^{+}CD3^{-}NK1.1^{-}CD11b^{+}Ly6C^{+}Ly6G^{-}), macrophages (CD45^{+}CD3^{-}NK1.1^{-}CD11b^{+} Ly6G^{-}Ly6C^{-} F4/80^{+}CD64^{+}), and neutrophils (CD45^{+}CD3^{-}NK1.1^{-}CD11b^{+}Ly6G^{+}Ly6C^{-}). The data is from (A) 3-10 mice per genotype consolidated from two independent experiments, or (B) 8-11 mice per genotype consolidated from three independent experiments. Bars represent means ± SEM; statistical analysis with ANOVA and Dunnett's post-hoc test, comparing each group to the control, * p<0.05, ** p<0.01, *** p<0.001, **** p<0.0001, NS - not significant. **(C-D)** Representative flow cytometry plots of the spleen of *Mysm1*$^{+/+}$, *Mysm1*$^{-/-}$, and *Mysm1*$^{DN/DN}$ mice gated on live cells and showing the depletion of **(C)** CD19^{+} B cells and **(D)** CD4^{+} and CD8^{+} T cells in *Mysm1*$^{-/-}$ and *Mysm1*$^{DN/DN}$ mice; the average frequencies of cells in the gates are presented as mean ± st. dev.

Figure 4.3.5 Supplemental analyses of the proportion of dead cells among hematopoietic and immune cells in *Mysm1*$^{DN/DN}$ relative to control *Mysm1*$^{+/+}$ mice, based on eFluor506 viability dye staining and flow cytometry.

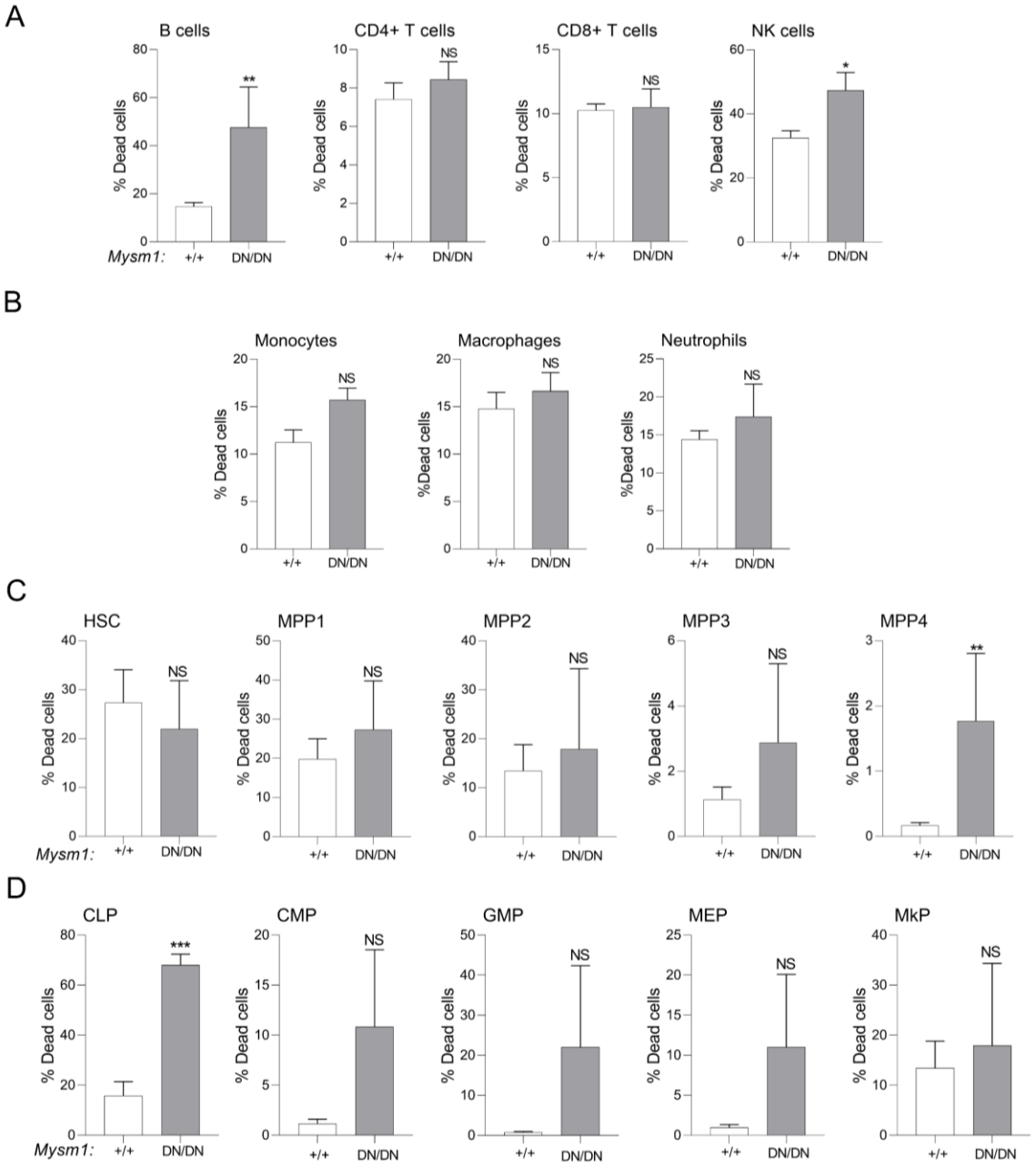

(A-B) Splenic immune cells were gated as follows: B cells ($CD19^+CD3^-$), CD4 T cells ($CD3^+CD4^+CD8^-$), CD8 T cells ($CD3^+CD4^-CD8^+$), NK cells ($CD3^-NK1.1^+$), monocytes ($CD45^+CD3^-NK1.1^-CD11b^+Ly6C^+Ly6G^-$), macrophages ($CD45^+CD3^-NK1.1^-CD11b^+Ly6G^-Ly6C^-F4/80^+CD64^+$), and neutrophils ($CD45^+CD3^-NK1.1^-CD11b^+Ly6G^+Ly6C^-$). **(C)** Bone marrow hematopoietic stem cells and multipotent progenitor cells were gated as LSK ($Lin^-cKit^+Sca1^+$), followed by $CD150^+CD48^-CD34^-Flt3^-$ for HSCs, $CD150^+CD48^-CD34^+Flt3^-$ for MPP1,

$CD150^{+}CD48^{+}CD34^{+}Flt3^{-}$ for MPP2, $CD150^{-}CD48^{+}CD34^{+}Flt3^{-}$ for MPP3, and $CD150^{-}CD48^{+}CD34^{+}Flt3^{+}$ for MPP4. **(D)** Bone marrow lineage committed progenitors were gated as follows: common lymphoid progenitors (CLP, $Lin^{-}IL7R\alpha^{+}cKit^{lo}Sca1^{lo}$), common myeloid progenitors (CMP, $Lin^{-}cKit^{+}Sca1^{-}CD34^{+}CD16/32^{-}$), granulocyte monocyte progenitors (GMP, $Lin^{-}cKit^{+}Sca1^{-}CD34^{+}CD16/32^{+}$), megakaryocyte erythroid progenitors (MEP, $Lin^{-}cKit^{+}Sca1^{-}CD34^{-}CD16/32^{-}$), and megakaryocyte progenitors (MkP, $Lin^{-}cKit^{+}Sca1^{-}CD150^{+}CD41^{+}$). Data is from 3 *Mysm1*$^{DN/DN}$ and 10 *Mysm1*$^{+/+}$ control mice consolidated from two independent experiments. Bars represent means ± SEM; statistical analyses with unpaired Student's *t*-test, * $p<0.05$, ** $p<0.01$, *** $p<0.001$, NS - not significant.

Figure 4.3.6 Depletion of splenic transitional, follicular, and marginal zone B cells with the loss of MYSM1 DUB catalytic activity.

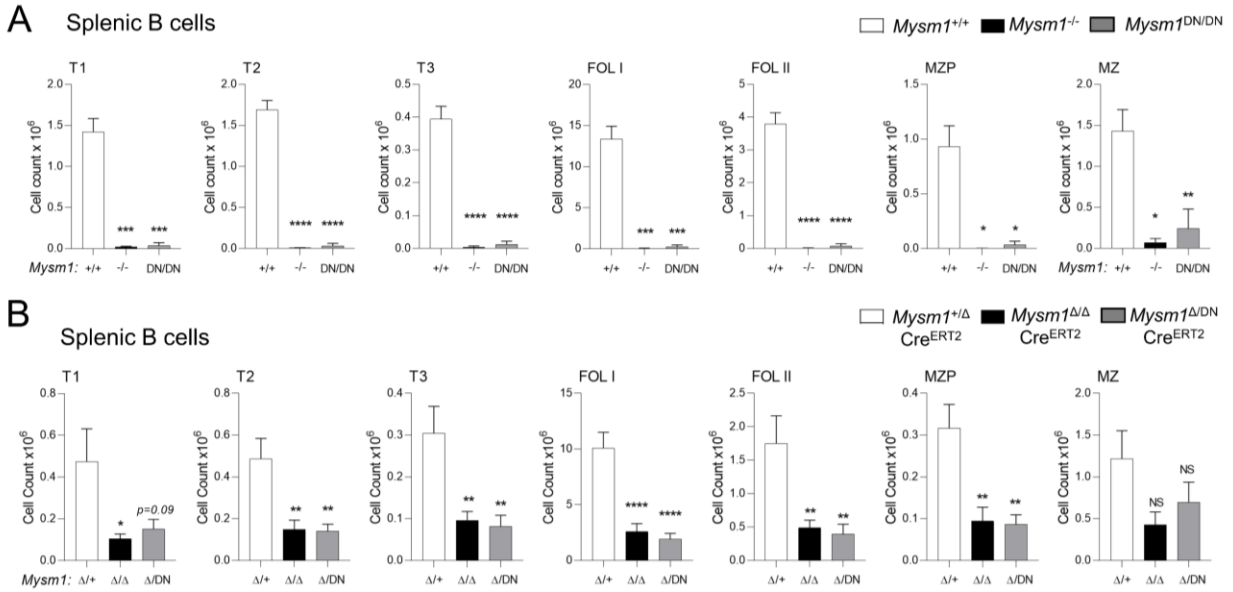

Flow cytometry analyses were performed on **(A)** *Mysm1*$^{+/+}$, *Mysm1*$^{-/-}$, and *Mysm1* $^{DN/DN}$ mice, and on **(B)** Cre^{ERT2} transgenic mice of *Mysm1*$^{fl/+}$, *Mysm1*$^{fl/fl}$, and *Mysm1*$^{fl/DN}$ genotypes at >20 weeks after tamoxifen injections, to quantify the following B cell populations: transitional 1 (T1, $CD19^{+}B220^{+}CD93^{+}IgM^{+}CD23^{-}$), transitional 2 (T2, $CD19^{+}B220^{+}CD93^{+}IgM^{+}CD23^{+}$), transitional 3 (T3, $CD19^{+}B220^{+}CD93^{+}IgM^{lo}CD23^{+}$), follicular I (FOLI, $CD19^{+}B220^{+}CD93^{-}CD21^{+}IgM^{+}IgD^{+}$), follicular II (FOLII, $CD19^{+}B220^{+}CD93^{-}CD21^{+}IgM^{hi}IgD^{+}$), marginal zone progenitors (MZP, $CD19^{+}B220^{+}CD93^{-}CD21^{hi}IgM^{hi}CD23^{+}$), and marginal zone B cells (MZ, $CD19^{+}B220^{+}CD93^{-}CD21^{hi}IgM^{hi}CD23^{-}$), as previously 1,2. The data is from (A) 3-10 mice per genotype consolidated from two independent experiments, or (B) 8-11 mice per genotype consolidated from three independent experiments. Bars represent means ± SEM; statistical analysis with ANOVA and Dunnett's post-hoc test, comparing each group to the control, * $p<0.05$, ** $p<0.01$, *** $p<0.001$, **** $p<0.0001$, NS - not significant.

4.3.8 Severe depletion of lymphocyte precursors in the Mysm1 $^{DN/DN}$ mice

We further analyzed for the B and T cell precursor subsets in the bone marrow and thymus of *Mysm1*$^{DN/DN}$ and *Mysm1*$^{-/-}$ mice, relative to the *Mysm1*$^{+/+}$ controls. We observed a strong depletion of most B cell precursor subsets, including pre-pro-B and pro-B cells (Fraction A-B), pre-B cells, and the immature and mature bone marrow B cell populations in the *Mysm1*$^{DN/DN}$ and *Mysm1*$^{-/-}$ mice (Figure 4.3.7A,C). Similarly, we observed a strong depletion of most thymocyte populations in the *Mysm1*$^{DN/DN}$ and *Mysm1*$^{-/-}$ mice (Figure 4.3.7B,D). Overall, this indicates that the loss of MYSM1 DUB catalytic activity or the loss of MYSM1 protein expression both results in a severe defect in B and T lymphocyte development.

Figure 4.3.7 Depletion of B and T lymphocyte precursors in the bone marrow and thymus in mice with the loss of MYSM1 DUB catalytic activity.

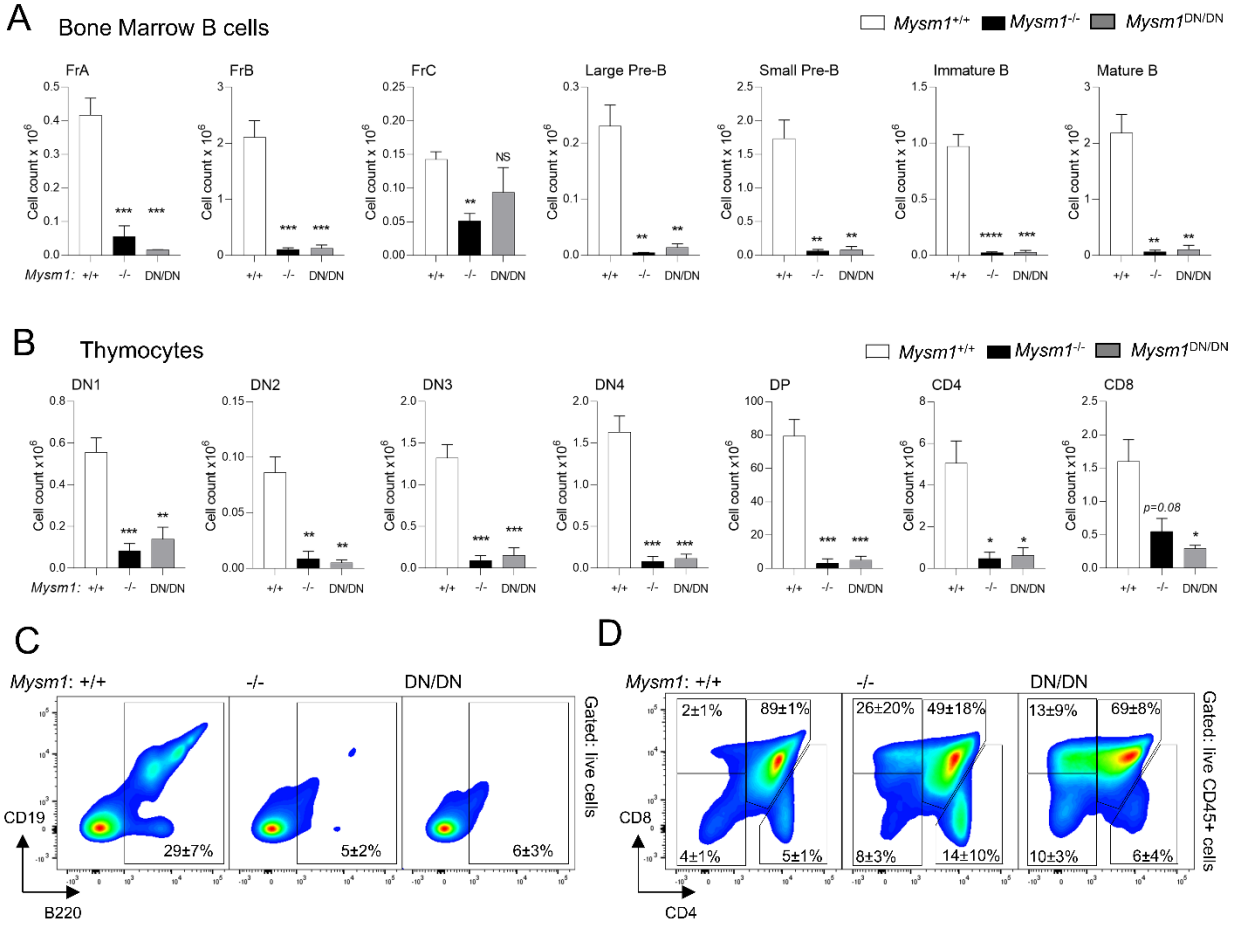

Flow cytometry analyses were performed on *Mysm1*$^{+/+}$, *Mysm1*$^{-/-}$, and *Mysm1*$^{DN/DN}$ mice, analyzing **(A)** the bone marrow for the following B cell populations: Fraction A (FrA, B220^{+}IgM^{-}IgD^{-}CD43^{+}CD24^{lo}BP1^{lo}), Fraction B (FrB, B220^{+}IgM^{-}IgD^{-}CD43^{+}CD24^{+}BP1^{lo}), Fraction C (FrC, B220^{+}IgM^{-}IgD^{-}CD43^{+}CD24^{+}BP1^{+}), large pre-B cells (B220^{+}CD19^{+}IgM^{-}IgD^{-}CD43^{-}IL7Rα^{hi}FSChi), small pre-B cells (B220^{+}CD19^{+}IgM^{-}IgD^{-}CD43^{-}IL7Rα^{lo}FSC^{lo}), immature B cells (B220^{+}IgM^{+}IgD^{-}), mature B cells (B220^{+}IgM^{+}IgD^{+}); and **(B)** the thymus for double negative thymocytes DN1 (CD45^{+}CD4^{-}CD8^{-}CD44^{+}CD25^{-}), DN2 (CD45^{+}CD4^{-}CD8^{-}CD44^{+}CD25^{+}), DN3 (CD45^{+}CD4^{-}CD8^{-}CD44^{-}CD25^{+}), and DN4 (CD45^{+}CD4^{-}CD8^{-}CD44^{-}CD25^{-}), double positive thymocytes (DP, CD45^{+}CD4^{+}CD8^{+}), and single positive thymocytes (CD45^{+}CD4^{+}CD8^{-} and CD45^{+}CD4^{-}CD8^{+}). The data is from 3-10 mice per genotype consolidated from two independent experiments. Bars represent means ± SEM; statistical analysis with ANOVA and Dunnett's post-hoc test, comparing each group to the control, * p<0.05, ** p<0.01, *** p<0.001; bone marrow cell counts are presented per two tibias and femurs. **(C)** Representative flow cytometry plots of the mouse bone marrow stained for B220 and CD19 B cell markers and **(D)** of the mouse thymus stained for CD4 and CD8; the average frequencies of cells in the gates are presented as mean ± st. dev.

4.3.9 ***Hematopoietic progenitor depletion and hematopoietic dysfunction in Mysm1$^{DN/DN}$ mice***

To further characterize the dysfunction in hematopoiesis resulting from the *in vivo* loss of MYSM1 DUB catalytic activity, *Mysm1*$^{DN/DN}$, *Mysm1*$^{-/-}$, and control *Mysm1*$^{+/+}$ mice were analyzed for the numbers of hematopoietic progenitor cells across the different lineages, as well as for the multipotent progenitors (MPPs) and hematopoietic stem cells (HSCs). We observed a significant depletion of common lymphoid (CLP), common myeloid (CMP), and granulocyte monocyte (GMP) progenitors in *Mysm1*$^{DN/DN}$ mice (Figure 4.3.8A), while changes in megakaryocyte erythroid (MEP) and megakaryocyte (MkP) progenitors did not reach statistical significance (Figure 4.3.8A). The numbers of HSC and MPP1-3 cells were highly variable between the *Mysm1*$^{DN/DN}$ mice, and showed trends for expansion, which however did not reach statistical significance (Figure 4.3.8B-C), and this likely reflects the competing effects of the loss of HSC quiescence and increased cell apoptosis, as previously reported in the *Mysm1*$^{-/-}$ mouse models [229, 239]. Importantly, there was a severe depletion of the lymphoid primed MPP4 cells in both *Mysm1*$^{DN/DN}$ and *Mysm1*$^{-/-}$ relative to control mice (Figure 4.3.8B-C), further supporting the essential role of MYSM1 DUB catalytic activity for lymphopoiesis. Furthermore, an increase in the proportion of dead cells was observed particularly for lymphoid biased MPP4 and CLP cells in *Mysm1*$^{DN/DN}$ relative to control *Mysm1*$^{+/+}$ mice (Figure 4.3.5C-D).

The dysfunction in lymphopoiesis and erythropoiesis in the *Mysm1*$^{DN/DN}$ mice was further demonstrated with colony-forming units (CFU) assays, showing a severe depletion of B-cell lineage and erythroid lineage CFUs in the *Mysm1*$^{DN/DN}$ and *Mysm1*$^{-/-}$ relative to the control mice (Figure 4.3.8D). No analysis of myeloid CFUs was conducted, as in previous studies myeloid CFU numbers in *Mysm1*$^{-/-}$ mice were not significantly impaired [180].

Figure 4.3.8 Hematopoietic dysfunction and altered hematopoietic progenitor cell numbers in *Mysm1*$^{DN/DN}$ mice.

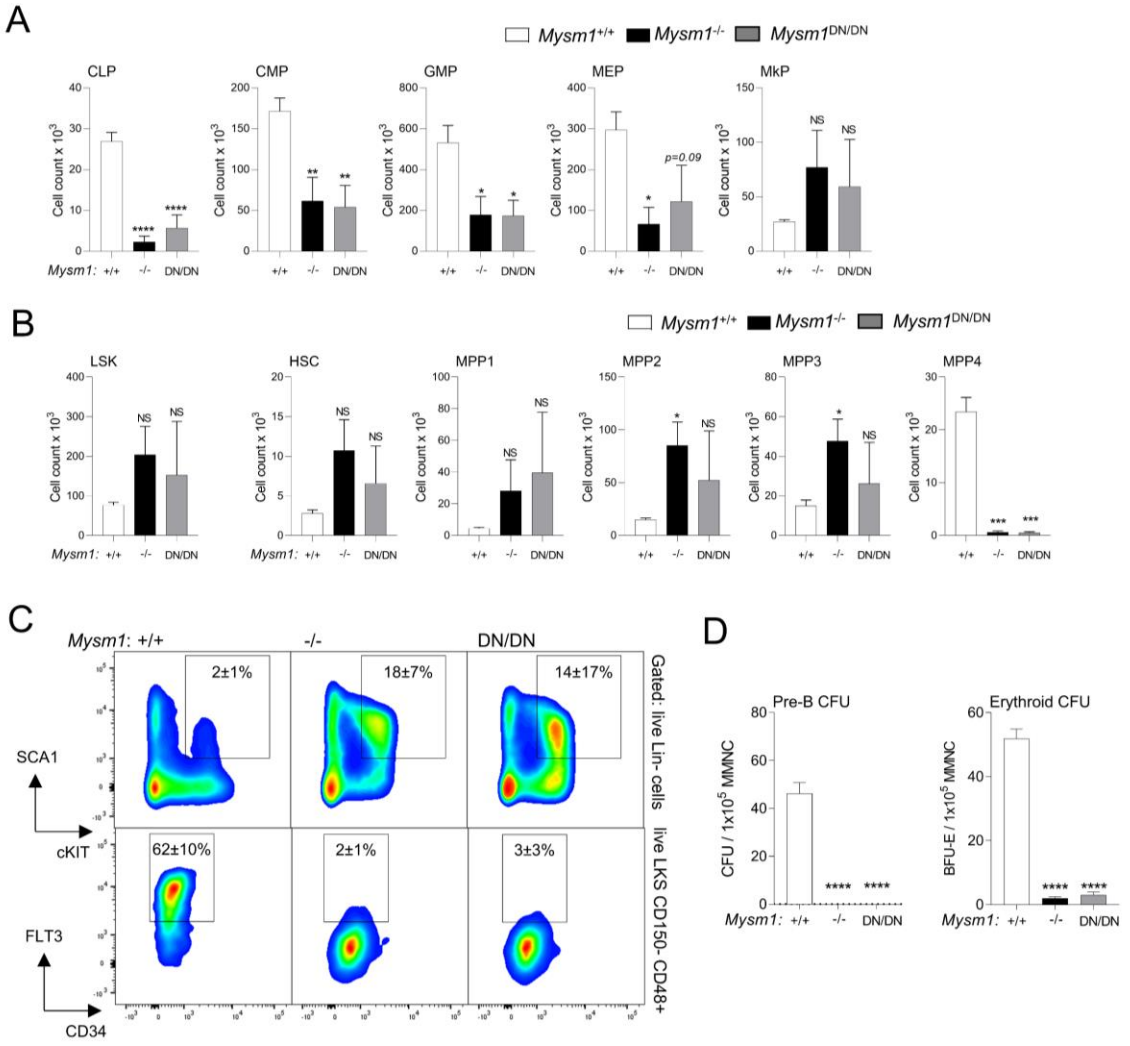

Flow cytometry analyses were performed on the bone marrow of *Mysm1*$^{+/+}$, *Mysm1*$^{-/-}$, and *Mysm1*$^{DN/DN}$ mice to quantify **(A)** common lymphoid progenitors (CLP, Lin$^-$IL7Rα$^+$cKit^{lo}Sca1^{lo}), common myeloid progenitors (CMP, Lin$^-$cKit$^+$Sca1$^-$CD34$^+$CD16/32$^-$), granulocyte monocyte progenitors (GMP, Lin$^-$cKit$^+$Sca1$^-$CD34$^+$CD16/32$^+$), megakaryocyte erythroid progenitors (MEP, Lin$^-$cKit$^+$Sca1$^-$CD34$^-$CD16/32$^-$), and megakaryocyte progenitors (MkP, Lin$^-$cKit$^+$Sca1$^-$CD150$^+$ CD41$^+$); **(B)** hematopoietic stem cells (HSCs) and multipotent progenitors (MPP1-4), gated as LSK (Lin$^-$cKit$^+$Sca1$^+$), followed by CD150$^+$CD48$^-$CD34$^-$Flt3$^-$ for HSCs, CD150$^+$CD48$^-$ CD34$^+$Flt3$^-$ for MPP1, CD150$^+$CD48$^+$CD34$^+$Flt3$^-$ for MPP2, CD150$^-$CD48$^+$CD34$^+$Flt3$^-$ for MPP3, and CD150$^-$CD48$^+$CD34$^+$Flt3$^+$ for MPP4. The data is from 3-10 mice per genotype consolidated from two independent experiments. Bars represent means ± SEM; statistical analysis with ANOVA and Dunnett's post-hoc test, comparing each group to the control, * p<0.05, ** p<0.01, *** p<0.001, **** p<0.0001, NS – not significant; bone marrow cell counts are presented per two

tibias and femurs. **(C)** Representative flow cytometry density plots of the bone marrow of *Mysm1*$^{+/+}$, *Mysm1*$^{-/-}$, and *Mysm1*$^{DN/DN}$ mice, gated on live Lin- cells and showing the LSK cell population (top), or gated on the LSK C150^{-}CD48^{+} cells and showing the Flt3^{lo} MPP3 and Flt3^{hi} MPP4 cells; the average frequency of cells in the gates is presented as mean ± st. dev. While the LSK cell numbers are highly variable (top), a strong depletion of the lymphoid-primed MPP4 cells is consistently observed in all the *Mysm1*$^{-/-}$ and *Mysm1*$^{DN/DN}$ mice (bottom). **(D)** Colony forming units (CFU) assays showing depletion of pre-B and erythroid BFU-E progenitors in *Mysm1*$^{DN/DN}$ and *Mysm1*$^{-/-}$ mouse bone marrow; MMNC – marrow mononuclear cells.

4.3.10 Cell intrinsic role of MYSM1 DUB catalytic activity in hematopoiesis

To directly test the cell-intrinsic requirement for the MYSM1 DUB catalytic activity in hematopoiesis, competitive bone marrow chimeras were set up. CD45.1^{+} wild type bone marrow was mixed in a 1:1 ratio with the bone marrow of CD45.2^{+} Cre^{ERT2} mice of *Mysm1*$^{+/fl}$, *Mysm1*$^{fl/fl}$, or *Mysm1*$^{DN/fl}$ genotypes, and transplanted into three independent groups of lethally irradiated recipients (Figure 4.3.9A). The recipient mice were bled at 12-weeks to confirm the normal reconstitution with donor bone marrow across the genotypes (data not shown), and subsequently all the mice were administered with tamoxifen to induce the *Mysm1*^{fl} to *Mysm1*$^{\Delta}$ allele conversion. The mice were analyzed for the relative contributions of the CD45.2^{+} bone marrow to the different hematopoietic lineage, across the three *Mysm1* genotypes.

We observed a significant reduction in the contribution of the *Mysm1*$^{DN/\Delta}$ donor hematopoiesis to the B cell, CD4 T cell, CD8 T cell, and NK cell populations in the mouse spleen (Figure 4.3.9B), to monocyte and neutrophil populations in both spleen and bone marrow (Figure 4.3.9B and not shown), and to all the leukocyte populations in the mouse blood (Figure 4.3.10A). Similar defects in the reconstitution were observed for the *Mysm1*$^{DN/\Delta}$ hematopoietic progenitor cells, including the lineage committed progenitors (CMPs, GMPs, CLPs, MEPs, and MkPs, Figure 4.3.9C), all the developing B cell subsets (Fractions A-C, pre-B, and immature B cells, Figure 4.3.10B), and the

majority of T cell precursor subsets within the thymus (Figure 4.3.10C). Among the multipotent HSC and MPP hematopoietic cells there was no defect in *Mysm1*$^{DN/\Delta}$ reconstitution of the early HSC and MPP1-2 cells, likely reflecting the balancing effects of the loss of quiescence and increase in apoptosis among these cells, as in the *Mysm1*$^{-/-}$ mouse models [229, 239], however impaired reconstitution was seen for the latter myeloid-biased MPP3 and lymphoid-biased MPP4 subsets (Figure 4.3.10D). Importantly, throughout the datasets presented above the *Mysm1*$^{DN/\Delta}$ phenotypes aligned very well with the *Mysm1*$^{\Delta/\Delta}$ group, both showing strong impairment of hematopoietic function relative to the *Mysm1*$^{+/\Delta}$ control (Figure 4.3.9, Figure 4.3.10). Overall, this demonstrates the essential and cell-intrinsic role of the MYSM1 DUB catalytic activity in the regulation of hematopoiesis, and suggests lack of significant MYSM1 mechanisms of action that are independent of its catalytic function.

Figure 4.3.9 Assessing the cell-intrinsic role of MYSM1 DUB catalytic activity in hematopoiesis and leukocyte development with competitive bone marrow transplantation.

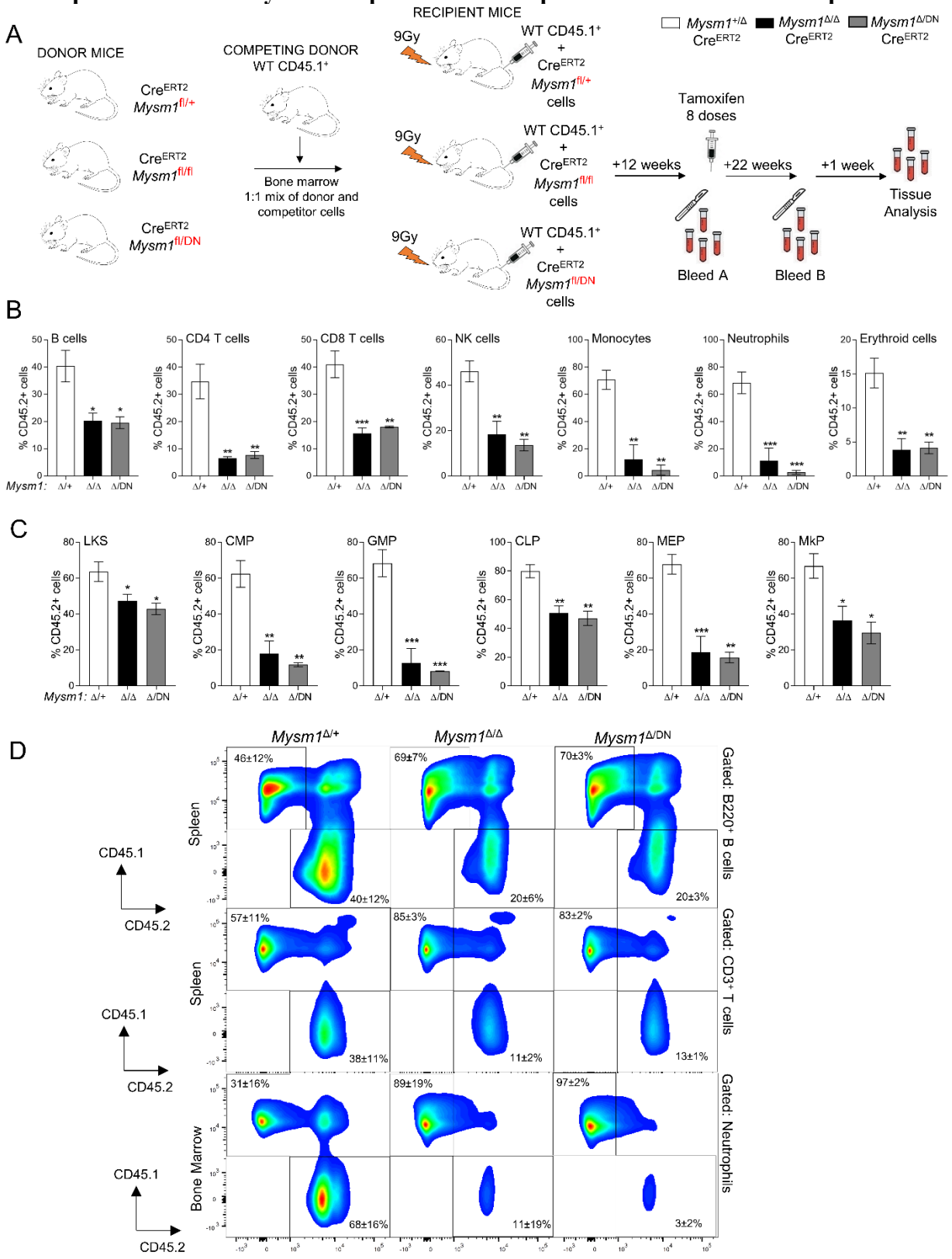

(A) Schematic representation of the mouse-to-mouse competitive bone marrow transplantation study. Wild type CD45.1^{+} bone marrow cells were mixed in a 1:1 ratio with Cre^{ERT2} transgenic bone marrow cells of *Mysm1*$^{fl/+}$, *Mysm1*$^{fl/fl}$, or *Mysm1*$^{fl/DN}$ genotypes, and the mixes were transplanted into three independent cohorts of lethally irradiated wild type CD45.1^{+} recipient mice. Following full hematopoietic reconstitution, the chimeric mice were administered with tamoxifen to induce the *Mysm1*^{fl} to *Mysm1*$^{\Delta}$ allele conversion. Clipart images were used toward the preparation of the Figure (*http://clipart-library.com*). **(B-C)** The relative contribution of *Mysm1*$^{\Delta/DN}$, *Mysm1*$^{\Delta/\Delta}$, and control *Mysm1*$^{\Delta/+}$ cells to the different hematopoietic and immune cell populations was evaluated by flow cytometry, quantifying the proportion of CD45.2^{+}CD45.1^{-} cells within each cell population. Data is from 3-5 mice per group; bars represent means ± SEM; statistical analysis uses ANOVA and Dunnett's post-hoc test comparing each group to the *Mysm1*$^{\Delta/+}$ control; * p<0.05, ** p<0.01, *** p<0.001, or NS - not significant. Data is presented for the following cell populations: **(B)** splenic B cells (CD19^{+}CD3^{-}), CD4 T cells (CD3^{+}CD4^{+}CD8^{-}), CD8 T cells (CD3^{+}CD4^{-}CD8^{+}), and NK cells (CD3^{-}NK1.1^{+}); bone marrow monocytes (CD11b^{+}Ly6C^{hi}Ly6G^{lo}), neutrophils (CD11b^{+}Ly6C^{lo}Ly6G^{hi}), and erythroid cells (CD71^{+}); **(C)** bone marrow stem and multipotent progenitors (LKS, Lin^{-}cKit^{+}Sca1^{+}), common myeloid progenitors (CMP, Lin^{-}cKit^{+}Sca1^{-}CD34^{+}CD16/32^{-}), granulocyte monocyte progenitors (GMP, Lin^{-}cKit^{+}Sca1^{-}CD34^{+}CD16/32^{+}), common lymphoid progenitors (CLP, Lin^{-}cKit^{lo}Sca1^{lo}IL7Ra^{+}CD16/32^{-}), megakaryocyte erythroid progenitors (MEP, Lin^{-}cKit^{+}Sca1^{-}CD34^{-}CD16/32^{-}), and megakaryocyte progenitors (MkP, Lin^{-}cKit^{+}Sca1^{-}CD16/32^{-}CD150^{+}CD41^{+}). **(D)** Representative flow cytometry plots showing the analyses of splenic B cells, splenic T cells, and bone marrow neutrophils for CD45.1 versus CD45.2 marker expression; percentage of cells in the gates is shown as mean ± st. dev. of all the mice in each group. Gates for CD45.1^{+} and CD45.2^{+} cells were set independently for each cell population using control non-chimeric WT-B6 (CD45.2) and WT-SJL (CD45.1) mice, as shown in Figure 4.3.10E.

Figure 4.3.10 Assessing the cell-intrinsic role of MYSM1 DUB catalytic activity in hematopoiesis and leukocyte development with competitive bone marrow transplantation.

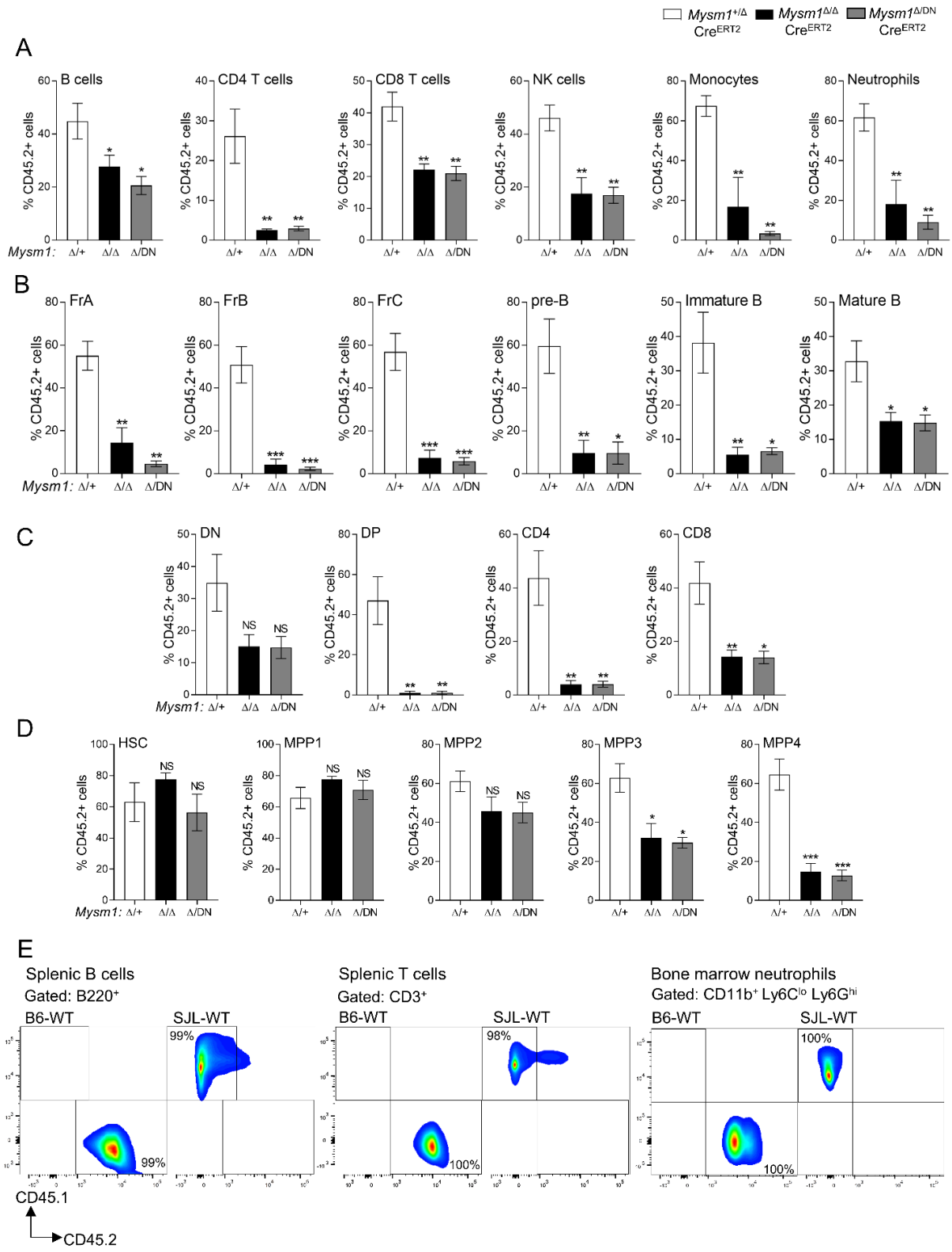

Wild type CD45.1$^+$ bone marrow cells were mixed in a 1:1 ratio with *CreERT2* transgenic bone marrow cells of *Mysm1*$^{fl/+}$, *Mysm1*$^{fl/fl}$, or *Mysm1*$^{fl/DN}$ genotypes, and the mixes were transplanted into three independent cohorts of lethally irradiated wild type CD45.1$^+$ recipient mice. Following full hematopoietic reconstitution by the donor bone marrows, the chimeric mice were administered with tamoxifen to induce the *Mysm1*^{fl} to *Mysm1*$^{\Delta}$ allele conversion. The relative contribution of *Mysm1*$^{\Delta/DN}$, *Mysm1*$^{\Delta/\Delta}$, and control *Mysm1*$^{\Delta/+}$ cells to the different hematopoietic and immune cell populations was evaluated by flow cytometry, gating on CD45.2$^+$CD45.1$^-$ cells. Data is from 3-5 mice per group; bars represent means ± SEM; statistical analysis with ANOVA and Dunnett's post-hoc test comparing each group to the *Mysm1*$^{\Delta/+}$ control; * p<0.05, ** p<0.01, *** p<0.001, or NS - not significant.
(A) Analysis of the mouse blood, gating on B cells (B220$^+$), CD4 T cells (CD3$^+$CD4$^+$CD8$^-$), CD8 T cells (CD3$^+$CD8$^+$CD4$^-$), NK cells (CD3$^-$NK1.1$^+$), monocytes (CD11b$^+$Ly6C^{hi}), and neutrophils (CD11b$^+$Ly6G^{hi}). **(B)** Analyses of B cell precursor cells in the mouse bone marrow, gating on B220$^+$ for all B cells, and on IgM$^-$CD43$^+$CD24$^-$ BP1- for Fraction A, IgM$^-$CD43$^+$CD24$^+$BP1$^-$ for Fraction B, IgM$^-$CD43$^+$CD24$^+$BP1$^+$ for Fraction C, IgM$^-$IgD$^-$CD43$^-$ for pre-B cells, IgM$^+$IgD$^-$ for immature B cells, and IgM$^+$IgD$^+$ for mature B cells. **(C)** Analyses of T cell development in the thymus, gating on CD4$^-$CD8$^-$ for double-negative thymocytes (DN), CD4$^+$CD8$^+$ for double-positive thymocytes (DP), CD4$^+$CD8$^-$ for CD4 single-positive, and CD4$^-$CD8$^+$ for CD8 single-positive thymocytes. **(D)** Analysis of hematopoietic stem cells (HSCs) and multipotent progenitors 1-4 (MPP1-4) in mouse bone marrow gated as Lin$^-$cKit$^+$Sca1$^+$ followed by CD150$^+$CD48$^-$CD34$^-$Flt3$^-$ for HSCs, CD150$^+$CD48$^-$CD34$^+$Flt3$^-$ for MPP1, CD150$^+$CD48$^+$CD34$^+$Flt3$^-$ for MPP2, CD150$^-$CD48$^+$CD34$^+$Flt3$^-$ for MPP3, and CD150$^-$CD48$^+$CD34$^+$Flt3$^+$ for MPP4 cells. **(E)** Setting the CD45.1$^+$ and CD45.2$^+$ gates for splenic B cells, splenic T cells, and bone marrow neutrophils, using control non-chimeric WT-B6 (CD45.2) and WT-SJL (CD45.1) mice; gates for each of the other cell populations were set independently with the same method.

4.3.11 MYSM1 is essential for dendritic cell (DC) lineage development

Dendritic cells (DCs), as mentioned before, are the most significant antigen presenting cells of the immune system, critical for the activation of naïve T cells and the induction of adaptive immune response in the context of infections, vaccinations, and antitumor immunity. A systemic and constitutive loss of MYSM1 in the *Mysm1*$^{-/-}$ mice was previously shown to result in a severe depletion of DCs from early stages in the DC lineage specification [237]. Here we set out to validate these studies, re-analyzing the numbers of pre-DCs in the bone marrow and DC subsets in the spleen of *Mysm1*$^{-/-}$ mice. Importantly, we also for the first time assessed the role of MYSM1 DUB catalytic activity in the DC lineage development, by conducting the same analyses on the *Mysm1*$^{DN/DN}$ mice, established in our recent work to express a catalytically inactive MYSM1

protein [277]. We observed a severe depletion of DC lineage cells in the bone marrow and of cDC1, cDC2a, cDC2b and pDC cells in the spleen of *Mysm1*$^{-/-}$ mice (Figure 4.3.11A-C), consistent with previous studies [237]. Furthermore, the *Mysm1*$^{DN/DN}$ mice demonstrated an equivalent highly significant depletion of DC lineage cells in the bone marrow and spleen (Figure 4.3.11A-C), indicating the essential role of the MYSM1 DUB catalytic activity for DC lineage specification and development.

Due to the complex developmental phenotypes of both *Mysm1*$^{-/-}$ and *Mysm1*$^{DN/DN}$ mice [180, 277], we also adopted the *Mysm1*^{fl} Cre^{ERT2} mouse strain for further studies of MYSM1 in the DC lineage, allowing for a tamoxifen induced deletion of *Mysm1* in phenotypically normal adult mice [234]. In our previous work, highly effective *Mysm1* deletion in HSPCs, hematopoietic, and lymphoid tissues has been demonstrated in this model [234, 244]. In the current study, we report a significant depletion of DC lineage cells in the bone marrow and of cDC1, cDC2a, cDC2b and pDC cells in the spleen of the tamoxifen treated *Mysm1*$^{fl/fl}$ Cre^{ERT2} and *Mysm1*$^{DN/fl}$ Cre^{ERT2}relative to control mice (Figure 4.3.12A-D). This demonstrates the essential role of MYSM1 and its DUB catalytic activity in the maintenance of DC development, independently of the complex developmental phenotypes of the previously studied murine models. Furthermore, the bone marrow of tamoxifen treated *Mysm1*$^{fl/fl}$ Cre^{ERT2} and *Mysm1*$^{DN/fl}$ Cre^{ERT2} mice also produced significantly lower numbers of BMDCs *in vitro* (Figure 4.3.13), further confirming that the loss of MYSM1 protein or its DUB catalytic activity throughout the hematopoietic cell hierarchy severely impairs DC development.

Figure 4.3.11 Constitutive systemic loss of MYSM1 expression or of its catalytic activity severely impair DC lineage development.

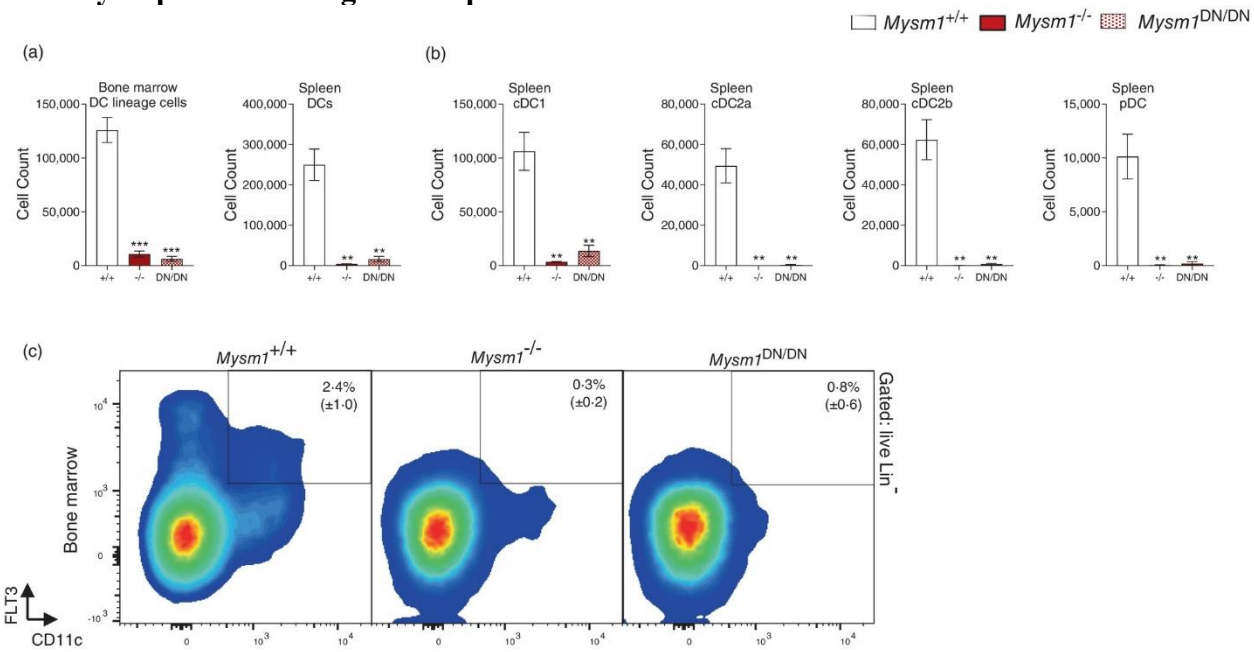

Mice of *Mysm1*$^{-/-}$, *Mysm1*$^{DN/DN}$, and control *Mysm1*$^{+/+}$ genotypes were analyzed by flow cytometry. **(A)** Absolute numbers of DC lineage cells in the bone marrow and of DCs in the spleen, gated as Lin$^-$Flt3$^+$CD11c$^+$SIRPα$^+$ and CD45$^+$Lin$^-$F4/80$^-$CD64$^-$CD11c$^+$MHCII$^+$ cells, respectively. **(B)** Absolute numbers of cDC1, cDC2a, cDC2b, and pDC subsets in the spleen. Cells were gated as CD45$^+$Lin$^-$F4/80$^-$CD64$^-$CD11c$^+$MHCII$^+$, followed by B220$^-$PDCA1$^-$XCR1$^+$ SIRPα$^-$ for cDC1, B220$^-$PDCA1$^-$XCR1$^-$SIRPα$^+$CLEC12a$^-$ for cDC2a, B220$^-$PDCA1$^-$XCR1$^-$SIRPα$^+$CLEC12a$^+$ for cDC2b, and B220$^+$PDCA1$^+$ for pDCs. Data are from n=4 *Mysm1*$^{-/-}$ and *Mysm1*$^{DN/DN}$ mice per group and n=10 *Mysm1*$^{+/+}$ control mice, consolidated from 2 independent experiments, and presented as mean ± SEM. Statistical analyses used ANOVA with Sidak's posthoc test, comparing each group to the *Mysm1*$^{+/+}$ control; ** p <0.01, *** p <0.001. **(C)** Representative flow cytometry plots of the mouse bone marrow, pre-gated on live lineage negative cells, and showing the depletion of Flt3$^+$CD11c$^+$ pre-DCs in the *Mysm1*$^{-/-}$ and *Mysm1*$^{DN/DN}$ mice. Numbers on the plots indicate the percentages of cells within each gate out of the parent population, presented as mean ± SD for all the mice in the group.

Figure 4.3.12 Inducible loss of MYSM1 expression or of its catalytic activity impair DC lineage development.

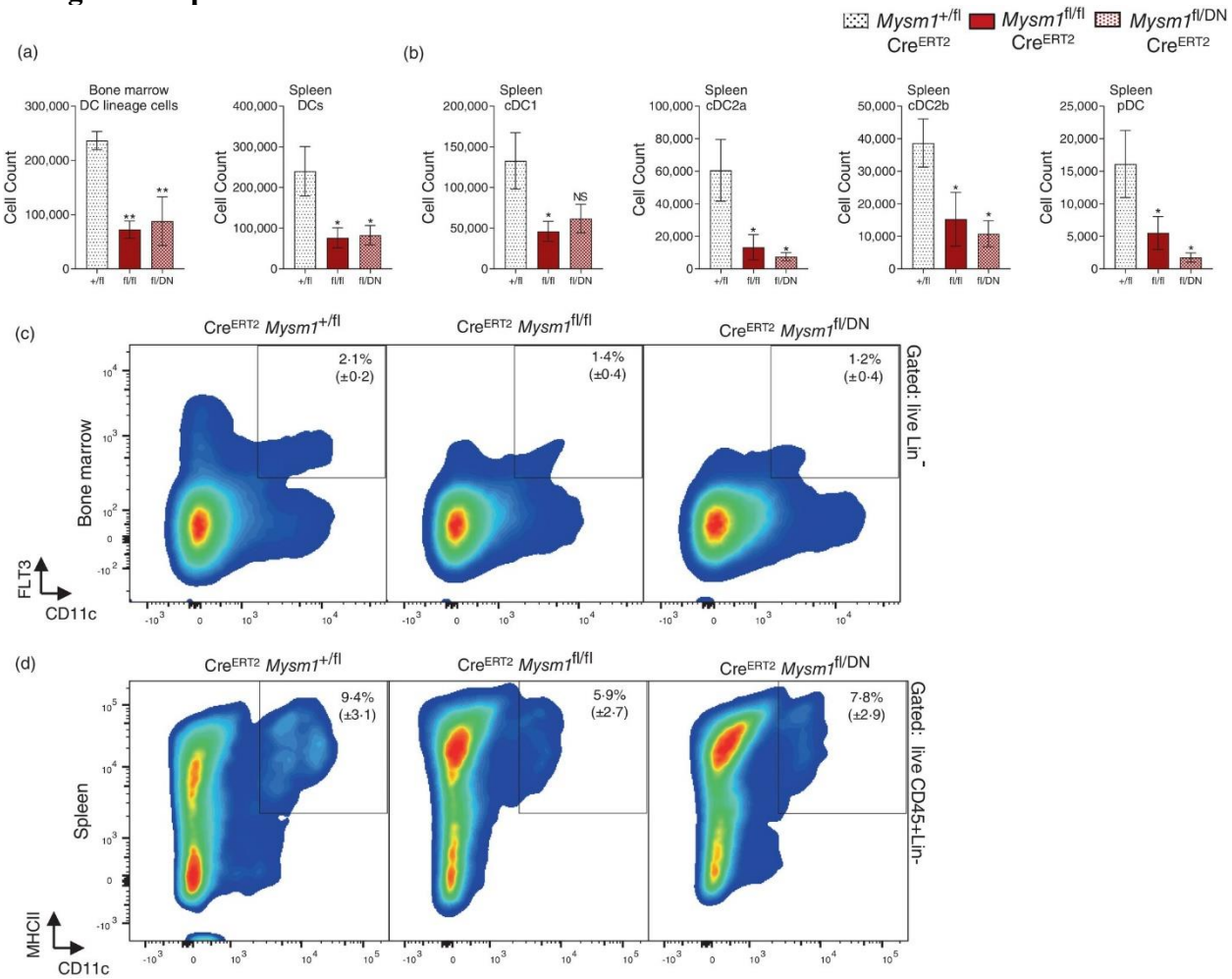

Cre^{ERT2} transgenic mice of *Mysm1*$^{fl/fl}$, *Mysm1*$^{DN/fl}$, and control *Mysm1*$^{+/fl}$ genotypes were analyzed by flow cytometry following tamoxifen treatment to induce a systemic *Mysm1*^{fl} to *Mysm1*$^{\Delta}$ allele conversion. **(A)** Absolute numbers of DC lineage cells in the bone marrow and of DCs in the spleen, gated as Lin^{-}Flt3^{+}CD11c^{+}SIRPα^{+} and CD45^{+}Lin^{-}F4/80^{-}CD64^{-}CD11c^{+}MHCII^{+} cells, respectively. **(B)** Absolute numbers of cDC1, cDC2a, cDC2b, and pDC subsets in the spleen. Cells were gated as CD45^{+}Lin^{-}F4/80^{-}CD64^{-}CD11c^{+}MHCII^{+}, followed by B220^{-}PDCA1^{-}XCR1^{+}SIRPα^{-} for cDC1, B220^{-}PDCA1^{-}XCR1^{-}SIRPα^{+}CLEC12a^{-} for cDC2a, B220^{-}PDCA1^{-}XCR1^{-}SIRPα^{+}CLEC12a^{+} for cDC2b, and B220^{+}PDCA1^{+} for pDCs. Data are from n=9-11 mice per group, consolidated from 3 independent experiments, and presented as mean ± SEM. Statistical analyses used ANOVA with Sidak's posthoc test, comparing each group to the *Mysm1*$^{fl/+}$ Cre^{ERT2} control; * p <0.05, ** p <0.01. **(C)** Representative flow cytometry plots of the mouse bone marrow, pre-gated on live lineage negative cells, and showing the depletion of Flt3^{+}CD11c^{+} pre-DCs in the tamoxifen treated *Mysm1*$^{fl/fl}$ Cre^{ERT2} and *Mysm1*$^{DN/fl}$ Cre^{ERT2} mice. **(D)** Representative flow cytometry plots of the spleen, pre-gated on live CD45^{+} lineage negative cells, and showing the depletion of CD11c^{+} MHCII^{+} DCs in tamoxifen treated *Mysm1*$^{fl/fl}$ Cre^{ERT2} and *Mysm1*$^{DN/fl}$ Cre^{ERT2} mice. Numbers on the plots indicate the percentages of cells within each gate out of the parent population, presented as mean ± SD for all the mice in the group.

Figure 4.3.13 Systemic inducible loss of MYSM1 expression or of its catalytic activity results in an impaired BMDC differentiation in culture.

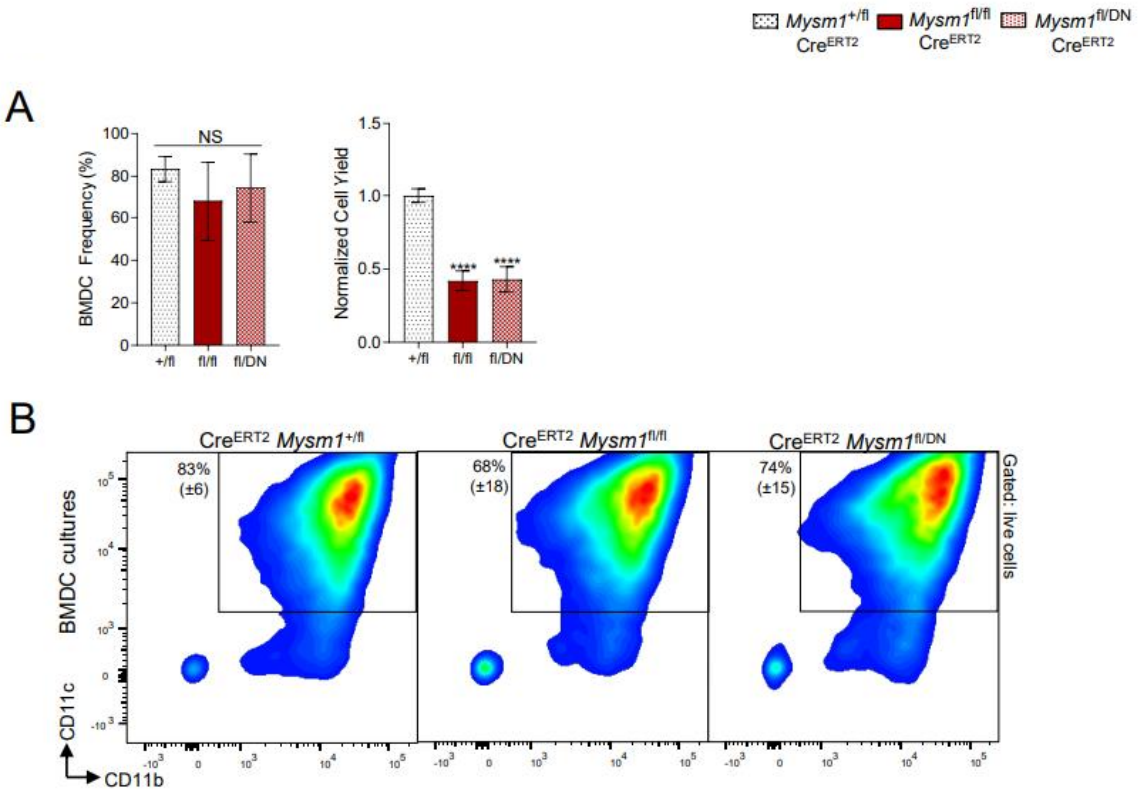

Flow cytometry analyses were conducted on the BMDC cultures set up with the bone marrow of tamoxifen treated Cre^{ERT2} transgenic mice of *Mysm1*$^{fl/fl}$, *Mysm1*$^{DN/fl}$, and control *Mysm1*$^{+/fl}$ genotypes. (A) Normal BMDC frequencies but depleted absolute cell numbers in the *Mysm1*$^{fl/fl}$ Cre^{ERT2} and *Mysm1*$^{DN/fl}$ Cre^{ERT2} BMDC cultures. Data are from $n = 7–8$ mice per group consolidated from two independent experiments; bars represent mean ± SEM; statistical analyses used ANOVA with Dunnett's post hoc test; NS, not significant, ****$p < 0.0001$. (B) Representative flow cytometry plots of the BMDC cultures from tamoxifen treated Cre^{ERT2} transgenic mice of *Mysm1*$^{fl/fl}$, *Mysm1*$^{DN/fl}$, and control *Mysm1*$^{+/fl}$ genotypes, showing the gating on BMDCs as live CD11b^{+}CD11^{hi} cells, and demonstrating similar high frequencies of cells with the BMDC surface markers across the *Mysm1* genotypes. Numbers on the plots indicate the percentages of cells within each gate out of the parent population, presented as mean ± SD of all the mice in the group.

4.3.12 Cell intrinsic MYSM1 in hematopoietic progenitors is essential for DC development

To test the cell intrinsic role of MYSM1 and its catalytic activity in hematopoietic progenitors for DC lineage development, competitive bone marrow chimeras were set up. CD45.1^{+} wild type bone marrow was mixed in a 1:1 ratio with the bone marrow of CD45.2^{+} Cre^{ERT2} mice of *Mysm1*$^{+/fl}$, *Mysm1*$^{fl/fl}$, or *Mysm1*$^{DN/fl}$ genotypes, and the mixes were transplanted into three independent groups of lethally irradiated recipients. The recipient mice were bled at 12-weeks to confirm normal reconstitution, and subsequently administered with tamoxifen to induce the *Mysm1*^{fl} allele deletion.

The mice were analyzed for the relative contribution of CD45.2^{+} hematopoietic stem and progenitor cells to the DC lineage, comparing across the three *Mysm1* genotypes (Figure 4.3.14A). We observed a highly significant reduction in the contribution of the *Mysm1*$^{fl/fl}$ Cre^{ERT2} and *Mysm1*$^{DN/fl}$ Cre^{ERT2} donor cells to all the DC populations in the spleen, bone marrow, and blood of the chimeric mice (Figure 4.3.14B-E, Figure 4.3.15A-B). Furthermore, the bone marrow of the chimeric mice demonstrated an impaired capacity to generate *Mysm1*$^{fl/fl}$ Cre^{ERT2} and *Mysm1*$^{DN/fl}$ Cre^{ERT2} BMDCs in culture (Figure 4.3.15C-D). This demonstrates the essential and cell intrinsic role of MYSM1 and its DUB catalytic activity in hematopoietic progenitors for the DC lineage development.

Figure 4.3.14 Cell intrinsic requirement for MYSM1 expression and its catalytic activity in the hematopoietic cells for DC lineage development, assessed with competitive bone marrow chimeras.

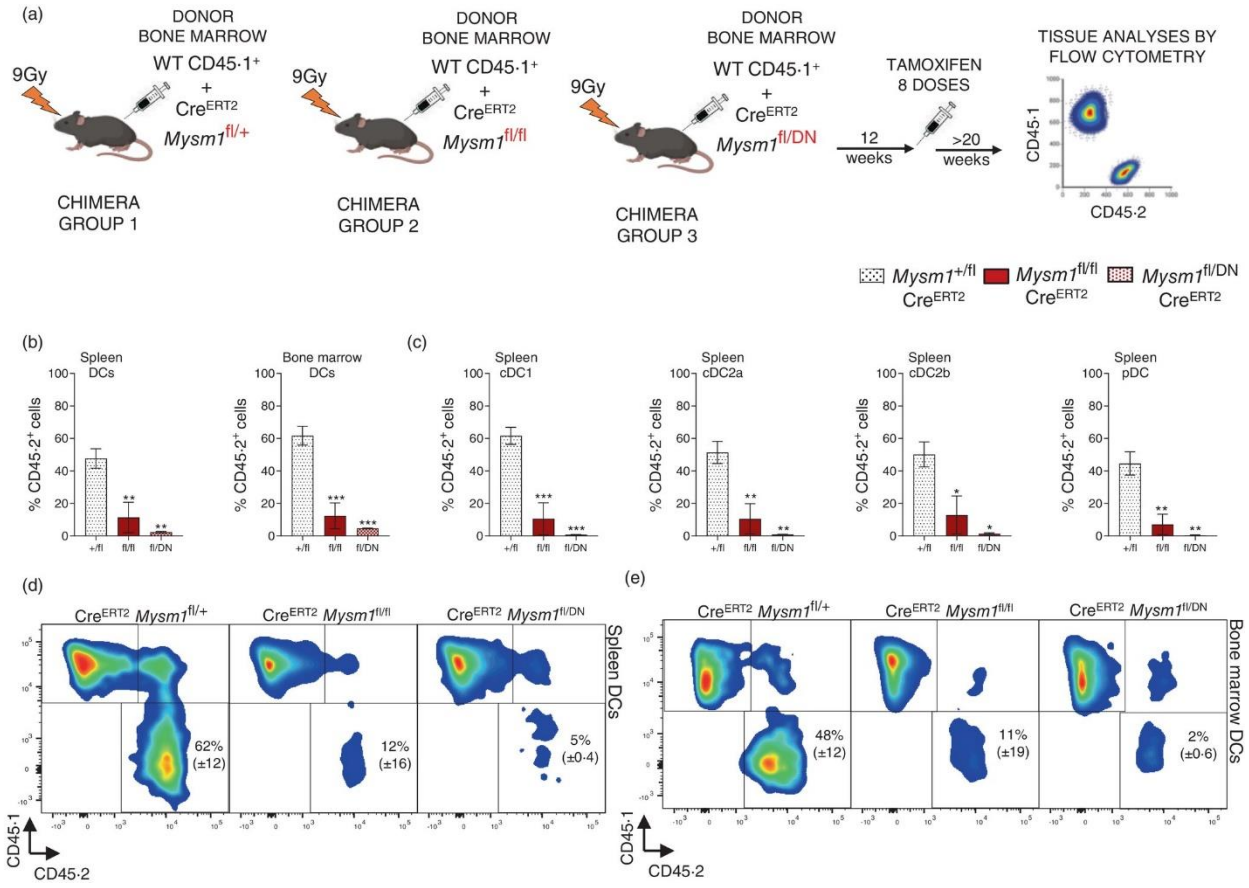

(**A**) Schematic representation of the mouse-to-mouse competitive bone marrow transplantation study. Wild type CD45.1$^+$ bone marrow cells were mixed in a 1:1 ratio with Cre^{ERT2} transgenic bone marrow cells of *Mysm1*$^{fl/+}$, *Mysm1*$^{fl/fl}$, or *Mysm1*$^{fl/DN}$ genotypes, and the mixes were transplanted into three independent cohorts of lethally irradiated wild type CD45.1$^+$ recipient mice, as described in [277]. Following full hematopoietic reconstitution, the chimeric mice were administered with tamoxifen to induce the *Mysm1*^{fl} to *Mysm1*$^{\Delta}$ allele conversion. (**B-C**) Relative contribution of *Mysm1*$^{\Delta/DN}$, *Mysm1*$^{\Delta/\Delta}$, and control *Mysm1*$^{\Delta/+}$ cells to the DC cell populations was evaluated by flow cytometry, quantifying the proportion of CD45.2$^+$CD45.1$^-$ cells within each cell population. Data are from n=3-5 mice per group, presented as mean ± SEM. Statistical analyses used ANOVA with Sidak's posthoc test, comparing each group to the *Mysm1*$^{\Delta/+}$ control; * p<0.05, ** p <0.01, *** p <0.001. DCs were gated as CD45$^+$Lin$^-$F4/80$^-$CD64$^-$CD11c$^+$MHCII$^+$ cells, followed by B220$^-$PDCA1$^-$XCR1$^+$SIRPα$^-$ for cDC1, B220$^-$PDCA1$^-$XCR1$^-$SIRPα$^+$CLEC12a$^-$ for cDC2a, B220$^-$PDCA1$^-$XCR1$^-$SIRPα$^+$CLEC12a$^+$ for cDC2b, and B220$^+$PDCA1$^+$ for pDCs, as shown in Figure S2. (**D-E**) Representative flow cytometry plots showing the analyses of splenic and bone marrow DCs in the chimeric mice for CD45.2 versus CD45.1 markers expression; percentage of cells in the gates is shown as mean ± SD of all the mice in each group. Gates for CD45.2$^+$ and CD45.1$^+$ cells were set independently for each DC cell population using control non-chimeric wild type B6-CD45.2 and SJL-CD45.1 mice, as shown in the Figure 4.3.15.

Figure 4.3.15 Cell intrinsic requirement for MYSM1 and its catalytic activity for DC lineage development and responses to microbial stimulation, assessed with competitive bone marrow chimeras.

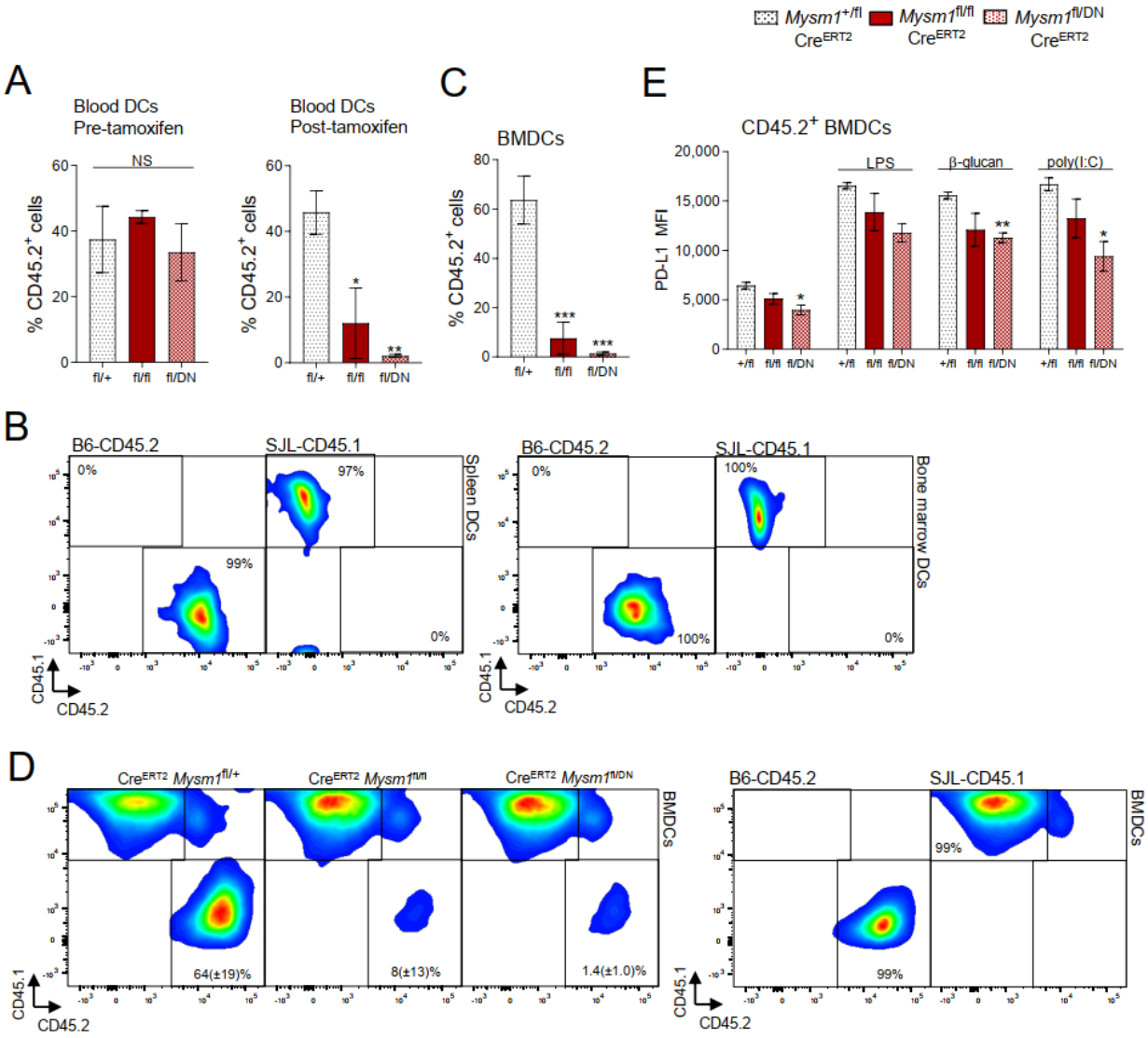

Chimeric mice were established as presented in Figure 4.3.14A. Briefly, wild type CD45.1$^+$ bone marrow was mixed in a 1:1 ratio with the bone marrow of *Mysm1*$^{fl/+}$ Cre^{ERT2}, *Mysm1*$^{fl/fl}$ Cre^{ERT2} , or *Mysm1*$^{fl/DN}$ Cre^{ERT2} mice, and the mixes were reconstituted into three independent cohorts of lethally irradiated wild type CD45.1$^+$ recipients. Following full hematopoietic reconstitution, the chimeric mice were administered with tamoxifen to induce the *Mysm1*^{fl} to *Mysm1*$^{\Delta}$ allele conversion. (A) Relative contributions of the *Mysm1*$^{fl/+}$ Cre^{ERT2}, *Mysm1*$^{fl/fl}$ Cre^{ERT2} , and *Mysm1*$^{fl/DN}$ Cre^{ERT2} donor bone marrows to the DC cell populations in the blood of the chimeric mice, pre- and post-tamoxifen treatment, evaluated by flow cytometry to quantify the proportion of CD45.2$^+$CD45.1$^-$ cells within the live CD11c$^+$MHCII$^+$ DC cell population. (B) Setting the gates to quantify the relative reconstitution of DC lineage cells by the CD45.2$^+$ versus CD45.1$^+$ donors:

DCs are gated as $CD45^+Lin^-F4/80^-CD64^-CD11c^+MHCII^+$ cells in the spleen and bone marrow of wild type non-chimeric B6-CD45.2 and SJL-CD45.1 mice in order to set the gates on the $CD45.2^+$ versus $CD45.1^+$ DC populations. (C, D) BMDC cultures setup with the bone marrow of the chimeric mice demonstrate the impaired contribution of *Mysm1*$^{fl/fl}$ Cre^{ERT2} and *Mysm1*$^{fl/DN}$ Cre^{ERT2} cells to BMDC development. (D) Flow cytometry plots analysing the BMDC cultures from the chimeric mice for CD45.2 versus CD45.1 markers; BMDCs are gated as live $CD11b^+CD11c^{hi}$ cells; percentages of cells in the gates are shown as mean ± SD for all the mice in each group. The gates for $CD45.2^+$ and $CD45.1^+$ cells were set using BMDC cultures from non-chimeric wild type B6-CD45.2 and SJL-CD45.1 mice. (E) Analysis of PD-L1 induction in response to microbial stimulation on the BMDCs derived from the chimeric mice, gating on live $CD11b^+CD11c^{hi}$ $CD45.2^+CD45.1^-$ cells. *Mysm1*$^{\Delta/DN}$ BMDCs exhibited reduced PD-L1 induction, with *Mysm1*$^{\Delta/\Delta}$ BMDCs showing a similar trend. In contrast, no defects in the induction of co-stimulatory and activation markers (CD86, CD40, MHCII) were observed for the *Mysm1*$^{\Delta/DN}$ or *Mysm1*$^{\Delta/\Delta}$ BMDCs (data not shown), and no impaired PD-L1 induction was observed for the control $CD45.2^-CD45.1^+$ BMDCs in the same co-cultures (data not shown). Data are from $n = 3–5$ mice per group, presented as mean ± SEM. Statistical analyses used ANOVA with Dunnett's post hoc test, comparing each group to the *Mysm1*$^{\Delta/+}$ control; $*p < 0.05$, $**p < 0.01$, $***p < 0.001$.

4.3.13 MYSM1 in hematopoietic progenitors affects DC transcriptional responses to stimulation

Given the primary function of MYSM1 as an epigenetic regulator [224, 225], we hypothesized that MYSM1 activities in the DC lineage specification may have downstream effects not only on DC numbers but also on the DC activation in responses to microbial stimulation. To explore such effects, BMDCs from the tamoxifen treated mice of Cre^{ERT2} *Mysm1*$^{fl/DN}$ and control Cre^{ERT2} *Mysm1*$^{+/fl}$ genotypes were subjected to bulk RNA-seq, with and without LPS stimulation (n=3-4 mice per group, Figure 4.3.16A). *Mysm1*$^{+/\Delta}$ BMDCs, used as the control group, showed normal transcriptional responses to LPS, consistent with the lack of significant phenotypes with a heterozygous loss of *MYSM1* in all previous studies in mouse and human [225]. Dimension reduction analysis of the BMDC gene expression profiles demonstrated a clear segregation based on the stimulation conditions (PC1, 51% variance, Figure 4.3.16B). Importantly, there was also a clear segregation of the gene expression profiles based on the *Mysm1* genotype for both untreated and LPS stimulated BMDCs (PC2, 18% variance, Figure 4.3.16B), demonstrating a major effect of a

pan-hematopoietic loss of MYSM1 function on the BMDC transcriptome. Differential gene expression analysis compared *Mysm1*$^{\Delta/DN}$ against control *Mysm1*$^{\Delta/+}$ BMDCs for each condition, and the genes with the fold change ≥ |1.5| and FDR ≤ 0.01 were considered significant. This identified 1019 dysregulated genes in the *Mysm1*$^{\Delta/DN}$ BMDCs in total, corresponding to 531 upregulated and 271 downregulated genes at steady-state and 300 upregulated and 141 downregulated genes following LPS stimulation. Hierarchical clustering segregated the genes differentially expressed in *Mysm1*$^{\Delta/DN}$ BMDCs into five major Clusters I-V (Figure 4.3.16C), and the gene ontology (GO) enrichment analysis was performed on the genes in each Cluster to investigate their biological functions (Figure 4.3.16D).

Clusters I-III corresponded to the genes downregulated in *Mysm1*$^{\Delta/DN}$ BMDCs under steady-state or LPS-stimulation conditions relative to control *Mysm1*$^{\Delta/+}$ BMDCs, with the Cluster I genes undergoing a downregulation in response to LPS across both *Mysm1* genotypes, and the Cluster II-III genes undergoing an upregulation in response to LPS at least in the control group (Figure 4.3.16C). GO analyses revealed that Cluster I was enriched for the genes engaged in ribosome biogenesis, consistent with the previous reports of MYSM1 function in the regulation of ribosomal genes in HSPCs [244, 307], while both Clusters I and II were enriched for the genes engaged in angiogenesis and responses to hypoxia (Figure 4.3.16D). Importantly, Cluster III was enriched for genes engaged in immune response and cell migration, with the genes downregulated in *Mysm1*$^{\Delta/DN}$ BMDCs including such immunological genes as *Il10*, *Il23a*, *Il33*, *Cxcl1*, *Cxcl11*, *Trem1*, and others (Figure 4.3.16D, Figure 4.3.17A).

Clusters IV-V encompassed the genes upregulated in *Mysm1*$^{\Delta/DN}$ relative to the control *Mysm1*$^{\Delta/+}$ BMDCs, of which Cluster IV genes were primarily downregulated and Cluster V genes primarily upregulated in the response to LPS stimulation (Figure 4.3.16C). GO analysis demonstrated that Cluster IV was strongly enriched for the genes engaged in cell cycle progression, including both cell division and DNA replication, and also for the genes engaged in DNA damage response and repair (Figure 4.3.16D), consistent with the previously established links between *Mysm1*-deficiency and p53-stress response induction in hematopoietic cells [238, 240, 308]. Importantly, Cluster V was enriched for the genes with immune functions, corresponding to the GO-terms 'immune system process', 'inflammatory response', 'regulation of cytokine production' and others (Figure 4.3.16D). Examples of the Cluster V genes upregulated in the *Mysm1*$^{\Delta/DN}$ relative to the control *Mysm1*$^{\Delta/+}$ BMDCs include the genes encoding microbial sensing machinery (*Tlr1*, *Tlr6*, *Tlr9*, *Ticam2*, *CD180*), cytokine response (*Il12b, Tnfrsf14*, *Ifitm3*), and MHCII-antigen presentation (*CIITA*, *H2-DMB1*, Figure 4.3.17B-D). Overall, we note that *Mysm1*$^{\Delta/DN}$ BMDCs demonstrated a downregulation of immunosuppressive *Il10*, Th17-polarizing *Il23*, and Th2-polarizing *Il33* genes (Cluster III, Figure 4.3.17A), and an upregulation of Th1-polarizing *Il12b* gene (Cluster V, Figure 4.3.17C). Together with the other transcriptional signatures, this demonstrates that the loss of MYSM1 function during DC-lineage specification results in the altered DC immune activation and polarization states.

To further explore the transcriptional signatures dysregulated in BMDCs as the result of a pan-hematopoietic loss of MYSM1 function, Gene Set Enrichment Analysis (GSEA) was performed [274]. *Mysm1*$^{\Delta/DN}$ BMDCs demonstrated an upregulation of the transcriptional signatures of cell cycle progression and downregulation of the transcriptional signatures of ribosome biogenesis (Figure

4.3.16E), as already reported in the GO-term analyses above (Figure 4.3.16D). Additionally, GSEA analysis indicated an upregulation of the transcriptional signatures related to 'aerobic respiration' and 'oxidative phosphorylation' in the *Mysm1*$^{\Delta/DN}$ BMDCs, suggesting altered metabolic profile of the cells, as well as downregulation of the transcriptional signatures of 'non-canonical WNT signaling' and 'response to interferon beta'. Overall, we conclude that the loss of MYSM1 DUB catalytic activity throughout DC lineage development results not only in a severe depletion of DC numbers, but also in the production of functionally altered DCs, with a dysregulation of many housekeeping transcriptional programs and a significantly altered induction of key immunological genes in response to microbial stimulation.

Figure 4.3.16 Pan-hematopoietic loss of MYSM1 function results in altered DC transcriptional profiles, including significant changes in the DC responses to microbial stimulation.

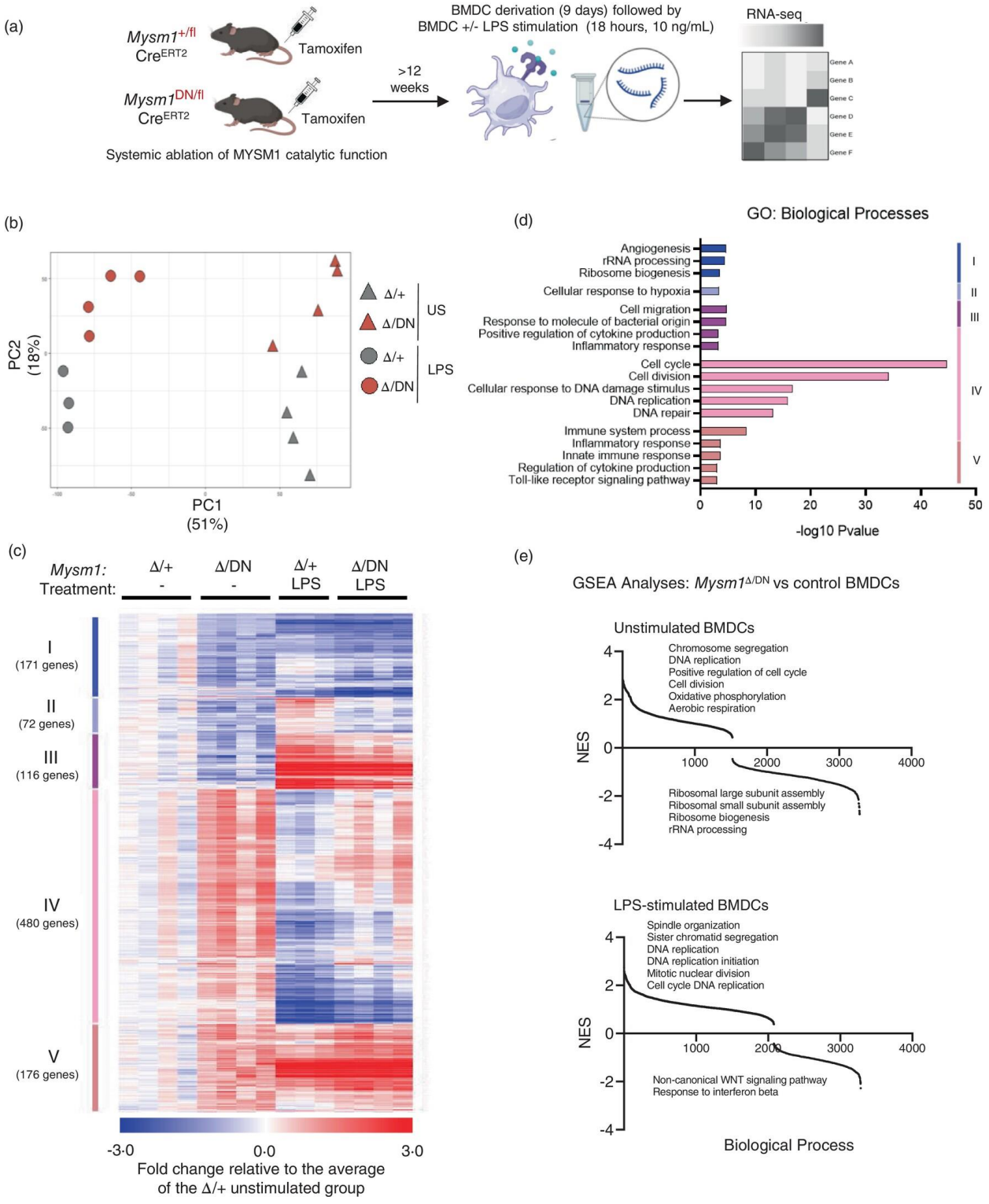

(A) Schematic of the bulk RNA-seq analyses of BMDCs derived from the tamoxifen treated Cre^{ERT2} transgenic mice of *Mysm1*$^{fl/DN}$ and control *Mysm1*$^{fl/+}$ genotypes, at steady-state and following LPS stimulation. Tamoxifen treated *Mysm1*$^{fl/DN}$ Cre^{ERT2} mice (Δ/DN) express a catalytically inactive MYSM1, whereas *Mysm1*$^{fl/+}$ Cre^{ERT2} control mice (Δ/+) express wild type MYSM1. Bone marrow was extracted at >12 weeks after the tamoxifen treatment, BMDCs derived *in vitro* over 9 days of culture, and subsequently harvested and cultured for further 18 hours either untreated or with LPS stimulation (10 ng/mL). **(B)** Partial component analysis plot demonstrating the gene expression profiles of *Mysm1*$^{Δ/DN}$ and control *Mysm1*$^{Δ/+}$ BMDCs with and without LPS stimulation, with the response to LPS described by the principal component 1 (PC1, 51% variability) and the differences between the genotypes by PC2 (18% variability). **(C)** Heatmap displaying 1015 genes significantly dysregulated between *Mysm1*$^{Δ/DN}$ and control *Mysm1*$^{Δ/+}$ BMDCs, at steady state and following LPS stimulation. The significance threshold is fold change $\geq |1.5|$ and FDR ≤ 0.01, and the data are presented relative to the average of the control unstimulated *Mysm1*$^{Δ/+}$ BMDC group. Hierarchical clustering of the genes was performed using Pearson correlation with average linkage to generate the Clusters I-V. **(D)** Gene ontology (GO) enrichment analysis of the differentially expressed genes in Clusters I-V; select representative biological process GO-terms are displayed. **(E)** Gene set enrichment analysis (GSEA) of the transcriptional signatures of *Mysm1*$^{Δ/DN}$ relative to control *Mysm1*$^{Δ/+}$ BMDCs, with and without LPS stimulation, showing the normalized enrichment scores (NES) for pre-established biological process transcriptional signatures. Select representative biological processes are labelled on the plot.

Figure 4.3.17 Examples of DC transcriptional changes resulting from a pan-hematopoietic loss of MYSM1 function, including the genes encoding important mediators of DC activation and immune response.

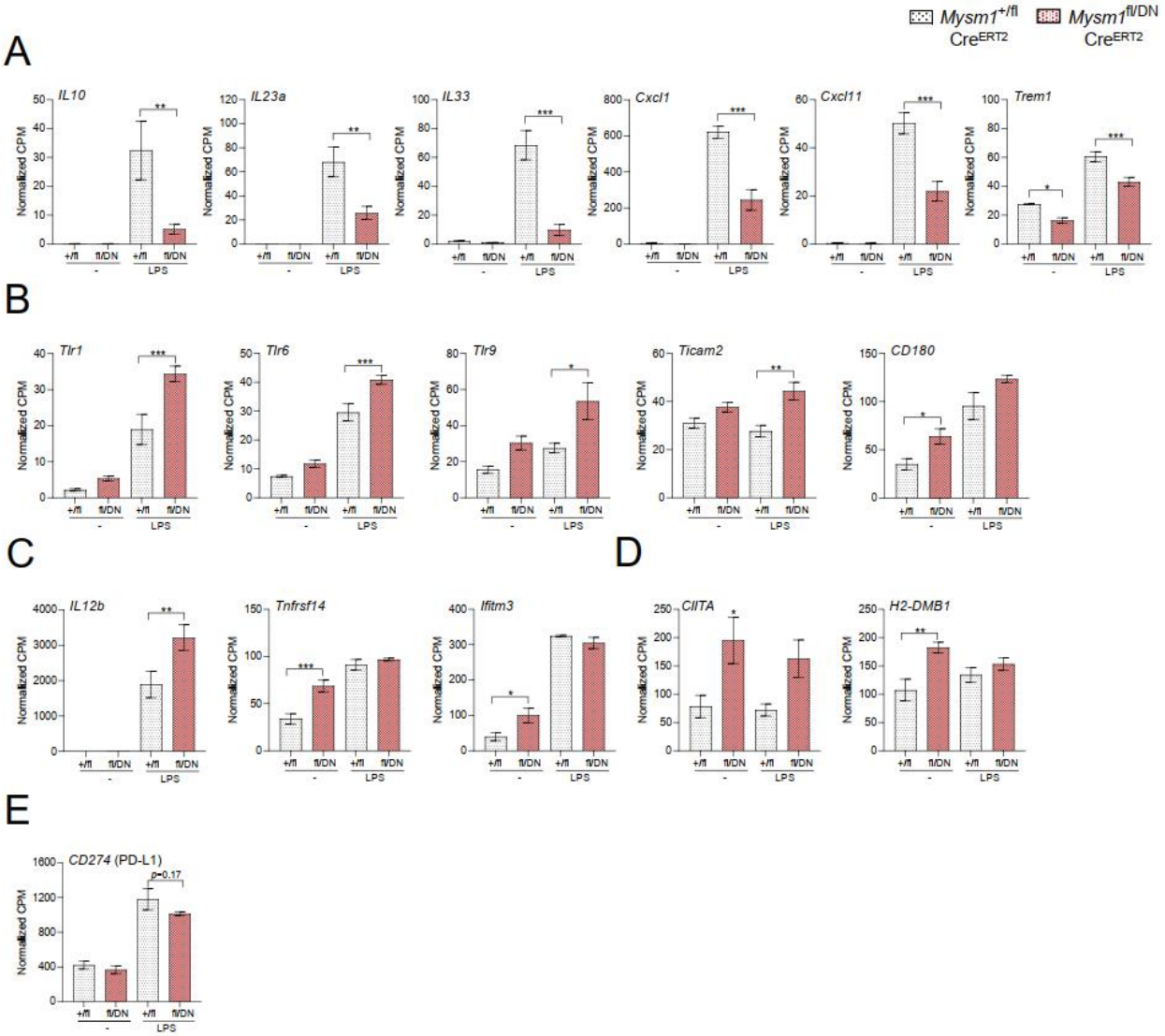

Normalized read counts per million (CPM) are presented from the bulk RNA-seq analyses of BMDCs from the tamoxifen treated *Mysm1*$^{fl/DN}$ Cre^{ERT2} and control *Mysm1*$^{fl/+}$ Cre^{ERT2} mice, at steady-state and following LPS stimulation, as shown in Figure 4.3.16. Data are from $n = 3–4$ mice per group and presented as mean ± SEM. Statistical analyses used ANOVA and Sidak's post hoc test, comparing to the *Mysm1*$^{fl/+}$ Cre^{ERT2} control group for each condition; $*p < 0.05$, $**p < 0.01$, $***p < 0.001$, or not significant if not indicated.

4.3.14 Loss of MYSM1 modulates DC responses to microbial stimulation

We further tested whether the changes in the responses of *Mysm1*$^{\Delta/DN}$ BMDCs to microbial stimulation alter their capacity to act as antigen presenting cells. For this purpose, BMDCs derived from tamoxifen treated mice of Cre^{ERT2} *Mysm1*$^{fl/DN}$ and control *Mysm1*$^{fl/+}$ genotypes were pre-stimulated with LPS in the presence of ovalbumin (OVA) and co-cultured with OVA-specific OT-II CD4 T cells. The T cells were analysed at days 3–4 for activation markers (CD44, CD69), cytokine production (IFNγ, IL-2, IL-4, IL-10), and for cell proliferation, comparing between the cultures containing *Mysm1*$^{\Delta/DN}$ and control BMDCs. This demonstrated a largely normal capacity of *Mysm1*$^{\Delta/DN}$ BMDCs for T cell activation, with a mild increase in the CD44 activation marker and a mild reduction in IL-2 production for the T cells in co-cultures with *Mysm1*$^{\Delta/DN}$ as compared to control BMDCs (Figure 4.3.18 A-D), but no differences in the induction of T cell proliferation (Figure 4.3.18 E-F), in the expression of CD69, IFNγ, IL-4, or IL-10 (Figure 4.3.18), or in T cell viability (Figure 4.3.18 G). Overall, we conclude that the loss of MYSM1 DUB catalytic activity in hematopoietic progenitors mildly modulates DC responses to microbial stimulation, however does not result in major changes in the DC capacity for antigen presentation or CD4 T cell activation.

Figure 4.3.18 Impact of a pan-hematopoietic loss of MYSM1 catalytic activity on the DC function as antigen presenting cells.

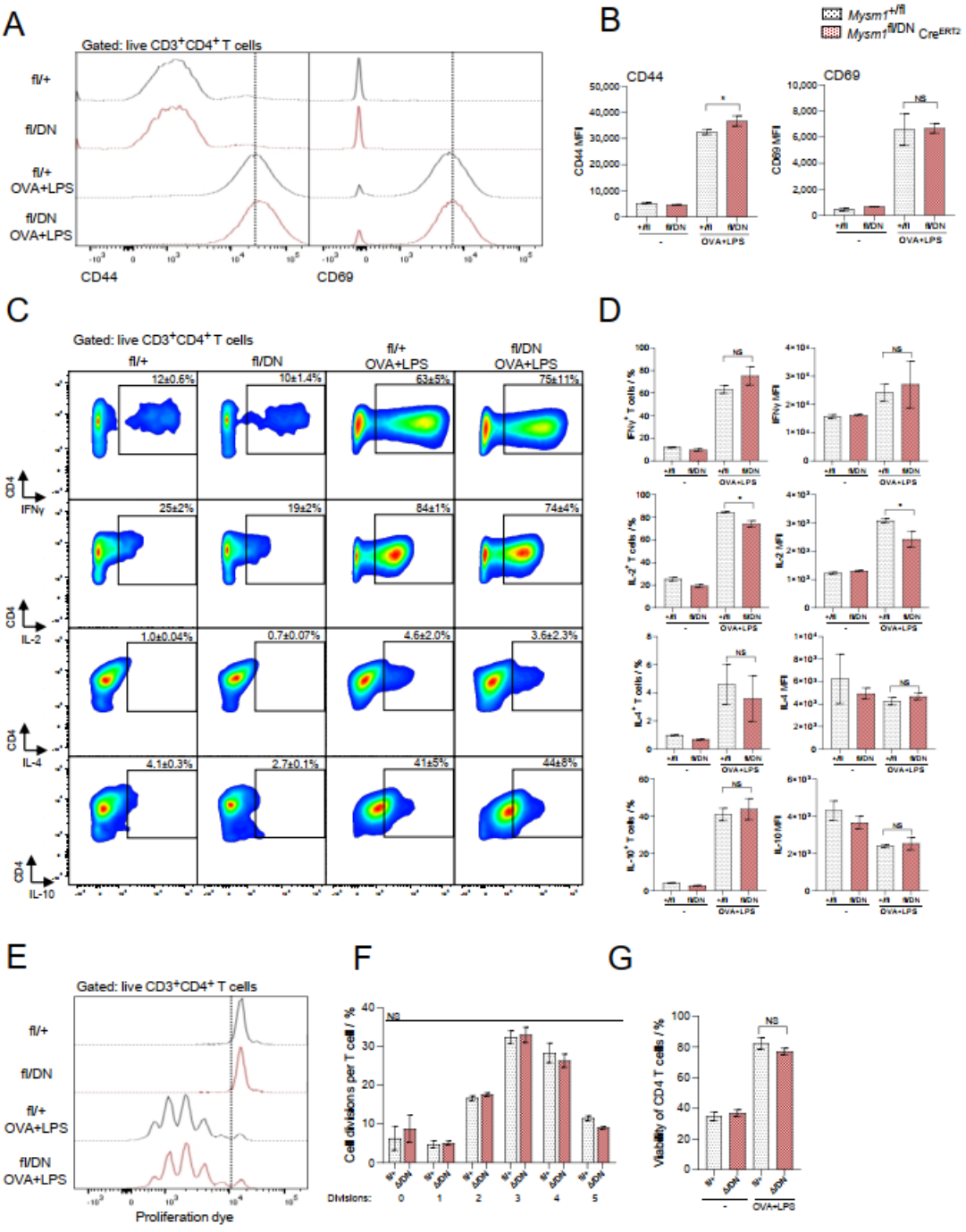

BMDCs derived from the tamoxifen treated mice of CreERT2 *Mysm1*fl/DN and control *Mysm1*fl/+ genotypes were either untreated or stimulated with LPS (10 ng/ml) in the presence of whole OVA (1mg/ml) for 18 hours. The BMDCs were subsequently cocultured with OVA-specific OT-II CD4 T cells in a 1:10 ratio for 3-4 days, and the T cells analyzed for the following readouts as a measure of DC function. **(A-B)** Analyses of the T cells for CD44 and CD69 activation markers at day 3 of

co-culture, comparing between the BMDC *Mysm1* genotypes and stimulation conditions. **(A)** Representative flow cytometry histograms of CD44 and CD69 staining, and **(B)** quantification of the CD44 and CD69 mean fluorescence intensity (MFI) gating on live CD3+CD4+ T cells. **(C-D)** Analyses of the T cells for IFNγ, IL-2, IL-4, and IL-10 cytokine production at day 4 of BMDC co-culture, comparing between the BMDC *Mysm1* genotypes and stimulation conditions. **(C)** Representative flow cytometry plots gated on live CD3+CD4+ T cells and showing intracellular cytokine staining; percentages of cells in the positive gates for all the mice in each group are indicated as mean ± S.D. **(D)** Quantification of T cell cytokine production, including the percentages of cytokine positive live CD3+CD4+ T cells, and the mean fluorescence intensities (MFI) of cytokine levels within the cytokine positive T cell populations. **(E-F)** Analyses of T cell proliferation at day 3 of co-culture, using a proliferation dye dilution assay and comparing between the BMDC *Mysm1* genotypes and stimulation conditions. **(E)** Representative flow cytometry plots of the proliferation dye dilution gating on live CD3+CD4+ T cells, and **(F)** quantification of the percentages of T cells in the culture that underwent 0-5 cell divisions are presented. **(G)** Analyses of T cell viability at day 3 of co-culture, comparing between the BMDC *Mysm1* genotypes and stimulation conditions. All data are from n=3 mice per group and presented as mean ± SEM. Statistical analyses used ANOVA and Sidak's posthoc test comparing between the *Mysm1* genotypes for each stimulation condition; * $p < 0.05$, NS – not significant.

Chapter 5: Conclusion and Discussion

5.1 Role of BAP1 in B lymphocyte development

In previous studies, we established the non-redundant and cell intrinsic role of BAP1 in the normal progression of B cell development[223]. Here, we propose that BAP1 plays a direct role in regulating the transcriptional programs essential for cell proliferation and cell cycle progression processes in pre-B cells, through its deubiquitinase (DUB) activity targeting histone H2AK119ub.

Our work has deepened the understanding of the molecular functions of BAP1 within the B cell lineage. To be more precise, using B cell precursor cell line Ba/F3 with CRISPR/Cas9 mediated *Bap1* deletion, we confirmed the role of BAP1 in the regulation of B cell proliferation. Moreover, using Ba/F3 cell lines, we mapped the genome-wide DNA-binding sites of BAP1 through ChIP-seq analysis, and observed a significant overrepresentation of BAP1 binding sites near genes that were dysregulated in our previous RNA-seq analyses using *Bap1*$^{fl/fl}$ mb1-Cre primary murine pre-B cells, particularly at downregulated genes involved in cell proliferation and cell cycle progression. Notably, the loss of BAP1 resulted in increased H2AK119ub levels at these sites. This finding supports our conclusion that BAP1, through its H2A-DUB catalytic activity, plays a direct role in regulating these genes. Overall, we hypothesize that the disruption of BAP1-regulated transcriptional programs related to cell proliferation and cycle progression contributes to the defects in B cell development observed in BAP1 deficiency.

The connection between the loss of BAP1 and reduced cell proliferation, as suggested in our study of the B cell lineage, is consistent across various cell types[203, 205, 222, 309]. As mentioned earlier, systemic inducible deletion of *Bap1* in mice impairs the proliferation of thymocytes and peripheral

CD4 T cells[222], indicating a shared role for BAP1 across different lymphoid cells. Erythrocyte and platelet depletions were also observed in this model but were not linked to cell proliferation defects[221]. BAP1 was also reported to be crucial for the proliferation of several non-hematopoietic cell lines, where it regulates the transcriptional programs related to cell cycle progression in collaboration with HCF1[197, 203, 205, 211, 309, 310]. However, it is worth noticing that BAP1's role in promoting cell proliferation is not universal: *Bap1* deletion in mice leads to an increase in myeloid leukocytes and progenitor cells, resembling the pathology of myelodysplastic syndrome (MDS) and chronic myelomonocytic leukemia (CMML)[221]. Such contrasting effects of BAP1 loss on myeloid versus lymphoid lineages are intriguing, especially given our findings showing a strong correlation in the genomic location of BAP1 binding sites across B cells, macrophages, and ES cells[221, 278], suggesting common transcriptional functions. The mechanisms behind these distinct outcomes of BAP1 loss on myeloid and lymphoid lineage cells merit further investigation, and may provide insights into the tumor suppressor roles of BAP1 and its ASXL binding partners[183, 191, 193].

As mentioned before, our findings show that BAP1 deficiency leads to an increase in histone H2AK119ub levels at BAP1 genomic binding sites in B cell precursors, both globally across the genome and locally at the promoters of BAP1-target genes involved in the regulation of B cell proliferation. This suggests that the function of BAP1 in B lymphocytes is, at least partially, tied to its DUB activity for histone H2AK119ub. Traditionally, the deposition of the H2AK119ub transcription repressive mark on chromatin by the PRC1 complex is associated with long-term silencing of developmentally regulated genes, thereby controlling cellular differentiation and lineage specification pathways[141, 143, 282]. More recently, the role of H2AK119ub in regulating other

transcriptional programs, such as those related to cell survival and apoptosis[311], as well as cell proliferation and cell cycle progression[312, 313, 314], has been recognized across different cell types. Our findings further emphasize the potential role of the H2AK119ub epigenetic mark and the machinery regulating its deposition and removal in controlling transcriptional programs related to cell proliferation in B lymphocytes.

It is worth noticing that BAP1 is not the only DUB expressed in B lymphocytes. Recent studies demonstrated that MYSM1 and USP16 are essential for B cell development[180, 232, 280, 315], while USP44 and USP21 are dispensable[181, 316]. Consolidation of various ChIP-seq datasets that analyzed the distribution of genomic binding sites of these DUBs in murine ESCs, hematopoietic and immune cells indicated co-localization of BAP1 majorly with USP16, minorly with USP22, but not with MYSM1[317]. Although the function of USP16 as a DUB for histone H2A was challenged by its primarily cytosolic localization[318], further investigation of the potential redundancy or interaction between BAP1 and other histone DUBs in B cells would benefit our understanding of the molecular mechanisms underlying the regulation of B cell differentiation and functions. Moreover, the interplay between histone modifications is also a critical aspect of the epigenetic regulatory mechanisms of gene expression. As mentioned earlier, the deposition of monoubiquitin at H2AK119 is influenced by the level of H3K27me3[142, 143, 144] and, in turn, affects the trimethylation at H3K27[145, 146] and H3K4[144]. Recent studies have revealed more details of the dynamic crosstalk between histone modification[319]. Our study confirms the essential gene regulatory role of BAP1 through its H2A-DUB catalytic activity in B cells. Further mechanistic exploration of BAP1 and its interaction with other chromatin-modifying enzymes in B

lymphocytes would shed light on the function of fundamental molecular machinery and on the future development of innovative therapeutic strategies.

The role of BAP1 as a tumor suppressor has also been intensively studied. Germline mutations in the *Bap1* gene in humans have been linked to cancers such as mesothelioma, uveal melanoma, and renal cell carcinoma[183, 193]. While *Bap1* mutations are not typically linked to B cell lymphomas, cases of non-Hodgkin lymphoma have been reported in patients carrying germline *Bap1* mutations[320]. Additionally, lymphomas with other genetic aberrations have been found to acquire *Bap1* gene silencing through epigenetic mechanisms[321]. These reports suggest that BAP1 might also act as a tumor suppressor in the B cell lineage, although further verification in murine models is needed. Interestingly, although it is not something we have tested systematically, we did not see an obvious increase in premature lethality or high-penetrance carcinogenesis in the *Bap1*$^{fl/fl}$ mb1-Cre mice. Future studies, such as screening for spontaneous lymphoma occurrence in these mice or tracking age-related phenotypes and lifespan of these animals, will be essential to explore the potential tumor suppressor role of BAP1 in B cells.

The molecular mechanisms underlying the tumor suppressor function of BAP1 are still in debate, particularly given the current study and many other reports supporting BAP1's role as a positive regulator of cell proliferation[203, 222, 223, 309]. In myeloid progenitor cells, BAP1's tumor suppressor activity has been associated with its antagonistic relationship with the PRC2 complex: the transformation of BAP1-deficient myeloid cells is linked to increased PRC2-mediated transcriptional repression, which can be reversed by the loss or inhibition of the PRC2 catalytic subunit EZH2[216, 322]. Similar mechanisms of BAP1's tumor suppressor role are implicated in

mesothelioma[216], but not in uveal melanoma cell lines[323]. Other proposed mechanisms connecting BAP1's molecular functions to its tumor suppressor activity include its roles in regulating pro-survival and pro-apoptosis transcriptional programs in cross-talk with PRC1[311], in promoting ferroptosis by repressing *SLC7A11* gene expression[196], in controlling cellular metabolic programs[204, 324, 325, 326], and in regulating Ca^{2+} signaling and apoptosis by deubiquitinating and stabilizing IP3R3 receptor-channels[207, 327]. In our previous study, SLC7A11 was not expressed in pre-B and immature B cells from either *Bap1*$^{fl/fl}$ mb1-Cre or control mice[223], indicating that BAP1's regulation of ferroptosis is unlikely to play significant roles in these B cell precursors. Consistently, genomic analyses in the current study demonstrated no significant overlap between the binding sites of BAP1 and of the PRC2 catalytic subunit EZH2 in the B cell lineage. Further research is needed to explore the molecular mechanisms of BAP1's tumor suppressor activities across different cell types, considering its apparent positive role in regulating cell proliferation in non-transformed cells from various tissues.

In summary, we highlight the non-redundant and cell-intrinsic role of BAP1 as an H2A-DUB in regulating the transcription programs essential for B cell development. We have attributed the impaired B lymphocyte development in BAP1 deficiency to defects in cell proliferation and cell cycle progression in pre-B cells[223]. Here, we propose a link between altered transcriptional profiles of the mentioned biological pathways and the elevated H2AK119ub levels in proximity to BAP1 binding sites in pre-B cells. However, it is worth noticing that BAP1 is expressed throughout B cell ontogeny, and our previous cell cycle analysis in *Bap1*$^{fl/fl}$ mb1-Cre mice revealed significant changes not only in pre-B cells but also in immature and mature B cells[223]. Therefore, BAP1 possibly acts as a transcriptional regulator throughout B cell development. Cell proliferation is

crucial not only for establishing and maintaining the pool of naïve B cells, but also for mediating humoral immune response, including clonal expansion of B cells during the germinal center reaction[104, 328]. In the next step of our research, we sought to explore the intrinsic role of BAP1 in B cells during humoral immune responses, including the germinal center (GC) reaction and the differentiation and persistence of plasma and memory B cells.

5.2 Role of BAP1 in humoral immunity

Through continuous investigation, here, we establish the essential and cell-intrinsic role of the chromatin-binding DUB BAP1 in B cells for the normal induction of humoral immune response using *Bap1*$^{fl/fl}$ Cγ1-cre mouse model, where *Bap1* deletion takes place selectively in mature activated B cell. We characterize the impact of BAP1-loss on the genome-wide distribution of the H2AK119ub epigenetic mark and on the B cell transcriptome, and discovers novel BAP1-regulated genes with critical roles in the regulation of GC reaction and antibody-mediated immunity.

It is important to note that BAP1 is a multifunctional DUB with many putative substrates[186]. Beyond histone H2AK119ub[135], BAP1 is reported to regulate the ubiquitination, stability, and activity of many transcription factors and enzymes at chromatin of various cell types, namely HCF1[197, 205, 211], YY1[197], FOXK1/2[201, 202], KLF5[203], PGC1α[204], and OGT[204, 221]. BAP1 can also modulate the ubiquitination and stability of IP3R3, regulating Ca^{2+} release from endoplasmic reticulum and cell viability[207]. Nevertheless, we demonstrate a major disruption in the H2AK119ub epigenetic landscape in BAP1 deficient B cells, with an increase in H2AK119ub specifically at the BAP1 genome-binding sites. This establishes the major non-redundant role of BAP1 as a DUB for

the H2AK119ub epigenetic mark in B cells and suggests this as the primary mechanism for the failure of B cell mediated immunity in the *Bap1*$^{fl/fl}$ Cγ1-Cre model. Possible roles of other BAP1 substrates in B cell physiology remain to be further explored in future work.

Analyzing the effects of BAP1-loss on the transcriptome of GC B cells in consolidation with the BAP1 ChIP-seq data, we identified putative novel BAP1-regulated genes with essential roles in the GC reaction and humoral immunity. Furthermore, the significant overlap in BAP1 ChIP-seq genome binding sites in our B cell datasets with previously published datasets from other cell types indicated the engagement of BAP1 in shared housekeeping transcriptional programs. Although, due to the broad BAP1 functions in both housekeeping and cell-type specific transcriptional programs, we cannot attribute all the observed phenotypes to a defined set of BAP1-target genes, our analyses provide many novel BAP1-regulated genes the dysregulation of which can contribute to the failure of humoral immunity in the *Bap1*$^{fl/fl}$ Cγ1-Cre model. This includes *Cblb* that encodes an E3 ubiquitin ligase known to target CD79a, CD79b, and IRF4 to regulate the GC-reaction[294, 295], as well as *Igf2bp3* that encodes a reader of the m6A RNA-modification, induced in GC B cells and essential for normal activation of humoral immunity[298]. Compensatory activity of the YTHDF2 m6A-binding protein has been reported in *Igf2bp3*-deficient GC B cells[298], and may contribute to the overexpression of the transcriptional signatures of mitochondrial biogenesis in the *Bap1*$^{fl/fl}$ Cγ1-Cre GC B cells. Downregulation of the transcriptional signatures of 'IL2 production' and 'T cell proliferation' in the *Bap1*$^{fl/fl}$ Cγ1-Cre GC B cells is also notable, as failure to receive T cell help is known to result in mitochondrial dysfunction and apoptosis in activated B cells[329, 330]. Another example of a novel BAP1-regulated gene identified in our work is *Litaf*, which encodes a repressor of *Bcl6*-expression and a regulator of autophagy in B cell lymphoma[296, 297],

and indeed autophagy plays an important role in the regulation of GC reaction and plasma cell maintenance[331, 332, 333, 334]. While our study focused on the BAP1-regulated transcriptional programs in GC B cells, its functions in the downstream checkpoints in humoral immunity, such as in plasma and memory B cells, remains to be further explored. The reduction in plasma cell numbers and antibody titers in the *Bap1*$^{fl/fl}$ Cγ1-Cre model is particularly notable, and our study did not quantify antigen specific plasma cells or assess the efficiency of *Bap1*-deletion within the plasma cell compartment. The roles and molecular mechanisms of BAP1 in plasma cell differentiation should be addressed in future work.

Loss of BAP1 in activated B cells in the *Bap1*$^{fl/fl}$ Cγ1-Cre mouse model resulted in a severe defect in antibody production, and we noted the more profound reduction in IgG as compared to IgM isotypes. We hypothesized that this may reflect the enhanced Cγ1-Cre activity in the B cells committed to undergo class switching to IgG1, or a direct role for BAP1 in the antibody class switching reaction. Indeed, epigenetic mechanisms are important across many checkpoints in antibody class switching, such as regulation of S-region accessibility and transcription, AID expression and targeting to chromatin, and in the DNA break-repair step[335]. For instance, BAP1 was previously shown to facilitate DNA repair through the homologous recombination (HR) pathway in DT40 B cell lymphoma[208]. However, we found normal class switching of *Bap1*$^{fl/fl}$ Cγ1-Cre B cells when normalized to the significant reduction in B cell proliferation. This result is consistent with the major roles of the other repair pathways in antibody class switching, namely non-homologous end joining (NHEJ) and microhomology-mediated end joining (MMEJ)[336], and also rules out non-redundant roles of BAP1 in steps upstream from DNA damage in class switching. Nonetheless, BAP1 functions in the class switching reaction may be redundant with other

chromatin associated DUBs[169], as for example the chromatin associated DUB USP22 was recently shown to promote DNA repair in antibody class switching[337]. Besides, the potential involvement of non-histone substrates of BAP1 in antibody class switching can also be further explored, as the DUB USP7 was recently reported to promotes IgA and inhibits IgG switching by deubiquitinating and stabilizing RUNX3[338].

Our current study focusses on the role of BAP1 specifically in mature activated B cells, with the *Bap1*$^{fl/fl}$ Cγ1-Cre model allowing the selective analyses of its B cell-intrinsic functions in the induction of humoral immune response. However, beyond this experimental model, it is important to consider that BAP1 activities in other cell types may also contribute to the regulation of antibody mediated immunity *in vivo*. BAP1 is known to play an important cell-intrinsic role in T cell development in the thymus, as well as in the peripheral T cell expansion under homeostatic conditions and in response to antigenic stimulation[222]. Furthermore, BAP1 activities in mesenchymal stromal cells (MSCs) are essential for normal B cell development in the bone marrow[339]. Therefore, in addition to the cell intrinsic roles of BAP1 in B cells, elucidated in our current work, BAP1 functions in T cells and stromal compartments need to be considered when assessing its systemic roles in the regulation of humoral immunity *in vivo*, as for example in carriers of germline *BAP1* mutations.

Our study establishes the critical role of BAP1 as a transcriptional and epigenetic regulator in the GC reaction, which is a common site of cell transformation that gives rise to B cell lymphomas[104, 340]. While BAP1 is a highly important tumor suppressor[186], as already discussed, lymphomas are not among the major cancer types associated with germline or acquired *Bap1* mutations, and our

current study didn't directly address the role of BAP1 in lymphomagenesis. Nevertheless, cases of non-Hodgkin lymphoma have been reported in carriers of germline *Bap1* mutations[320], and lymphomas with other genetic aberrations were shown to acquire *Bap1* gene silencing via epigenetic mechanisms[321]. Therefore, we anticipate that future work in the $Bap1^{fl/fl}$ Cγ1-Cre and other relevant murine models may further explore BAP1 functions as a tumor suppressor in B cell lymphoma.

In summary, our study provides novel insights into the epigenetic regulation of B lymphocyte biology and humoral immunity by BAP1, the major DUB for histone H2AK119ub, with potential implications for host responses to infections and vaccinations, and the mechanisms of B cell carcinogenesis.

5.3 Role of MYSM1 and its DUB activity in hematopoiesis

Beside investigating the role of BAP1 in B cell development and humoral immunity, we also explored the function of another histone H2A deubiquitinase (DUB), MYSM1, in hematopoiesis. In this study, we for the first time establish and characterize a mouse strain expressing a catalytically inactive $MYSM1^{D660N}$ protein. We demonstrate a profound similarity in the developmental, hematopoietic, and immune phenotypes of $Mysm1^{\Delta}$ and $Mysm1^{DN}$ mice, indicating the critical role of MYSM1 DUB catalytic activity in hematopoiesis and other aspects of mammalian physiology. While the depletion of hematopoietic cells and HSPC failure in functional assays were highly consistent between the $Mysm1^{-/-}$ and $Mysm1^{DN/DN}$ strains throughout this study, the $Mysm1^{DN/DN}$ strain showed high embryonic lethality, with only ~ 4% of $Mysm1^{DN/DN}$ offspring from an intercross of heterozygous parents, as compared to 10% for

the *Mysm1*$^{-/-}$ strain reported in previous studies[180]. Although these figures are not directly comparable between studies, it is interesting to note that increased embryonic lethality has been reported in other strains expressing catalytically inactive proteins relative to the corresponding knockout strains[341, 342]. This possibly indicates dominant-negative activity of the MYSM1^{D660N} catalytically inactive protein, such as blocking the access of compensatory proteins to its substrate.

While the current study provides an in-depth analysis of the role of MYSM1 DUB catalytic activity in hematopoiesis and leukocyte development, the International Mouse Phenotyping consortium[251, 343] and previously published studies report complex phenotypes in many other physiological systems in *Mysm1*$^{-/-}$ mice, including alterations in skeletal, skin, and adipose physiology[241, 300, 344, 345]. In future work, a broader comparison of *Mysm1*$^{-/-}$ and *Mysm1*$^{DN/DN}$ mouse strains will allow us to further explore the role of MYSM1 catalytic activity in these other physiological systems. Recent studies also established MYSM1 as a negative regulator of inflammatory responses to microbial stimuli in macrophages[235, 236, 305]. In these studies MYSM1 was shown to deubiquitinate TRAFs, RIP2, and STING proteins in the signal transduction cascades of innate immunity[235, 236, 305]. The *Mysm1*$^{DN/DN}$ mouse strain developed in our current work may be used to further validate the role of MYSM1 catalytic activity in the regulation of innate immune and inflammatory responses in vivo.

Although no molecular analyses for the mechanisms of hematopoietic failure were conducted in the *Mysm1*$^{DN/DN}$ and *Mysm1*$^{DN/\Delta}$ mouse models in the current study, the very high concordance of their phenotypes to those of the *Mysm1*$^{-/-}$ and *Mysm1*$^{\Delta/\Delta}$ mouse strains suggests that similar

molecular mechanisms are at play. Previously in the *Mysm1*$^{-/-}$ mice the hematopoietic failure was shown to be driven by the activation of p53 and the induction of its pro-apoptotic transcriptional programs[238, 239, 240]. Consistently, our current data showed some increase in cell death in *Mysm1*$^{DN/DN}$ relative to control *Mysm1*$^{+/+}$ hematopoietic and immune cells, supporting that similar mechanisms may also mediate the hematopoietic failure in *Mysm1*$^{DN/DN}$ mice.

With the validation of the role of MYSM1 DUB catalytic activity in hematopoiesis, it will be important to identify the full range of protein targets and substrates of MYSM1, for example through proteomics approaches[346, 347, 348]. While histone H2AK119ub is a highly abundant and well characterized MYSM1 substrate[169, 224], MYSM1 can also cleave K63, M1, K6, and K27 polyubiquitin in vitro[236] and regulates K63-polyubiquitination of TRAFs, RIP2, and STING proteins in macrophages[235, 236, 305]. Given the diverse and complex roles of ubiquitination in regulating chromatin accessibility, gene expression, genomic stability, signal transduction, protein localization and many other cellular processes[135, 169, 349], such studies may lead to the discovery of further novel MYSM1 substrates beyond histone H2AK119ub and advance the understanding of its functions and mechanisms of action.

Moreover, in the current work, we further characterize the role of MYSM1 in dendritic cells (DCs), and, for the first time, establish that MYSM1 is dispensable for DC maintenance and for DC antigen presenting capacity in response to microbial stimulation, with the essential role of MYSM1 being restricted to the early stages in the DC lineage specification. Our findings therefore indicate that MYSM1 acts specifically in HSPCs to sustain normal DC lineage development and to program

DCs for normal responses to microbial stimulation. Furthermore, we demonstrate the critical role of the DUB catalytic activity of MYSM1 for these functions.

These results resemble previous findings from the lymphoid cell lineage, where a severe arrest in lymphocyte development and the depletion of B and T cells is seen with systemic or pan-hematopoietic loss of *Mysm1*[180, 232], however the loss of MYSM1 at later stages in B and T cell development has only minor effects on lymphocyte numbers or their responses to stimulation[261, 350]. Consistent with the strong phenotypic similarities between *Mysm1*$^{-/-}$ mice with full loss of MYSM1 expression and *Mysm1*$^{DN/DN}$ mice with the loss of DUB catalytic activity, as discussed above, the loss of MYSM1 DUB catalytic activity showed the same impact on DC lineage development as the full loss of MYSM1 expression throughout all the DC experimental systems. This further supports the primary and indispensable function of MYSM1 as a DUB, likely for histone H2AK119ub[237] and possibly also for other substrates, in the DC lineage specification.

Our study further demonstrates that MYSM1 loss-of-function in early hematopoietic progenitors results in the production of functionally altered DCs, with significant changes in the expression of housekeeping transcriptional programs, including those engaged in cell cycle progression, ribosome biogenesis, metabolic and stress response regulation. Furthermore, MYSM1 loss-of-function in hematopoietic progenitors also alters the downstream responses of BMDCs to microbial stimulation, with altered expression of genes encoding cytokines, chemokines, pathogen sensing receptors, and antigen presentation machinery, as well as significant changes in cytokine production. In particular, we noticed enhanced expression IL-12 and reduced expression of IL-10 indicated by CPM counts. Such changes were confirmed by consistent alterations of IL-12 and IL-

10 protein levels[351], and may indicate an enhanced functional capacity of the BMDCs derived from *Mysm1*-deficient hematopoietic progenitors. However, studies in co-cultures with OT-II CD4 T cells demonstrated no major significant differences in the BMDC capacity to induce T cell activation and proliferation ex vivo. Nevertheless, it is important to note that such co-cultures may not fully model DC activities as antigen presenting cells in vivo, where the levels of antigen and microbial stimulation may be more limited, and complex cell migration dynamics are required to put the antigen presenting DCs and cognate T cells into contact within a polyclonal T cell repertoire. Therefore, our current study doesn't rule out that MYSM1 activities in hematopoietic progenitors may alter the capacity of the downstream DCs for antigen presentation and T cell activation in certain settings, beyond the ex vivo co-culture assays, and such effects will need to be explored in future work using in vivo models. Additionally, it will be important to assess the effects of MYSM1 on the DC capacity for antigen presentation and cross-presentation to CD8 T cells, not assessed in our current work. Furthermore, while BMDCs derived in GM-CSF containing bone marrow cultures are a highly common model for the study of DC cell biology[352], future work will need to explore to what extent MYSM1 functions in this model are conserved in DCs derived under Flt3-L culture conditions[353, 354] and also in primary DCs in vivo in murine tissues.

In previous studies, we illustrated the role of MYSM1 in maintaining the expression of genes encoding ribosomal proteins (*RP*-genes) in HSCs, yet observed no significant elevation of H2AK119ub levels at the MYSM1-binding sites within these *RP*-gene promoters[244]. With the *Mysm1*^{DN} mouse model established, it would be intriguing to analyze the expression levels of *RP*-genes in HSCs where MYSM1 exists in the catalytically inactive form. Moreover, MYSM1 was previously shown to interact with cMYC, a crucial transcriptional regulator for the genes encoding

the ribosomal and translational machinery, in B1a lymphocytes[230]. We recently established that the loss of MYSM1 in mouse models of cMYC-driven B cell lymphoma can protect against disease onset and progression[355]. At the cellular and molecular levels, the protective effects were attributed to the role of MYSM1 in the cMYC-dependent induction of the *RP*-genes, with MYSM1-loss resulting in reduced *RP*-gene transcript levels, reduced cellular protein synthesis rates, and the activation of p53 tumour suppressor[355]. Overall, these studies may suggest MYSM1 as a drug-target for cMYC driven hematologic malignancies; and the *Mysm1*^{DN} mouse strain described in our current work will allow to test whether the loss of MYSM1 DUB catalytic function can offer similar therapeutic benefits. This can serve as a proof-of-concept for the development of pharmacological MYSM1 inhibitors and for the assessment of their activities in experimental models of cMYC-driven hematologic malignancies. Furthermore, given the critical role of DCs as mediators of antitumor immunity and immunotherapy[356], our current work indicates the importance of further exploring how MYSM1 loss or the inhibition of its DUB catalytic activity will impact DC functions in the tumour microenvironment and the implications of such effects for anticancer immunity.

In summary, our study establishes the primary and indispensable function of MYSM1 as a DUB in vivo in the normal progression of mammalian development, hematopoiesis, and immune cell production. This work also provides a mouse model for further analyses of the roles of MYSM1 DUB catalytic functions in vivo in many other aspects of mammalian physiology.

5.4 Summary and final conclusions

In this study, we explored the roles of two deubiquitinases that can target histone H2AK119ub, BAP1 and MYSM1, in hematopoietic cell development and immune response. Overall, we

propose that BAP1 acts as an essential and cell-intrinsic regulator in B cell development and in antibody mediated immune response. We conclude that BAP1, although not functioning as an indispensable contributor to class switch recombination (CSR), directly regulates many transcriptional programs essential for B cell development, B cell activation, and the induction of humoral immune response. We claim that such regulatory function of BAP1 is exerted, at least partially, through its deubiquitinase (DUB) activity targeting histone H2AK119ub. Moreover, our study revealed a striking similarity between the developmental, hematopoietic, and immune phenotypes observed with the loss of MYSM1 DUB catalytic activity and those resulting from the complete loss of the MYSM1 protein. We thereby propose a critical and cell-intrinsic role of the DUB catalytic activity of MYSM1 in the regulation of hematopoiesis, including the development of lymphocytes and dendritic cells. Overall, our research enhances the understanding of the vital roles that BAP1 and MYSM1 play in hematopoiesis, leukocyte development, immune responses, and various other aspects of mammalian physiology.

Chapter 6 Uncategorized References

1. Alberts, B. *et al.* Renewal by multipotent stem cells: Blood cell formation. *Molecular Biology of the Cell. 4th edition*. Garland Science, 2002.

2. Orkin, S.H. & Zon, L.I. Hematopoiesis: an evolving paradigm for stem cell biology. *Cell* **132**, 631-644 (2008).

3. Dzierzak, E. & Speck, N.A. Of lineage and legacy–the development of mammalian hematopoietic stem cells. *Nature immunology* **9**, 129 (2008).

4. Mikkola, H.K. & Orkin, S.H.J.D. The journey of developing hematopoietic stem cells. **133**, 3733-3744 (2006).

5. Adams, G.B. & Scadden, D.T. The hematopoietic stem cell in its place. *Nature immunology* **7**, 333-337 (2006).

6. Ceredig, R., Rolink, A.G. & Brown, G. Models of haematopoiesis: seeing the wood for the trees. *J Nature Reviews Immunology* **9**, 293-300 (2009).

7. Kondo, M. Lymphoid and myeloid lineage commitment in multipotent hematopoietic progenitors. *Immunological reviews* **238**, 37-46 (2010).

8. King, K.Y. & Goodell, M.A. Inflammatory modulation of HSCs: viewing the HSC as a foundation for the immune response. *Nature Reviews Immunology* **11**, 685-692 (2011).

9. Cheng, H., Zheng, Z. & Cheng, T. New paradigms on hematopoietic stem cell differentiation. *Protein & cell* **11**, 34-44 (2020).

10. Janeway Jr, C., Travers, P. & Walport, M. *Immunobiology. 8th Edition*. Garland Science: New York, 2012.

11. Harly, C., Cam, M., Kaye, J. & Bhandoola, A. Development and differentiation of early innate lymphoid progenitors. *Journal of Experimental Medicine* **215**, 249-262 (2018).

12. Ishikawa, F. *et al.* The developmental program of human dendritic cells is operated independently of conventional myeloid and lymphoid pathways. *Blood, The Journal of the American Society of Hematology* **110**, 3591-3660 (2007).

13. Pietras, E.M. *et al.* Functionally distinct subsets of lineage-biased multipotent progenitors control blood production in normal and regenerative conditions. *Cell stem cell* **17**, 35-46 (2015).

14. Baldridge, M.T., King, K.Y., Boles, N.C., Weksberg, D.C. & Goodell, M.A. Quiescent haematopoietic stem cells are activated by IFN-γ in response to chronic infection. *Nature* **465**, 793-797 (2010).

15. Zhong, J.F. *et al.* Gene expression profile of murine long-term reconstituting vs. short-term reconstituting hematopoietic stem cells. *Proceedings of the National Academy of Sciences* **102**, 2448-2453 (2005).

16. Wilson, A. *et al.* Hematopoietic stem cells reversibly switch from dormancy to self-renewal during homeostasis and repair. *Cell* **135**, 1118-1129 (2008).

17. Rodriguez-Fraticelli, A.E. *et al.* Clonal analysis of lineage fate in native haematopoiesis. *Nature* **553**, 212-216 (2018).

18. Morrison, S.J. & Scadden, D.T. The bone marrow niche for haematopoietic stem cells. *Nature* **505**, 327-334 (2014).

19. Suda, T., Takubo, K. & Semenza, G.L. Metabolic regulation of hematopoietic stem cells in the hypoxic niche. *Cell stem cell* **9**, 298-310 (2011).

20. Domingues, M.J., Cao, H., Heazlewood, S.Y., Cao, B. & Nilsson, S.K. Niche extracellular matrix components and their influence on HSC. *Journal of cellular biochemistry* **118**, 1984-1993 (2017).

21. Clapes, T., Lefkopoulos, S. & Trompouki, E. Stress and non-stress roles of inflammatory signals during HSC emergence and maintenance. *Frontiers in immunology* **7**, 487 (2016).

22. Pellin, D. *et al.* A comprehensive single cell transcriptional landscape of human hematopoietic progenitors. *Nature communications* **10**, 2395 (2019).

23. Aristizábal, B. & González, Á. Innate immune system. *Autoimmunity: From Bench to Bedside [Internet]*. El Rosario University Press, 2013.

24. Alberts, B. *et al.* Lymphocytes and the cellular basis of adaptive immunity. *Molecular Biology of the Cell. 4th edition*. Garland Science, 2002.

25. Forthal, D.N. Functions of antibodies. *Microbiology spectrum* **2**, 10.1128/microbiolspec. aid-0019-2014 (2014).

26. LeBien, T.W. & Tedder, T.F. B lymphocytes: how they develop and function. *Blood, The Journal of the American Society of Hematology* **112**, 1570-1580 (2008).

27. Amezcua Vesely, M.C., Bermejo, D.A., Montes, C.L., Acosta-Rodríguez, E.V. & Gruppi, A. B-cell response during protozoan parasite infections. *Journal of parasitology research* **2012** (2012).

28. Borhis, G. & Richard, Y. Subversion of the B-cell compartment during parasitic, bacterial, and viral infections. *BMC immunology* **16**, 1-10 (2015).

29. Awasthi, A. & Kumar, H. T cell subtypes and its therapeutic potential in autoimmune diseases and cancer. *International Reviews of Immunology* **38**, 181-182 (2019).

30. Zhu, J. & Paul, W.E. CD4 T cells: fates, functions, and faults. *Blood, The Journal of the American Society of Hematology* **112**, 1557-1569 (2008).

31. Josefowicz, S.Z., Lu, L.-F. & Rudensky, A.Y. Regulatory T cells: mechanisms of differentiation and function. *Annual review of immunology* **30**, 531-564 (2012).

32. Mahnke, Y.D., Brodie, T.M., Sallusto, F., Roederer, M. & Lugli, E. The who's who of T-cell differentiation: human memory T-cell subsets. *European journal of immunology* **43**, 2797-2809 (2013).

33. Kurosaki, T., Shinohara, H. & Baba, Y. B cell signaling and fate decision. *Annual review of immunology* **28**, 21-55 (2009).

34. Ceredig, R. & Rolink, T. A positive look at double-negative thymocytes. *Nature Reviews Immunology* **2**, 888-897 (2002).

35. De Villartay, J.-P., Fischer, A. & Durandy, A. The mechanisms of immune diversification and their disorders. *Nature Reviews Immunology* **3**, 962-972 (2003).

36. Vettermann, C. & Schlissel, M.S. Allelic exclusion of immunoglobulin genes: models and mechanisms. *Immunological reviews* **237**, 22-42 (2010).

37. Schroeder Jr, H.W. & Cavacini, L. Structure and function of immunoglobulins. *Journal of allergy and clinical immunology* **125**, S41-S52 (2010).

38. Ceredig, R. & Rolink, A.G. The key role of IL-7 in lymphopoiesis. Seminars in immunology; 2012: Elsevier; 2012. p. 159-164.

39. Gaspar, H.B. Tearing RAGs apart. *Blood, The Journal of the American Society of Hematology* **123**, 156-157 (2014).

40. Coffman, R.L. Surface antigen expression and immunoglobulin gene rearrangement during mouse pre-B cell development. *Immunological reviews* **69**, 5-23 (1982).

41. Melchers, F. *et al.* The surrogate light chain in B-cell development. *Immunology today* **14**, 60-68 (1993).

42. Tze, L.E. *et al.* Basal immunoglobulin signaling actively maintains developmental stage in immature B cells. *PLoS biology* **3**, e82 (2005).

43. Sandel, P.C. & Monroe, J.G. Negative selection of immature B cells by receptor editing or deletion is determined by site of antigen encounter. *Immunity* **10**, 289-299 (1999).

44. Chen, J.W. *et al.* Positive and negative selection shape the human naive B cell repertoire. *The Journal of Clinical Investigation* **132** (2022).

45. Vale, A.M. & Schroeder Jr, H.W. Clinical consequences of defects in B-cell development. *Journal of Allergy and Clinical Immunology* **125**, 778-787 (2010).

46. Geisberger, R., Lamers, M. & Achatz, G. The riddle of the dual expression of IgM and IgD. *Immunology* **118**, 429-437 (2006).

47. Chung, J.B., Silverman, M. & Monroe, J.G. Transitional B cells: step by step towards immune competence. *Trends in immunology* **24**, 342-348 (2003).

48. Vossenkämper, A. & Spencer, J. Transitional B cells: how well are the checkpoints for specificity understood? *Archivum immunologiae et therapiae experimentalis* **59**, 379-384 (2011).

49. Carsetti, R., Köhler, G. & Lamers, M.C. Transitional B cells are the target of negative selection in the B cell compartment. *The Journal of experimental medicine* **181**, 2129-2140 (1995).

50. Flaishon, L. *et al.* Autocrine secretion of interferon γ negatively regulates homing of immature B cells. *The Journal of experimental medicine* **192**, 1381-1388 (2000).

51. Thomas, M.D., Srivastava, B. & Allman, D. Regulation of peripheral B cell maturation. *Cellular immunology* **239**, 92-102 (2006).

52. Oliver, A.M., Martin, F. & Kearney, J.F. IgMhighCD21high lymphocytes enriched in the splenic marginal zone generate effector cells more rapidly than the bulk of follicular B cells. *The Journal of Immunology* **162**, 7198-7207 (1999).

53. Martin, F. & Kearney, J.F. Marginal-zone B cells. *Nature Reviews Immunology* **2**, 323-335 (2002).

54. Montecino-Rodriguez, E. & Dorshkind, K. B-1 B cell development in the fetus and adult. *Immunity* **36**, 13-21 (2012).

55. Berland, R. & Wortis, H.H. Origins and functions of B-1 cells with notes on the role of CD5. *Annual review of immunology* **20**, 253-300 (2002).

56. Martin, F. & Kearney, J.F. B1 cells: similarities and differences with other B cell subsets. *Current opinion in immunology* **13**, 195-201 (2001).

57. Haas, K.M., Poe, J.C., Steeber, D.A. & Tedder, T.F. B-1a and B-1b cells exhibit distinct developmental requirements and have unique functional roles in innate and adaptive immunity to S. pneumoniae. *Immunity* **23**, 7-18 (2005).

58. Hardy, R.R. B-1 B cell development. *The Journal of Immunology* **177**, 2749-2754 (2006).

59. Delker, R.K., Fugmann, S.D. & Papavasiliou, F.N. A coming-of-age story: activation-induced cytidine deaminase turns 10. *Nature immunology* **10**, 1147-1153 (2009).

60. Feng, Y., Seija, N., Di Noia, J.M. & Martin, A. AID in antibody diversification: there and back again. *Trends in immunology* **41**, 586-600 (2020).

61. Di Noia, J.M. & Neuberger, M.S. Molecular mechanisms of antibody somatic hypermutation. *Annu. Rev. Biochem.* **76**, 1-22 (2007).

62. Shekhar, S. & Yang, X. The darker side of follicular helper T cells: from autoimmunity to immunodeficiency. *Cellular & molecular immunology* **9**, 380-385 (2012).

63. Gatto, D. & Brink, R. The germinal center reaction. *Journal of Allergy and Clinical Immunology* **126**, 898-907 (2010).

64. Colineau, L. *et al.* HIV-infected spleens present altered follicular helper T cell (Tfh) subsets and skewed B cell maturation. *PloS one* **10**, e0140978 (2015).

65. Tangye, S.G., Ma, C.S., Brink, R. & Deenick, E.K. The good, the bad and the ugly—T FH cells in human health and disease. *Nature Reviews Immunology* **13**, 412-426 (2013).

66. Allen, C.D. *et al.* Germinal center dark and light zone organization is mediated by CXCR4 and CXCR5. *Nature immunology* **5**, 943-952 (2004).

67. Roco, J.A. *et al.* Class-switch recombination occurs infrequently in germinal centers. *Immunity* **51**, 337-350. e337 (2019).

68. Stavnezer, J. & Schrader, C.E. IgH chain class switch recombination: mechanism and regulation. *The Journal of Immunology* **193**, 5370-5378 (2014).

69. Lieber, M.R. The mechanism of double-strand DNA break repair by the nonhomologous DNA end-joining pathway. *Annual review of biochemistry* **79**, 181-211 (2010).

70. Deriano, L. & Roth, D.B. Modernizing the nonhomologous end-joining repertoire: alternative and classical NHEJ share the stage. *Annual review of genetics* **47**, 433-455 (2013).

71. Kenter, A.L. *et al.* Three-dimensional architecture of the IgH locus facilitates class switch recombination. *Annals of the New York Academy of Sciences* **1267**, 86-94 (2012).

72. Wuerffel, R. *et al.* SS synapsis during class switch recombination is promoted by distantly located transcriptional elements and activation-induced deaminase. *Immunity* **27**, 711-722 (2007).

73. Guo, C. *et al.* Two forms of loops generate the chromatin conformation of the immunoglobulin heavy-chain gene locus. *Cell* **147**, 332-343 (2011).

74. Macri, C., Pang, E.S., Patton, T. & O'Keeffe, M. Dendritic cell subsets. Seminars in cell & developmental biology; 2018: Elsevier; 2018. p. 11-21.

75. Cabeza-Cabrerizo, M., Cardoso, A., Minutti, C.M., Pereira da Costa, M. & Reis e Sousa, C. Dendritic cells revisited. *Annual review of immunology* **39**, 131-166 (2021).

76. Steinman, R.M. & Cohn, Z.A. Identification of a novel cell type in peripheral lymphoid organs of mice: I. Morphology, quantitation, tissue distribution. *The Journal of experimental medicine* **137**, 1142-1162 (1973).

77. Collin, M. & Bigley, V. Human dendritic cell subsets: an update. *Immunology* **154**, 3-20 (2018).

78. Balan, S., Saxena, M. & Bhardwaj, N. Dendritic cell subsets and locations. *International review of cell and molecular biology* **348**, 1-68 (2019).

79. Sathe, P. & Wu, L. The network of cytokines, receptors and transcription factors governing the development of dendritic cell subsets. *Protein & cell* **2**, 620-630 (2011).

80. Martín, P. *et al.* Concept of lymphoid versus myeloid dendritic cell lineages revisited: both CD8α− and CD8α+ dendritic cells are generated from CD4lowlymphoid-committed precursors. *Blood, The Journal of the American Society of Hematology* **96**, 2511-2519 (2000).

81. Liu, K. & Nussenzweig, M.C. Origin and development of dendritic cells. *Immunological reviews* **234**, 45-54 (2010).

82. Chen, B., Zhu, L., Yang, S. & Su, W. Unraveling the heterogeneity and ontogeny of dendritic cells using single-cell RNA sequencing. *Frontiers in Immunology* **12**, 711329 (2021).

83. Brown, C.C. *et al.* Transcriptional basis of mouse and human dendritic cell heterogeneity. *Cell* **179**, 846-863. e824 (2019).

84. Antoniani, C., Romano, O. & Miccio, A. Concise review: epigenetic regulation of hematopoiesis: biological insights and therapeutic applications. *Stem cells translational medicine* **6**, 2106-2114 (2017).

85. Matthias, P. & Rolink, A.G. Transcriptional networks in developing and mature B cells. *Nature Reviews Immunology* **5**, 497 (2005).

86. Fischer, U. *et al.* Cell fate decisions: the role of transcription factors in early B-cell development and leukemia. *Blood cancer discovery* **1**, 224-233 (2020).

87. Urbánek, P., Wang, Z.-Q., Fetka, I., Wagner, E.F. & Busslinger, M. Complete block of early B cell differentiation and altered patterning of the posterior midbrain in mice lacking Pax5BSAP. *Cell* **79**, 901-912 (1994).

88. Lin, H. & Grosschedl, R. Failure of B-cell differentiation in mice lacking the transcription factor EBF. *Nature* **376**, 263-267 (1995).

89. Bain, G. *et al.* E2A proteins are required for proper B cell development and initiation of immunoglobulin gene rearrangements. *Cell* **79**, 885-892 (1994).

90. Cobaleda, C., Schebesta, A., Delogu, A. & Busslinger, M. Pax5: the guardian of B cell identity and function. *Nature immunology* **8**, 463-470 (2007).

91. Hagman, J. & Lukin, K. Transcription factors drive B cell development. *Current opinion in immunology* **18**, 127-134 (2006).

92. Miyai, T. *et al.* Three-step transcriptional priming that drives the commitment of multipotent progenitors toward B cells. *Genes & development* **32**, 112-126 (2018).

93. Kishi, H. *et al.* Lineage-specific regulation of the murine RAG-2 promoter: GATA-3 in T cells and Pax-5 in B cells. *Blood, The Journal of the American Society of Hematology* **95**, 3845-3852 (2000).

94. Miyazaki, K. & Miyazaki, M. The interplay between chromatin architecture and lineage-specific transcription factors and the regulation of rag gene expression. *Frontiers in immunology* **12**, 659761 (2021).

95. Lin, Y.C. *et al.* A global network of transcription factors, involving E2A, EBF1 and Foxo1, that orchestrates B cell fate. *Nature immunology* **11**, 635-643 (2010).

96. Amin, R.H. & Schlissel, M.S. Foxo1 directly regulates the transcription of recombination-activating genes during B cell development. *Nature immunology* **9**, 613-622 (2008).

97. Busslinger, M. Transcriptional control of early B cell development. *Annu. Rev. Immunol.* **22**, 55-79 (2004).

98. Wang, H., Morse, H.C. & Bolland, S. Transcriptional control of mature B cell fates. *Trends in Immunology* **41**, 601-613 (2020).

99. Song, S. & Matthias, P.D. The transcriptional regulation of germinal center formation. *Frontiers in immunology* **9**, 411463 (2018).

100. Basso, K. & Dalla-Favera, R. Roles of BCL6 in normal and transformed germinal center B cells. *Immunological reviews* **247**, 172-183 (2012).

101. Ochiai, K. *et al.* Transcriptional regulation of germinal center B and plasma cell fates by dynamical control of IRF4. *Immunity* **38**, 918-929 (2013).

102. Lee, C.H. *et al.* Regulation of the germinal center gene program by interferon (IFN) regulatory factor 8/IFN consensus sequence-binding protein. *The Journal of experimental medicine* **203**, 63-72 (2006).

103. Calado, D.P. *et al.* The cell-cycle regulator c-Myc is essential for the formation and maintenance of germinal centers. *Nature immunology* **13**, 1092-1100 (2012).

104. Basso, K. & Dalla-Favera, R. Germinal centres and B cell lymphomagenesis. *Nature Reviews Immunology* **15**, 172-184 (2015).

105. Chen, S. *et al.* Id3 orchestrates germinal center B cell development. *Molecular and cellular biology* **36**, 2543-2552 (2016).

106. Trabucco, S.E., Gerstein, R.M. & Zhang, H. YY1 regulates the germinal center reaction by inhibiting apoptosis. *The Journal of Immunology* **197**, 1699-1707 (2016).

107. Dominguez-Sola, D. *et al.* The FOXO1 transcription factor instructs the germinal center dark zone program. *Immunity* **43**, 1064-1074 (2015).

108. Shaffer, A. *et al.* XBP1, downstream of Blimp-1, expands the secretory apparatus and other organelles, and increases protein synthesis in plasma cell differentiation. *Immunity* **21**, 81-93 (2004).

109. Chiu, Y.-K. *et al.* Transcription factor ABF-1 suppresses plasma cell differentiation but facilitates memory B cell formation. *The Journal of Immunology* **193**, 2207-2217 (2014).

110. Meissner, A. Epigenetic modifications in pluripotent and differentiated cells. *Nature biotechnology* **28**, 1079 (2010).

111. Bernstein, B.E., Meissner, A. & Lander, E.S. The mammalian epigenome. *Cell* **128**, 669-681 (2007).

112. Wu, H. *et al.* Epigenetic regulation in B-cell maturation and its dysregulation in autoimmunity. *Cellular & Molecular Immunology* **15**, 676-684 (2018).

113. Carlberg, C. & Molnár, F. *Human epigenomics*. Springer, 2018.

114. Xu, Z., Zan, H., Pone, E.J., Mai, T. & Casali, P. Immunoglobulin class-switch DNA recombination: induction, targeting and beyond. *Nature Reviews Immunology* **12**, 517-531 (2012).

115. White, C.A. *et al.* Histone deacetylase inhibitors upregulate B cell microRNAs that silence AID and Blimp-1 expression for epigenetic modulation of antibody and autoantibody responses. *The Journal of Immunology* **193**, 5933-5950 (2014).

116. Laouar, Y., Welte, T., Fu, X.-Y. & Flavell, R.A. STAT3 is required for Flt3L-dependent dendritic cell differentiation. *Immunity* **19**, 903-912 (2003).

117. Carotta, S. *et al.* The transcription factor PU. 1 controls dendritic cell development and Flt3 cytokine receptor expression in a dose-dependent manner. *Immunity* **32**, 628-641 (2010).

118. Hambleton, S. *et al.* IRF8 mutations and human dendritic-cell immunodeficiency. *New England Journal of Medicine* **365**, 127-138 (2011).

119. Villar, J. & Segura, E. Recent advances towards deciphering human dendritic cell development. *Molecular immunology* **122**, 109-115 (2020).

120. Lee, J. *et al.* Lineage specification of human dendritic cells is marked by IRF8 expression in hematopoietic stem cells and multipotent progenitors. *Nature immunology* **18**, 877-888 (2017).

121. Ma, W. *et al.* Single cell RNA-Seq reveals pre-cDCs fate determined by transcription factor combinatorial dose. *BMC molecular and cell biology* **20**, 1-14 (2019).

122. Edelson, B.T. *et al.* Peripheral CD103+ dendritic cells form a unified subset developmentally related to CD8α+ conventional dendritic cells. *Journal of Experimental Medicine* **207**, 823-836 (2010).

123. Poulin, L.F. *et al.* DNGR-1 is a specific and universal marker of mouse and human Batf3-dependent dendritic cells in lymphoid and nonlymphoid tissues. *Blood, the Journal of the American Society of Hematology* **119**, 6052-6062 (2012).

124. Wu, L. *et al.* RelB is essential for the development of myeloid-related CD8α− dendritic cells but not of lymphoid-related CD8α+ dendritic cells. *Immunity* **9**, 839-847 (1998).

125. Hacker, C. *et al.* Transcriptional profiling identifies Id2 function in dendritic cell development. *Nature immunology* **4**, 380-386 (2003).

126. Allman, D. *et al.* Ikaros is required for plasmacytoid dendritic cell differentiation. *Blood* **108**, 4025-4034 (2006).

127. Cytlak, U. *et al.* Ikaros family zinc finger 1 regulates dendritic cell development and function in humans. *Nature communications* **9**, 1239 (2018).

128. Mastio, J. *et al.* Ikaros cooperates with Notch activation and antagonizes TGFβ signaling to promote pDC development. *PLoS Genetics* **14**, e1007485 (2018).

129. Schotte, R., Nagasawa, M., Weijer, K., Spits, H. & Blom, B. The ETS transcription factor Spi-B is required for human plasmacytoid dendritic cell development. *The Journal of experimental medicine* **200**, 1503-1509 (2004).

130. Reizis, B. Regulation of plasmacytoid dendritic cell development. *Current opinion in immunology* **22**, 206-211 (2010).

131. Sasaki, I. *et al.* Spi-B is critical for plasmacytoid dendritic cell function and development. *Blood, The Journal of the American Society of Hematology* **120**, 4733-4743 (2012).

132. Cisse, B. *et al.* Transcription factor E2-2 is an essential and specific regulator of plasmacytoid dendritic cell development. *Cell* **135**, 37-48 (2008).

133. Ghosh, H.S., Cisse, B., Bunin, A., Lewis, K.L. & Reizis, B. Continuous expression of the transcription factor e2-2 maintains the cell fate of mature plasmacytoid dendritic cells. *Immunity* **33**, 905-916 (2010).

134. Bhat, J. & Kabelitz, D. An introduction to immunology and epigenetics. *Epigenetics of the Immune System*. Elsevier, 2020, pp 1-23.

135. Barbour, H., Daou, S., Hendzel, M. & Affar, E.B. Polycomb group-mediated histone H2A monoubiquitination in epigenome regulation and nuclear processes. *Nature communications* **11**, 5947 (2020).

136. Yun, M., Wu, J., Workman, J.L. & Li, B. Readers of histone modifications. *Cell research* **21**, 564 (2011).

137. Bártová, E., Krejčí, J., Harničarová, A., Galiová, G. & Kozubek, S. Histone modifications and nuclear architecture: a review. *Journal of Histochemistry and Cytochemistry* **56**, 711-721 (2008).

138. Mariño-Ramírez, L., Kann, M.G., Shoemaker, B.A. & Landsman, D. Histone structure and nucleosome stability. *Expert review of proteomics* **2**, 719-729 (2005).

139. Gould, A. Functions of mammalian Polycomb group and trithorax group related genes. *Current opinion in genetics and development* **7**, 488-494 (1997).

140. Sha, K. & Boyer, L.A. *The chromatin signature of pluripotent cells*, vol. 1. Harvard Stem Cell Institute: Cambridge, MA, 2009.

141. Vidal, M. & Starowicz, K. Polycomb complexes PRC1 and their function in hematopoiesis. *Experimental hematology* **48**, 12-31 (2017).

142. Lee, M.G. *et al.* Demethylation of H3K27 regulates polycomb recruitment and H2A ubiquitination. *Science* **318**, 447-450 (2007).

143. Wang, H. *et al.* Role of histone H2A ubiquitination in Polycomb silencing. *Nature* **431**, 873-878 (2004).

144. Nakagawa, T. *et al.* Deubiquitylation of histone H2A activates transcriptional initiation via trans-histone cross-talk with H3K4 di-and trimethylation. *Genes and development* **22**, 37-49 (2008).

145. Kalb, R. *et al.* Histone H2A monoubiquitination promotes histone H3 methylation in Polycomb repression. *Nature structural & molecular biology* **21**, 569-571 (2014).

146. Cooper, S. *et al.* Jarid2 binds mono-ubiquitylated H2A lysine 119 to mediate crosstalk between Polycomb complexes PRC1 and PRC2. *Nature communications* **7**, 13661 (2016).

147. Lo, W.-S. *et al.* Phosphorylation of serine 10 in histone H3 is functionally linked in vitro and in vivo to Gcn5-mediated acetylation at lysine 14. *Molecular cell* **5**, 917-926 (2000).

148. Suryadinata, R., Roesley, S.N.A., Yang, G. & Šarčević, B. Mechanisms of generating polyubiquitin chains of different topology. *Cells* **3**, 674-689 (2014).

149. Sadowski, M. & Sarcevic, B. Mechanisms of mono-and poly-ubiquitination: Ubiquitination specificity depends on compatibility between the E2 catalytic core and amino acid residues proximal to the lysine. *Cell division* **5**, 1-5 (2010).

150. Weake, V.M. & Workman, J.L. Histone ubiquitination: triggering gene activity. *Molecular cell* **29**, 653-663 (2008).

151. Zhang, Y. Transcriptional regulation by histone ubiquitination and deubiquitination. *Genes and development* **17**, 2733-2740 (2003).

152. Yao, H. & Xu, J. Regulation of cancer immune checkpoint: mono-and poly-ubiquitination: tags for fate. *Regulation of Cancer Immune Checkpoints: Molecular and Cellular Mechanisms and Therapy*, 295-324 (2020).

153. Haglund, K., Di Fiore, P.P. & Dikic, I. Distinct monoubiquitin signals in receptor endocytosis. *Trends in biochemical sciences* **28**, 598-604 (2003).

154. Passmore, L.A. & Barford, D. Getting into position: the catalytic mechanisms of protein ubiquitylation. *Biochemical Journal* **379**, 513-525 (2004).

155. Ben-Saadon, R., Zaaroor, D., Ziv, T. & Ciechanover, A. The polycomb protein Ring1B generates self atypical mixed ubiquitin chains required for its in vitro histone H2A ligase activity. *Molecular cell* **24**, 701-711 (2006).

156. Goldknopf, I. *et al.* Isolation and characterization of protein A24, a" histone-like" non-histone chromosomal protein. *Journal of Biological Chemistry* **250**, 7182-7187 (1975).

157. Nickel, B.E. & Davie, J.R. Structure of polyubiquitinated histone H2A. *Biochemistry* **28**, 964-968 (1989).

158. Cao, J. & Yan, Q. Histone ubiquitination and deubiquitination in transcription, DNA damage response, and cancer. *Frontiers in oncology* **2**, 26 (2012).

159. Jason, L.J., Finn, R.M., Lindsey, G. & Ausió, J. Histone H2A ubiquitination does not preclude histone H1 binding, but it facilitates its association with the nucleosome. *Journal of Biological Chemistry* **280**, 4975-4982 (2005).

160. Zhang, Z. *et al.* Role of remodeling and spacing factor 1 in histone H2A ubiquitination-mediated gene silencing. *Proceedings of the National Academy of Sciences* **114**, E7949-E7958 (2017).

161. Huen, M.S. *et al.* RNF8 transduces the DNA-damage signal via histone ubiquitylation and checkpoint protein assembly. *Cell* **131**, 901-914 (2007).

162. Meas, R. & Mao, P. Histone ubiquitylation and its roles in transcription and DNA damage response. *DNA repair* **36**, 36-42 (2015).

163. Mattiroli, F. *et al.* RNF168 ubiquitinates K13-15 on H2A/H2AX to drive DNA damage signaling. *Cell* **150**, 1182-1195 (2012).

164. Gupta, A. *et al.* Role of 53BP1 in the regulation of DNA double-strand break repair pathway choice. *Radiation research* **181**, 1-8 (2014).

165. Densham, R.M. *et al.* Human BRCA1–BARD1 ubiquitin ligase activity counteracts chromatin barriers to DNA resection. *Nature structural & molecular biology* **23**, 647-655 (2016).

166. Bergink, S. *et al.* DNA damage triggers nucleotide excision repair-dependent monoubiquitylation of histone H2A. *Genes & development* **20**, 1343-1352 (2006).

167. Vissers, J.H., Nicassio, F., van Lohuizen, M., Di Fiore, P.P. & Citterio, E. The many faces of ubiquitinated histone H2A: insights from the DUBs. *Cell division* **3**, 1-14 (2008).

168. Jeusset, L.M. & McManus, K.J. Developing targeted therapies that exploit aberrant histone ubiquitination in cancer. *Cells* **8**, 165 (2019).

169. Belle, J.I. & Nijnik, A. H2A-DUBbing the mammalian epigenome: expanding frontiers for histone H2A deubiquitinating enzymes in cell biology and physiology. *The international journal of biochemistry and cell biology* **50**, 161-174 (2014).

170. Bajusz, I., Kovács, G. & Pirity, M.K. From flies to mice: the emerging role of non-canonical PRC1 members in mammalian development. *Epigenomes* **2**, 4 (2018).

171. Buchwald, G. *et al.* Structure and E3-ligase activity of the Ring–Ring complex of Polycomb proteins Bmi1 and Ring1b. *The EMBO journal* **25**, 2465-2474 (2006).

172. Eskeland, R. *et al.* Ring1B compacts chromatin structure and represses gene expression independent of histone ubiquitination. *Molecular cell* **38**, 452-464 (2010).

173. Leeb, M. & Wutz, A. Ring1B is crucial for the regulation of developmental control genes and PRC1 proteins but not X inactivation in embryonic cells. *The Journal of cell biology* **178**, 219-229 (2007).

174. Hanpude, P., Bhattacharya, S., Dey, A.K. & Maiti, T.K. Deubiquitinating enzymes in cellular signaling and disease regulation. *IUBMB life* **67**, 544-555 (2015).

175. Estavoyer, B. *et al.* Mechanisms orchestrating the enzymatic activity and cellular functions of deubiquitinases. *Journal of Biological Chemistry* **298** (2022).

176. Ng, H.-M., Wei, L., Lan, L. & Huen, M.S. The Lys63-deubiquitylating enzyme BRCC36 limits DNA break processing and repair. *Journal of Biological Chemistry* **291**, 16197-16207 (2016).

177. Sharma, N. *et al.* USP3 counteracts RNF168 via deubiquitinating H2A and γH2AX at lysine 13 and 15. *Cell cycle* **13**, 106-114 (2014).

178. Wang, Z. *et al.* USP51 deubiquitylates H2AK13, 15ub and regulates DNA damage response. *Genes & development* **30**, 946-959 (2016).

179. Uckelmann, M. *et al.* USP48 restrains resection by site-specific cleavage of the BRCA1 ubiquitin mark from H2A. *Nature communications* **9**, 229 (2018).

180. Nijnik, A. *et al.* The critical role of histone H2A-deubiquitinase Mysm1 in hematopoiesis and lymphocyte differentiation. *Blood* **119**, 1370-1379 (2012).

181. Lin, Y.H. *et al.* USP44 is dispensable for normal hematopoietic stem cell function, lymphocyte development, and B-cell-mediated immune response in a mouse model. *Experimental hematology* **72**, 1-8 (2019).

182. Jensen, D.E. *et al.* BAP1: a novel ubiquitin hydrolase which binds to the BRCA1 RING finger and enhances BRCA1-mediated cell growth suppression. *Oncogene* **16**, 1097-1112 (1998).

183. Abdel-Wahab, O. & Dey, A. The ASXL–BAP1 axis: new factors in myelopoiesis, cancer and epigenetics. *Leukemia* **27**, 10-15 (2013).

184. Murali, R., Wiesner, T. & Scolyer, R.A. Tumours associated with BAP1 mutations. *Pathology* **45**, 116-126 (2013).

185. Angeloni, D. Molecular analysis of deletions in human chromosome 3p21 and the role of resident cancer genes in disease. *Briefings in functional genomics and proteomics* **6**, 19-39 (2007).

186. Masclef, L. *et al.* Roles and mechanisms of BAP1 deubiquitinase in tumor suppression. *Cell Death & Differentiation* **28**, 606-625 (2021).

187. Pena-Llopis, S. *et al.* BAP1 loss defines a new class of renal cell carcinoma. *Nat Genet* **44**, 751-759 (2012).

188. Harbour, J.W. *et al.* Frequent mutation of BAP1 in metastasizing uveal melanomas. *Science* **330**, 1410-1413 (2010).

189. Bott, M. *et al.* The nuclear deubiquitinase BAP1 is commonly inactivated by somatic mutations and 3p21.1 losses in malignant pleural mesothelioma. *Nat Genet* **43**, 668-672 (2011).

190. Abdel-Wahab, O. & Dey, A. The ASXL-BAP1 axis: new factors in myelopoiesis, cancer and epigenetics. *Leukemia* **27**, 10-15 (2013).

191. Micol, J.B. & Abdel-Wahab, O. The Role of Additional Sex Combs-Like Proteins in Cancer. *Cold Spring Harb Perspect Med* **6** (2016).

192. Battaglia, A. The importance of multidisciplinary approach in early detection of BAP1 tumor predisposition syndrome: clinical management and risk assessment. *Clinical Medicine Insights: Oncology* **8**, CMO. S15239 (2014).

193. Carbone, M. *et al.* BAP1 and cancer. *Nature Reviews Cancer* **13**, 153-159 (2013).

194. Daou, S. *et al.* The BAP1/ASXL2 histone H2A deubiquitinase complex regulates cell proliferation and is disrupted in cancer. *Journal of Biological Chemistry* **290**, 28643-28663 (2015).

195. Sime, W. *et al.* BAP1 induces cell death via interaction with 14-3-3 in neuroblastoma. *Cell death & disease* **9**, 458 (2018).

196. Zhang, Y. *et al.* BAP1 links metabolic regulation of ferroptosis to tumour suppression. *Nature cell biology* **20**, 1181-1192 (2018).

197. Yu, H. *et al.* The ubiquitin carboxyl hydrolase BAP1 forms a ternary complex with YY1 and HCF-1 and is a critical regulator of gene expression. *Mol Cell Biol* **30**, 5071-5085 (2010).

198. Peng, H. *et al.* Familial and somatic BAP1 mutations inactivate ASXL1/2-mediated allosteric regulation of BAP1 deubiquitinase by targeting multiple independent domains. *Cancer research* **78**, 1200-1213 (2018).

199. Mashtalir, N. *et al.* Autodeubiquitination protects the tumor suppressor BAP1 from cytoplasmic sequestration mediated by the atypical ubiquitin ligase UBE2O. *Molecular cell* **54**, 392-406 (2014).

200. Campagne, A. *et al.* BAP1 complex promotes transcription by opposing PRC1-mediated H2A ubiquitylation. *Nature communications* **10**, 1-15 (2019).

201. Ji, Z. *et al.* The forkhead transcription factor FOXK2 acts as a chromatin targeting factor for the BAP1-containing histone deubiquitinase complex. *Nucleic acids research* **42**, 6232-6242 (2014).

202. Okino, Y., Machida, Y., Frankland-Searby, S. & Machida, Y.J. BRCA1-associated protein 1 (BAP1) deubiquitinase antagonizes the ubiquitin-mediated activation of FoxK2 target genes. *J Biol Chem* **290**, 1580-1591 (2015).

203. Qin, J. *et al.* BAP1 promotes breast cancer cell proliferation and metastasis by deubiquitinating KLF5. *Nat Commun* **6**, 8471 (2015).

204. Ruan, H.-B. *et al.* O-GlcNAc transferase/host cell factor C1 complex regulates gluconeogenesis by modulating PGC-1α stability. *Cell metabolism* **16**, 226-237 (2012).

205. Machida, Y.J., Machida, Y., Vashisht, A.A., Wohlschlegel, J.A. & Dutta, A. The deubiquitinating enzyme BAP1 regulates cell growth via interaction with HCF-1. *Journal of Biological Chemistry* **284**, 34179-34188 (2009).

206. Gearhart, P.J. & Wood, R.D. Emerging links between hypermutation of antibody genes and DNA polymerases. *Nature Reviews Immunology* **1**, 187-192 (2001).

207. Bononi, A. *et al.* BAP1 regulates IP3R3-mediated Ca(2+) flux to mitochondria suppressing cell transformation. *Nature* **546**, 549-553 (2017).

208. Yu, H. *et al.* Tumor suppressor and deubiquitinase BAP1 promotes DNA double-strand break repair. *Proc Natl Acad Sci U S A* **111**, 285-290 (2014).

209. Daou, S. *et al.* Monoubiquitination of ASXLs controls the deubiquitinase activity of the tumor suppressor BAP1. *Nat Commun* **9**, 4385 (2018).

210. Sahtoe, D.D., Van Dijk, W.J., Ekkebus, R., Ovaa, H. & Sixma, T.K. BAP1/ASXL1 recruitment and activation for H2A deubiquitination. *Nature communications* **7**, 1-13 (2016).

211. Misaghi, S. *et al.* Association of C-terminal ubiquitin hydrolase BRCA1-associated protein 1 with cell cycle regulator host cell factor 1. *Molecular and cellular biology* **29**, 2181-2192 (2009).

212. Baas, R., J. van der Wal, F., Bleijerveld, O.B., van Attikum, H. & Sixma, T.K. Proteomic analysis identifies novel binding partners of BAP1. *PLoS One* **16**, e0257688 (2021).

213. Reddington, C.J., Fellner, M., Burgess, A.E. & Mace, P.D. Molecular regulation of the polycomb repressive-deubiquitinase. *International journal of molecular sciences* **21**, 7837 (2020).

214. Conway, E. *et al.* BAP1 enhances Polycomb repression by counteracting widespread H2AK119ub1 deposition and chromatin condensation. *Molecular cell* **81**, 3526-3541. e3528 (2021).

215. Scheuermann, J.C. *et al.* Histone H2A deubiquitinase activity of the Polycomb repressive complex PR-DUB. *Nature* **465**, 243-247 (2010).

216. LaFave, L.M. *et al.* Loss of BAP1 function leads to EZH2-dependent transformation. *Nature medicine* **21**, 1344 (2015).

217. Pan, H. *et al.* BAP1 regulates cell cycle progression through E2F1 target genes and mediates transcriptional silencing via H2A monoubiquitination in uveal melanoma cells. *The international journal of biochemistry and cell biology* **60**, 176-184 (2015).

218. Zhao, L., Shah, J.A., Cai, Y. & Jin, J. 'O-GlcNAc Code'mediated biological functions of downstream proteins. *Molecules* **23**, 1967 (2018).

219. Mannino, M.P. & Hart, G.W. The beginner's guide to O-GlcNAc: From nutrient sensitive pathway regulation to its impact on the immune system. *Frontiers in Immunology* **13**, 828648 (2022).

220. Louie, B.H. & Kurzrock, R. BAP1: Not just a BRCA1-associated protein. *Cancer treatment reviews* **90**, 102091 (2020).

221. Dey, A. *et al.* Loss of the tumor suppressor BAP1 causes myeloid transformation. *Science* **337**, 1541-1546 (2012).

222. Arenzana, T.L. *et al.* Tumor suppressor BAP1 is essential for thymic development and proliferative responses of T lymphocytes. *Science immunology* **3**, eaal1953 (2018).

223. Lin, Y.H. *et al.* Regulation of B lymphocyte development by histone H2A deubiquitinase BAP1. *Frontiers in immunology* **12**, 626418 (2021).

224. Zhu, P. *et al.* A histone H2A deubiquitinase complex coordinating histone acetylation and H1 dissociation in transcriptional regulation. *Molecular cell* **27**, 609-621 (2007).

225. Fiore, A. *et al.* Deubiquitinase MYSM1 in the hematopoietic system and beyond: a current review. *International Journal of Molecular Sciences* **21**, 3007 (2020).

226. Bahrami, E. *et al.* Myb-like, SWIRM, and MPN domains 1 (MYSM1) deficiency: Genotoxic stress-associated bone marrow failure and developmental aberrations. *Journal of Allergy and Clinical Immunology* **140**, 1112-1119 (2017).

227. Le Guen, T. *et al.* An in vivo genetic reversion highlights the crucial role of Myb-Like, SWIRM, and MPN domains 1 (MYSM1) in human hematopoiesis and lymphocyte differentiation. *Journal of Allergy and Clinical Immunology* **136**, 1619-1626. e1615 (2015).

228. Birol, M. & Echalier, A. Structure and function of MPN (Mpr1/Pad1 N-terminal) domain-containing proteins. *Current Protein and Peptide Science* **15**, 504-517 (2014).

229. Wang, T. *et al.* The control of hematopoietic stem cell maintenance, self-renewal, and differentiation by Mysm1-mediated epigenetic regulation. *Blood, The Journal of the American Society of Hematology* **122**, 2812-2822 (2013).

230. Jiang, X.-X. *et al.* MYSM1/miR-150/FLT3 inhibits B1a cell proliferation. *Oncotarget* **7**, 68086 (2016).

231. Jiang, X.-X. *et al.* Epigenetic regulation of antibody responses by the histone H2A deubiquitinase MYSM1. *Scientific reports* **5**, 1-15 (2015).

232. Jiang, X.-X. *et al.* Control of B cell development by the histone H2A deubiquitinase MYSM1. *Immunity* **35**, 883-896 (2011).

233. Mathias, B. *et al.* MYSM1 attenuates DNA damage signals triggered by physiologic and genotoxic DNA breaks. *Journal of Allergy and Clinical Immunology* **153**, 1113-1124. e1117 (2024).

234. Förster, M. *et al.* Deubiquitinase MYSM1 is essential for normal fetal liver hematopoiesis and for the maintenance of hematopoietic stem cells in adult bone marrow. *Stem cells and development* **24**, 1865-1877 (2015).

235. Panda, S., Nilsson, J.A. & Gekara, N.O. Deubiquitinase MYSM1 regulates innate immunity through inactivation of TRAF3 and TRAF6 complexes. *Immunity* **43**, 647-659 (2015).

236. Panda, S. & Gekara, N.O. The deubiquitinase MYSM1 dampens NOD2-mediated inflammation and tissue damage by inactivating the RIP2 complex. *Nature communications* **9**, 4654 (2018).

237. Won, H. *et al.* Epigenetic control of dendritic cell development and fate determination of common myeloid progenitor by Mysm1. *Blood, The Journal of the American Society of Hematology* **124**, 2647-2656 (2014).

238. Belle, J.I. *et al.* p53 mediates loss of hematopoietic stem cell function and lymphopenia in Mysm1 deficiency. *Blood* **125**, 2344-2348 (2015).

239. Belle, J. *et al.* Repression of p53-target gene Bbc3/PUMA by MYSM1 is essential for the survival of hematopoietic multipotent progenitors and contributes to stem cell maintenance. *Cell Death and Differentiation* **23**, 759-775 (2016).

240. Gatzka, M. *et al.* Interplay of H2A deubiquitinase 2A-DUB/Mysm1 and the p19ARF/p53 axis in hematopoiesis, early T-cell development and tissue differentiation. *Cell Death & Differentiation* **22**, 1451-1462 (2015).

241. Wilms, C. *et al.* 2A-DUB/Mysm1 regulates epidermal development in part by suppressing p53-mediated programs. *International Journal of Molecular Sciences* **19**, 687 (2018).

242. Zhang, Y. & Lu, H. Signaling to p53: ribosomal proteins find their way. *Cancer cell* **16**, 369-377 (2009).

243. Golomb, L., Volarevic, S. & Oren, M. p53 and ribosome biogenesis stress: the essentials. *FEBS letters* **588**, 2571-2579 (2014).

244. Belle, J.I. *et al.* MYSM1 maintains ribosomal protein gene expression in hematopoietic stem cells to prevent hematopoietic dysfunction. *JCI insight* **5** (2020).

245. Langlais, D., Couture, C., Balsalobre, A. & Drouin, J. The Stat3/GR interaction code: predictive value of direct/indirect DNA recruitment for transcription outcome. *Molecular cell* **47**, 38-49 (2012).

246. Langmead, B., Trapnell, C., Pop, M. & Salzberg, S.L. Ultrafast and memory-efficient alignment of short DNA sequences to the human genome. *Genome biology* **10**, R25 (2009).

247. Zhang, Y. *et al.* Model-based analysis of ChIP-Seq (MACS). *Genome biology* **9**, R137 (2008).

248. Heinz, S. *et al.* Simple combinations of lineage-determining transcription factors prime cis-regulatory elements required for macrophage and B cell identities. *Molecular cell* **38**, 576-589 (2010).

249. Thorvaldsdottir, H., Robinson, J.T. & Mesirov, J.P. Integrative Genomics Viewer (IGV): high-performance genomics data visualization and exploration. *Brief Bioinform* **14**, 178-192 (2013).

250. McLean, C.Y. *et al.* GREAT improves functional interpretation of cis-regulatory regions. *Nature biotechnology* **28**, 495-501 (2010).

251. White, J.K. *et al.* Genome-wide generation and systematic phenotyping of knockout mice reveals new roles for many genes. *Cell* **154**, 452-464 (2013).

252. Skarnes, W.C. *et al.* A conditional knockout resource for the genome-wide study of mouse gene function. *Nature* **474**, 337-342 (2011).

253. Bradley, A. *et al.* The mammalian gene function resource: the International Knockout Mouse Consortium. *Mamm Genome* **23**, 580-586 (2012).

254. Hobeika, E. *et al.* Testing gene function early in the B cell lineage in mb1-cre mice. *Proceedings of the National Academy of Sciences* **103**, 13789-13794 (2006).

255. Casola, S. *et al.* Tracking germinal center B cells expressing germ-line immunoglobulin gamma1 transcripts by conditional gene targeting. *Proc Natl Acad Sci U S A* **103**, 7396-7401 (2006).

256. Nakamura, M. *et al.* High frequency class switching of an IgM+ B lymphoma clone CH12F3 to IgA+ cells. *Int Immunol* **8**, 193-201 (1996).

257. Ran, F.A. *et al.* Genome engineering using the CRISPR-Cas9 system. *Nat Protoc* **8**, 2281-2308 (2013).

258. Litzler, L.C. *et al.* Protein arginine methyltransferase 1 regulates B cell fate after positive selection in the germinal center in mice. *J Exp Med* **220** (2023).

259. Cao, A.T. *et al.* Interleukin (IL)-21 promotes intestinal IgA response to microbiota. *Mucosal Immunol* **8**, 1072-1082 (2015).

260. Nojima, T. *et al.* In-vitro derived germinal centre B cells differentially generate memory B or plasma cells in vivo. *Nat Commun* **2**, 465 (2011).

261. Forster, M. *et al.* MYSM1-dependent checkpoints in B cell lineage differentiation and B cell-mediated immune response. *J Leukoc Biol* **101**, 643-654 (2017).

262. Litzler, L.C. *et al.* PRMT5 is essential for B cell development and germinal center dynamics. *Nat Commun* **10**, 22 (2019).

263. McAllister, E.J., Apgar, J.R., Leung, C.R., Rickert, R.C. & Jellusova, J. New Methods To Analyze B Cell Immune Responses to Thymus-Dependent Antigen Sheep Red Blood Cells. *J Immunol* **199**, 2998-3003 (2017).

264. Tung, L.T. *et al.* p53-dependent induction of P2X7 on hematopoietic stem and progenitor cells regulates hematopoietic response to genotoxic stress. *Cell Death Dis* **12**, 923 (2021).

265. Bolger, A.M., Lohse, M. & Usadel, B. Trimmomatic: a flexible trimmer for Illumina sequence data. *Bioinformatics* **30**, 2114-2120 (2014).

266. Kim, D., Paggi, J.M., Park, C., Bennett, C. & Salzberg, S.L. Graph-based genome alignment and genotyping with HISAT2 and HISAT-genotype. *Nature biotechnology* **37**, 907-915 (2019).

267. Pertea, M., Kim, D., Pertea, G.M., Leek, J.T. & Salzberg, S.L. Transcript-level expression analysis of RNA-seq experiments with HISAT, StringTie and Ballgown. *Nature protocols* **11**, 1650-1667 (2016).

268. Kim, D., Langmead, B. & Salzberg, S.L. HISAT: a fast spliced aligner with low memory requirements. *Nature methods* **12**, 357-360 (2015).

269. Liao, Y., Smyth, G.K. & Shi, W. featureCounts: an efficient general purpose program for assigning sequence reads to genomic features. *Bioinformatics* **30**, 923-930 (2014).

270. Bolstad, B. preprocessCore: A collection of pre-processing functions. R package version 1.44.0. *https://github.com/bmbolstad/preprocessCore* (2018).

271. Robinson, M.D. & Oshlack, A. A scaling normalization method for differential expression analysis of RNA-seq data. *Genome biology* **11**, R25 (2010).

272. Mevik, B.H. & Wehrens, R. The pls Package: Principal Component and Partial Least Squares Regression in R. *Journal of Statistical Software* **18** (2007).

273. Huang, D.W. *et al.* The DAVID Gene Functional Classification Tool: a novel biological module-centric algorithm to functionally analyze large gene lists. *Genome biology* **8**, R183 (2007).

274. Subramanian, A. *et al.* Gene set enrichment analysis: a knowledge-based approach for interpreting genome-wide expression profiles. *Proc Natl Acad Sci U S A* **102**, 15545-15550 (2005).

275. Skarnes, W. *et al.* A conditional knockout resource for genome-wide analysis of mouse gene function. *Nature* **474**, 337-342 (2011).

276. Petrov, J.C. & Nijnik, A. Mysm1 expression in the bone marrow niche is not essential for hematopoietic maintenance. *Exp Hematol* **47**, 76-82 e73 (2017).

277. Liang, Y. *et al.* Deubiquitinase catalytic activity of MYSM1 is essential in vivo for hematopoiesis and immune cell development. *Sci Rep* **13**, 338 (2023).

278. Kweon, S.-M. *et al.* An adversarial DNA N6-methyladenine-sensor network preserves polycomb silencing. *Molecular cell* **74**, 1138-1147. e1136 (2019).

279. Micol, J.-B. *et al.* ASXL2 is essential for haematopoiesis and acts as a haploinsufficient tumour suppressor in leukemia. *Nature communications* **8**, 15429 (2017).

280. Frangini, A. *et al.* The aurora B kinase and the polycomb protein ring1B combine to regulate active promoters in quiescent lymphocytes. *Molecular cell* **51**, 647-661 (2013).

281. Kleiman, E., Jia, H., Loguercio, S., Su, A.I. & Feeney, A.J. YY1 plays an essential role at all stages of B-cell differentiation. *Proceedings of the National Academy of Sciences* **113**, E3911-E3920 (2016).

282. Steffen, P.A. & Ringrose, L. What are memories made of? How Polycomb and Trithorax proteins mediate epigenetic memory. *Nature reviews molecular cell biology* **15**, 340-356 (2014).

283. Li, Z. *et al.* ASXL1 interacts with the cohesin complex to maintain chromatid separation and gene expression for normal hematopoiesis. *Science advances* **3**, e1601602 (2017).

284. Lara-Astiaso, D. *et al.* Immunogenetics. Chromatin state dynamics during blood formation. *Science* **345**, 943-949 (2014).

285. Allman, D. & Pillai, S. Peripheral B cell subsets. *Curr Opin Immunol* **20**, 149-157 (2008).

286. Tas, J.M.J. *et al.* Antibodies from primary humoral responses modulate the recruitment of naive B cells during secondary responses. *Immunity* **55**, 1856-1871 e1856 (2022).

287. Kolovos, P. *et al.* PR-DUB maintains the expression of critical genes through FOXK1/2- and ASXL1/2/3-dependent recruitment to chromatin and H2AK119ub1 deubiquitination. *Genome Res* **30**, 1119-1130 (2020).

288. Delgado-Benito, V. *et al.* The Chromatin Reader ZMYND8 Regulates Igh Enhancers to Promote Immunoglobulin Class Switch Recombination. *Mol Cell* **72**, 636-649 e638 (2018).

289. Yoshida, H. *et al.* The cis-Regulatory Atlas of the Mouse Immune System. *Cell* **176**, 897-912 e820 (2019).

290. Ohtsuka, M. *et al.* NFAM1, an immunoreceptor tyrosine-based activation motif-bearing molecule that regulates B cell development and signaling. *Proc Natl Acad Sci U S A* **101**, 8126-8131 (2004).

291. Li, X. *et al.* CRAC Channel Controls the Differentiation of Pathogenic B Cells in Lupus Nephritis. *Front Immunol* **12**, 779560 (2021).

292. Kubo, M. *et al.* Leucine-rich repeat kinase 2 is a regulator of B cell function, affecting homeostasis, BCR signaling, IgA production, and TI antigen responses. *J Neuroimmunol* **292**, 1-8 (2016).

293. Wheeler, M.L., Dong, M.B., Brink, R., Zhong, X.P. & DeFranco, A.L. Diacylglycerol kinase zeta limits B cell antigen receptor-dependent activation of ERK signaling to inhibit early antibody responses. *Sci Signal* **6**, ra91 (2013).

294. Li, X. *et al.* Cbl and Cbl-b control the germinal center reaction by facilitating naive B cell antigen processing. *J Exp Med* **217** (2020).

295. Li, X. *et al.* Cbl Ubiquitin Ligases Control B Cell Exit from the Germinal-Center Reaction. *Immunity* **48**, 530-541 e536 (2018).

296. Shi, Y. *et al.* The feedback loop of LITAF and BCL6 is involved in regulating apoptosis in B cell non-Hodgkin's-lymphoma. *Oncotarget* **7**, 77444-77456 (2016).

297. Bertolo, C. *et al.* LITAF, a BCL6 target gene, regulates autophagy in mature B-cell lymphomas. *Br J Haematol* **162**, 621-630 (2013).

298. Grenov, A.C. *et al.* The germinal center reaction depends on RNA methylation and divergent functions of specific methyl readers. *J Exp Med* **218** (2021).

299. Alsultan, A., Shamseldin, H.E., Osman, M.E., Aljabri, M. & Alkuraya, F.S. MYSM1 is mutated in a family with transient transfusion-dependent anemia, mild thrombocytopenia,

and low NK-and B-cell counts. *Blood, The Journal of the American Society of Hematology* **122**, 3844-3845 (2013).

300. Haffner-Luntzer, M. *et al.* Loss of p53 compensates osteopenia in murine Mysm1 deficiency. *FASEB J* **32**, 1957-1968 (2018).

301. Huang, X.F. *et al.* Mysm1 is required for interferon regulatory factor expression in maintaining HSC quiescence and thymocyte development. *Cell Death Dis* **7**, e2260 (2016).

302. Ambroggio, X.I., Rees, D.C. & Deshaies, R.J. JAMM: a metalloprotease-like zinc site in the proteasome and signalosome. *PLoS Biol* **2**, E2 (2004).

303. Pulver, E.M. *et al.* A BRCA1 Coiled-Coil Domain Variant Disrupting PALB2 Interaction Promotes the Development of Mammary Tumors and Confers a Targetable Defect in Homologous Recombination Repair. *Cancer Res* **81**, 6171-6182 (2021).

304. Zavolan, M. *et al.* Impact of alternative initiation, splicing, and termination on the diversity of the mRNA transcripts encoded by the mouse transcriptome. *Genome Res* **13**, 1290-1300 (2003).

305. Tian, M. *et al.* MYSM1 Represses Innate Immunity and Autoimmunity through Suppressing the cGAS-STING Pathway. *Cell Rep* **33**, 108297 (2020).

306. Klinger, M.H. & Jelkmann, W. Role of blood platelets in infection and inflammation. *J Interferon Cytokine Res* **22**, 913-922 (2002).

307. Zhao, J. *et al.* Human hematopoietic stem cell vulnerability to ferroptosis. *Cell* **186**, 732-747 e716 (2023).

308. Belle, J.I. *et al.* Repression of p53-Target Gene Bbc3/PUMA by MYSM1 Is Essential for Survival of Multipotent Hematopoietic Progenitor and Contributes to Stem Cell Maintenance. *Cell death and differentiation* **23**, 759-775 (2015).

309. Eletr, Z.M. & Wilkinson, K.D. An emerging model for BAP1's role in regulating cell cycle progression. *Cell biochemistry and biophysics* **60**, 3-11 (2011).

310. Zargar, Z.U. & Tyagi, S. Role of host cell factor-1 in cell cycle regulation. *Transcription* **3**, 187-192 (2012).

311. He, M. *et al.* Intrinsic apoptosis shapes the tumor spectrum linked to inactivation of the deubiquitinase BAP1. *Science* **364**, 283-285 (2019).

312. Piunti, A. *et al.* Polycomb proteins control proliferation and transformation independently of cell cycle checkpoints by regulating DNA replication. *Nature communications* **5**, 3649 (2014).

313. Bravo, M.n. *et al.* Polycomb RING1A-and RING1B-dependent histone H2A monoubiquitylation at pericentromeric regions promotes S-phase progression. *Journal of cell science* **128**, 3660-3671 (2015).

314. Martinez, A.-M. & Cavalli, G. The role of polycomb group proteins in cell cycle regulation during development. *Cell cycle* **5**, 1189-1197 (2006).

315. Gu, Y. *et al.* The histone H2A deubiquitinase Usp16 regulates hematopoiesis and hematopoietic stem cell function. *Proceedings of the National Academy of Sciences* **113**, E51-E60 (2016).

316. Pannu, J. *et al.* Ubiquitin specific protease 21 is dispensable for normal development, hematopoiesis and lymphocyte differentiation. *PLoS One* **10**, e0117304 (2015).

317. Wang, H., Langlais, D. & Nijnik, A. Histone H2A deubiquitinases in the transcriptional programs of development and hematopoiesis: a consolidated analysis. *The International Journal of Biochemistry & Cell Biology* **157**, 106384 (2023).

318. Sen Nkwe, N. *et al.* A potent nuclear export mechanism imposes USP16 cytoplasmic localization during interphase. *Journal of cell science* **133**, jcs239236 (2020).

319. Ito, S., Umehara, T. & Koseki, H. Polycomb-mediated histone modifications and gene regulation. *Biochemical Society Transactions* (2024).

320. Walpole, S. *et al.* Comprehensive study of the clinical phenotype of germline BAP1 variant-carrying families worldwide. *JNCI: Journal of the National Cancer Institute* **110**, 1328-1341 (2018).

321. Yamagishi, M. *et al.* Targeting excessive EZH1 and EZH2 activities for abnormal histone methylation and transcription network in malignant lymphomas. *Cell reports* **29**, 2321-2337. e2327 (2019).

322. Wang, L. *et al.* Resetting the epigenetic balance of Polycomb and COMPASS function at enhancers for cancer therapy. *Nature medicine* **24**, 758-769 (2018).

323. Schoumacher, M. *et al.* Uveal melanoma cells are resistant to EZH2 inhibition regardless of BAP1 status. *Nature medicine* **22**, 577-578 (2016).

324. Bononi, A. *et al.* Germline BAP1 mutations induce a Warburg effect. *Cell Death & Differentiation* **24**, 1694-1704 (2017).

325. Baughman, J.M. *et al.* NeuCode proteomics reveals Bap1 regulation of metabolism. *Cell reports* **16**, 583-595 (2016).

326. Dai, F. *et al.* BAP1 inhibits the ER stress gene regulatory network and modulates metabolic stress response. *Proceedings of the National Academy of Sciences* **114**, 3192-3197 (2017).

327. Affar, E.B. & Carbone, M. BAP1 regulates different mechanisms of cell death. *Cell death & disease* **9**, 1151 (2018).

328. Mesin, L., Ersching, J. & Victora, G.D. Germinal center B cell dynamics. *Immunity* **45**, 471-482 (2016).

329. Akkaya, M. *et al.* Second signals rescue B cells from activation-induced mitochondrial dysfunction and death. *Nat Immunol* **19**, 871-884 (2018).

330. Tesi, A. *et al.* An early Myc-dependent transcriptional program orchestrates cell growth during B-cell activation. *EMBO Rep* **20**, e47987 (2019).

331. He, C. *et al.* CD36 and LC3B initiated autophagy in B cells regulates the humoral immune response. *Autophagy* **17**, 3577-3591 (2021).

332. Raso, F. *et al.* alphav Integrins regulate germinal center B cell responses through noncanonical autophagy. *J Clin Invest* **128**, 4163-4178 (2018).

333. Martinez-Martin, N. *et al.* A switch from canonical to noncanonical autophagy shapes B cell responses. *Science* **355**, 641-647 (2017).

334. Sandoval, H., Kodali, S. & Wang, J. Regulation of B cell fate, survival, and function by mitochondria and autophagy. *Mitochondrion* **41**, 58-65 (2018).

335. Vaidyanathan, B. & Chaudhuri, J. Epigenetic Codes Programing Class Switch Recombination. *Front Immunol* **6**, 405 (2015).

336. Saha, T., Sundaravinayagam, D. & Di Virgilio, M. Charting a DNA Repair Roadmap for Immunoglobulin Class Switch Recombination. *Trends Biochem Sci* **46**, 184-199 (2021).

337. Li, C. *et al.* The H2B deubiquitinase Usp22 promotes antibody class switch recombination by facilitating non-homologous end joining. *Nat Commun* **9**, 1006 (2018).

338. Zhao, B. *et al.* USP7 promotes IgA class switching through stabilizing RUNX3 for germline transcription activation. *Cell reports* **43** (2024).

339. Jeong, J. *et al.* BAP1 shapes the bone marrow niche for lymphopoiesis by fine-tuning epigenetic profiles in endosteal mesenchymal stromal cells. *Cell Death Differ* **29**, 2151-2162 (2022).

340. Mlynarczyk, C., Fontán, L. & Melnick, A. Germinal center-derived lymphomas: The darkest side of humoral immunity. *Immunological reviews* **288**, 214-239 (2019).

341. Daniel, J.A. *et al.* Loss of ATM kinase activity leads to embryonic lethality in mice. *J Cell Biol* **198**, 295-304 (2012).

342. Jiang, W. *et al.* Differential phosphorylation of DNA-PKcs regulates the interplay between end-processing and end-ligation during nonhomologous end-joining. *Mol Cell* **58**, 172-185 (2015).

343. Dickinson, M.E. *et al.* High-throughput discovery of novel developmental phenotypes. *Nature* **537**, 508-514 (2016).

344. Liakath-Ali, K. *et al.* Novel skin phenotypes revealed by a genome-wide mouse reverse genetic screen. *Nature communications* **5**, 3540 (2014).

345. Wang, Y.H. *et al.* Mysm1 epigenetically regulates the immunomodulatory function of adipose-derived stem cells in part by targeting miR-150. *Journal of Cellular and Molecular Medicine* **23**, 3737-3746 (2019).

346. Bushman, J.W. *et al.* Proteomics-Based Identification of DUB Substrates Using Selective Inhibitors. *Cell Chem Biol* **28**, 78-87 e73 (2021).

347. Rossio, V. *et al.* Proteomics of broad deubiquitylase inhibition unmasks redundant enzyme function to reveal substrates and assess enzyme specificity. *Cell Chem Biol* **28**, 487-502 e485 (2021).

348. Ramirez, J. *et al.* A Proteomic Approach for Systematic Mapping of Substrates of Human Deubiquitinating Enzymes. *Int J Mol Sci* **22** (2021).

349. Mattiroli, F. & Penengo, L. Histone ubiquitination: an integrative signaling platform in genome stability. *Trends in Genetics* **37**, 566-581 (2021).

350. Förster, M. *et al.* A role for the histone H2A deubiquitinase MYSM 1 in maintenance of CD 8+ T cells. *Immunology* **151**, 110-121 (2017).

351. Mousa, M. *et al.* Chromatin-binding deubiquitinase MYSM1 acts in haematopoietic progenitors to control dendritic cell development and to program dendritic cell responses to microbial stimulation. *Immunology* **172**, 109-126 (2024).

352. Inaba, K. *et al.* Generation of large numbers of dendritic cells from mouse bone marrow cultures supplemented with granulocyte/macrophage colony-stimulating factor. *J Exp Med* **176**, 1693-1702 (1992).

353. Xu, Y., Zhan, Y., Lew, A.M., Naik, S.H. & Kershaw, M.H. Differential development of murine dendritic cells by GM-CSF versus Flt3 ligand has implications for inflammation and trafficking. *J Immunol* **179**, 7577-7584 (2007).

354. Brasel, K., De Smedt, T., Smith, J.L. & Maliszewski, C.R. Generation of murine dendritic cells from flt3-ligand-supplemented bone marrow cultures. *Blood* **96**, 3029-3039 (2000).

355. Lin, Y.H. *et al.* Loss of MYSM1 inhibits the oncogenic activity of cMYC in B cell lymphoma. *Journal of Cellular and Molecular Medicine* **25**, 7089-7094 (2021).

356. Wculek, S.K. *et al.* Dendritic cells in cancer immunology and immunotherapy. *Nat Rev Immunol* **20**, 7-24 (2020).